International Atomic Energy Agency

INDC(NDS)-272
Distr.: G+Sp

INDC INTERNATIONAL NUCLEAR DATA COMMITTEE

# CO-ORDINATED RESEARCH PROGRAMME ON MEASUREMENT AND ANALYSIS FOR 14 MeV NEUTRON-INDUCED DOUBLE-DIFFERENTIAL NEUTRON EMISSION CROSS SECTIONS NEEDED FOR FISSION AND FUSION REACTOR TECHNOLOGY

Summary Report of the
Third and Final Research-Co-ordination Meeting
organized by the
International Atomic Energy Agency and held at
Chiang Mai, Thailand, 31 March - 2 April 1992

Prepared by
Wang DaHai
Nuclear Data Section
International Atomic Energy Agency

March 1993

IAEA NUCLEAR DATA SECTION, WAGRAMERSTRASSE 5, A-1400 VIENNA

**INDC(NDS)-272**
Distr.: G+Sp

# CO-ORDINATED RESEARCH PROGRAMME ON MEASUREMENT AND ANALYSIS FOR 14 MeV NEUTRON-INDUCED DOUBLE-DIFFERENTIAL NEUTRON EMISSION CROSS SECTIONS NEEDED FOR FISSION AND FUSION REACTOR TECHNOLOGY

Summary Report of the
Third and Final Research-Co-ordination Meeting
organized by the
International Atomic Energy Agency and held at
Chiang Mai, Thailand, 31 March - 2 April 1992

Prepared by
Wang DaHai
Nuclear Data Section
International Atomic Energy Agency

March 1993

Reproduced by the IAEA in Austria
March 1993
93-01000

## TABLE OF CONTENTS*

Footnote

1. The presentations of the participants of the third RCM have been included.

2. Under the CRP, some papers have been published which are not included in this report. They are:

   (a) INDC report: *INDC(GDR)-058*, September 1990
   The neutron emission cross section of V, Ta and W at 14 MeV neutron incidence energy
   By H. Al Obiesi et.al.

   (b) INDC report: *INDC(JPN)-146/L*, December 1990
   Measurement of double-differential neutron-emission cross-sections at 14.1 MeV for Ti, Mo and Sn
   By A. Takahashi et.al.

   (c) INDC report: *INDC(JPN)-118/L*, January 1989
   Measurement and analysis of double-differential neutron emission cross sections at $E_n$ = 14.1 MeV for $^{93}$Nb and $^{181}$Ta
   By A. Takahashi et.al.

   (d) INDC report: *INDC(CCP)-315*, September 1990
   Differential neutron emission and inelastic cross section from $^{208}$Pb and $^{209}$Bi at 14.1 MeV incident energy
   By S.P. Simakov et.al.

   (e) Measurement of double-differential neutron-emission cross sections at 14 MeV
   Beijing International Symposium on Fast Neutron Physics, 9-13 September 1991
   By A. Takahashi

## SUMMARY

The third and final IAEA Research Co-ordination Meeting on Measurements and Analysis of 14 MeV Neutron-Induced Double-Differential Neutron Emission Cross Sections (DDX) needed for Fission and Fusion Reactor Technology was held at Chiang Mai, Thailand, during 31 March - 2 April 1992. This report summarizes the conclusions and recommendations which were agreed by all participants and includes the reports presented by the participants of the meeting.

The principal objectives of the RCM were to discuss and evaluate the final results of the measurements and analyses carried out by each participating laboratory under the CRP, to recommend "best" data resulting from this CRP, to review the status and remaining gaps in the required data and, if necessary, to identify further measurements and calculations to fill these gaps.

The meeting was attended by 7 scientists from 7 countries, who are the principal scientific investigators of the CRP, and 2 other scientists from Japan, as observers.

The meeting agenda and the list of participants are attached to the full report as Appendices I and II respectively.

The main conclusions of the RCM are as follows:

(1) Extensive new measurements have been carried out under the CRP for 14 MeV neutron-induced double-differential neutron emission cross sections of $^{6}$Li, $^{7}$Li, Be, V, Cr, Fe, Nb, Mo, W, Ta, Bi and $^{238}$U, which are very important for fission and fusion reactor technology. The accuracy of the above data has been approved. An uncertainty of $\leq 10\%$ for the energy-differential cross sections has been obtained.

(2) Based on the new experimental data, new evaluations have been carried out for the above mentioned nuclides. The new evaluation data are strongly recommended to the FENDL nuclear data library which will be mainly used by the ITER project.

(3) Judging by the results mentioned above, it is concluded that the CRP has been very successful.

(4) The CRP may be terminated at this stage formally, the measurements and evaluations of the double-differential neutron emission cross section (DDX) data for the FENDL library should, however, be continued. Therefore, it is recommended that the IAEA should hold a Consultants' Meeting to discuss the DDX data for checking the nuclear model calculations.

# *Part I: Summary Report*

## 1. Introduction

Double-differential neutron emission cross sections (DDX) induced by 14 MeV neutrons are required for nuclear energy applications, especially for fusion reactor analysis, e.g. tritium breeding in blankets, nuclear heating, radiation shielding and material damage. Now large uncertainties and discrepancies of the DDX data are existing.

The IAEA Co-ordinated Research Programme (CRP) on Measurements and Analysis of 14 MeV Neutron-Induced Double-Differential Neutron Emission Cross Sections needed for Fission and Fusion Reactor Technology was started at the end of 1987. The main objectives of the CRP were to improve the current status of data for 14 MeV neutron induced DDX of several isotopes and elements which are very important for fission and fusion reactor technology but not satisfactory for these technologies.

Seven laboratories have participated in the CRP. The are:

(1) Institut für Radiumforschung und Kernphysik (IRK), Vienna, Austria
(principal investigator: ***G. Winkler***; Research Agreement)

(2) China Institute of Atomic Energy (CIAE), Beijing, China
(principal investigator: ***Sa Jun***; Research Contract)

(3) Technical University Dresden, Germany
(principal investigator: ***K. Seidel;*** *Research Agreement)*

*(4) Esfahan Nuclear Technology Centre, Esfahan, Iran*
*(principal investigator:* ***J. Rahighi***; Research Contract)

(5) Osaka University, Osaka, Japan
(principal investigator: ***A. Takahashi***; Research Agreement)

(6) Institute of Physics and Power Engineering, Obninsk, Russian Federation
(principal investigator: ***S.P. Simakov***; Research Agreement)

(7) Chiang Mai University, Chiang Mai, Thailand
(principal investigator: ***T. Vilaithong***; Research Contract)

The first Research Co-ordination Meeting (RCM) took place on 20-22 April 1988 in Vienna. The participants of the CRP analyzed the DDX data status and selected the isotopes and elements which should be included in the CRP. The selected isotopes and elements are: $^{6}$Li, $^{7}$Li, $^{9}$Be, V, Cr, Fe, Nb. Mo, W, Ta, Bi and $^{238}$U.

The second RCM was held on 18-20 June 1990 in Vienna. The participants of the meeting exchanged the experience on the measurements and evaluations and discussed in detail the technical problems.

The summary reports of the RCMs were published as **INDC(NDS)-207/L** and **INDC(NDS)-240**, respectively.

The third and final RCM was held at Chiang Mai, Thailand, during 31 March to 2 April 1992. The principal objectives of the RCM were

(a) to discuss and evaluate the final results of the measurements and analyses carried out by each participating laboratory under this CRP;

(b) to evaluate and recommend "best" data resulting from this CRP;

(c) to review the status and remaining gaps in the required data and, if necessary, to identify further measurements and calculations to fill these gaps.

## 2. Organization of the Meeting

The Agenda of the meeting is listed in Appendix I. The nine participants (seven principal scientific investigators, two observers from Japan), who attended the meeting, are listed in Appendix II.

## 3. Reports by participants of the third RCM

Seven participants of the CRP presented final reports on their work under the CRP. The observers presented their recent work on DDX experiments and evaluations. The activity programme of the individual laboratories are summarised in Appendix III.

## 4. Summary of conclusions and recommendations

(a) The main objectives of the CRP were to improve the current status of data for 14 MeV neutron induced double-differential neutron emission cross sections (DDX) of $^{6}$Li, $^{7}$Li, $^{9}$Be, V, Cr, Fe, Nb, Mo, W, Ta, Bi and $^{238}$U which are very important for fission and fusion reactor technology, but not satisfactory for these technologies. Judging by the reports from individual laboratories, the CRP has been very successful in fulfilling these objectives to a considerable extent.

(b) Extensive new measurements have been carried out under the CRP for the above mentioned nuclides. The bombarding energies used are not only at 14 MeV but also are from 5 - 10 MeV. A novel time-of-flight technique has been developed for the 10 MeV neutron energy eliminating the disturbing interference of D-D break-up neutrons. New evaluation based on the experimental data improved the accuracies close to the levels required for fission and fusion reactor design.

(c) Based on the new experimental data, new evaluation has been carried out for the above mentioned nuclides. Accuracies needed for fission and fusion reactor design have been improved with evaluation of experimental DDX data. Therefore, the participants of the RCM strongly recommend the new evaluation data to the FENDL project.

(d) The discussion of the data status revealed that

(i) **Experimental data**

- For nuclides summarized in Table 1 (Appendix IV), recent experimental data for 14 MeV incident energy show general agreement in angle-integrated spectra, i.e. EDX (energy differential cross section) except for the low and high energy region of secondary neutrons.

- In the high energy region, the data are rather uncertain because of the tail of elastic-peak and of structures due to direct reaction. For improvement of the data status and for assessment of nuclear model, experimental data with higher energy resolution are required.

- The experimental DDX data for low energy part (En 1 MeV) are few and discrepant because of experimental difficulties. They are important for assessment of DDX for (n,2n) reactions, especially for Be, Pb, Bi etc. Therefore, new measurements are encouraged to extend to lower energy range by improving experimental techniques.

- On the angular distribution, discrepancies between the experimental data are much larger than on EDX (Table 1 and 2). A quantitative comparison of angular distributions is required . Detailed comparison on angular distributions are planned at IRK, Vienna, on the basis of reduced Legendre coefficients.

- For nuclides noted in Table 2, new data are highly requested since experimental EDX/DDX data are discrepant or very few.

- For incident energies lower than 14 MeV, experimental data are very few and this makes it difficult to assess the validity of evaluated nuclear data files. Then, new experiments are highly encouraged especially in the range of 8-13 MeV. Experiments are in progress in CIAE using a unique experimental technique.

(ii) **Evaluation Files**

The evaluated data files, as shown in Table 1, are not satisfactory in many cases both in EDXs and DDXs. For most cases, the evaluated data files do not provide angular dependence of emission spectra and are not sufficient for neutron transport calculations. At present, marked disagreement exists between the evaluations even for Fe which is of prime importance as structural material and as the standard data.

- It was recommended to improve the evaluation of emission spectra and to provide DDX data appropriately taking account of angular dependence.

- It was recommended to evaluate fine structures in the high energy region since recent high resolution data enables such evaluations. They will be useful as the standard for evaluations and experiments.

(iii) **Benchmarking of Evaluated Data and Model Calculations**

For the assessment of an evaluated data file, integral data sensitive to DDX are highly needed. In addition to past experiments, new integral experiments are in progress or planned in several laboratories for shielding benchmark of ITER.

- These experiments should be analyzed taking account of energy-angle correlation, i.e. angle-dependence of emission spectra to describe the neutron transport and related phenomena adequately.

- For the nuclear model codes, international comparisons were done previously. An benchmark comparison between the codes will be useful not only for EDX but also for the angular distribution.

(e) The discussion also revealed that the multistep scattering could be a very large source of systematic errors in general and it was recommended to exchange the detailed information about the mutliple scattering correction among the laboratories. It is recommended that the IRK Group, Vienna, should collect the information and compare the correction results.

(f) For the measurements of the DDX data for isotopes, it is recommended that IAEA should financially support the exchange of enriched isotopic samples.

(g) As there were so many technical discussions, more than three days, maybe five days, are needed for the RCM.

(h) For testing the nuclear model codes, the incident neutron energy should be extended from 14 to 30 MeV.

(i) The participants concluded that the CRP may be terminated at this stage formally, the measurements and evaluations of the DDX data for the FENDL project should, however, be continued. Therefore it is recommended that the IAEA should hold a Consultants' Meeting in conjunction with the next FENDL meeting to discuss the DDX data (for example, data of carbon, iron and lead) for checking and nuclear model calculations and experimental techniques including data processing.

# *Part II: Contributed Papers*

# The IRK Time-of-Flight Facility for Measurements of Double-Differential Neutron Emission Cross Sections

Andreas Pavlik, Alfred Priller, Peter Steier,
Herbert Vonach and Gerhard Winkler
Institut für Radiumforschung und Kernphysik der Universität Wien
Boltzmanngasse 3
A-1090 Wien, Austria

**Abstract:** In order to improve the present experimental data base of energy- and angular-differential neutron emission cross sections for incident neutrons in the 14 MeV range, a new time-of-flight facility was installed at the Institut für Radiumforschung und Kernphysik (IRK), Vienna. Combined with a pulsed neutron generator of Cockcroft-Walton type it incorporates a flight-path in an evacuated tube system particularly designed to more precisely measure the high-energy part of the secondary (inelastic) neutron spectra. The goal of background reduction in this energy range was definitely achieved. For every secondary neutron detected, the recoil energy, the flight-time and information on the pulse shape is recorded in listmode. Software packages were developed for reduction of the multiparameter data to sorted neutron and $\gamma$-ray spectra yielding the double-differential scattering cross sections, for the calculation of the primary neutron energy-profiles and the scattering-angle profiles for the different sample positions, and for estimating the influence of multiple scattering in the sample.

## 1. Introduction

The new time-of-flight facility installed at the IRK, Vienna, during the last few years is an improved version of the old time-of-flight set-up described by Winkler et al. [1]. The principle of varying the scattering angle by moving the sample along the axis of a fixed cylindrical detector access channel with fixed neutron source and fixed neutron detector was maintained. This permits heavy shielding of the neutron detector against background. The new design features aimed at eliminating the essential drawbacks of the old version as there were:

a) Since tight collimation is not possible with a scattering sample at varying distances from the detector and the neutron source, there exists a considerable background due to air-scattered neutrons from the air volume seen by the detector, in particular from regions close to the collimator aperture.

b) The mean energy varied with the changing of the scattering angle, i.e. the sample position , causing problems with the interpretation of the measured data [1,2].

Therefore in the new set-up

a) the neutron production target and the sample were positioned in a cylindrical tube system, which can be evacuated in order to significantly reduce the number of air-scattered neutrons and to eliminate the need of neutron air-attenuation corrections for different lengths of the flight-path.

b) In order to keep the mean energy of the effective source neutrons constant when changing the scattering sample position, the scattering geometry was set up in a way that the mean angle between the direction of the effective source neutrons and the direction of the deuteron beam initiating the $T(d,n)^4He$ source reaction was kept constant at 90°, independent of the scattering sample postition on the detector collimator axis.

The operation of the new facility was unfortunately hampered by the renovation of the institute building (from the middle of 1985 until the end of 1987), the break down of the

high voltage power supply of the neutron generator (middle of 1988), and by other necessary services (replacement of worn-out parts) and improvements of the IRK neutron generator. In addition, the energy-dependent efficiency of the main neutron detector had to be remeasured. The electronics for pulse processing, data acquisition and remote control of the sample positioning system had to be readjusted. Several neutron yield monitor circuits were installed and the monitor responses were calibrated.

At the CRP held in Vienna (1990), the participants proposed to perform measurements on $^{6}$Li, $^{7}$Li, $^{9}$Li, Na, Mg, P, S, Cl, K, Ca and F. At that time the IRK intended to investigate Mg and S [3]. In the meantime it was decided not to do so since Mg and S consist of several stable elements and therefore are not very suitable for comparisons with model calculations. Now sodium was chosen at the IRK as the sample element of primary interest having only one stable isotope. Difficulties had to be encountered when producing an air-tight and pure sample of this material (diameter 30 mm, length 120 mm, mass ≈ 82 g). For checking the performance of the new facility, measurements with a lead sample (diameter 19 mm, length 120 mm, mass ≈ 386 g) are also planned. The double-differential cross sections of lead have been evaluated recently from several data sets in the literature [4].

## 2. The IRK neutron generator

The IRK pulsed neutron generator of Cockcroft-Walton type produces neutrons in the 14 MeV region via the T(d,n)$^{4}$He reaction [5]. Deuterium gas is ionized in a radio frequency source driven by a transmitter with a frequency of 72 MHz and a power consumption of ≈ 200 W. The source delivers 2.5 - 3.5 mA of $D^{+}$ and $D^{++}$ ions (ratio about 1:1). The extraction channel is fabricated from titanium being less subject to sputtering compared to aluminium. The ions are pre-accelerated by a voltage of about 30 kV. The ion beam is chopped by writing it periodically (every 400 ns) across a narrow slit. A 90° double-focusing magnet selects and bends the $d^{+}$-ion bunches into a double-gap buncher (driving frequency 15 MHz, gap separation ≈ 6 cm). The ions are further accelerated to about 230 - 240 keV energy and hit a solid-state tritium-titanium-copper target. The stop signal for the time-of-flight measurements is obtained from the beam bunches by means of a pick-off cylinder about 20 cm up-stream of the neutron production target. The time structure of the neutron bunches at 2.5 MHz repetition frequency as obtained with a small 3-mm thick plastic scintillator, 40 cm away from the target, is shown in Fig. 1. The average target current is around 5 $\mu$A giving about $10^{9}$ neutrons per second with a new target, bunched into pulses with less than 2 ns FWHM. The neutron generator room, heavily shielded by concrete walls, is about 6.5 m * 6.8 m wide and 5.2 m high.

## 3. Experimental set-up

The essential features of the layout of the scattering chamber and the flight-path are shown in Fig. 2. The whole flight path of the neutrons is contained in an evacuated tube system centered around the detector collimator axis. The scattering chamber consists of a cylindrical steel vessel about 5 m high and 80 cm in diameter. This large size is needed in order to reduce the influence of neutrons scattered from the walls of this vacuum vessel on the secondary neutron spectrum to a negligible level (< 1%). The target is positioned by a low-mass target holder, with the beam spot center 15 cm off the detector collimator axis, inside a thin Al tube (1 mm thick) separating the beam line vacuum from the scattering

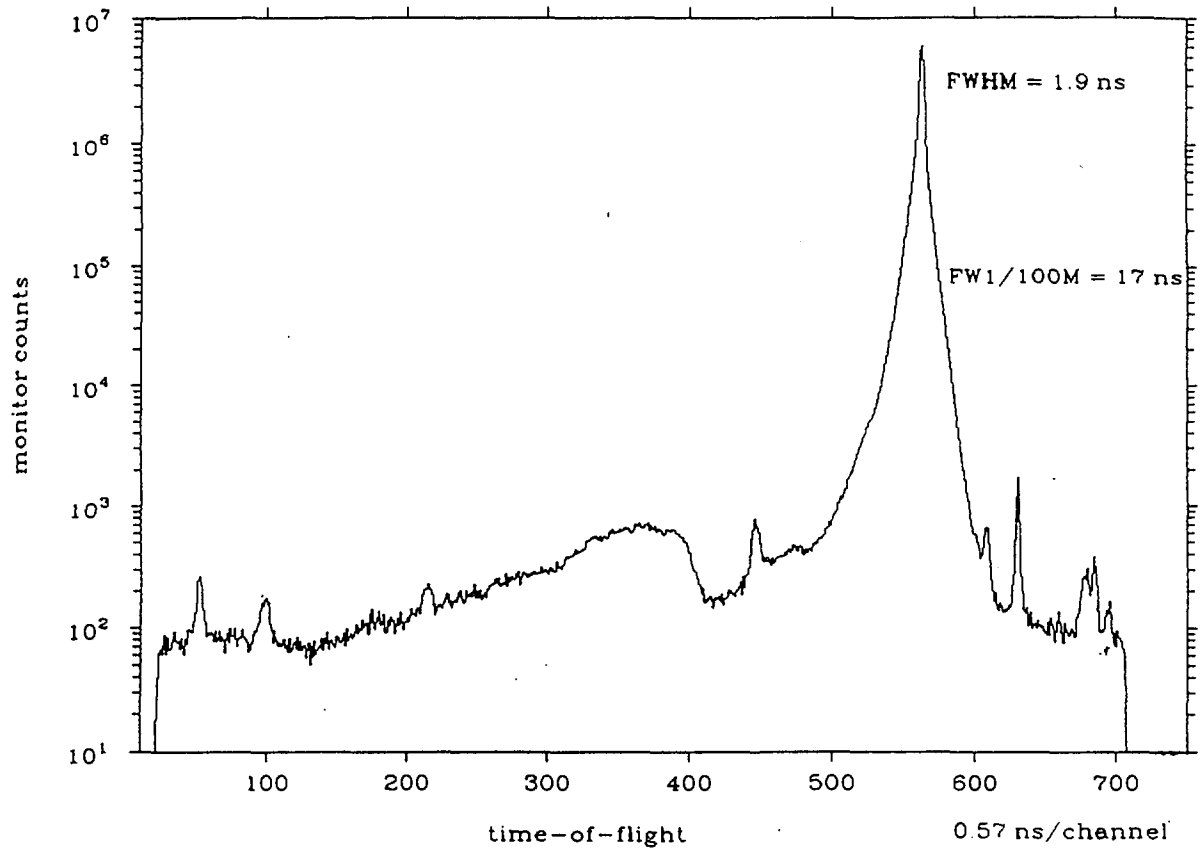


Fig. 1 Time structure of the primary source neutrons during one pulse cycle (400 ns) showing the achieved time resolution of the pulsing system and the (very low) neutron background between successive pulses exhibiting some small spikes due to buncher operation.

chamber vacuum. The beam spot is 234 cm above the floor of the accelerator room; cooling is achieved mainly by radiant cooling. A hole had been drilled through the floor of the accelerator room (concrete doped with boric acid). This opening acts as a collimator and a feed-through for the flight-path extension tube (inner diameter 16 cm). At the end of this extension tube, in the room below the neutron generator, the main neutron detector is located with its own heavy shielding for reducing the regular neutron and gamma-ray background not correlated with accelerator operation. The entrance face of the scintillator cell is shielded against soft photons by a 2-mm thick lead cap. An additional collimator limiting the detector acceptance angle is on top of the flight-path extension tube. The main neutron detector consists of a cylindrical NE213 liquid scintillator cell (12.7 cm diameter, 5.1 cm thick) mounted on a Philips XP 2041 fast photomultiplier.

The scattering geometry to measure double-differential neutron scattering cross sections is as follows:

- The beam spot center and the center of symmetry of the (preferably cylindrical) sample lie in a plane perpendicular to the incident deuteron ion beam.
- The axis of symmetry of the sample is always perpendicular to this plane, i.e. parallel to the deuteron beam, which runs horizontally.
- The scattering angle is changed by moving the sample along the collimator axis, which is the axis of symmetry of the main neutron detector.
- The mean energy of the incident neutrons thus does not change with the sample position [6].
- The flight path is (625 ± 1) cm long for a scattering angle of 90° and depends on the scattering angle (sample position). The design of the collimating system ensures that the

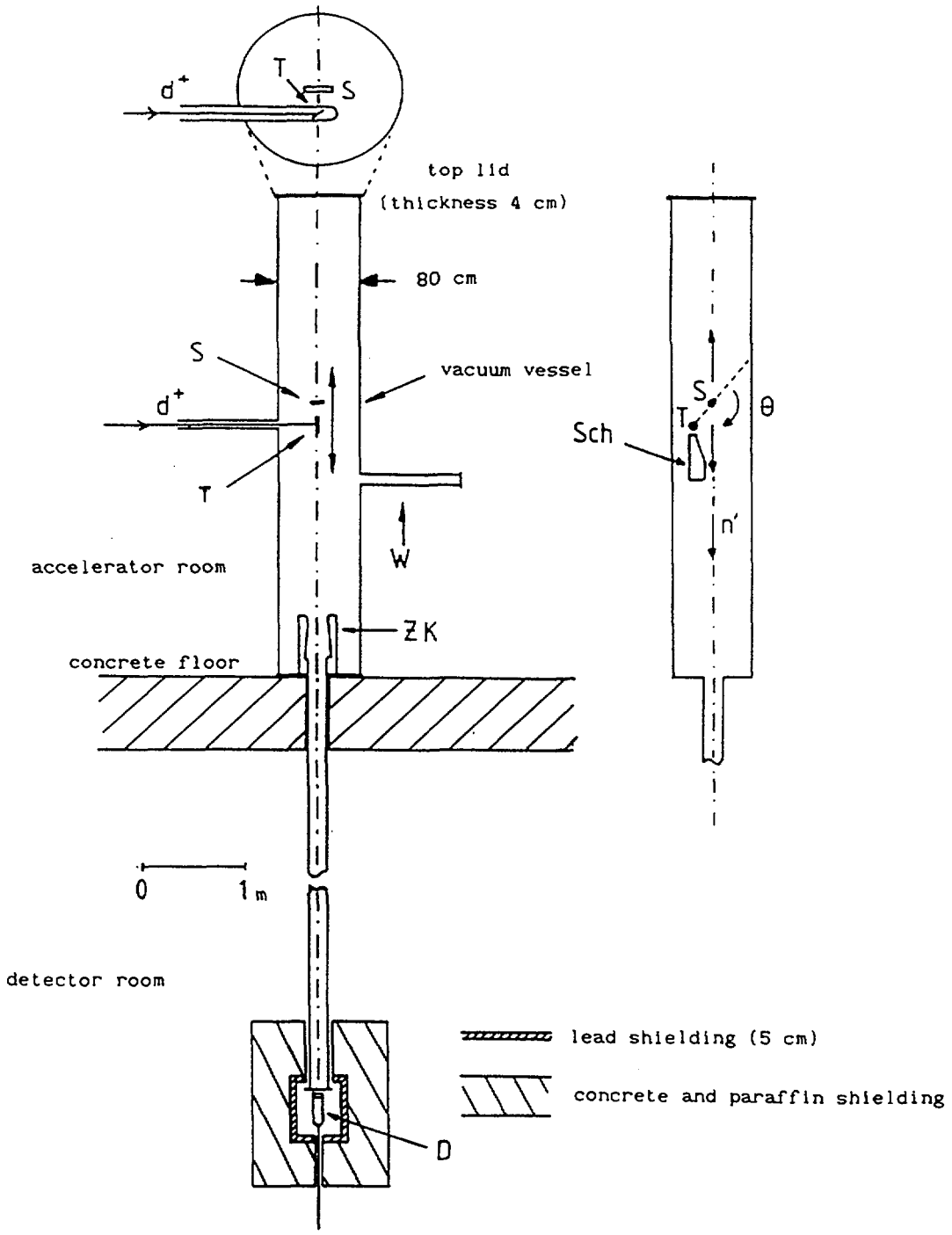


S.....scattering sample

↕.....direction of sample movement

T.....neutron-production target

$d^+$....deuteron beam

n'....scattered neutrons

θ ....scattering angle

Sch...shadow cone (copper)

Zk....additional collimator (polyethylene)

W.....storage container for sample-out measurements

Fig. 2 The new IRK Time-of-Flight Facility (expanded view from the top)

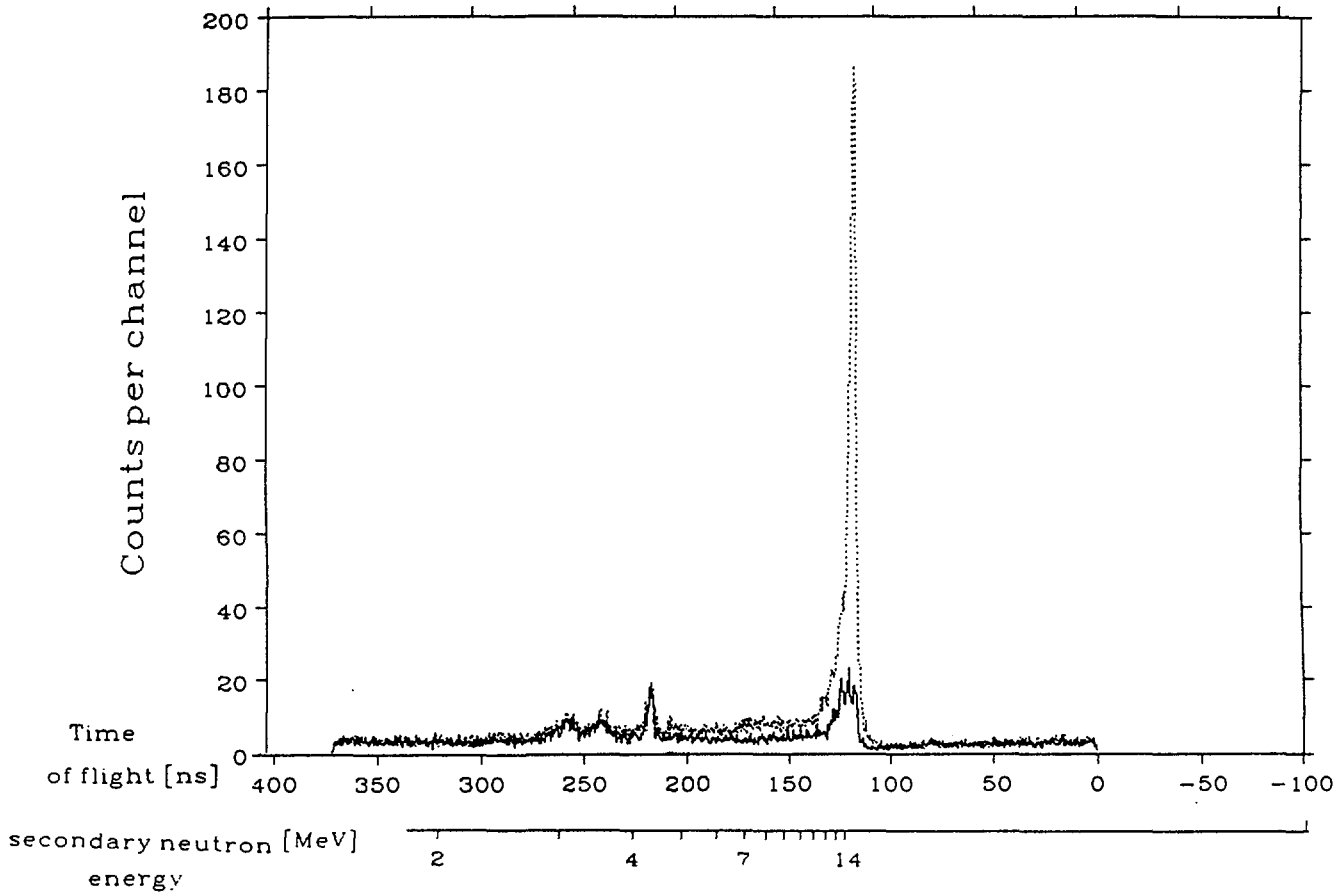


Fig. 3 Accelerator-correlated background time-of-flight spectrum with the flight-path tube system under normal air pressure (dotted line) and evacuated to a pressure 10 Pa (full line) as measured with the main neutron detector (detector threshold: Compton edge of $^{137}Cs$) and normalized to a source yield of $10^{13}$ neutrons.

whole sample is within the circle of vision of each point of the detector, irrespective of the scattering angle in order to maintain the determined detection efficiency.

- A shadow cone (50 cm long) made of copper shields the collimator entrance from direct source neutrons.

- The sample can be moved in vacuum by remote control. For measurements of the neutron-generator dependent background by means of sample-out measurements, the sample is stored in a stand-by side tube.

The suppression of background by evacuating the flight-path is demonstrated in Fig. 3 by sample-out measurements. The huge peak due to air-scattered neutrons and its tail towards lower secondary neutron energies is drastically reduced. Thus the uncertainties introduced by subtracting the accelerator-correlated background are also reduced within the mentioned energy region due to a much better signal-to-background ratio.

Besides the main neutron detector three other neutron monitors are involved in the measurements. The above mentioned fast neutron detector with a small 3-mm thick and 2-cm diameter plastic scintillator is positioned at an angle of 135° relative to the deuteron beam at a distance of 40 cm from the neutron production target. It views the neutron source directly and besides monitoring the time structure of the neutron flux it serves as a calibrated fluence monitor for spectrum normalizing. Another NE213 scintillation neutron detector with a larger response, 12.7 cm in diameter and 2.6 cm thick, sitting at an angle of $\approx 99°$ relative to the deuteron beam and about 4 m away from the target, is used for adjusting the operation parameters and for surveillance of the stability of the pulsed

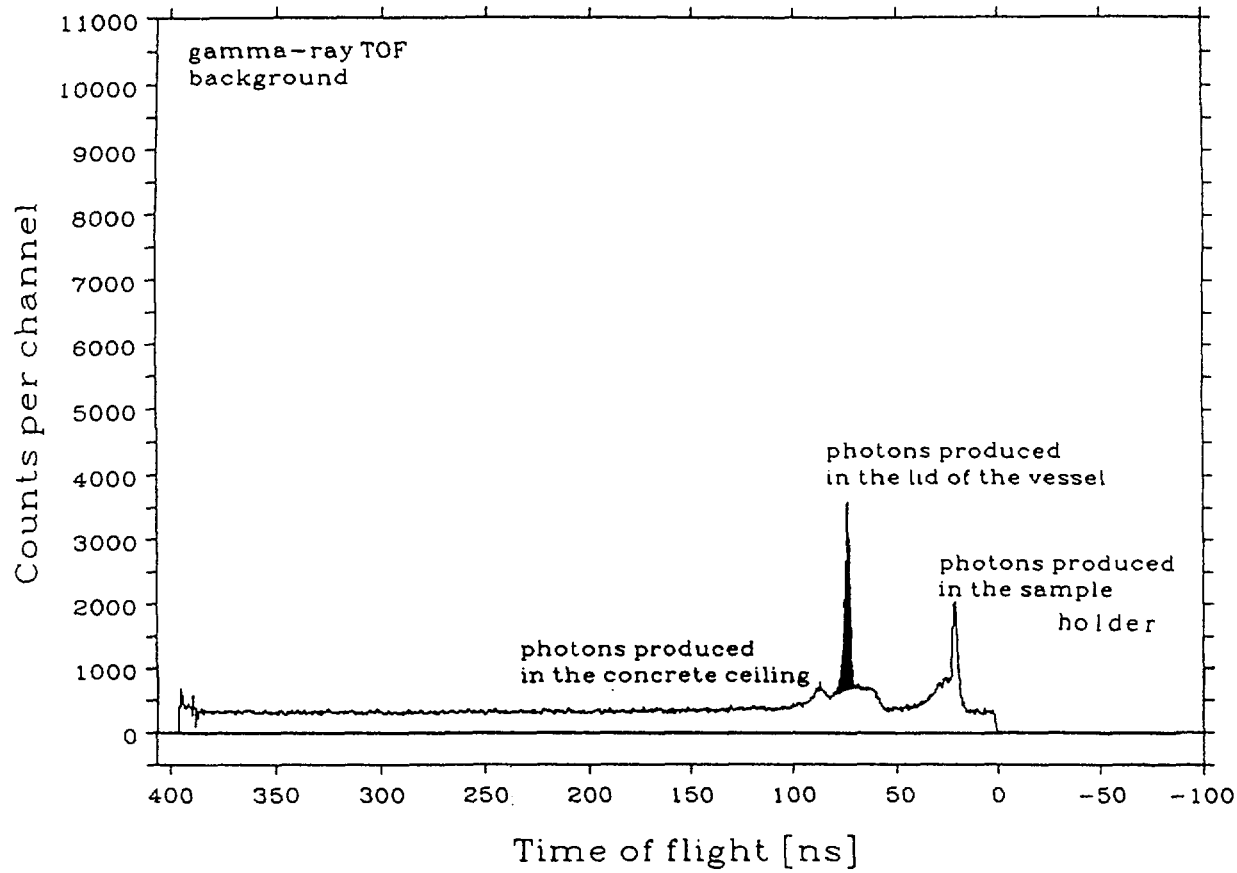


Fig. 4 Time-of-flight spectrum produced by gamma-rays only as obtained with the main neutron detector referred to a neutron source yield of $10^{13}$ neutrons. The peak at the time-of-flight of 19.6 ns stems from inelastic neutron interactions in the sample holder, the peak at the time-of-flight of 73.2 ns from interactions in the top lid of the vacuum tube, which favourably can be used as additional fluence and surveillance monitor. Relatively weak peaks show up at all positions where the corresponding neutron time-of-flight spectrum exhibits peaks (due to inelastic neutron interactions with material surrounding the neutron detector).

neutron generator. Its 14-MeV time-of-flight peak quickly indicates the achieved time structure and possible drifts of the accelerating voltages. The lower threshold of the latter two neutron monitors is adjusted at a pulse size corresponding to one half of the 14-MeV proton recoil edge. Furthermore a $^3$He counter is located in a hole in the 1.5-m thick concrete shielding wall of the accelerator room. It turned out that the photons produced in the iron top lid of the vacuum vessel, always present in the gamma ray spectrum of the main detector, additionally serve as a very handy supplemetary neutron fluence and surveillance monitor (see Fig. 4). The overall time resolution exhibited by the corresponding prominent gamma-ray is around 2.5 ns. Taking into account the neutron flight-path uncertainty of about 5 cm due to the scintillator thickness, this enables an energy resolution of about 450 keV for 14 MeV neutrons with the given flight-path length. The energy spread of the primary source neutrons varies between 120 keV and about 250 keV (FWHM) depending on the scattering sample position [6].

Since the measurements are very low in intensity a compromise has to be made between a tolerable net count rate and several effects that reduce the quality of the experiment and increase with the sample size. The criteria given in Ref. [1] and detailed calculations reported in Ref. [7] show that the choice of cylindrical scattering samples (12 cm long and 1 to 2 cm in diameter) is a good one.

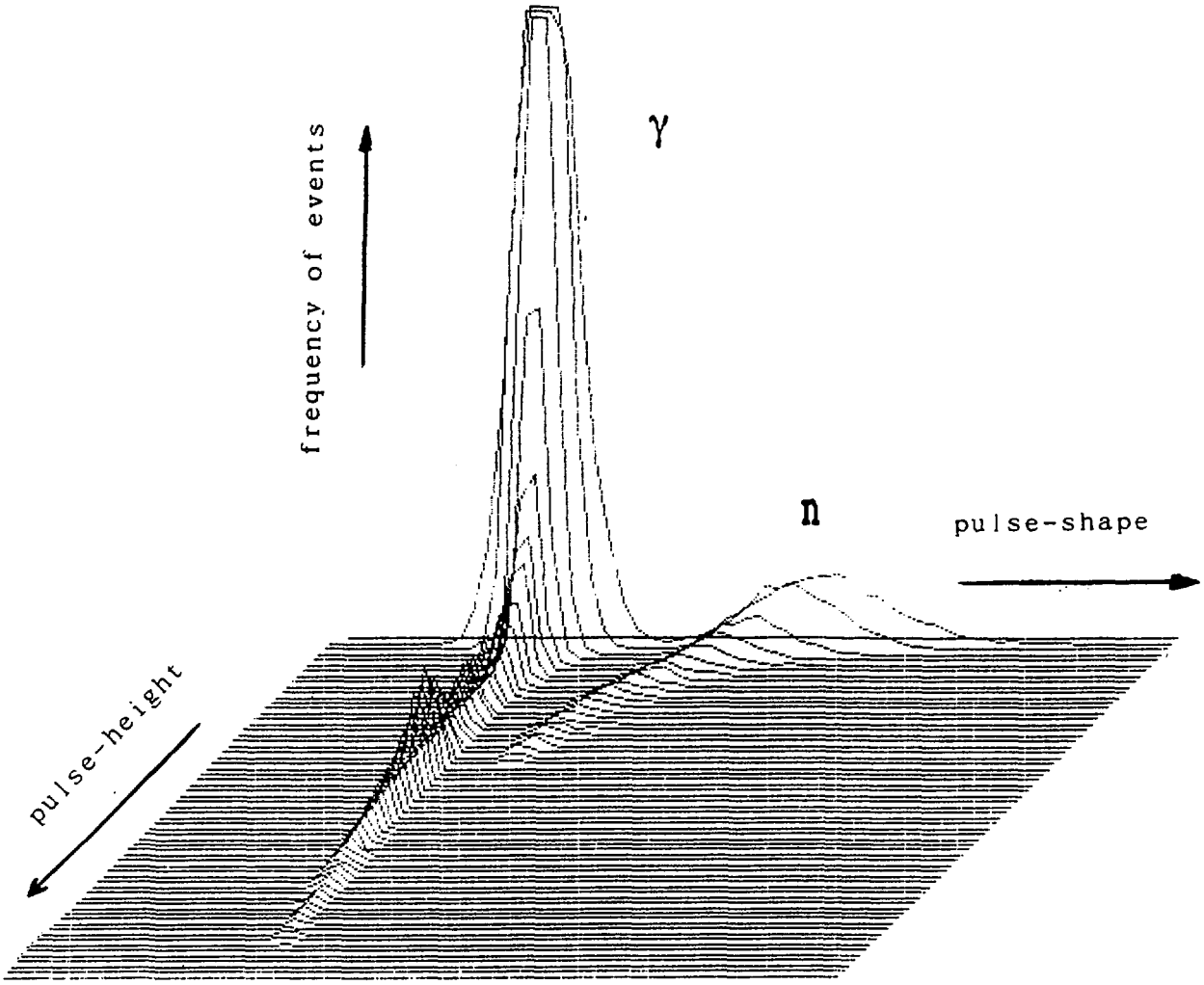


Fig. 5 Two-dimensional spectrum of detector events; frequency of events depending on pulse-height and pulse-shape

## 4. Data acquisition

A fast stop pulse for all time-of-flight measurements is derived from the capacitive beam pick-off by a zero-crossing discriminator. A stop efficiency of 100% can be achieved for every beam burst.

The signal path of the main neutron detector involves three circuits each of which feeds an ADC: a pulse-shape discrimination circuit providing the separation of gamma-ray and neutron pulses, a slow analog circuit for processing the recoil energy information, and the time-of-flight circuit. If all conditions applied to the signals by hardware are met, a triple coincidence provides a common gate signal for the three ADCs (incorporated in a SILENA 4418/V module) interfaced to a PDP 11/34 computer for data storage and on-line display. For every detector event thus the information is made up of three words which are stored in listmode. The PDP 11/34 or a VAX-station II can both be used for sorting and off-line analysis of the data. The actual lower threshold of the pulse height distribution spectra can be set during the data reduction process. The threshold set by hardware is less than half of the pulse-height corresponding to the Compton edge produced with a source of $^{137}Cs$. Sixteen scalers connected to critical points of the electronics set-up and controlled by the on-line computer serve to check pulse processing and stability of the electronics.

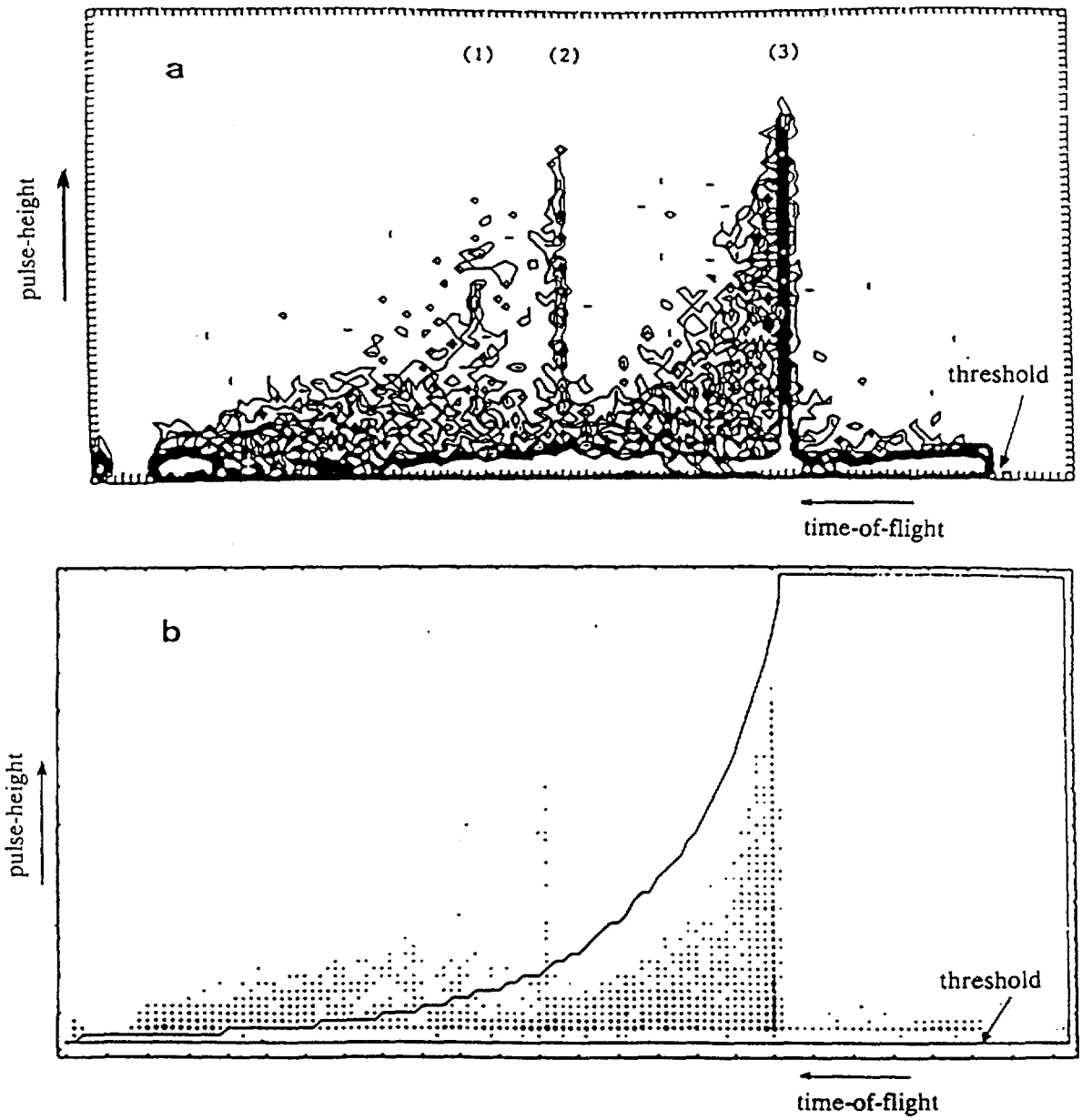


Fig. 6 Contour-plot **a** and intensity scan **b** of a two-dimensionally sorted neutron TOF-spectrum; pulse-height versus time-of-flight. The solid line in **b** marks the border between valid (below line) and non-valid events (above line). The marked areas in plot **a** correspond to elastically scattered neutrons from the environment: (1) from the ceiling of the accelerator room, (2) from the top lid of the vaccuum tube and (3) from the elastic scattering from the sample or directly from the neutron production target.

## 5. Data reduction

The first step in off-line multiparameter data analysis of the listmode data is generating TOF spectra including all events produced by neutrons with a pulse-height above a given level. The separation between gamma- and neutron pulses is performed by two-dimensional sorting pulse-height versus pulse-shape cross-over time and taking only the neutron or gamma-ray "hill", respectively (Fig. 5).

Fig. 6 shows neutron events two-dimensionally sorted according to time-of-flight versus pulse height (recoil energy) as a contour plot as well as an intensity scan. There is a unique relation between the time-of-flight and the maximum recoil energy for a neutron

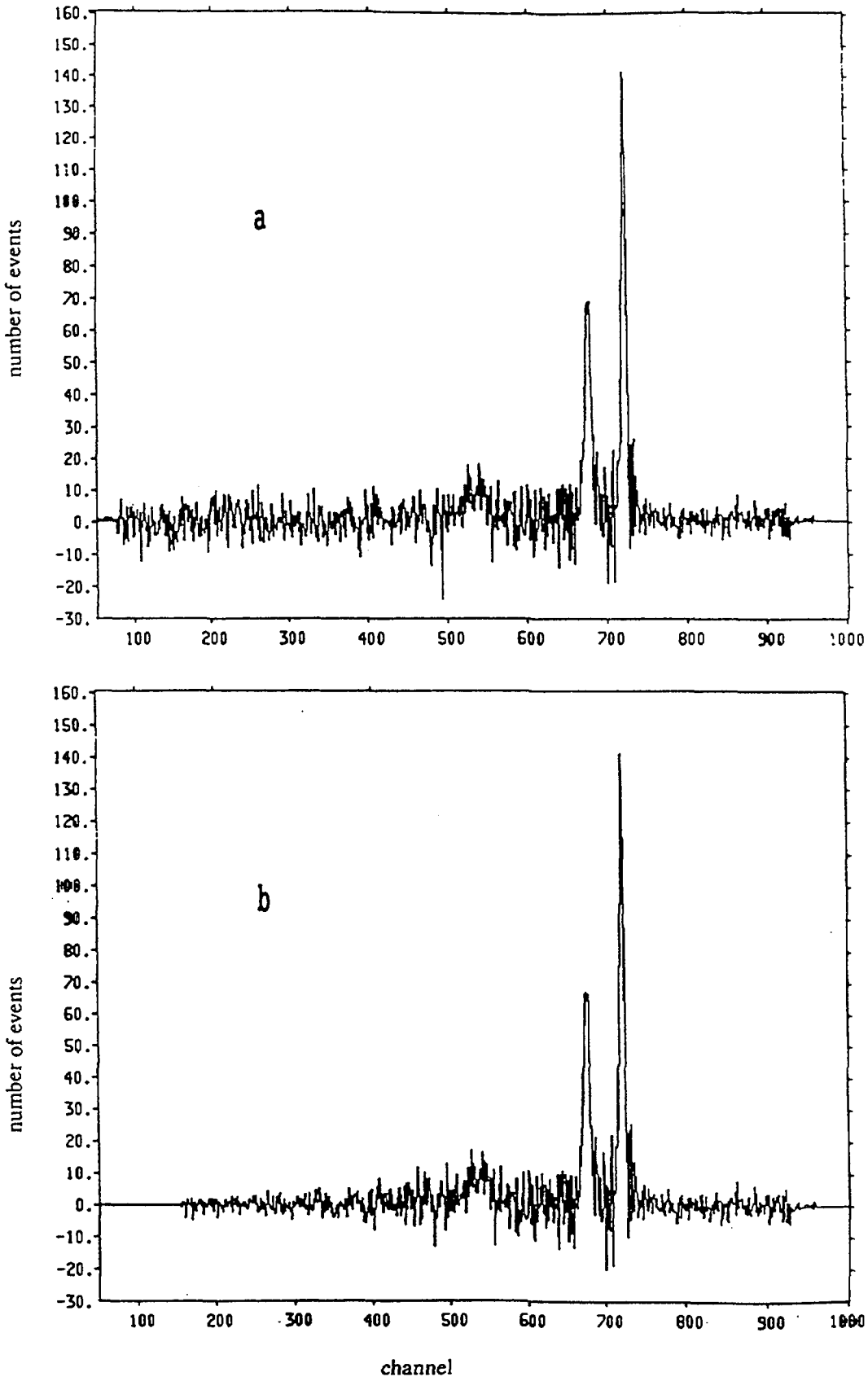


Fig. 7 Background-subtracted neutron TOF spectrum for carbon: scattering angle in the laboratory system 51.5°, sample diameter 1 cm, 12 cm long, yield 2 x $10^{12}$ neutrons, 0.426 ns/channel, Cs threshold

a without rejection
b sorting procedure applied (non-valid events rejected)

starting from the scattering sample (indicated by a full line in Fig. 6). Events showing a pulse-height significantly higher than the flight-time corresponding maximum can be identified as background events and therefore be rejected. This type of accelerator-correlated background mainly stems from elastic and inelastic scattering from the ceiling of the neutron generator room and from the top-lid of the vacuum tube system. Since this type of events will be corrected automatically by subtracting the corresponding background spectrum obtained with a sample-out measurement, the rejection in both measurements reduces the statistical fluctuations (uncertainties) in the lower-energy region of the inelastic net (background-subtracted) neutron spectra significantly (see Fig. 7a and 7b).

Sample-in and sample-out measurements have to be normalized to the same neutron yield using the neutron monitors. Two types of background have to be distinguished:

a) a background independent of the neutron generator with events equally distributed in the TOF spectrum. Its intensity is proportional to the duration of the individual measurement.

b) a background correlated with the accelerator operation exhibiting a flight-time dependent structure with an intensity proportional to the neutron yield.

The uncorrelated background has to be subtracted first from all measured spectra. Then the accelerator-correlated background corrected for the uncorrelated background has to be subtracted from the sample spectra.

The responses of the neutron fluence monitors were calibrated to absolute neutron source yields by irradiating small pure Al foils at definite distances from the target and measuring the $^{24}Na$ activity by means of a NaI(Tl) well-type detector [8,9] using the well-known $^{27}Al(n,\alpha)^{24}Na$ cross section [10].

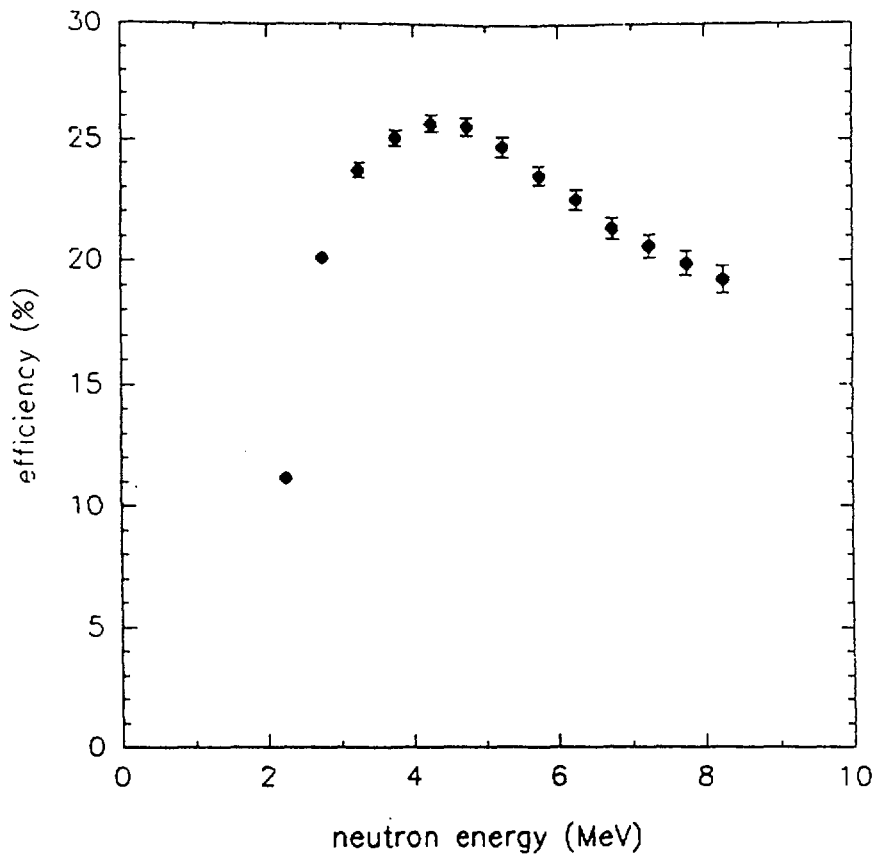


Fig. 8 Efficiency of the main neutron detector measured with a $^{252}Cf$ source. The threshold set by software corresponds to the Compton edge produced with a source of $^{137}Cs$.

The efficiency of the main neutron detector up to a secondary neutron energy of 9 MeV was calibrated using a $^{252}Cf$ source ($10^5$ neutrons/sec) in the 90° position of the scattering sample. A low-mass ionization chamber encasing the $^{252}Cf$ source served as fission-fragment detector providing the start signal for the time-of-flight measurement. Applying the coincidence relations between the fission chamber and the neutron detector response [11], the latter can be converted to absolute efficiencies shown in Fig. 8. This calibration is checked by measuring the scattering of neutrons from hydrogene in polyethylene samples (separate runs with graphite scatterers are necessary to correct the contribution of the carbon in polyethylene). In the energy region beyond 9 MeV the efficiency was determined via elastic neutron scattering on carbon samples. The shape of this extrapolation is to be checked by Monte-Carlo simulation.

The neutron emission cross sections are calculated differently whether they are deduced from resolved peaks belonging to discrete levels in the final nucleus or whether they are deduced from the continuum of the spectra. Integration over the peak is done for distinguishable discrete levels and angle-differential cross sections for neutron scattering on those specific levels are calculated.

For the continuum part the TOF-spectra are transformed into energy spectra in the center-of-mass system. Energy bins of suitable size (according to the resolution of the measurement) are chosen for the integration of counts within the corresponding time-of-flight limits to calculate double-differential neutron emission cross sections. Corrections for absorption and multiple scattering are applied.

Acknowledgements:

We thank the Physikalisch-Technische Bundesanstalt in Braunschweig, Germany, for supplying us with the $^{252}Cf$-source and Prof.Dr.G. Schöck and Dr.W. Pichl of the Institut für Festkörperphysik, Universität Wien, Austria, for their assistance in casting the Na-sample.

**References:**

[1] G. Winkler, K. Hansjakob and G. Staffel:
Measurement of differential elastic and inelastic scattering cross sections with 14 MeV neutrons on barium and chromium. Proc. Int. Conf. on Nucl. Cross sections for Technology, Univ. of Tennessee, Knoxville, Oct. 22-16, 1979, ed. J.L. Fowler, C.H. Johnson and C.D. Bowman, Nat. Bureau of Standards Spec. Publ. 594, p. 150.

[2] G. Winkler, A. Chalupka, K. Hansjakob, G. Staffel, F. Weninger and H. Vonach:
Final report on the work performed at the Institut für Radiumforschung und Kernphysik under contract no. 732-77-10 SISPC between the European Communities (Euratom) and the IRK of the University of Vienna, Univ. of Vienna (1979).

[3] Wang DaHai:
Summary Report of the Second Research Co-ordination Meeting organized by the International Atomic Energy Agency, held in Vienna, Austria, 18-20 June 1990, Report INDC(NDS)-240/L, IAEA, Vienna (1990).

[4] R. Edelmaier:
Mehrfachstreuung und Absorption von Neutronen in ausgedehnten Streuproben. Diplomarbeit (Master thesis), University of Vienna (1989).

[5] G. Stengl:
Sitzungsberichte Österr. Akad. Wiss., mathem.-naturw. Klasse, Abt. II, 185 (1976) 291.

[6] A. Pavlik and G. Winkler:
Calculation of the energy spread and the average neutron energy of 14 MeV neutrons produced via the T(d,n)$^4$He reaction in solid Ti-T targets. Report INDC(AUS)-011/LI or INT(86)-6, IAEA, Vienna (1986).

[7] A. Pavlik, G. Staffel, H. Vonach, G. Winkler:
Unelastische Streuung von 14 MeV Neutronen an Kernen im Massenbereich 10-120. Abschlußbericht zum Jubiläumsfondsprojekt Nr. 1762, Institut für Radiumforschung und Kernphysik der Universität Wien (1989, unpublished).

[8] G. Winkler and A. Pavlik:
Some Aspects of Activity Measurements with NaI(Tl) Well-Type Detectors. Int. J. Appl. Radiat. Isot. 34, (1983) 547.

[9] A. Pavlik and G. Winkler:
Survey of standardization possibilities with a NaI(Tl) well-type detector. Int.J.Appl.Radiat.Isot. 34 (1983) 1167.

[10] M. Wagner, H. Vonach, A. Pavlik, B. Strohmaier, S. Tagesen and J. Martinez-Rico:
Evaluation of cross sections for 14 important neutron-dosimetry reactions. Physics Data 13-5, Fachinformationszentrum Karlsruhe (1990)

[11] R. Böttger, H. Klein, A. Chalupka and B. Strohmaier:
Investigation of the spectral fluence of neutrons from spontaneous fission of $^{252}$Cf by means of time-of-flight spectrometry. Nucl.Sci.Eng. 106 (1990) 377.

# Evaluation of the Angle-Integrated Neutron Emission Cross Sections for Cr, Fe, Ni, Nb, Mo, Ta, W and Bi

Andreas Pavlik, Alfred Priller and Herbert Vonach

Institut für Radiumforschung und Kernphysik der Universität Wien
Boltzmanngasse 3
A-1090 Wien, Austria

**Abstract:** The evaluation of the angle-integrated neutron emission cross sections of 1988 was updated for the elements Cr, Fe, Ni, Nb, Mo, Ta, W and Bi, as new experimental results have been become available in the course of this CRP. The nominal incident neutron energy was chosen to be 14.1 MeV. Cross sections were evaluated for a secondary neutron energy range 0.25 to 12 MeV in energy groups increasing from 0.25 to 1 MeV width with increasing neutron energy. Uncertainties of the evaluated cross sections were calculated taking into account both the uncertainties of the individual experiments and the general consistency of the data. In addition correlation matrices were derived describing the correlations between the neutron emission cross sections for the same element and different secondary neutron energies. The updated evaluation results confirm essentially the old ones, but have become more reliable due to the improved experimental data base.

## 1. Introduction

Secondary neutron emission spectra resulting from the interaction of 14 MeV neutrons with nuclei have been widely used as experimental data base for evaluations based on nuclear model calculations. These evaluations, especially for the creation of evaluated data files for fusion reactor design, have mostly been performed in the form of calculations based on the statistical model, considering in addition precompound emission and direct reactions. The model parameters were thereby adjusted to give an optimum overall fit to the existing experimental data. In such evaluation processes the comparison with secondary neutron emission spectra at 14 MeV incident neutron energy has been used to determine the relative magnitudes of preequilibrium and equilibrium particle emission.

As the entire experimental data base was not easily accessible, many evaluators used a rather arbitrarily chosen subset of the existing experimental data for comparison with the results of their model calculations. To improve this situation it was the goal of the evaluation program at IRK to provide a single recommended set of evaluated neutron emission cross sections including uncertainty information for each of the elements studied. This work lead to a report published 1988 [1] which contains evaluated energy differential cross sections for the elements Cr, Fe, Ni, Cu, Nb, Mo, Ta, W, Pb and Bi. This evaluated data set combines the information of all existing measurements available to us in the year 1987.

In the meantime a number of high-quality measurements of neutron emission cross sections was performed in the course of this CRP, therefore the evaluation of 1988 was updated with consideration of the recent experimental data, which were available for the elements Cr, Fe, Ni, Nb, Mo, Ta, W, and Bi.

## 2. Evaluation Method

### 2.1. Preparation of the Evaluation Input

The evaluations are performed in a way very similar to that one originally developed for the evaluation of neutron dosimetry cross sections [2,3]. According to the different nature of neutron emission cross sections from activation cross sections the preprocessing of the data, that is the preparation of the input for the actual evaluation process has to be performed in a way different from the procedures described in Refs. 2 and 3. As full details are given in Ref. 1, we will give only a brief description in this paper.

For this evaluation a nominal incident neutron energy of 14.1 MeV was chosen and the secondary neutron energy range was for practical reasons restricted to E' = 0.25 MeV to E' = 12 MeV. In principle it would be desirable to have an evaluation over the whole secondary neutron energy range 0 to 14 MeV. But the lack of reliable experimental data for low secondary neutron energies resulted in the lower limit of E' = 0.25 MeV. Above E' = 12 MeV, that is below an excitation energy of 2 MeV in the residual nucleus, the concept of energy differential continuum cross sections becomes less meaningful due to inelastic scattering to a small number of discrete levels.

The experimental data base has become available from publications, data files, and by direct communications with experimentalists in the form of double differential cross sections or angle-integrated cross sections, either in the laboratory system or in the center-of-mass system. The data base was restricted to experiments in the "14 MeV range", that means to experiments with incident neutron energies between 13.5 to 14.8 MeV. Further more, some experiments used techniques, where the incident neutron energy was dependent on the scattering angle.

As the goal of this evaluation was to provide a recommended set of angle-integrated neutron emission cross sections in the center-of-mass system, a number of processing steps had to be performed prior to the numerical evaluation procedure.

The following steps were applied to double differential cross section data, if necessary:

Transformation of the cross sections to the center-of-mass system.
Correction of the cross sections to the nominal incident neutron energy of 14.1 MeV.
Estimation of correction factors for multiple scattering.
Integrations of the double differential cross sections by fitting Legendre polynomials to the data.

For a few data sets published already as angle-integrated cross sections, corrections had to be applied, if the integration was performed in the laboratory system, or if the incident neutron energy was different from 14.1 MeV. For the available data sets both corrections were found to be important only for the elements Cr, Fe, and Ni in the range E' = 0.25 to 2.5 MeV (see Ref. 1 for details).

Some data sets were in addition renormalized due to changes in standards used, e.g. the shape of the $^{252}Cf$ spontaneous fission neutron spectrum employed for the determination of the neutron detector efficiency.

One of the most important facts within the evaluation process is to determine the relative weights to be given to the various data. As the weight factor is given in the usual way by $1/\sigma^2$, effective $1\sigma$ uncertainties of all experimental data points have to be

estimated as accurate as possible. The uncertainties given for the majority of the experimental data were statistical uncertainties only, and systematic uncertainties had to be added quadratically. The systematic uncertainties were taken from the error analyses of the experimentalists, if available. Otherwise they were estimated by the evaluators according to the experimental details reported. In addition an uncertainty of the secondary energy E' stemming from uncertainties in the time-of-flight measurements was estimated for each data point.

Examples for the evaluation input, that are the cross sections and their uncertainties from all experiments, processed, partially corrected and renormalized as described above, are shown in Figures 1 to 3 for the elements Fe, Ni, and Ta.

### 2.2. Evaluation Procedure

The evaluation itself was performed using the methods and procedures described in Refs. 2 and 3. Essentially the evaluation process contains the following steps:

1) The neutron energy range (0.25 to 12 MeV) is divided into a suitable group structure to calculate evaluated group cross sections. The group structure should be compatible with the energy resolutions of the experiments. Also every experiment covering the energy range $E'_1$ to $E'_2$ should be represented by at least one point within $E_1$ and $E_2$. Therefore a rather coarse group structure compared to the resolution of some recent high-resolution experiments had to be chosen.

2) Preliminary evaluated cross sections are calculated as weighted average from all input data within one group. If several data points from one experiment are within one energy group it is assumed that they are completely correlated. Therefore prior to the averaging process mentioned above all cross section data from one experiment within each group are combined to one cross section value by calculating the average cross section and the linear mean uncertainty.

3) The slope of that preliminary evaluated cross section curve is used to transform for each input data point the uncertainty in the energy scale into an uncertainty of the cross section, which is combined quadratically with the original uncertainty of the cross section to a total uncertainty.

4) As cross section changes of about 10 to 20% have to be admitted within each group, all input cross section values have to be renormalized to the energy of the group center. This is also done using the slope of the preliminary cross section curve.

5) The final evaluated group cross sections are calculated as weighted average of the renormalized cross sections. The inverse squares of the total uncertainties are used as statistical weight. If several data points from one experiment are within one energy group, they are again assumed to be completely correlated and processed in the same way as during step 2.

6) Both the external uncertainty (derived from the scatter of the data) and the internal uncertainty (derived from the uncertainties of the data points according to error propagation) of the weighted average are calculated. The larger of them is then assigned as $1\sigma$ uncertainty of the evaluated group cross section.

7) In addition approximate values of relative correlation coefficients and covariances are calculated according to the procedure described in Refs. 2 and 3. It is assumed that the data from different experiments are completely uncorrelated. The correlation amongst the data from one experiment for the same element is described by an average correlation

coefficient. The covariances and therefrom the relative correlation coefficients of the evaluated neutron emission cross sections are then calculated for each element from this average correlation coefficients and the uncertainties of the evaluation input by employing the (generalized) rules of error propagation.

## 3. New Data Received in the Course of this CRP

Until the end of 1991, the deadline for this evaluation work, we had received experimental results from the participating laboratories TU Dresden, Osaka University, Tohoku University, FEI Obninsk, and Chiang Mai University. Later we got additional data from FEI Obninsk for the element iron and preliminary results for niobium from IAE Beijing. The additional data from FEI were also included in the present evaluation; the data from IAE are preliminary and not yet corrected for flux attenuation, multiple scattering and finite geometry, and could therefore not be considered. A summary of the new data sets is given in Table 1. The measurements from TU Dresden and Osaka University were assumed to be continuations (with different elements) of the experiments *Elfruth 86* and *Takahashi 86* already included in our data base.

**Table 1:** Summary of the new data

| Experiment | Laboratory | Elements | Type of data | Energy [MeV] | |
|---|---|---|---|---|---|
| *Elfruth 86* | TU Dresden | Ta, W | EDX | 14.1 | |
| *Takahashi 86* | Osaka Univ. | Cr, Fe, Ni, Nb, Mo, Ta, W, Bi | EDX | 14.1 | W and Bi data rejected |
| *Baba 88* | Tohoku Univ. | Cr, Fe, Ni, Nb, Ta, Bi | EDX | 14.1 | |
| *Simakov 91* | FEI Obninsk | W, Bi<br>Fe | EDX<br>DDX | 14.1<br>13.5 - 14.8 | dependent on scattering angle |
| *Vilaithong 91* | Chiang Mai Univ. | Fe | DDX | 14.1 | |

The following procedure was applied to the double differential cross sections from *Simakov 91* and *Vilaithong 91* (for further details see Ref. 1, Appendix 1):

For each scattering angle the cross section values as well as the secondary neutron energy group limits were transformed to the center-of-mass system using relativistic reaction kinematics. In the next step the data sets from *Simakov 91,* for four of the five scattering angles measured, had to be corrected for the incident neutron energies being different from the nominal energy of 14.1 MeV. Only for high secondary neutron energies (E' > 9 MeV) corrections were applied. In this energy range the secondary neutron spectrum is determined by inelastic scattering to discrete levels and the neutron energies corresponding to the excitation of this levels have a constant energy difference to the incident neutron energy. Thus the discrete level part is simply shifted, if one compares neutron emission spectra for different incident neutron energies. The correction was done

by changing the group widths in the rather flat part of the spectrum (in the energy region between 7 MeV and 9 MeV), while leaving the double differential cross section values unchanged. Thus the flat part of the spectrum was expanded or contracted, respectively, and the part with energies above 9 MeV was shifted. For low secondary neutron energies (E' around 1 MeV) double differential neutron emission cross sections for Fe depend significantly from the incident neutron energy due to the gradient of the (n,2n) cross section curve in the 14 MeV range. As for the experiment of *Simakov 91* the incident neutron energy averaged over all scattering angles measured is 14.1 MeV, the influence of this energy dependency on the angle-integrated cross sections is small and could be neglected.

For both experiments, *Simakov 91* and *Vilaithong 91* then a new unified group structure was established and for each of this groups the angle-integrated cross section was obtained by fitting Legendre polynomials to the data.

A careful examination of all angle-integrated cross section data lead to the following rejections of data and restrictions of the accepted neutron energy range:

The data of *Takahashi 86* for W and Bi showed large deviations from all other data in the energy region around E' = 8 MeV. A comparison of the raw data of this experiment and the data corrected for finite sample size effects and the effective spectrum of the neutron source showed unrealistic correction factors. As the calculation of the correction factors for W and Bi was based on data from the libraries ENDF/B-IV and ENDL-86, respectively, whereas for the other elements the evaluated data library JENDL-3 was used, the deviations for W and Bi probably stem from the input data for the correction procedure. The cross sections for W and Bi from *Takahashi 86* were therefore not included into the data base.

The cross sections for Cr and Ni from the work of *Baba 88* are clearly to high for secondary neutron energies below 2 MeV, due to problems with the detector efficiency for low energies [4]. Therefore the accepted secondary energy range was restricted to E' = 2 to 12 MeV for these two elements.

The data point for Bi at E' = 0.4 MeV reported by *Simakov 91* showed an unrealistic low value, probably also due to detector threshold problems. So the accepted energy range was restricted to E' = 0.5 to 12 MeV for this data set.

**Table 2:** Secondary neutron energy range and systematic uncertainties

| Experiment | Elements | Secondary neutron Energy range | Systematic uncertainty added quadratically |
|---|---|---|---|
| *Elfruth 86* | Ta, W | 1.5 - 12.0 MeV | 7.5 % |
| *Takahashi 86* | Cr, Fe, Ni, Nb, Mo, Ta | 1.0 - 12.0 MeV | 4.6 - 6.8 % [a] |
| *Baba 88* | Cr, Ni | 1.9 - 12.0 MeV[b] | included |
| | Fe, Nb, Ta, Bi | 0.9 - 12.0 MeV | |
| *Simakov 91* | Fe | 0.25 -12.0 MeV | 6 % |
| | W | 0.7 - 12.0 MeV[b] | 7 % |
| | Bi | 0.5 - 12.0 MeV | 6 % |
| *Vilaithong 91* | Fe | 2.25 -12.0 MeV | 6 % |

[a] Dependent on E', according to uncertainty analysis of the author.
[b] Secondary neutron energy range restricted by the evaluators.

Systematic uncertainties as given in Table 2 were added quadratically, if not already included in the uncertainties reported. For the data set given by *Vilaithong 91* a systematic uncertainty of 6% was estimated by the evaluators, for the other experiments systematic uncertainties reported by the experimentalists were used.

The uncertainties in the secondary neutron energy scale were estimated according to the procedure given in Ref. 1. No further corrections or renormalizations seemed to be necessary for any of the new data sets.

## 4. Results and Discussions

With the recently measured cross sections the data base has been clearly improved. For Ni in the energy range E' > 7 MeV the results of *Takahashi 83*, which do not agree with the values of *Hermsdorf 74* are now confirmed by two further measurements as shown in Figure 2. For the element Mo the energy range E' > 6 MeV now is covered by two measurements (*Takahashi 83* and *Takahashi 86*) which can be considered as independent experiments as different experimental set-ups were used. Neutron emission cross section for the entire range up to 12 MeV now exist for Ta. There are, however, discrepancies between the results given by *Elfruth 86* and the results of *Takahashi 86* and *Baba 88*, respectively, as seen in Figure 3. Significant improvements of the data base also appear for W and Bi.

For the majority of the elements studied, the secondary neutron energy range E' = 0.25 MeV to 1 MeV is still covered by only one experiment (*Vonach 80*). Though this experiment was dedicated to the measurement of neutron emission cross sections for low secondary neutron energies, a check by an independent experiment would be desirable.

The evaluation itself was performed using the procedure described in Section 2.2. The evaluated neutron emission cross sections and their uncertainties are given in Tables 3 to 10. The new evaluation results confirm essentially the old ones. Due to the improved data base the evaluation has become more reliable and the uncertainty limits could be decreased. As an example the evaluated cross sections for Fe compared to the results of Ref. 1 are given in Figure 4.

Covariances and correlations matrices were calculated using the estimated average correlation coefficients as given in Table 11 for the new data sets and in Ref. 1 for the old ones. As an example for a correlation matrix the correlation coefficients for the evaluated cross sections for Fe are given in Table 12. The correlation matrices for the other elements are obtainable from the authors on request.

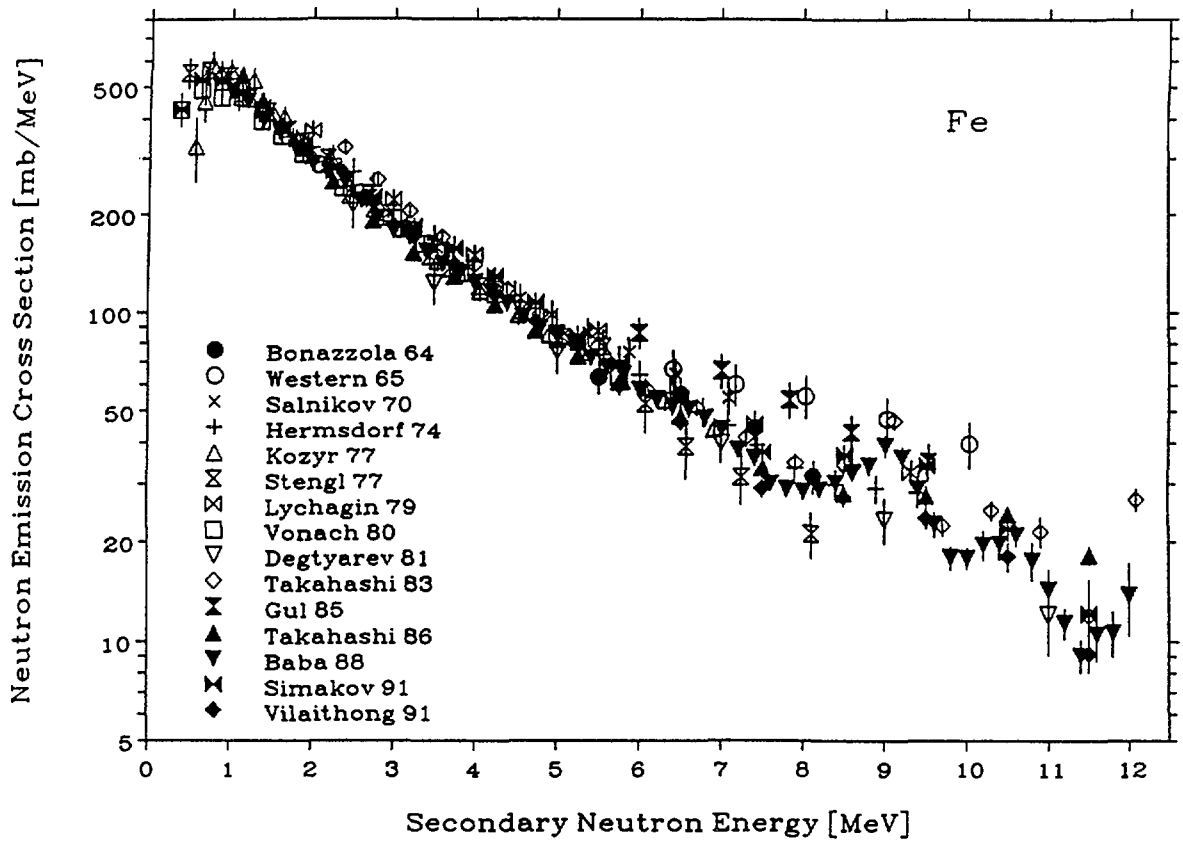


**Figure 1:** The experimental data base for the element Fe

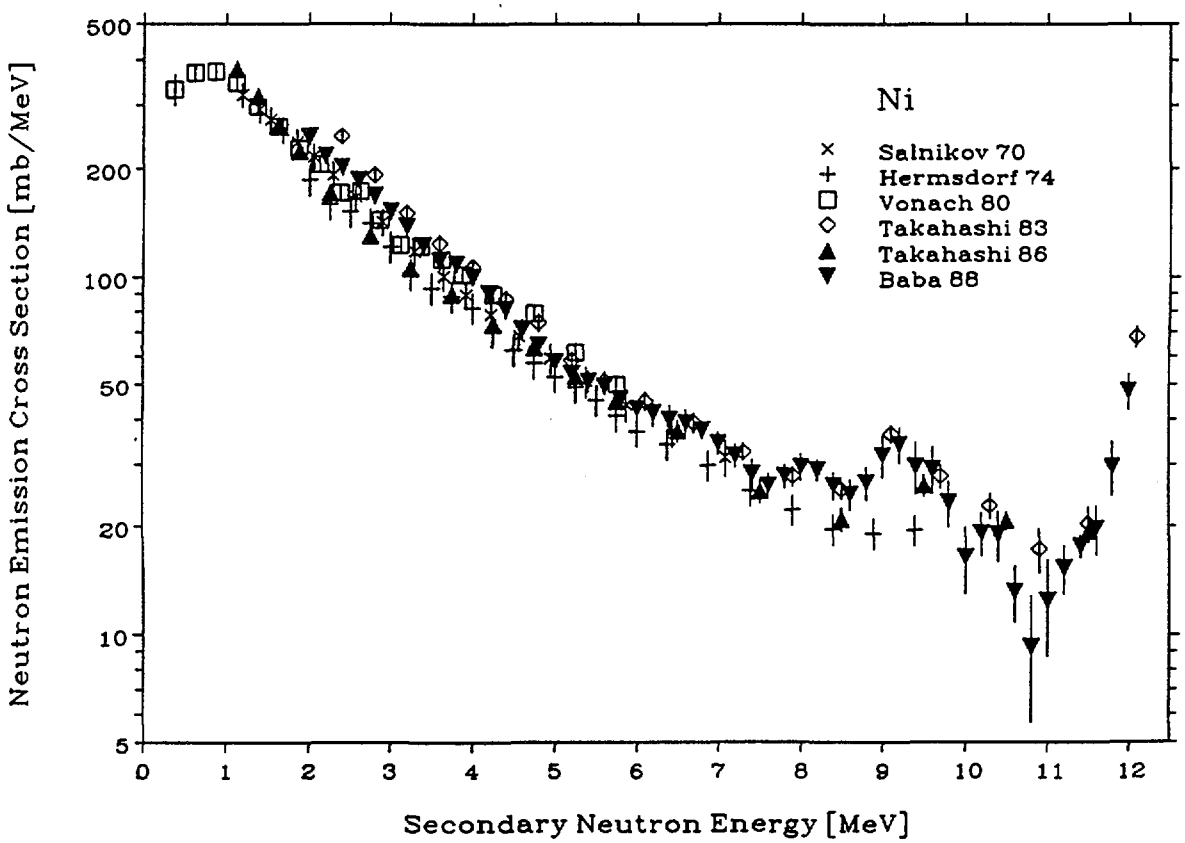


**Figure 2:** The experimental data base for the element Ni

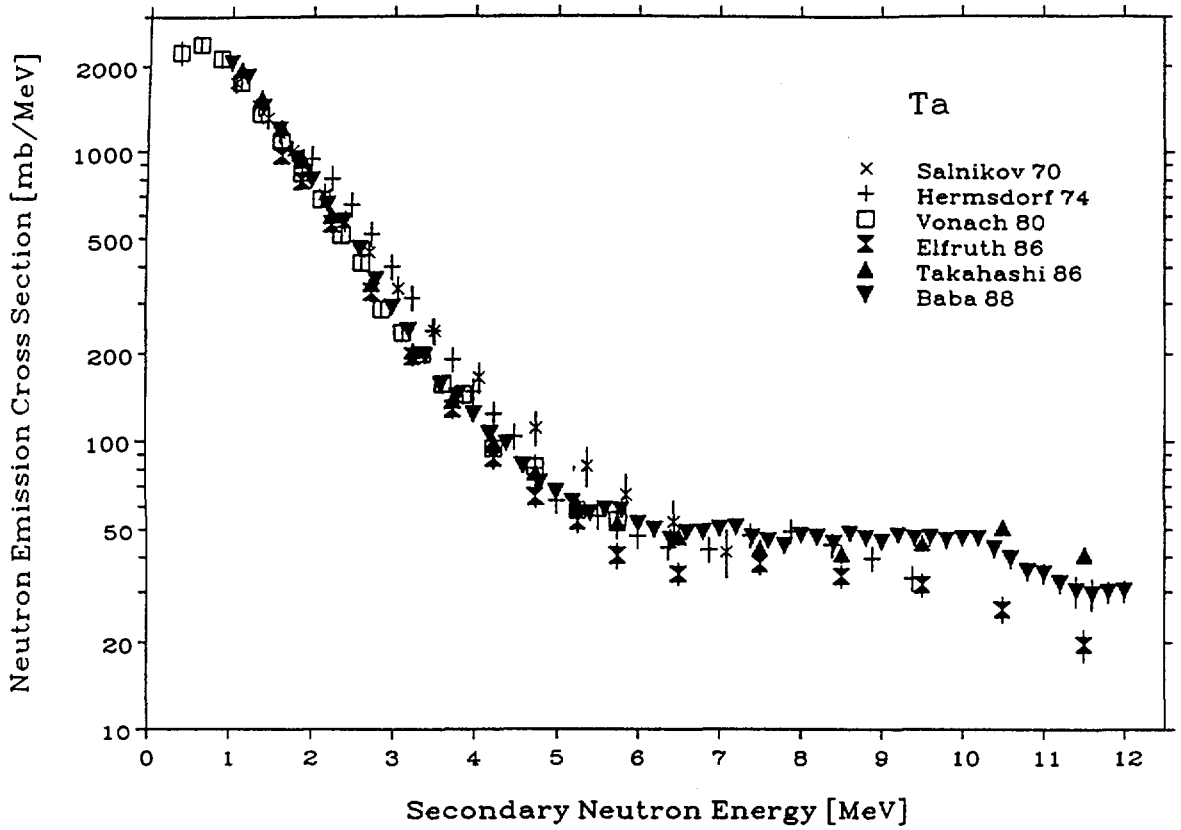


**Figure 3:** The experimental data base for the element Ta

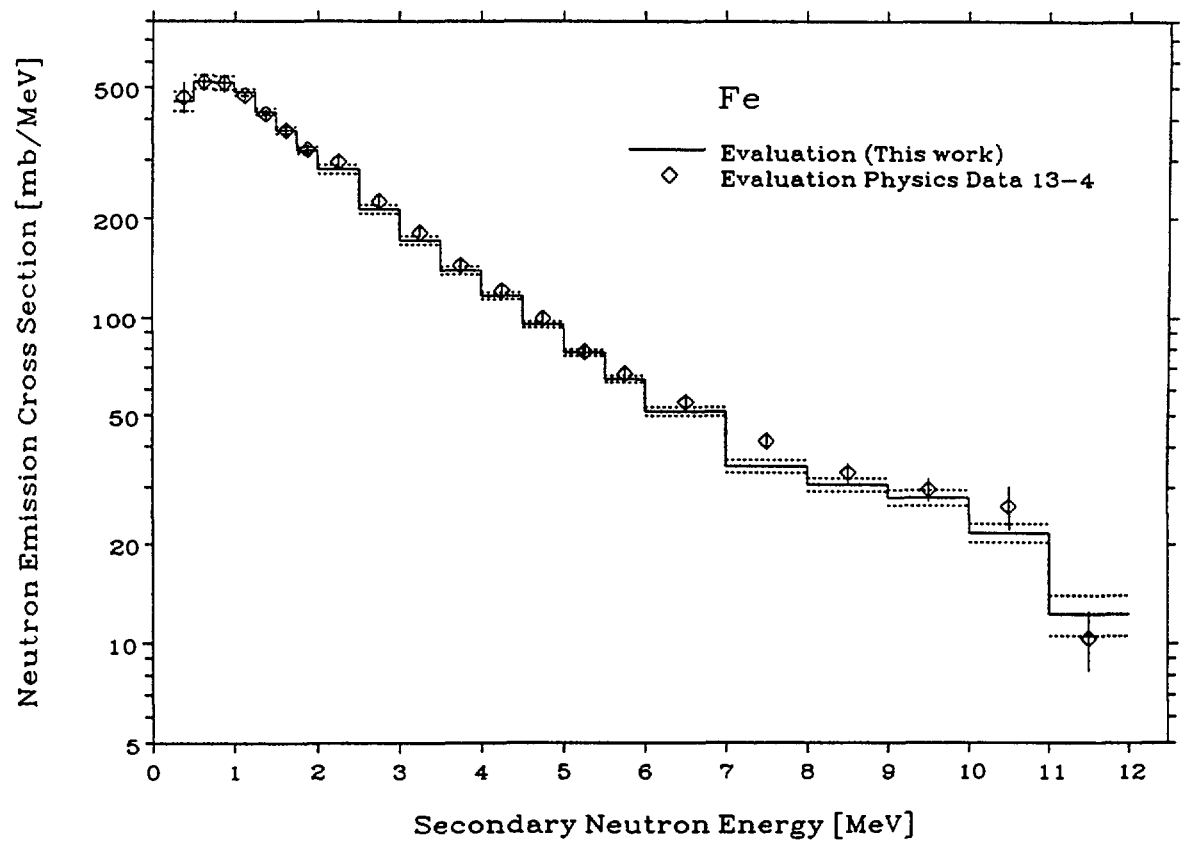


**Figure 4:** The evaluated neutron emission cross sections for Fe compared to the results of Ref. 1

**Table 3:** Evaluated neutron emission cross sections for the element Cr for E = 14.1 MeV

| Secondary neutron energy range [MeV] | Neutron emission cross section [mb/MeV] |
|---|---|
| 0.25 - 0.50 | 432.4 ± 43.2 |
| 0.50 - 0.75 | 447.8 ± 21.7 |
| 0.75 - 1.00 | 428.5 ± 21.3 |
| 1.00 - 1.25 | 436.4 ± 21.4 |
| 1.25 - 1.50 | 372.7 ± 12.5 |
| 1.50 - 1.75 | 333.8 ± 10.9 |
| 1.75 - 2.00 | 299.5 ± 10.4 |
| 2.00 - 2.50 | 286.0 ± 18.9 |
| 2.50 - 3.00 | 224.4 ± 14.7 |
| 3.00 - 3.50 | 176.4 ± 10.7 |
| 3.50 - 4.00 | 143.6 ± 7.0 |
| 4.00 - 4.50 | 115.4 ± 5.1 |
| 4.50 - 5.00 | 96.0 ± 4.1 |
| 5.00 - 5.50 | 75.4 ± 4.2 |
| 5.50 - 6.00 | 61.9 ± 3.4 |
| 6.00 - 7.00 | 52.4 ± 2.4 |
| 7.00 - 8.00 | 35.0 ± 2.8 |
| 8.00 - 9.00 | 25.3 ± 1.5 |
| 9.00 - 10.00 | 26.9 ± 1.2 |
| 10.00 - 11.00 | 19.9 ± 0.9 |
| 11.00 - 12.00 | 24.4 ± 2.8 |

**Table 4:** Evaluated neutron emission cross sections for the element Fe for E = 14.1 MeV

| Secondary neutron energy range [MeV] | Neutron emission cross section [mb/MeV] |
|---|---|
| 0.25 - 0.50 | 453.6 ± 30.7 |
| 0.50 - 0.75 | 521.1 ± 24.8 |
| 0.75 - 1.00 | 516.0 ± 24.8 |
| 1.00 - 1.25 | 483.6 ± 11.3 |
| 1.25 - 1.50 | 421.8 ± 10.1 |
| 1.50 - 1.75 | 370.1 ± 8.7 |
| 1.75 - 2.00 | 321.3 ± 7.4 |
| 2.00 - 2.50 | 281.9 ± 9.1 |
| 2.50 - 3.00 | 213.2 ± 6.6 |
| 3.00 - 3.50 | 172.0 ± 4.8 |
| 3.50 - 4.00 | 139.3 ± 3.9 |
| 4.00 - 4.50 | 116.7 ± 2.8 |
| 4.50 - 5.00 | 95.3 ± 2.1 |
| 5.00 - 5.50 | 77.9 ± 1.7 |
| 5.50 - 6.00 | 64.7 ± 1.5 |
| 6.00 - 7.00 | 51.5 ± 1.5 |
| 7.00 - 8.00 | 34.9 ± 1.6 |
| 8.00 - 9.00 | 30.6 ± 1.5 |
| 9.00 - 10.00 | 27.9 ± 1.5 |
| 10.00 - 11.00 | 21.7 ± 1.5 |
| 11.00 - 12.00 | 12.2 ± 1.7 |

**Table 5:** Evaluated neutron emission cross sections for the element Ni for E = 14.1 MeV

| Secondary neutron energy range [MeV] | Neutron emission cross section [mb/MeV] |
|---|---|
| 0.25 - 0.50 | 331.8 ± 33.2 |
| 0.50 - 0.75 | 368.5 ± 15.8 |
| 0.75 - 1.00 | 371.7 ± 16.0 |
| 1.00 - 1.25 | 352.8 ± 11.6 |
| 1.25 - 1.50 | 302.9 ± 9.6 |
| 1.50 - 1.75 | 261.8 ± 8.1 |
| 1.75 - 2.00 | 227.0 ± 7.1 |
| 2.00 - 2.50 | 196.5 ± 13.3 |
| 2.50 - 3.00 | 155.8 ± 10.0 |
| 3.00 - 3.50 | 121.2 ± 6.7 |
| 3.50 - 4.00 | 101.0 ± 4.9 |
| 4.00 - 4.50 | 83.1 ± 3.8 |
| 4.50 - 5.00 | 68.1 ± 3.1 |
| 5.00 - 5.50 | 54.7 ± 1.7 |
| 5.50 - 6.00 | 46.6 ± 1.4 |
| 6.00 - 7.00 | 37.7 ± 1.4 |
| 7.00 - 8.00 | 27.2 ± 1.2 |
| 8.00 - 9.00 | 22.7 ± 1.7 |
| 9.00 - 10.00 | 24.3 ± 2.8 |
| 10.00 - 11.00 | 19.9 ± 1.3 |
| 11.00 - 12.00 | 19.3 ± 1.1 |

**Table 6:** Evaluated neutron emission cross sections for the element Nb for E = 14.1 MeV

| Secondary neutron energy range [MeV] | Neutron emission cross section [mb/MeV] |
|---|---|
| 0.25 - 0.50 | 1277.0 ± 72.2 |
| 0.50 - 0.75 | 1316.0 ± 46.7 |
| 0.75 - 1.00 | 1331.0 ± 55.0 |
| 1.00 - 1.25 | 1120.0 ± 36.9 |
| 1.25 - 1.50 | 963.0 ± 27.0 |
| 1.50 - 1.75 | 825.4 ± 17.4 |
| 1.75 - 2.00 | 696.7 ± 17.3 |
| 2.00 - 2.50 | 514.6 ± 11.0 |
| 2.50 - 3.00 | 355.7 ± 9.2 |
| 3.00 - 3.50 | 237.2 ± 6.6 |
| 3.50 - 4.00 | 171.7 ± 5.0 |
| 4.00 - 4.50 | 121.5 ± 3.2 |
| 4.50 - 5.00 | 93.5 ± 2.6 |
| 5.00 - 5.50 | 72.4 ± 2.2 |
| 5.50 - 6.00 | 58.7 ± 1.5 |
| 6.00 - 7.00 | 46.9 ± 1.4 |
| 7.00 - 8.00 | 34.6 ± 1.1 |
| 8.00 - 9.00 | 25.6 ± 1.3 |
| 9.00 - 10.00 | 22.4 ± 1.6 |
| 10.00 - 11.00 | 28.4 ± 1.4 |
| 11.00 - 12.00 | 46.9 ± 3.4 |

**Table 7:** Evaluated neutron emission cross sections for the element Mo for E = 14.1 MeV

| Secondary neutron energy range [MeV] | Neutron emission cross section [mb/MeV] |
|---|---|
| 0.25 - 0.50 | 1233.0 ± 123.3 |
| 0.50 - 0.75 | 1383.0 ± 62.0 |
| 0.75 - 1.00 | 1211.0 ± 56.5 |
| 1.00 - 1.25 | 1059.0 ± 39.4 |
| 1.25 - 1.50 | 852.2 ± 28.8 |
| 1.50 - 1.75 | 706.5 ± 23.4 |
| 1.75 - 2.00 | 576.2 ± 19.3 |
| 2.00 - 2.50 | 462.3 ± 29.6 |
| 2.50 - 3.00 | 316.9 ± 15.1 |
| 3.00 - 3.50 | 214.2 ± 7.0 |
| 3.50 - 4.00 | 152.3 ± 5.1 |
| 4.00 - 4.50 | 113.7 ± 3.9 |
| 4.50 - 5.00 | 85.9 ± 3.4 |
| 5.00 - 5.50 | 68.4 ± 2.8 |
| 5.50 - 6.00 | 54.5 ± 2.6 |
| 6.00 - 7.00 | 44.6 ± 2.3 |
| 7.00 - 8.00 | 34.5 ± 2.1 |
| 8.00 - 9.00 | 26.8 ± 2.8 |
| 9.00 - 10.00 | 28.3 ± 2.1 |
| 10.00 - 11.00 | 39.6 ± 1.9 |
| 11.00 - 12.00 | 62.9 ± 2.8 |

**Table 8:** Evaluated neutron emission cross sections for the element Ta for E = 14.1 MeV

| Secondary neutron energy range [MeV] | Neutron emission cross section [mb/MeV] |
|---|---|
| 0.25 - 0.50 | 2239.0 ± 223.9 |
| 0.50 - 0.75 | 2396.0 ± 120.5 |
| 0.75 - 1.00 | 2132.0 ± 110.4 |
| 1.00 - 1.25 | 1834.0 ± 64.0 |
| 1.25 - 1.50 | 1448.0 ± 42.1 |
| 1.50 - 1.75 | 1117.0 ± 40.0 |
| 1.75 - 2.00 | 870.8 ± 24.0 |
| 2.00 - 2.50 | 612.5 ± 19.0 |
| 2.50 - 3.00 | 365.3 ± 18.3 |
| 3.00 - 3.50 | 216.7 ± 11.6 |
| 3.50 - 4.00 | 143.2 ± 7.3 |
| 4.00 - 4.50 | 100.0 ± 5.0 |
| 4.50 - 5.00 | 76.0 ± 3.7 |
| 5.00 - 5.50 | 59.0 ± 2.1 |
| 5.50 - 6.00 | 51.8 ± 2.8 |
| 6.00 - 7.00 | 43.3 ± 2.8 |
| 7.00 - 8.00 | 43.7 ± 2.0 |
| 8.00 - 9.00 | 40.8 ± 2.6 |
| 9.00 - 10.00 | 38.9 ± 3.7 |
| 10.00 - 11.00 | 40.5 ± 7.3 |
| 11.00 - 12.00 | 31.5 ± 6.4 |

**Table 9:** Evaluated neutron emission cross sections for the element W for E = 14.1 MeV

| Secondary neutron energy range [MeV] | Neutron emission cross section [mb/MeV] |
|---|---|
| 0.25 - 0.50 | 2210.0 ± 221.0 |
| 0.50 - 0.75 | 2445.0 ± 112.2 |
| 0.75 - 1.00 | 2326.0 ± 91.6 |
| 1.00 - 1.25 | 1907.0 ± 100.0 |
| 1.25 - 1.50 | 1536.0 ± 107.3 |
| 1.50 - 1.75 | 1236.0 ± 64.5 |
| 1.75 - 2.00 | 948.9 ± 40.3 |
| 2.00 - 2.50 | 599.5 ± 36.5 |
| 2.50 - 3.00 | 352.2 ± 18.8 |
| 3.00 - 3.50 | 218.6 ± 10.7 |
| 3.50 - 4.00 | 142.8 ± 7.7 |
| 4.00 - 4.50 | 99.2 ± 6.1 |
| 4.50 - 5.00 | 75.3 ± 5.0 |
| 5.00 - 5.50 | 59.8 ± 2.8 |
| 5.50 - 6.00 | 51.0 ± 3.5 |
| 6.00 - 7.00 | 43.2 ± 3.7 |
| 7.00 - 8.00 | 39.3 ± 3.9 |
| 8.00 - 9.00 | 38.5 ± 3.5 |
| 9.00 - 10.00 | 39.7 ± 3.1 |
| 10.00 - 11.00 | 36.7 ± 2.0 |
| 11.00 - 12.00 | 30.9 ± 2.5 |

**Table 10:** Evaluated neutron emission cross sections for the element Bi for E = 14.1 MeV

| Secondary neutron energy range [MeV] | Neutron emission cross section [mb/MeV] |
|---|---|
| 0.25 - 0.50 | 1770.0 ± 177.0 |
| 0.50 - 0.75 | 1843.0 ± 64.8 |
| 0.75 - 1.00 | 1893.0 ± 69.7 |
| 1.00 - 1.25 | 1854.0 ± 78.8 |
| 1.25 - 1.50 | 1720.0 ± 57.0 |
| 1.50 - 1.75 | 1567.0 ± 49.0 |
| 1.75 - 2.00 | 1396.0 ± 63.4 |
| 2.00 - 2.50 | 1057.0 ± 58.2 |
| 2.50 - 3.00 | 724.1 ± 31.3 |
| 3.00 - 3.50 | 457.9 ± 15.8 |
| 3.50 - 4.00 | 311.2 ± 10.3 |
| 4.00 - 4.50 | 208.9 ± 7.1 |
| 4.50 - 5.00 | 150.5 ± 5.4 |
| 5.00 - 5.50 | 104.2 ± 3.9 |
| 5.50 - 6.00 | 79.6 ± 3.2 |
| 6.00 - 7.00 | 59.8 ± 2.7 |
| 7.00 - 8.00 | 56.1 ± 3.6 |
| 8.00 - 9.00 | 63.7 ± 4.3 |
| 9.00 - 10.00 | 61.6 ± 3.3 |
| 10.00 - 11.00 | 39.3 ± 5.4 |
| 11.00 - 12.00 | 46.9 ± 3.1 |

**Table 11:** The average correlation coefficients $B_{nnk}$ estimated to calculate covariances of the evaluated results

| Experiment | $B_{nnk}$ |
|---|---|
| *Elfruth 86* | 0.65 |
| *Takahashi 86* | 0.60 |
| *Baba 88* | 0.65 |
| *Simakov 91* | 0.60 |
| *Vilaithong 91* | 0.70 |

**Table 12:** Correlation matrix for the evaluated neutron emission cross sections for the Element Fe. Correlations are given in %

| Group number | 1 | 2 | 3 | 4 | 5 | 6 | 7 | 8 | 9 | 10 | 11 | 12 | 13 | 14 | 15 | 16 | 17 | 18 | 19 | 20 | 21 | Group energy [MeV] |
|---|---|---|---|---|---|---|---|---|---|---|---|---|---|---|---|---|---|---|---|---|---|---|
| 1 | 100 | 56 | 55 | 40 | 41 | 39 | 39 | 31 | 28 | 27 | 26 | 26 | 25 | 24 | 23 | 14 | 13 | 13 | 13 | 14 | 7 | 0.25 - 0.50 |
| 2 | | 100 | 60 | 44 | 43 | 40 | 42 | 31 | 29 | 27 | 27 | 26 | 25 | 23 | 22 | 12 | 8 | 9 | 7 | 8 | 3 | 0.50 - 0.75 |
| 3 | | | 100 | 45 | 44 | 42 | 43 | 33 | 30 | 29 | 28 | 28 | 27 | 25 | 24 | 14 | 9 | 10 | 8 | 9 | 4 | 0.75 - 1.00 |
| 4 | | | | 100 | 62 | 61 | 62 | 51 | 51 | 49 | 49 | 48 | 48 | 46 | 43 | 36 | 31 | 30 | 24 | 32 | 28 | 1.00 - 1.25 |
| 5 | | | | | 100 | 62 | 62 | 52 | 51 | 50 | 50 | 48 | 49 | 47 | 44 | 37 | 33 | 31 | 26 | 34 | 29 | 1.25 - 1.50 |
| 6 | | | | | | 100 | 62 | 52 | 52 | 51 | 51 | 49 | 50 | 48 | 45 | 38 | 34 | 32 | 27 | 36 | 31 | 1.50 - 1.75 |
| 7 | | | | | | | 100 | 52 | 52 | 50 | 50 | 49 | 50 | 47 | 45 | 38 | 33 | 32 | 26 | 35 | 30 | 1.75 - 2.00 |
| 8 | | | | | | | | 100 | 60 | 62 | 59 | 62 | 60 | 58 | 60 | 53 | 52 | 49 | 46 | 48 | 46 | 2.00 - 2.50 |
| 9 | | | | | | | | | 100 | 60 | 63 | 60 | 62 | 61 | 58 | 55 | 52 | 50 | 46 | 50 | 51 | 2.50 - 3.00 |
| 10 | | | | | | | | | | 100 | 59 | 62 | 60 | 58 | 60 | 54 | 53 | 50 | 47 | 49 | 47 | 3.00 - 3.50 |
| 11 | | | | | | | | | | | 100 | 59 | 61 | 62 | 58 | 55 | 53 | 51 | 47 | 50 | 52 | 3.50 - 4.00 |
| 12 | | | | | | | | | | | | 100 | 61 | 59 | 60 | 55 | 53 | 50 | 47 | 50 | 48 | 4.00 - 4.50 |
| 13 | | | | | | | | | | | | | 100 | 61 | 59 | 57 | 53 | 53 | 45 | 53 | 51 | 4.50 - 5.00 |
| 14 | | | | | | | | | | | | | | 100 | 57 | 57 | 55 | 54 | 49 | 51 | 53 | 5.00 - 5.50 |
| 15 | | | | | | | | | | | | | | | 100 | 58 | 56 | 55 | 49 | 51 | 49 | 5.50 - 6.00 |
| 16 | | | | | | | | | | | | | | | | 100 | 58 | 60 | 50 | 55 | 52 | 6.00 - 7.00 |
| 17 | | | | | | | | | | | | | | | | | 100 | 59 | 58 | 55 | 56 | 7.00 - 8.00 |
| 18 | | | | | | | | | | | | | | | | | | 100 | 52 | 56 | 55 | 8.00 - 9.00 |
| 19 | | | | | | | | | | | | | | | | | | | 100 | 50 | 52 | 9.00 - 10.00 |
| 20 | | | | | | | | | | | | | | | | | | | | 100 | 58 | 10.00 - 11.00 |
| 21 | | | | | | | | | | | | | | | | | | | | | 100 | 11.00 - 12.00 |

## References


1. A. Pavlik and H. Vonach, Evaluation of the angle-integrated neutron emission cross sections from the interaction of 14 MeV neutrons with medium and heavy nuclei, Physics Data 13-4, Fachinformationszentrum Karlsruhe (1988)
2. S. Tagesen, H. Vonach and B. Strohmaier, Evaluation of the cross sections for the reactions $^{24}Mg(n,p)^{24}Na$, $^{64}Zn(n,p)^{64}Cu$, $^{63}Cu(n,2n)^{62}Cu$ and $^{90}Zr(n,2n)^{89}Zr$, Physics Data 13-1, Fachinformationszentrum Karlsruhe (1988)
3. H. Vonach and S. Tagesen, Proc. Conf. on Nuclear Data Evaluation Methods and Procedures, Brookhaven National Laboratory, 22. - 25. Sep. 1980, (Report BNL-NCS-51363), Vol. II, p. 621, BNL, Upton (1981)
4. M. Baba, Tohoku University, Sendai, Private Communication (1991)


## References of the Experimental Data Base


*Bonazzola 64*: G. C. Bonazzola et al., *Nucl. Phys.* **51**, 353 (1964)

*Western 65*: G.T. Western et al., Report WL-TR-64-140, General Dynamics, Fort Worth (1965)

*Salnikov 70*: O.A. Salnikov et al., *Yad. Fiz.* **12**, 1132 (1970), (*Sov. J. Nucl. Phys.* **12**, 620 (1970))
O.A. Salnikov et al., *Yad. Fiz.* **20**, 852 (1974), (*Sov. J. Nucl. Phys.* **20**, 454 (1975))

*Hermsdorf 74*: D. Hermsdorf et al., *Kernenergie* **17**, 176 (1974)
D. Hermsdorf et al., *Kernenergie* **17**, 259 (1974)
D. Hermsdorf et al., Report ZfK-277(Ü), Zentralinstitut für Kernforschung, Rossendorf bei Dresden (1975)
D. Seeliger, Private Communication (1984)

*Kozyr 77*: Yu. E. Kozyr and G.A. Prokopets, *Yad. Fiz.* **26**, 927 (1977), (*Sov. J. Nucl. Phys.* **26**, 489 (1977))
Yu. E. Kozyr and G.A. Prokopets, *Yad. Fiz.* **27**, 616 (1978), (*Sov. J. Nucl. Phys.* **27**, 329 (1978))

*Stengl 77*: G. Stengl, M. Uhl and H. Vonach, *Nucl. Phys.* **A290**, 109 (1977)

*Lychagin 79*: A.A. Lychagin et al., Report FEI-923, FEI, Obninsk (1979)

*Vonach 80*: H. Vonach, A. Chalupka, F. Wenninger and G. Staffel, Proc. Symp. on Neutron Cross Sections from 10 to 50 MeV, Brookhaven National Laboratory, 12. - 14. May 1980, (Report BNL-NCS-51245), Vol I, p. 343, BNL, Upton, (1980)
F. Wenniger, Thesis, University of Vienna (1980)

*Degtyarev 81*: A.P. Degtyarev et al., *Yad. Fiz.* **34**, 299 (1981), (*Sov. J. Nucl. Phys.* **34**, 169 (1981))

*Takahashi 83*: A. Takahashi et al., Report OKTAVIAN-A-83-01, Osaka University, Osaka (1983)
A. Takahashi et al., *J. Nucl. Sci. Technol.* **21**, 577 (1984)

*Gul 85*: K. Gul et al., *Phys. Rev. C* **31**, 69 (1985)
K. Gul et al., *Phys. Rev. C* **31**, 74 (1985)
K. Gul et al., Report INDC(PAK)-006, IAEA, Vienna (1986)

*Elfruth 86*: T. Elfruth et al., Report INDC(GDR)-044, IAEA, Vienna (1986)
T. Elfruth, Private Communication (1986 and 1991)
H. Al Obiesi et al., Report INDC(GDR)-058, IAEA, Vienna (1990)

*Takahashi 86*: A. Takahashi, Proc. 1985 Seminar on Nuclear Data, (Report JAERI-M-86-080), p. 190, JAERI, Tokai (1986)
A. Takahashi et. al, *J. Nucl. Sci and Technol.*, **25**, 215 (1988)
A. Takahashi, Private Communication (1987 and 1991)

*Baba 88*: M. Baba et al., Proc. Int. Conf. Nucl. Data for Science and Technology, Mito, 30. May - 5. June 1988, (S. Igarasi ed.), p. 291, Saikon Publ. Comp., Tokyo (1988)
M. Baba, Private Communication (1991)

*Simakov 91*: S.P. Simakov, Private Communication (1991)
S. P. Simakov et al., Report INDC (CCP)-315, IAEA, Vienna (1990)

*Vilaithong 91*: T. Vilaithong, Private Communication (1991)

# MEASUREMENT OF DOUBLE DIFFERENTIAL NEUTRON EMISSION CROSS SECTIONS FOR $^{238}U$ AND $^{209}Bi$ AT INCIDENT NEUTRON ENERGY OF 9.6 MeV

TANG HONGQING, QI BUJIA, ZHOU ZUYING, SA JUN, KE ZUNJIAN, ZHOU CHENWEI, XIA HAIHONG AND SHEN GUANREN

*China Institute of Atomic Energy*
*P. O. Box 275-46, Beijing 102413, P. R. China*

ABSTRACT

There are scarce measurements of secondary neutron double differential cross sections in the incident energy range 9-13 MeV upto now. A main difficulty for this is lack of an applicable monoenergetic neutron source. When monoenergetic neutron energy reaches 8 MeV, the break-up neutrons from the d+D or p+T reaction starts to become significant. It is difficult to get a pure secondary neutron spectrum induced only by monoenergetic neutrons. To solve this problem an abnormal fast neutron TOF facility was designed and tested.

Double differential neutron emission cross sections of $^{238}U$ and $^{209}Bi$ at 9.6 MeV were obtained by combining the data measured by both normal and abnormal TOF spectrometers and a good agreement between measurement and calculation was achieved.

## 1. Introduction

So far only 4 elements which are Li, Be, B and C have been measured at 10 MeV at LANL using an H(t, n) reaction neutron source[1,2]. $^{7}Li$ was also measured in Geel laboratory in the incident neutron energy bins of 9.6-11.7 and 11.7-13.8MeV[3].

Why is the measurement of double differential cross sections in this energy region so few? The difficulty comes from monoenergetic neutron source. As we know, for the conventional neutron source, like d+D and p+T reactions, when the monoenergetic neutron energy reaches 8 MeV, the break-up neutrons will occur. The ratio of the break-up neutrons to the monoenergetic ones increases with increasing of neutron energy. The break-up neutrons will interfere secondary neutron spectrum measurement. To solve this problem, a lot of efforts have been made in different laboratories [4-7]. Our method is described in the following section.

## 2. Experimental Arrangement

The normal fast neutron TOF spectrometer in CIAE is shown in Fig.1. The detailed description can be found in ref. [8].

Fig. 2 shows the incident neutron TOF spectrum of d+D reaction at the bombarding energy $E_d$ = 7.0 MeV (the monoenergetic neutron energy is about 10 MeV), measured by the normal TOF spectrometer. From the

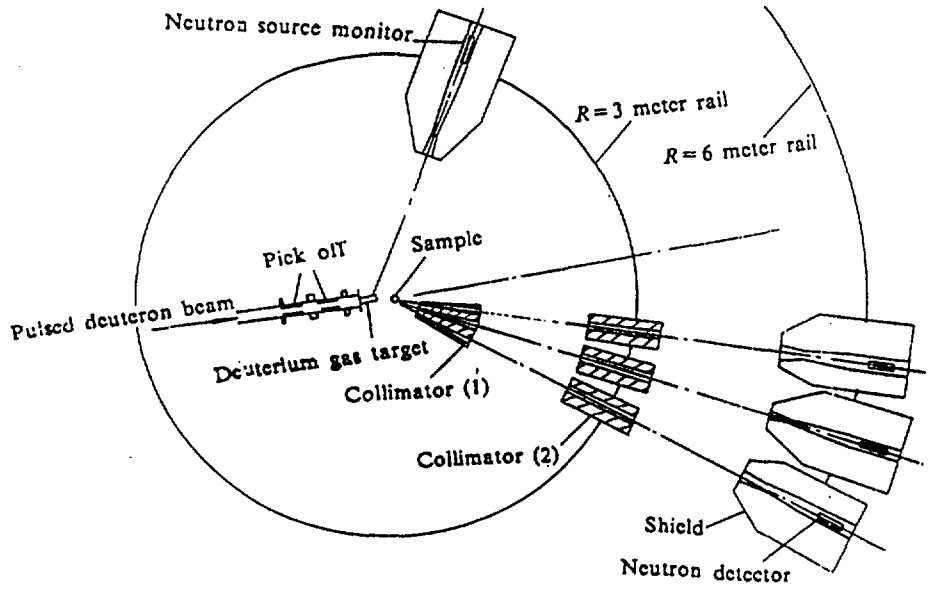


Fig. 1. Normal fast neutron TOF spectrometer

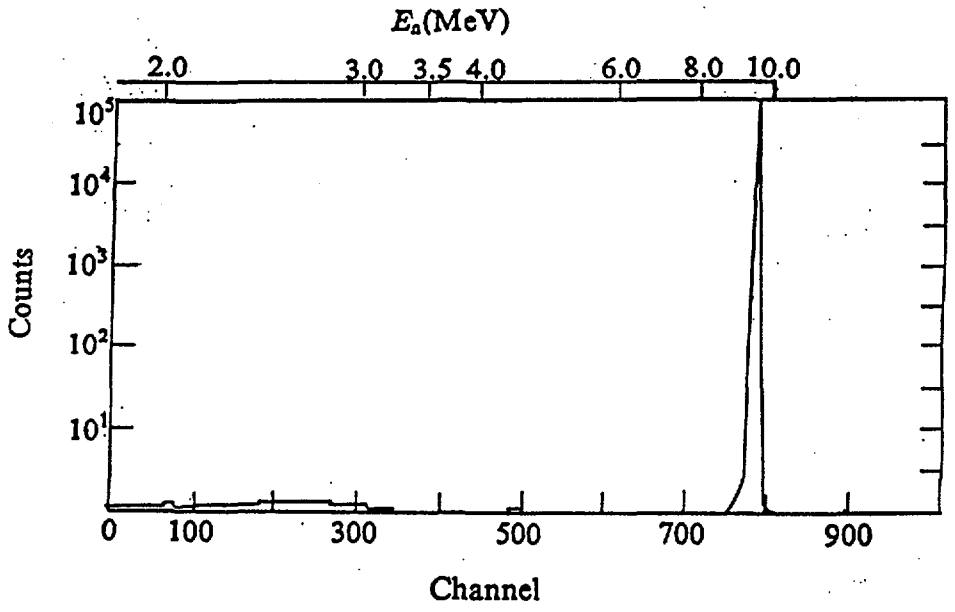


Fig. 2. TOF spectrum of the d+D reaction neutrons at 0 deg. at bombarding energy $E_d$=7.0 MeV

figure it can be seen that the break-up neutron with energy below 3.5 MeV is the major trouble for secondary neutron spectrum measurement. Because of its interference, the lower energy part below 3.5 MeV of the spectrum is contaminated, as seen in Fig. 3. It is hard to get a pure secondary neutron spectrum for 10 MeV incident monoenergetic neutrons.

To eliminate source break-up neutron interference, an unusual arrangement was made ( we call it abnormal TOF spectrometer shown in Fig.4 ). Double differential cross sections in lower energy part (En<4MeV) was obtained using this unusual geometry. The idea of our method, the abnormal fast neutron TOF spectrometer, is using such a long distance, 2.2 m instead of 20 cm in the normal geometry, between neutron source and sample that there is a big time gape between monoenergetic and break-up neutrons of the d+D reaction in the TOF spectrum measured at

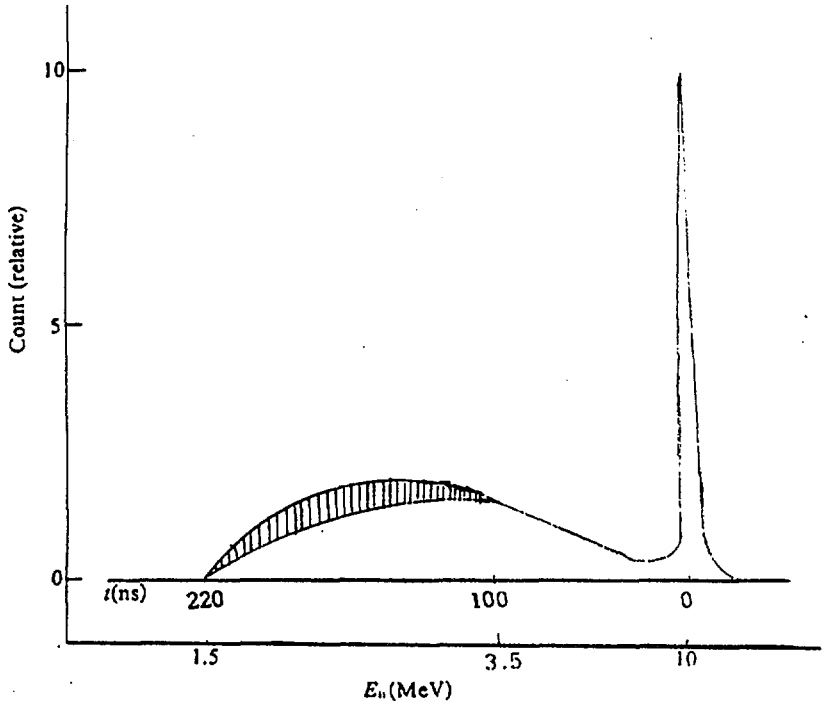


Fig. 3. Secondary neutron TOF spectrum induced by d+D reaction neutrons measured by the normal TOF spectrometer, hatched area is the contribution of break-up neutrons of the d+D reaction

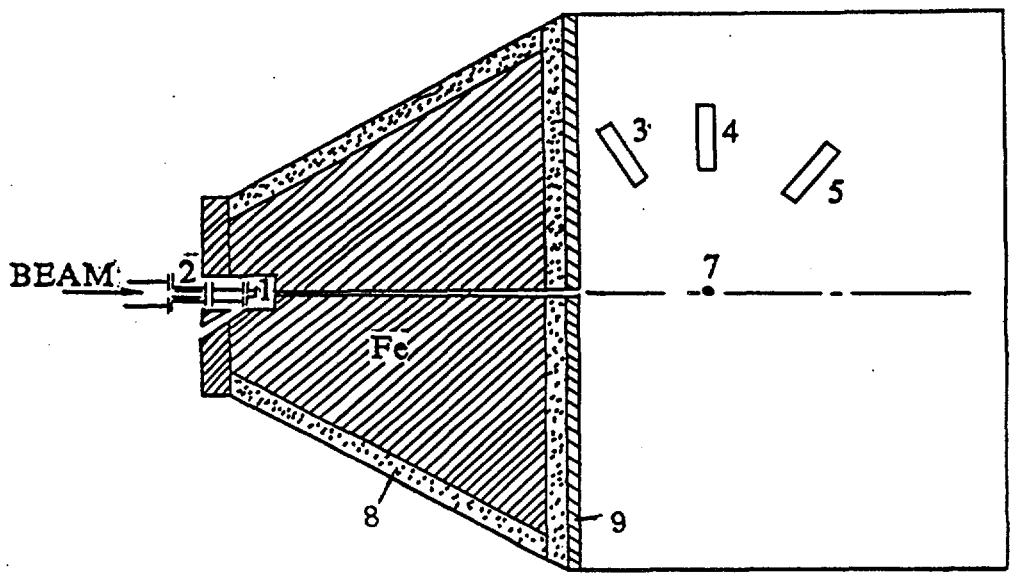


Fig. 4. Schematic diagram of the abnormal fast neutron TOF spectrometer
1- neutron source 2- beam pick-off
3, 4 and 5 - neutron detectors, 7 - sample
8- paraffin +lithium carbonate
9- lead

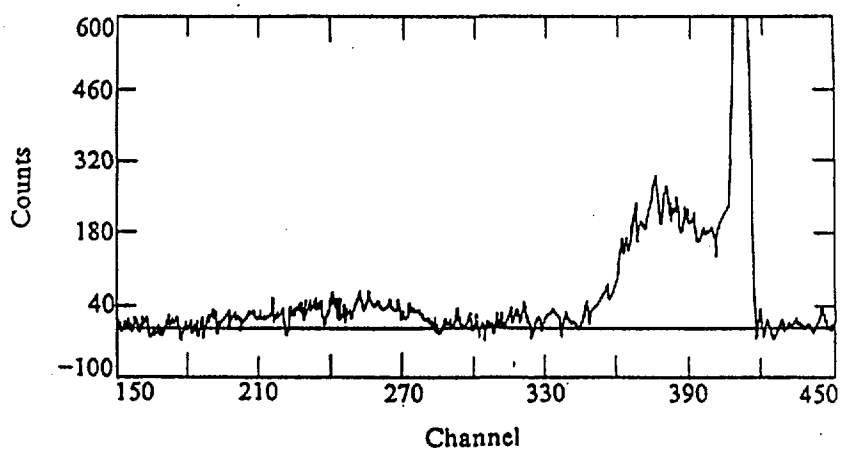


Fig. 5. TOF spectrum of secondary neutrons of $^{238}U$ induced by d+D reaction neutrons with monoenergy of 9.6 MeV measured by the abnormal TOF spectrometer, 45 degs., random background subtracted

the sample position. Two groups of secondary neutrons which are induced by monoenergetic and break-up neutrons respectively would be still separate enough from each other in the TOF spectrum when the detectors were located as far as 70 cm from the sample. The flight time of the two groups of secondary neutrons induced by 10 and 3.5 MeV neutrons under the above arrangement is listed in table 1. As the table indicates, the separation of these two groups of neutrons is 20.5 ns for the detector bias of 1.5 MeV and 11.2 ns for 1.0 MeV bias

Double differential cross sections in higher energy part (En>4MeV) was obtained by using the normal fast neutron TOF spectrometer. The final results of double differential cross sections in the whole energy region were given by combination of these two datum sets.

Fig. 5 shows the secondary neutron TOF spectrum of $^{238}U$ induced by 9.6 MeV monoenergetic and break-up neutrons of the d+D reaction measured by the abnormal TOF spectrometer. It is obvious that secondary neutrons are distributed in two groups which are induced by monoenergetic and break-up neutrons of the d+D reaction. Therefore, the contamination of break-up neutrons from the neutron source to the wanted secondary neutron spectrum can be fully eliminated and a pure secondary neutron spectrum induced only by monoenergetic neutrons can be obtained.

To get a net secondary neutron spectrum at an angle four runs of measurements are needed. The first run is performed with "sample in" and "target gas in". The second is done with "sample out" but "target gas in". The third is made with "sample in" but "target gas out". The fourth is for "sample out" and "target gas out". The net TOF spectrum of secondary neutrons is obtained by the following formula:

run 1 - run 2 - run 3 + run 4

Fig. 6 shows the individual and net neutron TOF spectra of $^{238}U$ induced by 9.6 MeV neutrons.

The secondary neutron TOF spectrum was converted into energy spectrum. Double differential cross sections of $^{238}U$ at 45° at the incident neutron energy of 9.6 MeV measured by both normal and abnormal TOF spectrometers are shown in Fig. 7, symbolized with circles and crosses

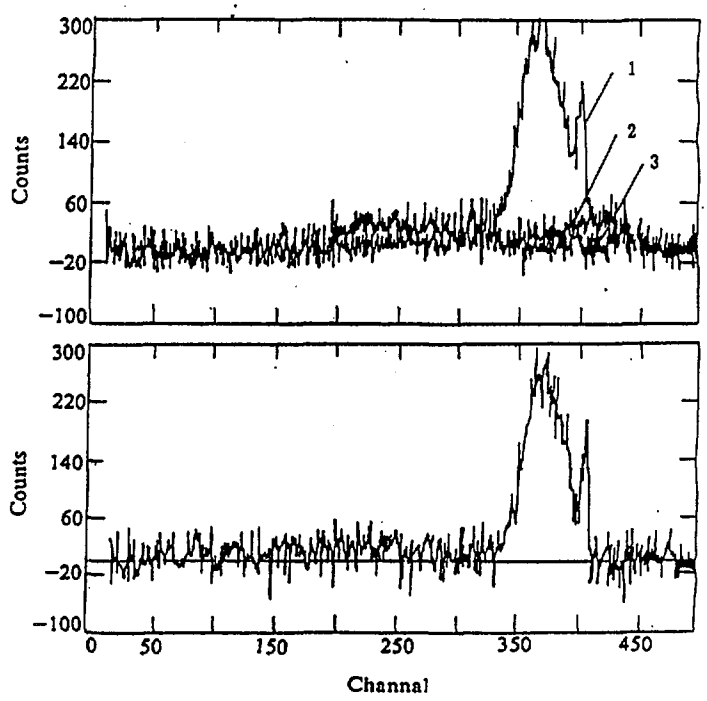


Fig. 6. Neutron TOF spectra of $^{238}U$ induced by 9.6 MeV neutrons at 120 degs. random background subtracted
Top:1- sample in and target gas in 2- sample out and target gas in 3-sample in,target gas out 4- sample out, target gas out (not shown)
Bottom: [1] - [2] - [3] + [4]

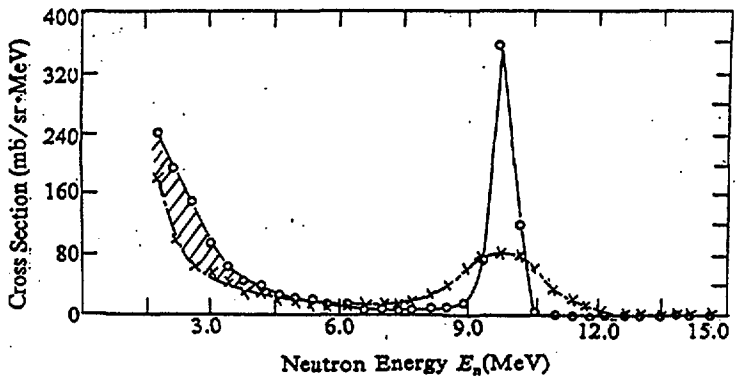


Fig. 7. Double differential neutron emission spectra of $^{238}U$ induced by 9.6 MeV neutrons at 45 degs
o : data by normal TOF spectrometer --:data by abnormal one

respectively. The shadow area is the source break-up neutron contribution which is moved away in the spectrum measured by the abnormal TOF facility.

## 3. Results

The double differential cross sections of secondary neutrons of $^{238}U$ and $^{209}Bi$ at 9.6 MeV have been measured so far. The final result was given in the following way. The double differential cross sections above 4 MeV were taken from the data measured by the normal TOF spectrometer

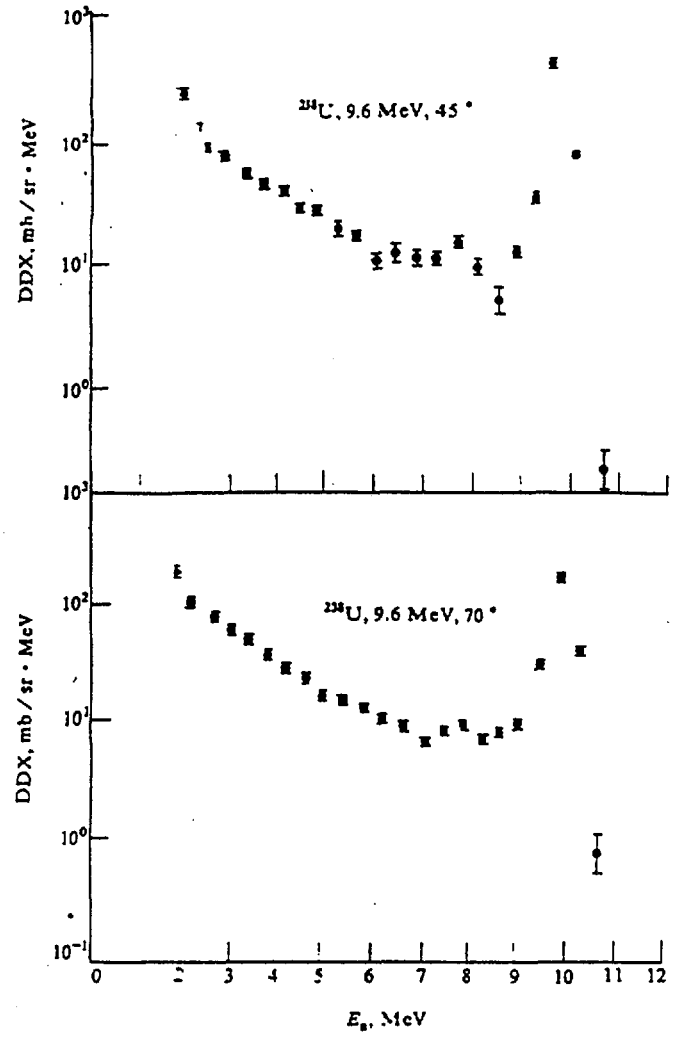


Fig. 8. Double differential cross sections of $^{238}U$ at 9.6 MeV 45 degs. and 70 degs.

to keep good energy resolution. The double differential cross sections below 4 MeV were given by the result obtained by the abnormal TOF device. Fig. 8 and 9 show the double differential cross sections of $^{238}U$ at 9.6 MeV. The secondary neutron double differential cross sections of $^{209}Bi$ at 9.6 MeV incident neutron energy at 45°, 70°, and 110° are shown in Fig. 10 and 11. All the data were corrected for neutron flux attenuation, multiple scattering and finite geometry with a Monte-Carlo code.

A semiclassical model, the computer code UNF written by J. Zhang[9] and DWBA, was used to calculate DDX for $^{209}Bi$. The cross sections, EDX and DDX from 14 reaction channels especially include those from the discret levels of these 14 channels can be calculated using UNF. The $J\pi$-dependent master equation , exciton state densities with the exact Pauli exclusion correction and pick-up mechanism in emission of composite particle (such as $\alpha$, d, t ) have been introduced in the exciton model. From reproduction of the total cross sections, non-elastic cross sections and elastic scattering angular distributions taken from ENDF/B-6 a set of optical potential was obtained for $^{209}Bi$[10] and then DDX were prodicted. A good agreement was obtained between the measurement and calculation, as can be seen in Fig. 10 and 11.

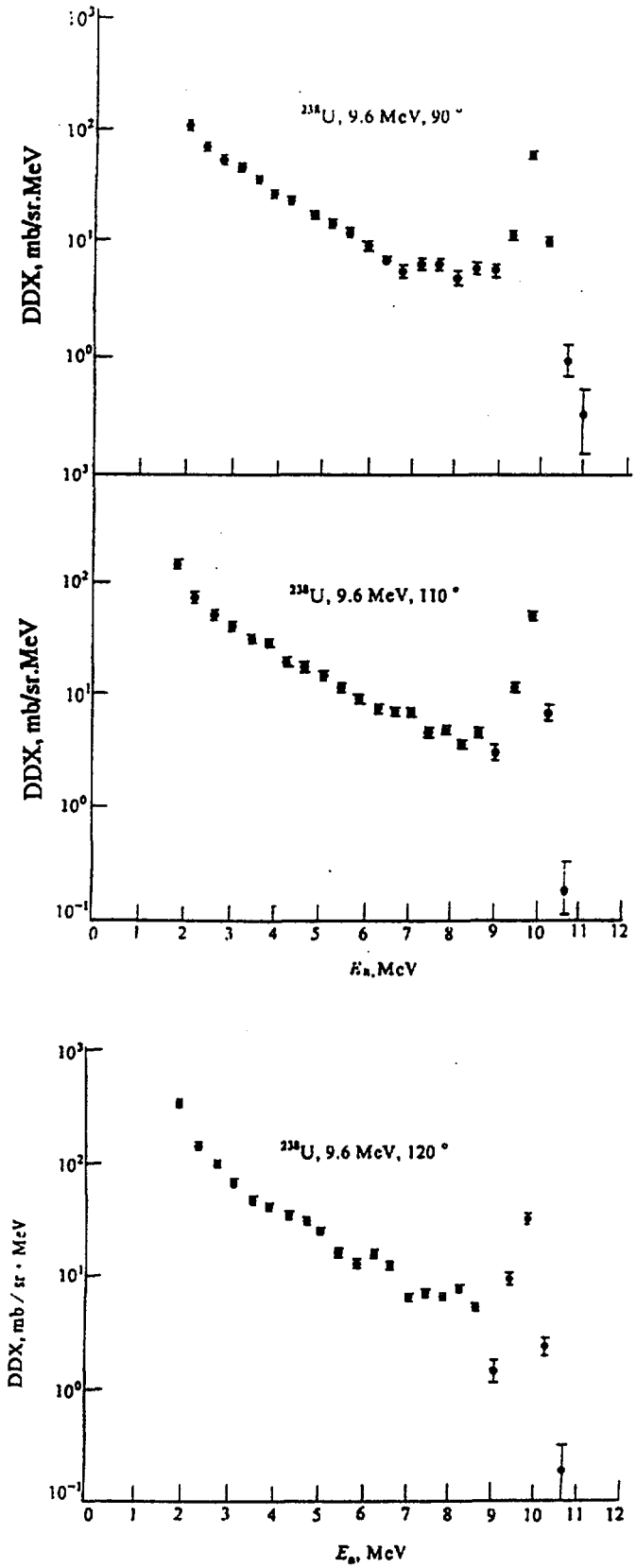


Fig.9. Double differential cross sections of $^{238}U$ at 9.6 MeV 90 degs.,.110 degs. and 120 degs.

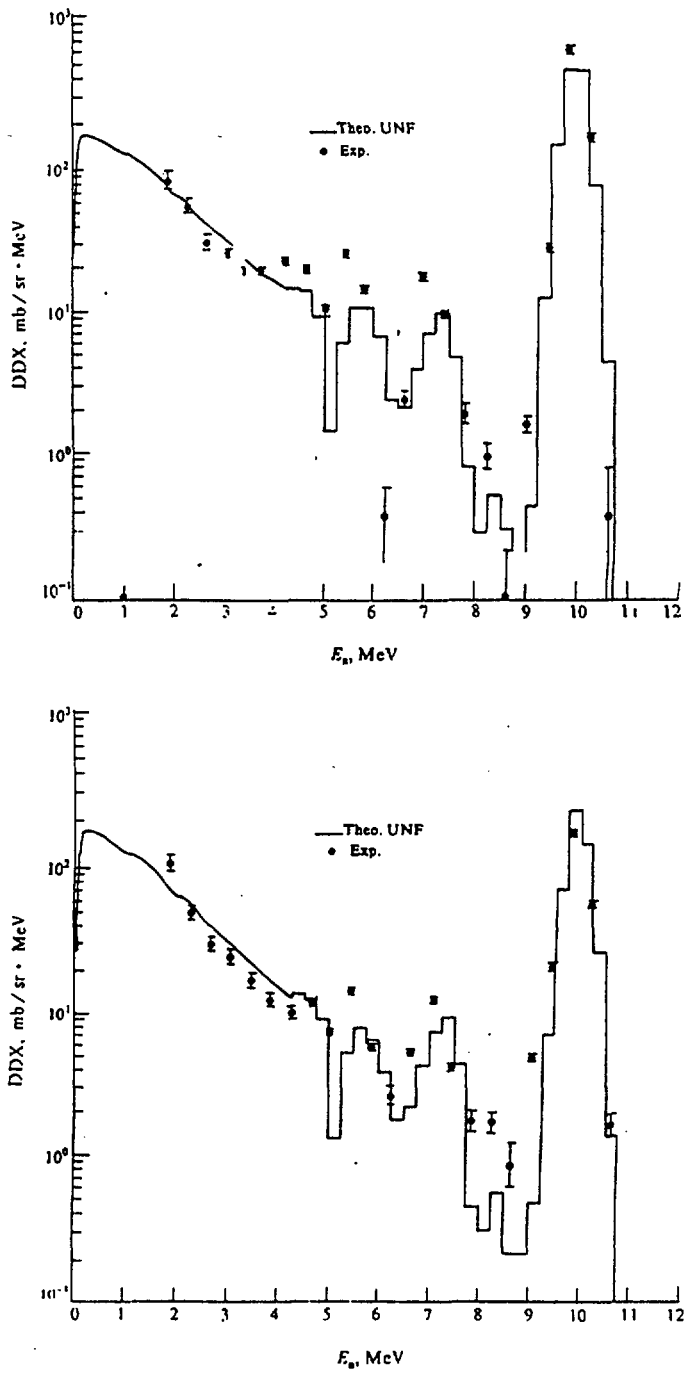


Fig. 10. Double differential cross sections of $^{209}Bi$ at 9.6 MeV
Top: 45 degs. Bottom: 70 degs.

## 4. Discussion and Conclusion

As we know, the most promising method for measuring double differential cross sections of secondary neutrons in the incident neutron energy range 9 to 13 MeV is accelerating triton and using the H(t, n) reaction as a monoenergetic neutron source. However, this is not an easy way for most of laboratories. People have explored different approaches as mentioned in section 1, but few effective methods have been found in real use. The method developed in CIAE can be used to solve the problem with conventional neutron sources at the price of losing counting rate and energy resolution.

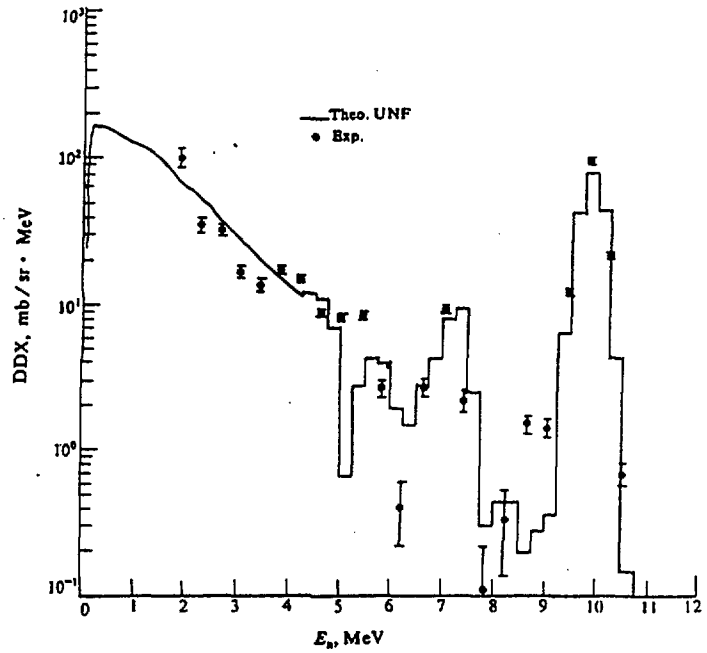


Fig. 11. Double differential cross sections of $^{209}Bi$ at 9.6 MeV 110 degs.

The counting rate is a factor of 0.6, compared with that of the normal arrangement (supposing the distance between neutron source and sample is 20 cm and that between sample and neutron detector is 6 m for the normal TOF spectrometer). At present three neutron detectors are used in the measurement simultaneously. To increase the datum acquisition rate we plan to add three more neutron detectors. Because the neutron source is massively shielded in the forward semisphere, it is easy to put more neutron detectors without additional shielding.

Now the threshold of the spectrometer is set at 1.5 MeV and the time separation in the spectrum between the secondary neutrons of the lowest energy (1.5 MeV) induced by monoenergetic neutrons and the one of highest energy (3.5 MeV) induced by break-up neutrons of the d+D reaction is about 20 ns. If the threshold is 1 MeV, the separation will be 11.2 ns,which is much larger than the time resolution (the full width at half maximum for elastic scattering neutron peak is 1.6 ns). Therefore, the threshold of the detector can be extended to 1 MeV or a little bit lower

Table 1 Flight time of secondary neutrons induced by monoenergetic and break-up neutrons of the d+D reaction under the following arrangement:
d1: the distance between neutron source and sample
d2: the distance between neutron detector and sample

| primary neutron | | secondary neutron | | total |
|---|---|---|---|---|
| $E_n$ (MeV) | d1=220cm | $E_n'$ (MeV) | d2=70cm | |
| 10 | 50.3ns | 10 | 16.0ns | 66.3ns |
| 10 | 50.3ns | 1.5 | 41.3ns | 91.6ns |
| 10 | 50.3ns | 1.0 | 50.6ns | 100.9ns |
| 3.5 | 85.0ns | 3.5 | 27.1ns | 112.1ns |
| 3.5 | 85.0ns | 1.5 | 41.3ns | 126.3ns |
| 3.5 | 85.0ns | 1.0 | 50.6ns | 135.6ns |

without difficulty for 10 MeV incident neutrons. For the incident neutron energy of 13 MeV, the bias of the neutron detector should be higher (about 2.2 MeV).

The energy resolution is about 2.4% for 10 MeV neutrons measured by the normal TOF spectrometer and about 12% for 4 MeV neutrons measured by the abnormal TOF spectrometer.

In conclusion, the preliminary results show that our method can be used for secondary neutron double differential cross section measurement in the incident neutron energy range 9 to 13 MeV.

References


1. D. M. Drake et al., *Nucl. Sci. and Eng.* 63 (1977) 401
2. M. Drosg et al., *Rad. Effect* 92 (1986) 145; P. W. Lisowski et al., LANL, *LA8342* (1980)
3. E. Dekempeneer et al., *Nucl. Sci. and Eng.* 97 (1987) 353
4. R. C. Byrd et al., *Annual Report-TUNL* XXI (1981-1982) p. 18
5. Wang Xiaozhong et al., Neutron Physics Lab, CIAE, *Laboratory Report* (1989)
6. Qi Bujia, Tang Hongqing, Zhou Zuying et al., *Proc. of Inter. Conf. on Nucl. Data for Science and Tech.* (Jülich, Germany, May, 1991)
7. S. Chiba et al., *the proceedings of Beijing Inter. Symp. on Fast Neutron Phys. Sep. (1991)*
8. Sa Jun, Tang Hongqing, Zhou Zuying et al., "A muti-detector fast neutron TOF spectrometer at the HI-13 tandem accelerator", *Beijing National Tandem Accelerator Laboratory Progress Report* (1988 - 1989)P. 119
9. Zhang Jingshang, *the proceedings of Beijing Inter. Symp. on Fast Neutron Phys. Sep. (1991)*
10. Xia Haihong et al., *Chinese J. Nucl. Phys (1992).*

# Evaluation of the 14.1 MeV Neutron Induced Double-Differential Neutron Emission Cross Sections of $^{51}V$

T. Elfruth, K. Seidel, S. Unholzer
Technische Universität Dresden, Institut für Kern- und Atomphysik
Mommsenstraße 13, D-O-8027 Dresden, Germany

**Abstract :** For the fusion reactor structure material vanadium the recently measured double-differential neutron emission cross sections deviate from the evalauted data of libraries more than the accuracy needed. The experimental data are used to derive evaluated experimental cross sections at 14.1 MeV neutron incidence energy as a step to improve the situation.

## 1. Introduction

Vanadium is one of the structure materials in fusion reactor designs. For neutron transport calculations of the reactor components energy- and angle-differential neutron emission cross sections (DDX) are needed with an accuracy of $\lesssim$ 10 % [1]. Comparing the recent experimental results at $E_o$ = 14 MeV with the evaluated data of libraries (Fig. 1) significant differences of the spectral shapes and of the angular distributions are obvious. They exceed the data accuracy needed.

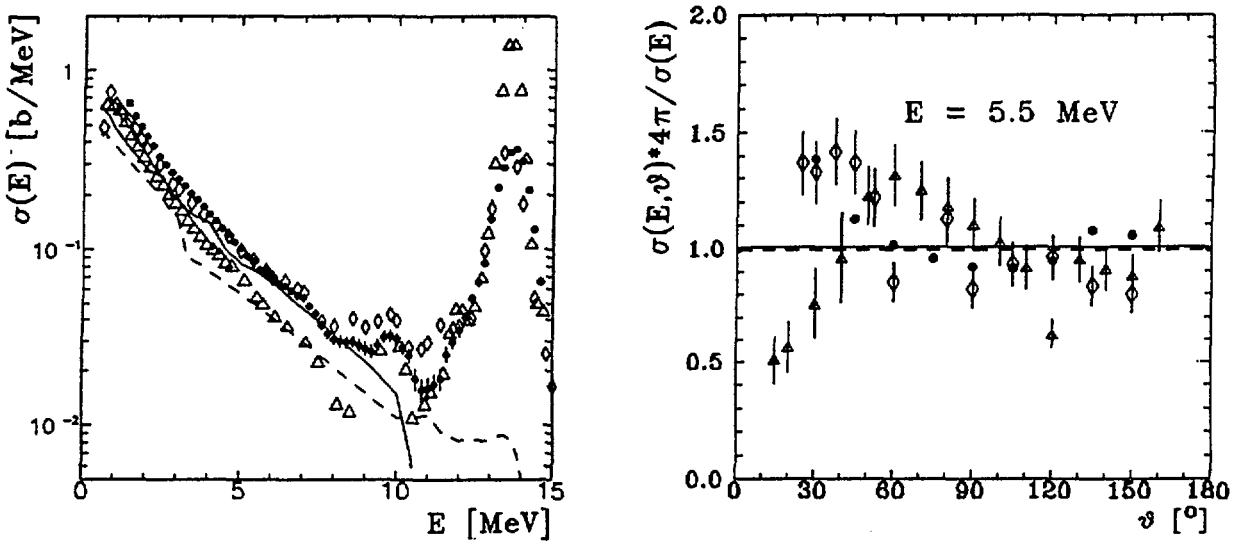


**Fig. 1:** Energy distribution of the neutrons emitted after 14 MeV neutron bombardment (left hand) and angular distribution at 5.5 MeV neutron emission energy (right hand). Experimental data: • [2], △ [3], ◇ [4]. Library data: ENDF/B-VI (solid line), ENDL-83 (dashed line)

In the present work the recent experimental data are used for the evaluation of the DDX at $E_o$ = 14.1 MeV. The procedure is described in paragraph 2. The results are presented in paragraph 3.

## 2. Evaluation

Experimental data were recently published by groups of TU Dresden [2,5], of Osaka University [3], and of Tohoku University [4].
The neutron incidence energies $E_o$ in these works are somewhat different, especially in the dependence on the angle $\vartheta$ where the neutron emission is observed. The influence on the emission spectra is the larger as the spectrum part has structures. That is illustrated in Fig. 2, where the energy-differential neutron emission cross section $\sigma$(E) calculated with the statistical model code EXIFON (details in Ref. [5,6]) for $E_o$ = 14.0 MeV and for $E_o$ = 14.2 MeV are compared to the distribution obtained for $E_o$ = 14.1 MeV.

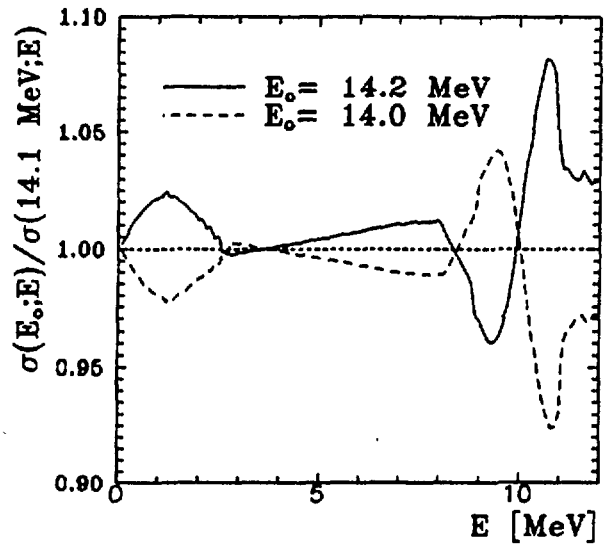


**Fig. 2:** Ratio of $\sigma$(E) for $E_o$ = 14.2 MeV and $E_o$ = 14.0 MeV, respectively, to $\sigma$(E) calculated with the code EXIFON for $E_o$ = 14.1 MeV.

Therefore, the DDX were corrected to $E_o$ = 14.1 MeV for each $\vartheta$.
Following the procedure of Pavlik and Vonach [7] $\sigma(E,\vartheta)$ was divided into a part dominated by emissions from separated levels and a continuum part of emissions. After the separation of the continuous part the "level part" of the spectra was shifted according to the Q-values of the (n,n')-processes. The continuous part was corrected by EXIFON calculations.
The corrected $\sigma(E,\vartheta)$ were used to derive energy-group averaged DDX. Their angular distribution was described by

$$\sigma(E,\vartheta) = \frac{\sigma(E)}{4\pi}\sum_{l=0}^{l_{max}}(2\cdot l+1)\cdot f_l \cdot P_l(cos(\vartheta)) \qquad (1)$$

To realize a linear equation of the parameters to be fitted the coefficients $a_l$,

$$a_i = \frac{\sigma(E)}{4\pi}(2\cdot l+1)f_i\,, \qquad (2)$$

were used as parameters.
The fit was carried out with a weighting of the experimental data according to their uncertainties. The uncertainties of the data are divided into short-range errors (S: e.g. statistical errors), long-range errors (L: full correlation over the whole range of E, e.g. source strength monitoring uncertainty) and medium-range errors (M: correlation length of several MeV, e.g. uncertainties of the detector efficiency or finite sample size corrections).
In addition to the uncertainties given by the authors themselves the following drawbacks of the experiments were fixed as additional systematic errors:

- Ref. [3] (in the calculation of $f_l$'s used for E $\geq$ 6 MeV only)
  - artificial structure in the angular distributions for $\vartheta \leq 60$ deg. (e.g. Fig. 1);
  - artificial $f_1$ asymmetry (Fig. 5)
  - finite sample size correction.
- Ref. [4] (in the calculation of $\sigma$(E) used for E $\leq$ 10 MeV only)
  - energy resolution in the high-energy part;
  - no peak separation of the elastically scattered neutrons.
- In all experiments the error of the detector efficiency was enlarged by 5 % in the vicinity of the detection threshold.

The possible influence of elastically scattered neutrons, resolved with finite resolution, on the Legendre polynomial coefficients is shown is Fig. 3. To avoid this influence the elastic scattering peak was separated from the data of Ref. [5] using the experimental peak shape.

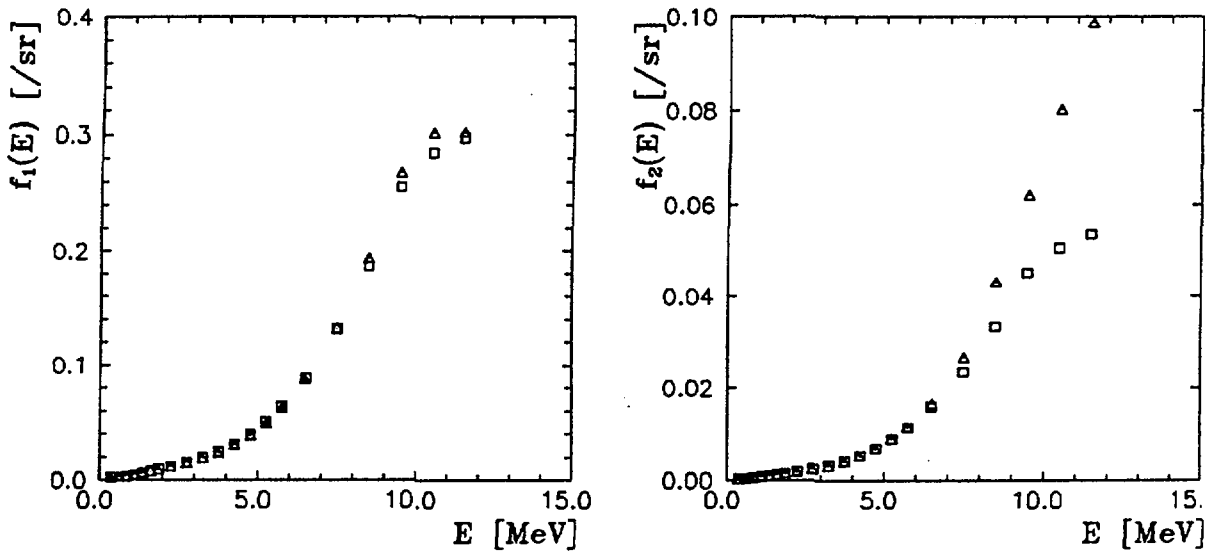


**Fig. 3:** Influence of the finite resolution of elastically scattered neutrons on the Legendre coefficients, obtained from DDX calculated by EXIFON without (□) and with (△) adding the peak of elastically scattered neutrons with the experimental peak shape of Ref. [5].

Table 1 shows the systematic uncertainties according to the group structure implemented in the evaluation. The $\Delta\sigma(E_i, \vartheta)$ were assumed to be not dependent on $\vartheta$. For each file k of the experimental data the total uncertainty $\Delta\sigma_k(E_i, \vartheta)$ was calculated as root-mean-square of the $\Delta\sigma_k^j(E_i, \vartheta)$ with j=S,M,L from Tab. 1 and the statistical uncertainties given by the authors.

An example of the evaluation is shown in Fig. 4. The fits with $l_{max} = 2$ were used for the evaluated experimental DDX.

For $E_i \leq 1$ MeV the DDX were calculated with the EXIFON-code because of lack and uncertainty, respectively, of the experimental data.

For the calculation of the relative $\sigma$(E) correlation matrix the procedure of Vonach et al. [7,8] was adopted.

**Table 1:** Systematic uncertainties ($\frac{\Delta\sigma}{\sigma}\cdot 100$) of the experimental $\sigma(E_i,\vartheta)$ for the energy-group structure $E_i$ used in the evaluation.

| k | $E_i$ [MeV] | | 0.00-0.25 | 0.50-0.75 | 1.00-1.25 | 1.50-1.75 | 2.00-2.50 | 3.00-3.50 |
|---|---|---|---|---|---|---|---|---|
| 1 | | S | 0.0 | 0.0 | 0.0 | 0.0 | 0.0 | 0.0 |
| 1 | Tohoku Univ. | M | 10.0 | 10.0 | 10.0 | 10.0 | 10.0 | 7.0 |
| 1 | | L | 4.0 | 4.0 | 4.0 | 4.0 | 4.0 | 4.0 |
| 2 | | S | 0.0 | 0.0 | 0.0 | 0.0 | 0.0 | 0.0 |
| 2 | TU Dresden | M | 10.0 | 10.0 | 10.0 | 10.0 | 10.0 | 7.0 |
| 2 | | L | 4.0 | 4.0 | 4.0 | 4.0 | 4.0 | 4.0 |
| 3 | | S | 0.0 | 0.0 | 0.0 | 0.0 | 0.0 | 0.0 |
| 3 | Osaka Univ. | M | 12.0 | 12.0 | 12.0 | 12.0 | 12.0 | 10.0 |
| 3 | | L | 10.0 | 10.0 | 10.0 | 10.0 | 10.0 | 10.0 |

| k | $E_i$ [MeV] | | 3.50-4.00 | 4.50-5.00 | 5.50-6.00 | 7.00-8.00 | 9.00-10.0 | 11.0-12.0 |
|---|---|---|---|---|---|---|---|---|
| 1 | | S | 0.0 | 0.0 | 0.0 | 0.0 | 0.0 | 0.0 |
| 1 | Tohoku Univ. | M | 7.0 | 7.0 | 7.0 | 7.0 | 20.0 | 20.0 |
| 1 | | L | 4.0 | 4.0 | 4.0 | 4.0 | 4.0 | 4.0 |
| 2 | | S | 0.0 | 0.0 | 0.0 | 0.0 | 0.0 | 0.0 |
| 2 | TU Dresden | M | 7.0 | 7.0 | 7.0 | 7.0 | 7.0 | 7.0 |
| 2 | | L | 4.0 | 4.0 | 4.0 | 4.0 | 4.0 | 4.0 |
| 3 | | S | 0.0 | 0.0 | 0.0 | 0.0 | 0.0 | 0.0 |
| 3 | Osaka Univ. | M | 10.0 | 10.0 | 10.0 | 10.0 | 10.0 | 10.0 |
| 3 | | L | 10.0 | 10.0 | 10.0 | 10.0 | 10.0 | 10.0 |

S = short-range-, M = medium-range- , L = long-range

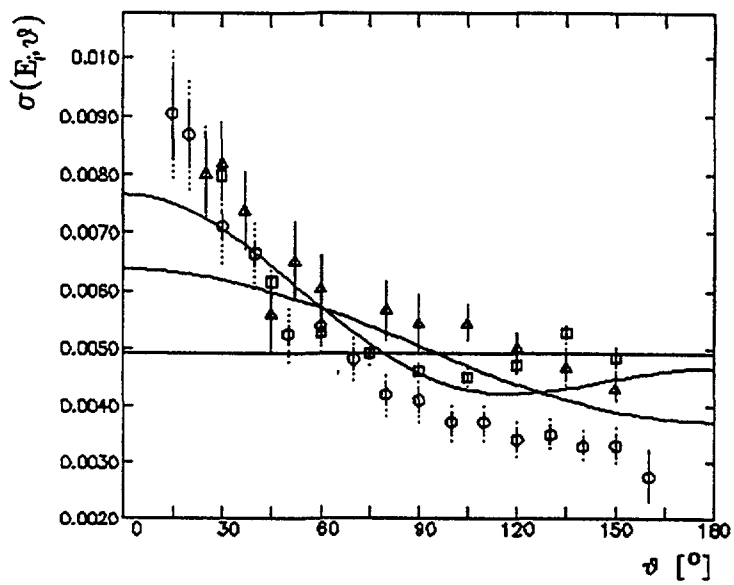


**Fig. 4:** DDX for the emission energy group $E_i$ = 6.0 - 7.0 MeV. The experimental data of Ref. [2] (□), Ref. [3] (o) and Ref. [4] (△) are shown with their statistical (solid) and systematic (dotted) uncertainties. The solid lines represent fits according to equation (1) with $l_{max}$ = 0, 1 and 2, respectively.

The correlation coefficients $C_{i,i'}$ for the uncertainties of the evaluated $\sigma(E)$ were calculated by a weighted average over all data sets k of the energy groups i and i', respectively, using the inverse squares of the group DDX errors $\Delta\sigma_k(E_i)$ and $\Delta\sigma_k(E_{i'})$ as statistical weights.

$$C_{i,i'} = \frac{1}{\Delta\sigma(E_i)_{int}\cdot\Delta\sigma(E_{i'})_{int}}\cdot\sum_{\forall k} A_{ik}\cdot A_{i'k}\cdot\Delta\sigma_k(E_i)\cdot\Delta\sigma_k(E_{i'})\cdot C_k^{ii'} \qquad (3)$$

The weighting factors $A_{ik}$ and $A_{i'k}$ are defined as

$$A_{ik} = \frac{(\frac{1}{\Delta\sigma_k(E_i)})^2}{\sum_{\forall k''}(\frac{1}{\Delta\sigma_{k''}(E_i)})^2} \quad \text{and} \quad A_{i'k} = \frac{(\frac{1}{\Delta\sigma_k(E_{i'})})^2}{\sum_{\forall k''}(\frac{1}{\Delta\sigma_{k''}(E_{i'})})^2} \quad \text{, respectively.} \tag{4}$$

The quantities $\Delta\sigma(E_i)_{int}$ and $\Delta\sigma(E_{i'})_{int}$ are the internal errors of the evaluated cross sections calculated by

$$\Delta\sigma(E_i)_{int} = \frac{1}{N} \cdot \sqrt{\sum_{k=1}^{N} A_{ik} \cdot \Delta\sigma_k^2(E_i)} \tag{5}$$

The correlation coefficient $C_k^{ii'}$ of each data set k was derived from the analysis of the systematic uncertainties by dividing $\Delta\sigma_k(E_i)$ into a correlated $\Delta\sigma_k(E_i)_{corr}$ and an uncorrelated part $\Delta\sigma_k(E_i)_{uncorr}$.

$$C_k^{ii'} = \frac{\Delta\sigma_k^2(E_i)_{corr}}{\Delta\sigma_k^2(E_i)} \tag{6}$$

with

$$\Delta\sigma_k^2(E_i)_{corr} = [\Delta\sigma_k^L(E_i)]^2 + 0.5 \cdot ([\Delta\sigma_k^M(E_i)]^2 + [\Delta\sigma_k^M(E_{i'})]^2) \cdot e^{-\frac{(E_i - E_{i'})^2}{2 \cdot L_{corr}^2}} \tag{7}$$

The correlation length $L_{corr}$ for the medium-range errors was assumed to be 4 MeV.

## 3. Results

The results of the DDX-evaluation carried out with the programme EVALUATE [9] are given in Tables 2 - 4.

**Table 2:** Evaluated experimental $\sigma(E)$, $f_1$ and $f_2$ for $^{51}V$ at $E_o$ = 14.1 MeV ($f_o \equiv 1/sr$)

| $E_i$ [MeV] | $\sigma(E)$ [b/MeV] | $\delta\sigma$[%] | $f_1$ [/sr] | $\delta f_1$ [%] | $f_2$ [/sr] | $\delta f_2$ [%] |
|---|---|---|---|---|---|---|
| 0.00 - 0.25 | 0.36888E+00 | | 0.20460E-02 | | 0.33236E-03 | |
| 0.25 - 0.50 | 0.81359E+00 | | 0.22018E-02 | | 0.35491E-03 | |
| 0.50 - 0.75 | 0.82121E+00 | | 0.26244E-02 | | 0.38629E-03 | |
| 0.75 - 1.00 | 0.72948E+00 | | 0.38554E-02 | | 0.70367E-03 | |
| 1.00 - 1.25 | 0.64477E+00 | 2.32 | 0.31107E-01 | 70.47 | 0.15292E-01 | 70.30 |
| 1.25 - 1.50 | 0.53659E+00 | 2.26 | 0.30572E-01 | 70.60 | 0.16055E-01 | 63.21 |
| 1.50 - 1.75 | 0.48010E+00 | 1.37 | 0.23074E-01 | 48.25 | 0.14106E-01 | 45.37 |
| 1.75 - 2.00 | 0.40511E+00 | 1.35 | 0.20230E-01 | 54.96 | 0.17446E-01 | 36.17 |
| 2.00 - 2.50 | 0.31930E+00 | 1.29 | 0.27712E-01 | 38.14 | 0.14185E-01 | 41.90 |
| 2.50 - 3.00 | 0.23646E+00 | 1.29 | 0.32398E-01 | 32.96 | 0.18164E-01 | 32.99 |
| 3.00 - 3.50 | 0.19529E+00 | 1.10 | 0.30032E-01 | 28.55 | 0.20589E-01 | 25.41 |
| 3.50 - 4.00 | 0.15289E+00 | 1.18 | 0.21444E-01 | 43.67 | 0.76310E-02 | 74.41 |
| 4.00 - 4.50 | 0.12704E+00 | 1.17 | 0.33428E-01 | 27.37 | 0.18922E-01 | 29.74 |
| 4.50 - 5.00 | 0.10530E+00 | 1.19 | 0.41195E-01 | 23.07 | 0.30867E-01 | 18.72 |
| 5.00 - 5.50 | 0.84619E-01 | 1.24 | 0.43061E-01 | 22.88 | 0.30531E-01 | 19.85 |
| 5.50 - 6.00 | 0.70111E-01 | 1.29 | 0.87421E-01 | 8.67 | 0.37068E-01 | 17.11 |
| 6.00 - 7.00 | 0.57953E-01 | 1.20 | 0.10892E+00 | 6.45 | 0.45634E-01 | 12.74 |
| 7.00 - 8.00 | 0.39754E-01 | 1.34 | 0.13544E+00 | 5.83 | 0.68613E-01 | 9.46 |
| 8.00 - 9.00 | 0.28100E-01 | 1.55 | 0.17755E+00 | 5.08 | 0.78912E-01 | 9.28 |
| 9.00 - 10.00 | 0.26790E-01 | 1.59 | 0.18644E+00 | 4.96 | 0.83512E-01 | 9.14 |
| 10.00 - 11.00 | 0.17721E-01 | 2.03 | 0.26727E+00 | 4.44 | 0.95773E-01 | 10.14 |
| 11.00 - 12.00 | 0.11770E-01 | 2.87 | 0.14915E+00 | 11.95 | 0.13852E+00 | 9.93 |

The coefficients $f_1$ and $f_2$ are shown in Fig. 5. The energy dependence of the evaluated $f_1$ and $f_2$ can by parametrized by

$$f_1(E) = 0.002418 \cdot E^2 - 0.002542 \cdot E + 0.0122 \text{ , and}$$

$$f_2(E) = 0.0008425 \cdot E^2 + 0.0009666 \cdot E + 0.00513 .$$

**Table 3:** Relative correlation matrix of $\sigma(E)$

| energy [MeV] | 0.00 - 0.25 | 0.25 - 0.50 | 0.50 - 0.75 | 0.75 - 1.00 | 1.00 - 1.25 | 1.25 - 1.50 | 1.50 - 1.75 | 1.75 - 2.00 |
|---|---|---|---|---|---|---|---|---|
| 0.00 - 0.25 | 100.0 | 100.0 | 100.0 | 100.0 | 0.0 | 0.0 | 0.0 | 0.0 |
| 0.25 - 0.50 | | 100.0 | 100.0 | 100.0 | 0.0 | 0.0 | 0.0 | 0.0 |
| 0.50 - 0.75 | | | 100.0 | 100.0 | 0.0 | 0.0 | 0.0 | 0.0 |
| 0.75 - 1.00 | | | | 100.0 | 0.0 | 0.0 | 0.0 | 0.0 |
| 1.00 - 1.25 | | | | | 100.0 | 66.6 | 67.2 | 67.5 |
| 1.25 - 1.50 | | | | | | 100.0 | 69.2 | 69.7 |
| 1.50 - 1.75 | | | | | | | 100.0 | 80.7 |
| 1.75 - 2.00 | | | | | | | | 100.0 |

| energy [MeV] | 2.00 - 2.50 | 2.50 - 3.00 | 3.00 - 3.50 | 3.50 - 4.00 | 4.00 - 4.50 | 4.50 - 5.00 | 5.00 - 5.50 | 5.50 - .00 |
|---|---|---|---|---|---|---|---|---|
| 0.00 - 0.25 | 0.0 | 0.0 | 0.0 | 0.0 | 0.0 | 0.0 | 0.0 | 0.0 |
| 0.25 - 0.50 | 0.0 | 0.0 | 0.0 | 0.0 | 0.0 | 0.0 | 0.0 | 0.0 |
| 0.50 - 0.75 | 0.0 | 0.0 | 0.0 | 0.0 | 0.0 | 0.0 | 0.0 | 0.0 |
| 0.75 - 1.00 | 0.0 | 0.0 | 0.0 | 0.0 | 0.0 | 0.0 | 0.0 | 0.0 |
| 1.00 - 1.25 | 74.0 | 68.4 | 54.4 | 48.5 | 40.4 | 33.5 | 28.0 | 24.1 |
| 1.25 - 1.50 | 76.7 | 71.4 | 57.2 | 51.4 | 43.0 | 36.0 | 30.2 | 26.1 |
| 1.50 - 1.75 | 82.0 | 78.6 | 71.9 | 64.1 | 61.1 | 55.9 | 49.8 | 44.7 |
| 1.75 - 2.00 | 82.4 | 79.7 | 73.1 | 65.6 | 62.8 | 57.7 | 51.6 | 46.5 |
| 2.00 - 2.50 | 100.0 | 83.9 | 77.4 | 70.3 | 67.4 | 62.1 | 55.8 | 50.4 |
| 2.50 - 3.00 | | 100.0 | 79.0 | 72.9 | 71.2 | 66.7 | 60.7 | 55.6 |
| 3.00 - 3.50 | | | 100.0 | 71.9 | 72.3 | 69.5 | 64.9 | 60.8 |
| 3.50 - 4.00 | | | | 100.0 | 70.2 | 68.5 | 64.8 | 61.5 |
| 4.00 - 4.50 | | | | | 100.0 | 73.1 | 70.3 | 67.8 |
| 4.50 - 5.00 | | | | | | 100.0 | 72.5 | 71.0 |
| 5.00 - 5.50 | | | | | | | 100.0 | 71.5 |
| 5.50 - 6.00 | | | | | | | | 100.0 |

| energy [MeV] | 6.00 - 7.00 | 7.00 - 8.00 | 8.00 - 9.00 | 9.00 -10.00 | -11.00 | -12.00 |
|---|---|---|---|---|---|---|
| 0.00 - 0.25 | 0.0 | 0.0 | 0.0 | 0.0 | 0.0 | 0.0 |
| 0.25 - 0.50 | 0.0 | 0.0 | 0.0 | 0.0 | 0.0 | 0.0 |
| 0.50 - 0.75 | 0.0 | 0.0 | 0.0 | 0.0 | 0.0 | 0.0 |
| 0.75 - 1.00 | 0.0 | 0.0 | 0.0 | 0.0 | 0.0 | 0.0 |
| 1.00 - 1.25 | 25.5 | 15.2 | 10.9 | 7.2 | 4.5 | 3.3 |
| 1.25 - 1.50 | 27.6 | 16.6 | 11.9 | 7.8 | 4.9 | 3.4 |
| 1.50 - 1.75 | 39.6 | 30.4 | 27.3 | 18.7 | 14.7 | 10.3 |
| 1.75 - 2.00 | 41.5 | 31.7 | 28.4 | 19.3 | 15.1 | 10.4 |
| 2.00 - 2.50 | 45.5 | 34.5 | 30.5 | 20.5 | 15.7 | 10.7 |
| 2.50 - 3.00 | 51.1 | 39.2 | 34.9 | 23.3 | 17.7 | 11.8 |
| 3.00 - 3.50 | 57.5 | 46.5 | 43.4 | 30.2 | 24.1 | 17.5 |
| 3.50 - 4.00 | 59.3 | 48.8 | 45.8 | 32.0 | 25.2 | 17.9 |
| 4.00 - 4.50 | 66.5 | 56.3 | 54.0 | 38.0 | 30.1 | 21.3 |
| 4.50 - 5.00 | 70.8 | 61.8 | 60.5 | 43.1 | 34.2 | 24.0 |
| 5.00 - 5.50 | 72.7 | 65.1 | 65.1 | 47.1 | 37.6 | 26.3 |
| 5.50 - 6.00 | 63.2 | 55.1 | 27.9 | 36.3 | 22.9 | 15.1 |
| 6.00 - 7.00 | 100.0 | 61.4 | 35.1 | 42.9 | 27.7 | 18.3 |
| 7.00 - 8.00 | | 100.0 | 37.2 | 47.0 | 31.6 | 21.4 |
| 8.00 - 9.00 | | | 100.0 | 33.1 | 24.2 | 17.0 |
| 9.00 - 10.00 | | | | 100.0 | 35.2 | 26.0 |
| 10.00 - 11.00 | | | | | 100.0 | 21.0 |
| 11.00 - 12.00 | | | | | | 100.0 |

**Table 4:** Relative covariance matrices of the fit parameters $a_0$, $a_1$, $a_2$

E = 0.00 - 0.25 MeV

| i\k | 0 | 1 | 2 |
|---|---|---|---|
| 0 | 100.0 | 0.5 | -48.9 |
| 1 | | 100.0 | 0.6 |
| 2 | | | 100.0 |

E = 0.25 - 0.50 MeV

| i\k | 0 | 1 | 2 |
|---|---|---|---|
| 0 | 100.0 | 0.5 | -48.9 |
| 1 | | 100.0 | 0.7 |
| 2 | | | 100.0 |

E = 0.50 - 0.75 MeV

| i\k | 0 | 1 | 2 |
|---|---|---|---|
| 0 | 100.0 | 0.8 | -48.8 |
| 1 | | 100.0 | 0.8 |
| 2 | | | 100.0 |

E = 0.75 - 1.00 MeV

| i\k | 0 | 1 | 2 |
|---|---|---|---|
| 0 | 100.0 | 1.0 | -48.6 |
| 1 | | 100.0 | 1.1 |
| 2 | | | 100.0 |

E = 1.00 - 1.25 MeV

| i\k | 0 | 1 | 2 |
|---|---|---|---|
| 0 | 100.0 | 3.4 | -23.9 |
| 1 | | 100.0 | -16.8 |
| 2 | | | 100.0 |

E = 1.25 - 1.50 MeV

| i\k | 0 | 1 | 2 |
|---|---|---|---|
| 0 | 100.0 | -1.1 | -22.9 |
| 1 | | 100.0 | -16.6 |
| 2 | | | 100.0 |

E = 1.50 - 1.75 MeV

| i\k | 0 | 1 | 2 |
|---|---|---|---|
| 0 | 100.0 | 1.9 | -6.2 |
| 1 | | 100.0 | -4.5 |
| 2 | | | 100.0 |

E = 1.75 - 2.00 MeV

| i\k | 0 | 1 | 2 |
|---|---|---|---|
| 0 | 100.0 | -0.2 | 0.0 |
| 1 | | 100.0 | -3.7 |
| 2 | | | 100.0 |

E = 2.00 - 2.50 MeV

| i\k | 0 | 1 | 2 |
|---|---|---|---|
| 0 | 100.0 | -0.5 | -1.9 |
| 1 | | 100.0 | -3.8 |
| 2 | | | 100.0 |

E = 2.50 - 3.00 MeV

| i\k | 0 | 1 | 2 |
|---|---|---|---|
| 0 | 100.0 | 2.4 | -3.1 |
| 1 | | 100.0 | -0.1 |
| 2 | | | 100.0 |

E = 3.00 - 3.50 MeV

| i\k | 0 | 1 | 2 |
|---|---|---|---|
| 0 | 100.0 | 6.6 | -1.3 |
| 1 | | 100.0 | 3.2 |
| 2 | | | 100.0 |

E = 3.50 - 4.00 MeV

| i\k | 0 | 1 | 2 |
|---|---|---|---|
| 0 | 100.0 | 11.9 | 5.0 |
| 1 | | 100.0 | 9.5 |
| 2 | | | 100.0 |

E = 4.00 - 4.50 MeV

| i\k | 0 | 1 | 2 |
|---|---|---|---|
| 0 | 100.0 | 9.4 | 1.3 |
| 1 | | 100.0 | 5.8 |
| 2 | | | 100.0 |

E = 4.50 - 5.00 MeV

| i\k | 0 | 1 | 2 |
|---|---|---|---|
| 0 | 100.0 | 11.3 | 6.5 |
| 1 | | 100.0 | 7.0 |
| 2 | | | 100.0 |

E = 5.00 - 5.50 MeV

| i\k | 0 | 1 | 2 |
|---|---|---|---|
| 0 | 100.0 | 13.4 | 7.0 |
| 1 | | 100.0 | 7.7 |
| 2 | | | 100.0 |

E = 5.50 - 6.00 MeV

| i\k | 0 | 1 | 2 |
|---|---|---|---|
| 0 | 100.0 | 21.2 | 11.1 |
| 1 | | 100.0 | 14.9 |
| 2 | | | 100.0 |

E = 6.00 - 7.00 MeV

| i\k | 0 | 1 | 2 |
|---|---|---|---|
| 0 | 100.0 | 28.1 | 12.8 |
| 1 | | 100.0 | 22.5 |
| 2 | | | 100.0 |

E = 7.00 - 8.00 MeV

| i\k | 0 | 1 | 2 |
|---|---|---|---|
| 0 | 100.0 | 31.3 | 21.5 |
| 1 | | 100.0 | 24.2 |
| 2 | | | 100.0 |

E = 8.00 - 9.00 MeV

| i\k | 0 | 1 | 2 |
|---|---|---|---|
| 0 | 100.0 | 36.3 | 26.4 |
| 1 | | 100.0 | 22.8 |
| 2 | | | 100.0 |

E = 9.00 - 10.00 MeV

| i\k | 0 | 1 | 2 |
|---|---|---|---|
| 0 | 100.0 | 34.2 | 26.2 |
| 1 | | 100.0 | 20.0 |
| 2 | | | 100.0 |

E = 10.00 - 11.00 MeV

| i\k | 0 | 1 | 2 |
|---|---|---|---|
| 0 | 100.0 | 36.4 | 30.7 |
| 1 | | 100.0 | 23.2 |
| 2 | | | 100.0 |

E = 11.00 - 12.00 MeV

| i\k | 0 | 1 | 2 |
|---|---|---|---|
| 0 | 100.0 | 20.8 | 38.2 |
| 1 | | 100.0 | 14.7 |
| 2 | | | 100.0 |

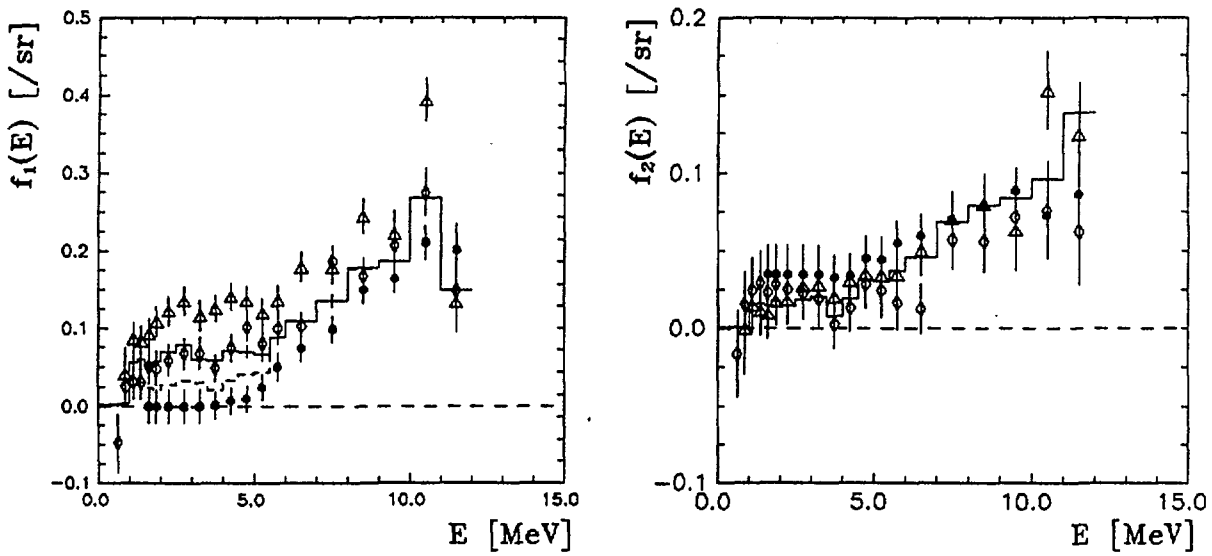


**Fig. 5:** Coefficients of equ. (1) derived from the experimental data sets (△ [3], ◇ [4], • [5]) and the evaluated coefficients obtained from all data (solid histogram) and obtained without the data of [3] below 6 MeV (dashed histogram), respectively.

Fig. 6 presents the evaluated experimental $\sigma$(E) together with both the experimental data and the evaluated data of the libraries ENDF/B-VI and ENDL-83, respectively.

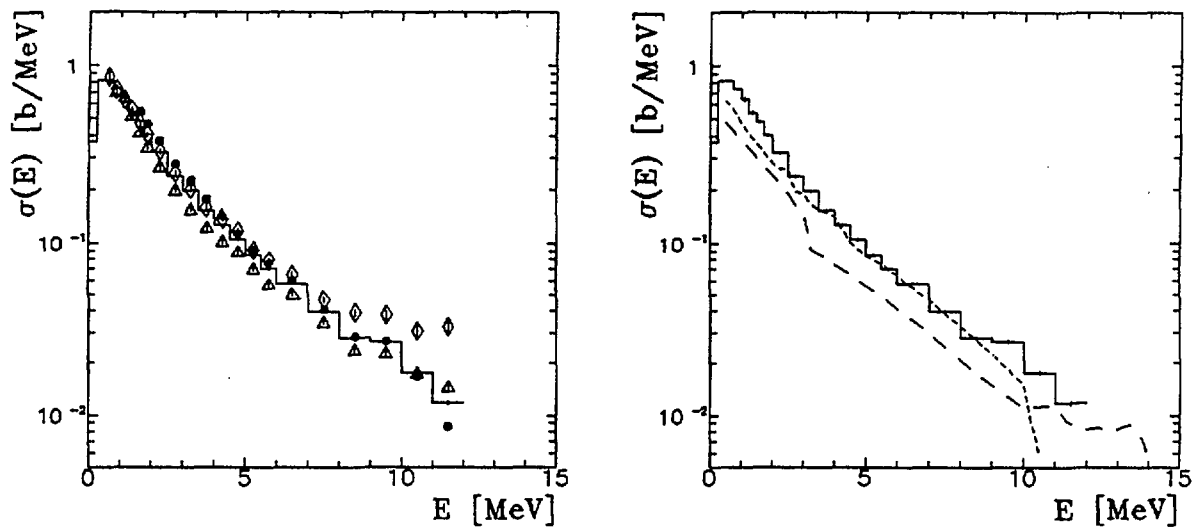


**Fig. 6:** Comparison of the evaluated experimental $\sigma$(E) (solid histogram) with measured data (left hand; △ [3], ◇ [4], • [5]) and with ENDF/B-VI (short-dashed line) and ENDL-83 (dashed line) data, respectively.

In Fig. 7 the evaluated experimental $\sigma$(E) is compared with a statistical model calculation using the EXIFON-code. The calcualated $\sigma$(E) is in better agreement with the evaluated experimental data than the library cross sections.
An incorrect (n,2n)-cross section in the libraries as well as inadequate shapes of the energy distributions may be the reason for the deviation to the library data.

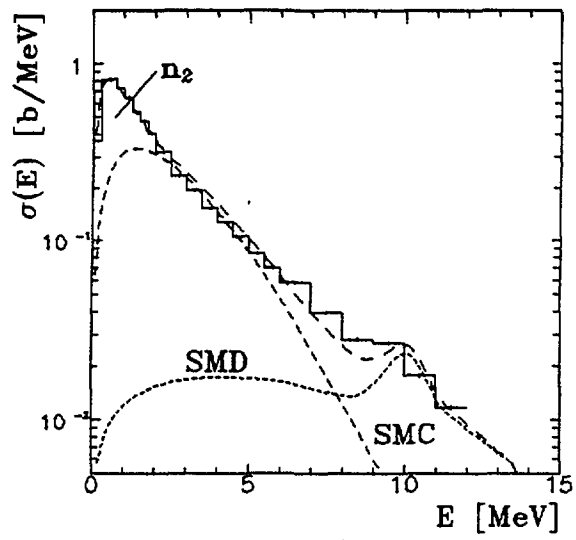


**Fig. 7:** Comparison of the evaluated experimental $\sigma(E)$ for $E_o$ = 14.1 MeV neutron incidence energy (solid histogram) with a statistical model calculation using the EXIFON-code.

## 4. Conclusions

Evaluated experimental DDX were derived from the recent DDX-experiments for $^{51}V$ at 14.1 MeV incidence energy with an accuracy needed for fusion reactor design. They deviate from the evaluated data of the libraries ENDF/B-VI and ENDL-83. Statistical model calculations with the code EXIFON are in good agreement with the data obtained and may be used for data calculation at lower incidence energies.

## References

[1] Nuclear Data for Fusion Reactor Technology, in Proc. Adv. Group Meeting of the IAEA, Gaussig 1986, IAEA-TECDOC-487, IAEA, Vienna, 1988

[2] H. Al Obiesi et al., in Proc. Int. Conf. on Nuclear Data for Science and Technology, 13 - 17 May 1991, Juelich, in press

[3] A. Takahashi et al., OKTAVIAN-Report A-87-03, Osaka University (1987)

[4] M. Baba et al., JAERI-01-88-065, p. 365, Tokai, 1988

[5] H. Al Obiesi et al., INDC(GDR)-058/L, IAEA, Vienna, 1988

[6] H. Kalka, INDC(GDR)-059/L, IAEA, Vienna, 1990

[7] A. Pavlik and H. Vonach, Physics Data 13 – 4 (1988)

[8] S. Tagesen et al., Physics Data 13 – 1 (1979)

[9] T. Elfruth and T. Hehl, Programme EVALUATE - An Evaluation Programme for DDX, TU Dresden, 1990, unpublished

# Measurement, Evaluation and Analysis of 14.1 MeV Neutron Induced Double-Differential Neutron Emission Cross Sections of $^{238}U$

T. Elfruth, K. Seidel, S. Unholzer
Technische Universität Dresden
Institut für Kern- und Atomphysik
Mommsenstraße 13, D-O-8027 Dresden
Germany

**Abstract:** Double-differential neutron emission cross sections of $^{238}U$ have been measured at 14.1 MeV neutron incidence energy. Evaluated double-differential neutron emission cross sections are derived from all available experimental data and compared with the evaluated data of nuclear data libraries. Discrepancies larger than the data accuracy needed are observed. A theoretical analysis of the neutron emission at 14 MeV reveals that pre-equilibrium emission components are not adequately included in the library data. The model used for the interpretation consistently describes the neutron emission at lower incidence energies too.

## 1 Introduction

Double-differential neutron emission cross sections (DDX) are of major importance for the design of D-T fusion reactor components. In particular, for fusion-fission hybrid reactor projects the 14 MeV neutron induced emission cross sections of $^{238}U$ are of interest. Moreover, the 14 MeV data are reference point for the evaluation of DDX at lower incidence energies. The data are needed with accuracies of $\lesssim$ 10 % [1].
In the present work DDX of $^{238}U$ are measured at 14.1 MeV incidence energy. These data and all other available experimental results are used to derive evaluated experimental DDX. It will be shown that evaluated data of libraries deviate from these evaluated experimental cross sections more than the accuracy needed, especially at higher emission energies. The data are analysed with a statistical model of multistep-direct and multistep-compound reactions.

## 2 Measurement

Neutron emission spectra were measured with time-of-flight spectroscopy at a pulsed D-T neutron generator. The experimental arrangement is shown in Fig. 1. The neutron flight-path was about 5 m. Neutron emission spectra from a ring sample (inner diameter 8 cm; outer diameter 12 cm, thickness 0.6 cm) were taken at emission angles $\vartheta = 15^o \cdots 165^o$ in steps of 15°. The flight-path was arranged perpendicularly to the deuteron beam to minimize the influence of the neutron source anisotropy on the neutron emission spectra. The neutron generation was determined by counting the $\alpha$-particles of the source reaction. The data corrected for differential nonlinearity of the spectrometer, dead time, uncorrelated background, source anisotropy, flux attenuation and multiple scattering in the sample were transformed from time to energy spectra. The peak of the elastically scattered neutrons was separated from the spectrum of inelastically scattered neutrons using the experimental peak shape. More details are described in Ref. [2] and in a contribution to this meeting.

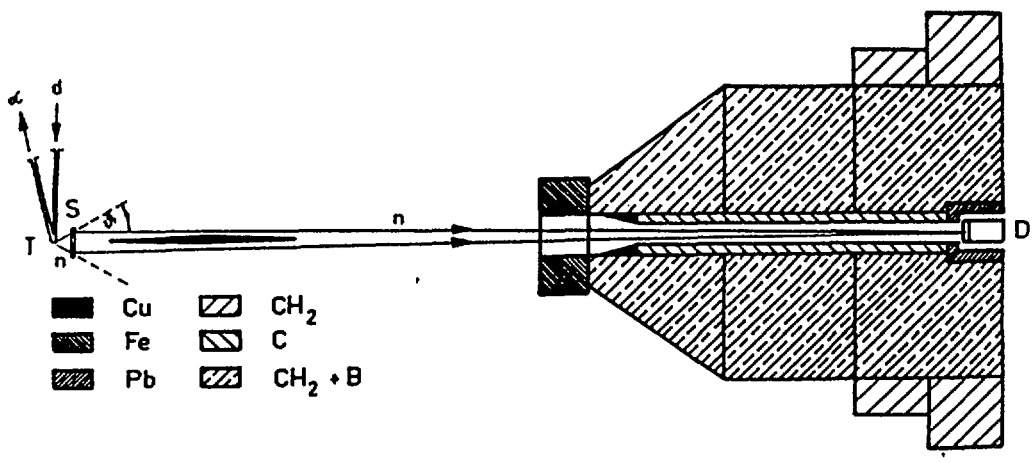


**Fig. 1:** Set-up for the measurement of double-differential neutron emission cross sections. T - $^3$H(d,n) pulsed neutron source; S - sample ring; $\vartheta$ - neutron emission angle; D - neutron time-of-flight detector

The obtained experimental results are compared in Fig. 2 with available experimental data sets of other groups.
The systematic uncertainties of the present data were found to be

| | | |
|---|---|---|
| due to source strength determination | 4 | %, |
| detector effiency determination | 5 | %, |
| and finite sample size correction | 3 | %. |

## 3 Evaluation

Experimental data were published by Kammerdiener [3], Voignier et al. [4], Shen Guanren et al. [5] and Degtjarev et al. [6]. If necessary, the data were corrected to the neutron incidence energy of 14.1 MeV. Following the procedure of Pavlik and Vonach [7] the energy-differential neutron spectrum at a fixed emission angle was divided into a part dominated by emissions from separated levels and in a continuum part of emissions. After separation of the continuous part the "level part" of the spectrum was shifted according to the Q-values in the (n,n')-processes. The continuous part was corrected by statistical model calculations described below. After this, group-averaged DDX were derived for an error-weighted fit with the function

$$\sigma(E,\vartheta) = \frac{\sigma(E)}{4\pi} \sum_{l=0}^{l_{max}} (2 \cdot l + 1) \cdot f_l \cdot P_l(cos(\vartheta))$$

To realize a linear equation of the fit parameters the coefficients $a_l$, with

$$a_i = \frac{\sigma(E)}{4\pi} \cdot (2 \cdot l + 1) \cdot f_i \ ,$$

were used as fit parameters.
In the analysis of the experimental data the uncertainties of the data were divided into short-range errors (e.g. statistical errors given by the authors), long-range errors (full correlation over the whole emission energy range, e.g. source strength uncertainty) and medium-range errors (correlation length of several MeV, e.g. uncertainties of the detector efficiency or finite sample size corrections).

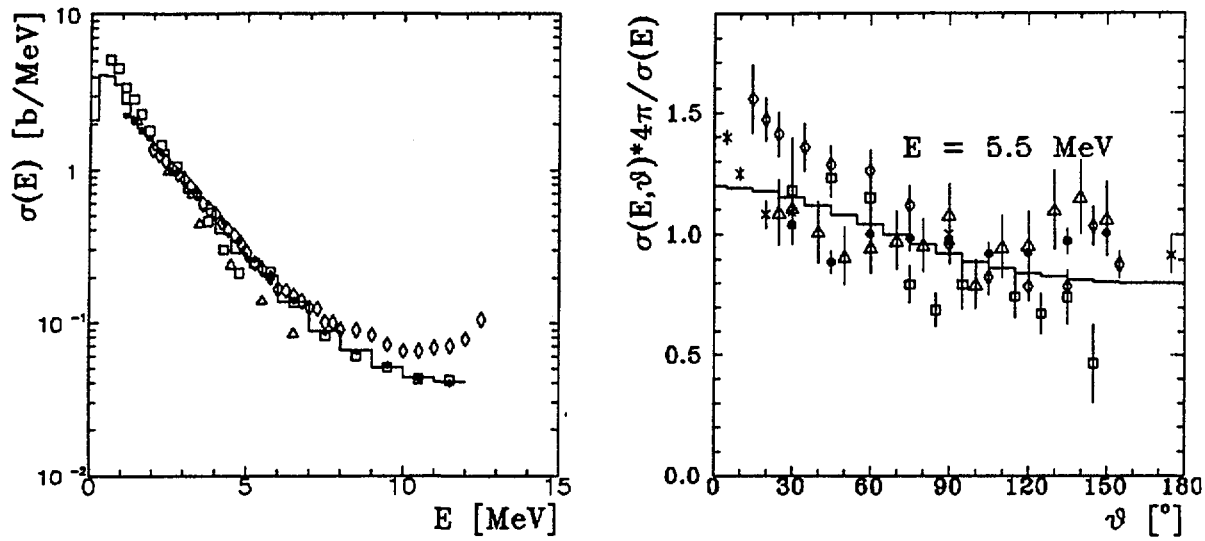


**Fig. 2:** Energy distribution of the neutrons emitted after 14.1 MeV neutron bombardment and relative angular distribution at 5.5 MeV neutron emission energy.
Experimental data: □ [3], △ [4], ◇ [5], * [6], (•) present work; evaluated data: histogram ;

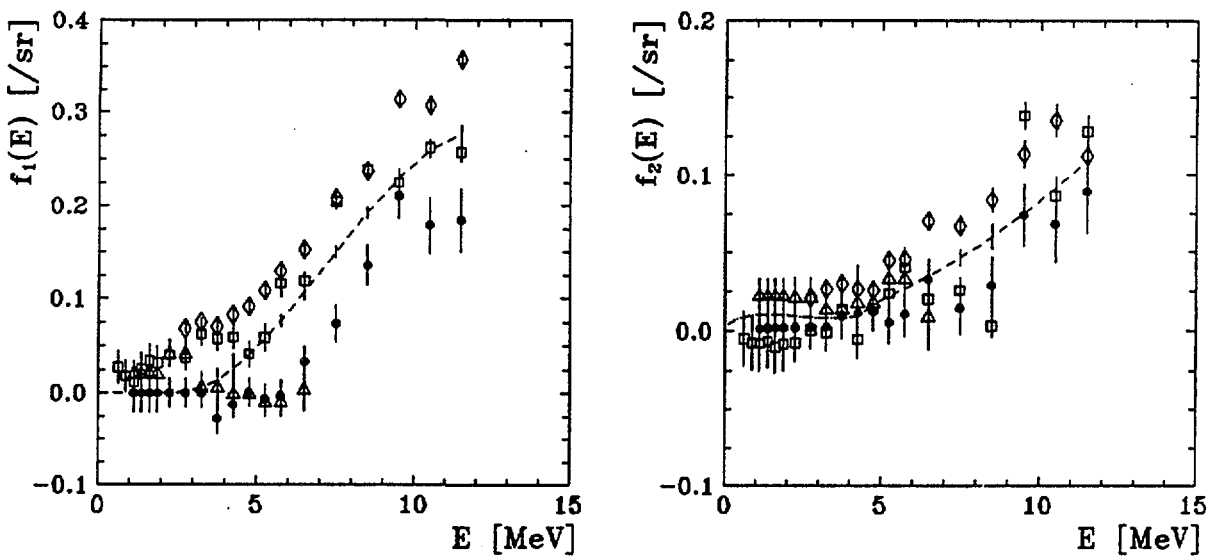


**Fig. 3:** Legendre coeffients $f_1$ and $f_2$ of the neutron emission
Experimental data: □ [3], △ [4], ◇ [5], * [6], (•) present work; evaluated data: dashed line)

In addition to the uncertainties given by the authors themselves the following drawbacks of the experiments were fixed as additional systematic errors:

- Ref. [3] (used for E > 1 MeV)
  - artificial structure in the spectra around 5 MeV and different slopes below and above;
  - step-like angular distributions.
- Ref. [4] (used for the evaluation of the $f_l$'s, only)
  - energy groups of 1 MeV width;
  - large deviations from the results of the other experiments (also for other nuclides and especially at lower energies).

- Ref. [5]
  - energy resolution in the high-energy part;
  - no peak separation of the elastically scattered neutrons.
- In all experiments the error of the detector efficiency was enlarged by 5 % in the vicinity of the detection threshold;

The results of the DDX-evaluation carried out with the programme EVALUATE [9] are given in Tables 1 - 3.

**Table 1:** Evaluated experimental $\sigma$(E), $f_1$ and $f_2$ for $^{238}$U at $E_o$ = 14.1 MeV

| E [MeV] | σ[b/MeV] | δσ[%] | $f_1$[/sr] | δ$f_1$[%] | $f_2$[/sr] | δ$f_2$[%] |
|---|---|---|---|---|---|---|
| 0.00 - 0.25 | 0.21210E+01 | | 0.11200E-02 | | 0.45110E-02 | |
| 0.25 - 0.50 | 0.40910E+01 | | 0.71100E-03 | | 0.70080E-02 | |
| 0.50 - 0.75 | 0.40540E+01 | | 0.11750E-02 | | 0.86000E-02 | |
| 0.75 - 1.00 | 0.35910E+01 | 4.29 | 0.17790E-02 | | 0.97200E-02 | |
| 1.00 - 1.25 | 0.26900E+01 | 2.80 | 0.25410E-02 | | 0.10320E-01 | |
| 1.25 - 1.50 | 0.21969E+01 | 1.79 | 0.34930E-02 | | 0.10500E-01 | |
| 1.50 - 1.75 | 0.18727E+01 | 1.79 | 0.46310E-02 | | 0.10400E-01 | |
| 1.75 - 2.00 | 0.16452E+01 | 1.78 | 0.59790E-02 | | 0.10080E-01 | |
| 2.00 - 2.50 | 0.13494E+01 | 1.67 | 0.84570E-02 | | 0.94250E-02 | |
| 2.50 - 3.00 | 0.97323E+00 | 1.10 | 0.12670E-01 | | 0.85995E-02 | |
| 3.00 - 3.50 | 0.70523E+00 | 0.97 | 0.18080E-01 | | 0.81500E-02 | |
| 3.50 - 4.00 | 0.55262E+00 | 1.04 | 0.24900E-01 | | 0.95270E-02 | |
| 4.00 - 4.50 | 0.38598E+00 | 1.11 | 0.33327E-01 | | 0.91091E-02 | |
| 4.50 - 5.00 | 0.28614E+00 | 1.12 | 0.40559E-01 | 25.19 | 0.17278E-01 | 25.21 |
| 5.00 - 5.50 | 0.25577E+00 | 1.10 | 0.57465E-01 | 11.77 | 0.21728E-01 | 21.84 |
| 5.50 - 6.00 | 0.20461E+00 | 1.16 | 0.76235E-01 | 8.31 | 0.26568E-01 | 12.02 |
| 6.00 - 7.00 | 0.13689E+00 | 1.09 | 0.10688E+00 | 7.89 | 0.34529E-01 | 13.17 |
| 7.00 - 8.00 | 0.88320E-01 | 1.15 | 0.14997E+00 | 3.89 | 0.46492E-01 | 10.36 |
| 8.00 - 9.00 | 0.65667E-01 | 1.25 | 0.19223E+00 | 3.09 | 0.59988E-01 | 13.22 |
| 9.00 - 10.00 | 0.50621E-01 | 1.44 | 0.22997E+00 | 3.88 | 0.75016E-01 | 6.57 |
| 10.00 - 11.00 | 0.43514E-01 | 1.49 | 0.25952E+00 | 3.23 | 0.91577E-01 | 8.11 |
| 11.00 - 12.00 | 0.40713E-01 | 1.76 | 0.27718E+00 | 3.30 | 0.10967E+00 | 8.24 |

For energies below 1 MeV the spectrum was calculated using the statistical model described below.
For the calculation of the relative $\sigma$(E) correlation matrix the procedure of Vonach et al. [7,8] was adopted. The correlation length for the medium-range errors was assumed to be 4 MeV.

Results of the evaluation are compared in Fig. 4 with data of the libraries ENDL-83 and ENDF/B-VI. Discrepancies are observed in $\sigma$(E) for E > 8 MeV and to some degree in the whole spectrum shape. The shape of the angular distribution at 5.5 MeV is well described by the ENDF/B-VI data, the data of ENDL-83 and older libraries show isotropy.

# 4 Analysis

$\sigma$(E) is calculated as sum of cross sections $\sigma_i$(E) of all possible neutron emission chances $n_i$. As shown in Fig. 5 at each stage of the deexciting system, neutron emission competes with $\gamma$-emission, and also with fission additionally leading to fission neutrons ($n_f$). The $n_1$ are assumed to be emitted in the pre-equilibrium and in the equlibrium phase of the reaction. Pre-equilibrium neutrons arise from multistep-direct (SMD) and from multistep-compound (SMC) processes. Their statistical treatment with the code EXIFON [10] includes as one- and two-step direct processes both, single-particle and collective excitations ($2^+$ and $3^-$

Table 2: Relative correlation matrix of $\sigma$(E)

| energy [MeV] | 0.00 - 0.25 | 0.25 - 0.50 | 0.50 - 0.75 | 0.75 - 1.00 | 1.00 - 1.25 | 1.25 - 1.50 | 1.50 - 1.75 | 1.75 - 2.00 |
|---|---|---|---|---|---|---|---|---|
| 0.00 - 0.25 | 100.0 | 100.0 | 100.0 | 100.0 | 0.0 | 0.0 | 0.0 | 0.0 |
| 0.25 - 0.50 | | 100.0 | 100.0 | 100.0 | 0.0 | 0.0 | 0.0 | 0.0 |
| 0.50 - 0.75 | | | 100.0 | 100.0 | 0.0 | 0.0 | 0.0 | 0.0 |
| 0.75 - 1.00 | | | | 100.0 | 0.0 | 0.0 | 0.0 | 0.0 |
| 1.00 - 1.25 | | | | | 100.0 | 90.2 | 89.2 | 86.9 |
| 1.25 - 1.50 | | | | | | 100.0 | 89.3 | 87.5 |
| 1.50 - 1.75 | | | | | | | 100.0 | 87.7 |
| 1.75 - 2.00 | | | | | | | | 100.0 |

| energy [MeV] | 2.00 - 2.50 | 2.50 - 3.00 | 3.00 - 3.50 | 3.50 - 4.00 | 4.00 - 4.50 | 4.50 - 5.00 | 5.00 - 5.50 | 5.50 - 6.00 |
|---|---|---|---|---|---|---|---|---|
| 0.00 - 0.25 | 0.0 | 0.0 | 0.0 | 0.0 | 0.0 | 0.0 | 0.0 | 0.0 |
| 0.25 - 0.50 | 0.0 | 0.0 | 0.0 | 0.0 | 0.0 | 0.0 | 0.0 | 0.0 |
| 0.50 - 0.75 | 0.0 | 0.0 | 0.0 | 0.0 | 0.0 | 0.0 | 0.0 | 0.0 |
| 0.75 - 1.00 | 0.0 | 0.0 | 0.0 | 0.0 | 0.0 | 0.0 | 0.0 | 0.0 |
| 1.00 - 1.25 | 83.4 | 91.8 | 93.7 | 81.3 | 71.6 | 64.7 | 56.8 | 51.0 |
| 1.25 - 1.50 | 84.8 | 94.1 | 96.2 | 84.4 | 74.9 | 68.1 | 59.7 | 53.7 |
| 1.50 - 1.75 | 85.7 | 95.7 | 98.2 | 87.0 | 77.9 | 71.2 | 62.6 | 56.4 |
| 1.75 - 2.00 | 86.2 | 97.0 | 99.6 | 89.5 | 81.0 | 74.7 | 65.3 | 58.7 |
| 2.00 - 2.50 | 100.0 | 99.7 | 100.0 | 94.6 | 87.3 | 81.8 | 71.0 | 63.6 |
| 2.50 - 3.00 | | 100.0 | 82.5 | 77.4 | 68.0 | 63.1 | 56.0 | 49.3 |
| 3.00 - 3.50 | | | 100.0 | 77.7 | 69.7 | 66.3 | 60.6 | 54.8 |
| 3.50 - 4.00 | | | | 100.0 | 70.0 | 68.3 | 62.2 | 56.2 |
| 4.00 - 4.50 | | | | | 100.0 | 65.6 | 60.5 | 55.3 |
| 4.50 - 5.00 | | | | | | 100.0 | 62.8 | 58.1 |
| 5.00 - 5.50 | | | | | | | 100.0 | 58.0 |
| 5.50 - 6.00 | | | | | | | | 100.0 |

| energy [MeV] | 6.00 - 7.00 | 7.00 - 8.00 | 8.00 - 9.00 | 9.00 -10.00 | 10.00 -11.00 | 11.00 -12.00 |
|---|---|---|---|---|---|---|
| 0.00 - 0.25 | 0.0 | 0.0 | 0.0 | 0.0 | 0.0 | 0.0 |
| 0.25 - 0.50 | 0.0 | 0.0 | 0.0 | 0.0 | 0.0 | 0.0 |
| 0.50 - 0.75 | 0.0 | 0.0 | 0.0 | 0.0 | 0.0 | 0.0 |
| 0.75 - 1.00 | 0.0 | 0.0 | 0.0 | 0.0 | 0.0 | 0.0 |
| 1.00 - 1.25 | 42.6 | 29.8 | 20.5 | 13.8 | 10.3 | 7.2 |
| 1.25 - 1.50 | 45.2 | 31.7 | 21.8 | 14.7 | 10.8 | 7.5 |
| 1.50 - 1.75 | 47.9 | 33.6 | 23.1 | 15.6 | 11.3 | 7.7 |
| 1.75 - 2.00 | 50.5 | 35.7 | 24.5 | 16.6 | 11.9 | 8.0 |
| 2.00 - 2.50 | 56.6 | 40.7 | 28.3 | 19.7 | 14.0 | 9.3 |
| 2.50 - 3.00 | 39.9 | 26.9 | 17.0 | 9.5 | 6.2 | 6.0 |
| 3.00 - 3.50 | 45.7 | 32.5 | 21.5 | 13.1 | 9.2 | 9.2 |
| 3.50 - 4.00 | 48.2 | 34.6 | 22.5 | 13.7 | 9.2 | 9.2 |
| 4.00 - 4.50 | 48.6 | 35.9 | 23.4 | 14.5 | 9.5 | 9.8 |
| 4.50 - 5.00 | 53.3 | 40.5 | 26.6 | 17.0 | 10.9 | 10.8 |
| 5.00 - 5.50 | 54.4 | 42.4 | 28.8 | 18.8 | 12.2 | 11.4 |
| 5.50 - 6.00 | 54.7 | 44.1 | 30.9 | 21.0 | 13.8 | 12.8 |
| 6.00 - 7.00 | 100.0 | 48.3 | 35.0 | 25.5 | 16.6 | 16.8 |
| 7.00 - 8.00 | | 100.0 | 36.0 | 29.7 | 19.8 | 20.0 |
| 8.00 - 9.00 | | | 100.0 | 27.9 | 19.8 | 23.0 |
| 9.00 - 10.00 | | | | 100.0 | 23.5 | 30.3 |
| 10.00 - 11.00 | | | | | 100.0 | 32.0 |
| 11.00 - 12.00 | | | | | | 100.0 |

phonons). The SMC-neutron emission is calculated by solving the master equation from 5-exciton states up to the equilibrium of excited particles and holes. The $n_2$ and $n_3$ are emitted from the equilibrated system. The $n_f$ are evaporated from the accelerated fragments. Not specific input parameters, but a surface-delta interaction of $V_o$ = 19.4 MeV, $r_o$ = 1.4 fm, the single-particle level density g = A/13 $MeV^{-1}$ and phonon data from mass-number dependent systematics are used. The angular distribution is calculated with the assumption that the SMD-component is anisotropic and can be parametrized with the Kalbach-Mann-formula. A detailed description of the calculation procedure for $^{238}U$ can be found in Ref. [11].

**Table 3:** Relative covariance matrices of the fit parameters $a_0$, $a_1$, $a_2$

E = 0.00 - 0.25 MeV

| i\k | 0 | 1 | 2 |
|---|---|---|---|
| 0 | 100.0 | | |
| 1 | | | |
| 2 | | | |

E = 0.25 - 0.50 MeV

| i\k | 0 | 1 | 2 |
|---|---|---|---|
| 0 | 100.0 | | |
| 1 | | | |
| 2 | | | |

E = 0.50 - 0.75 MeV

| i\k | 0 | 1 | 2 |
|---|---|---|---|
| 0 | 100.0 | | |
| 1 | | | |
| 2 | | | |

E = 0.75 - 1.00 MeV

| i\k | 0 | 1 | 2 |
|---|---|---|---|
| 0 | 100.0 | | |
| 1 | | | |
| 2 | | | |

E = 1.00 - 1.25 MeV

| i\k | 0 | 1 | 2 |
|---|---|---|---|
| 0 | 100.0 | -4.1 | -4.6 |
| 1 | | 100.0 | -3.3 |
| 2 | | | 100.0 |

E = 1.25 - 1.50 MeV

| i\k | 0 | 1 | 2 |
|---|---|---|---|
| 0 | 100.0 | -4.0 | -4.4 |
| 1 | | 100.0 | -3.3 |
| 2 | | | 100.0 |

E = 1.50 - 1.75 MeV

| i\k | 0 | 1 | 2 |
|---|---|---|---|
| 0 | 100.0 | -4.1 | -4.0 |
| 1 | | 100.0 | -3.5 |
| 2 | | | 100.0 |

E = 1.75 - 2.00 MeV

| i\k | 0 | 1 | 2 |
|---|---|---|---|
| 0 | 100.0 | -5.4 | -3.2 |
| 1 | | 100.0 | -4.2 |
| 2 | | | 100.0 |

E = 2.00 - 2.50 MeV

| i\k | 0 | 1 | 2 |
|---|---|---|---|
| 0 | 100.0 | -6.8 | -2.9 |
| 1 | | 100.0 | -5.5 |
| 2 | | | 100.0 |

E = 2.50 - 3.00 MeV

| i\k | 0 | 1 | 2 |
|---|---|---|---|
| 0 | 100.0 | -9.3 | -22.4 |
| 1 | | 100.0 | -22.7 |
| 2 | | | 100.0 |

E = 3.00 - 3.50 MeV

| i\k | 0 | 1 | 2 |
|---|---|---|---|
| 0 | 100.0 | -9.0 | -22.0 |
| 1 | | 100.0 | -27.3 |
| 2 | | | 100.0 |

E = 3.50 - 4.00 MeV

| i\k | 0 | 1 | 2 |
|---|---|---|---|
| 0 | 100.0 | -13.6 | -16.8 |
| 1 | | 100.0 | -30.4 |
| 2 | | | 100.0 |

E = 4.00 - 4.50 MeV

| i\k | 0 | 1 | 2 |
|---|---|---|---|
| 0 | 100.0 | -12.6 | -10.8 |
| 1 | | 100.0 | -27.3 |
| 2 | | | 100.0 |

E = 4.50 - 5.00 MeV

| i\k | 0 | 1 | 2 |
|---|---|---|---|
| 0 | 100.0 | -13.1 | -11.0 |
| 1 | | 100.0 | -24.9 |
| 2 | | | 100.0 |

E = 5.00 - 5.50 MeV

| i\k | 0 | 1 | 2 |
|---|---|---|---|
| 0 | 100.0 | -6.5 | -8.9 |
| 1 | | 100.0 | -21.0 |
| 2 | | | 100.0 |

E = 5.50 - 6.00 MeV

| i\k | 0 | 1 | 2 |
|---|---|---|---|
| 0 | 100.0 | -2.2 | -2.1 |
| 1 | | 100.0 | -11.5 |
| 2 | | | 100.0 |

E = 6.00 - 7.00 MeV

| i\k | 0 | 1 | 2 |
|---|---|---|---|
| 0 | 100.0 | 0.8 | 3.0 |
| 1 | | 100.0 | -9.7 |
| 2 | | | 100.0 |

E = 7.00 - 8.00 MeV

| i\k | 0 | 1 | 2 |
|---|---|---|---|
| 0 | 100.0 | 19.2 | 2.2 |
| 1 | | 100.0 | 4.2 |
| 2 | | | 100.0 |

E = 8.00 - 9.00 MeV

| i\k | 0 | 1 | 2 |
|---|---|---|---|
| 0 | 100.0 | 33.0 | 1.0 |
| 1 | | 100.0 | 18.8 |
| 2 | | | 100.0 |

E = 9.00 - 10.00 MeV

| i\k | 0 | 1 | 2 |
|---|---|---|---|
| 0 | 100.0 | 30.9 | 29.9 |
| 1 | | 100.0 | 20.5 |
| 2 | | | 100.0 |

E = 10.00 - 11.00 MeV

| i\k | 0 | 1 | 2 |
|---|---|---|---|
| 0 | 100.0 | 44.1 | 26.3 |
| 1 | | 100.0 | 27.9 |
| 2 | | | 100.0 |

E = 11.00 - 12.00 MeV

| i\k | 0 | 1 | 2 |
|---|---|---|---|
| 0 | 100.0 | 56.8 | 41.9 |
| 1 | | 100.0 | 42.1 |
| 2 | | | 100.0 |

Results of the calculations for $E_o$ = 14.1 MeV are shown in Fig. 6 together with the evaluated experimental cross sections. Energy spectrum and angular distribution of the neutron emission are well described by the model.

To check the adopted model and the global input parameters used at lower incidence energies the neutron emission spectra were calculated for $E_o = 6 \cdots 9.6$ MeV and are compared in Fig. 7 with experimental data. Additionally, the emission of neutrons from U in coincidence with fission events was calculated for $E_o = 6 \cdots 14.2$ MeV and is compared with experimental results. Angular distributions are discussed in Ref. [12]. The agreement of all calculated spectra and angular distributions with the experimental data is sufficient. Summarizing can be concluded that the model used describes the main emission components adequately.

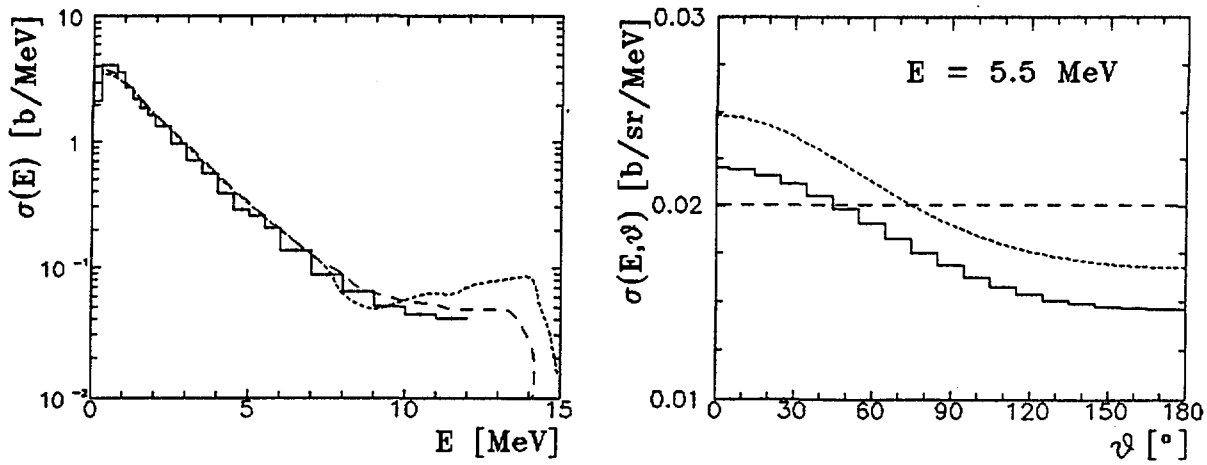


**Fig. 4:** Comparison of $\sigma$(E) and of the DDX at E = 5.5 MeV as evaluated from the experimental data at $E_o$ = 14.1 MeV neutron incidence energy (solid histogram) with the data of the libraries ENDF/B-VI (short-dashed line) and ENDL-83 (dashed line).

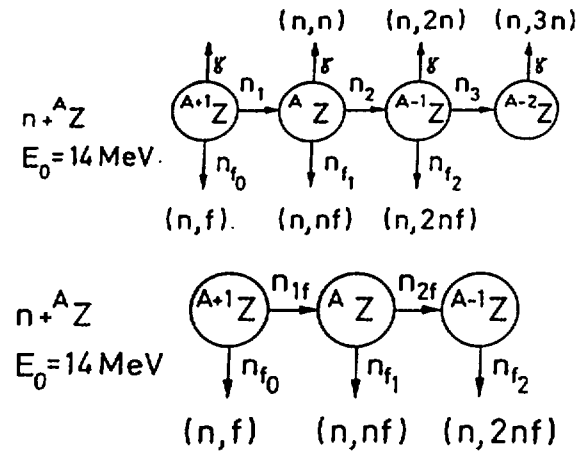


**Fig. 5:** Chances of neutron emission of a heavy nucleus (mass number A, proton number Z) bombarded with 14 MeV neutrons.
Upper part: all chances. Lower part: only those chances having a coincidence with fission

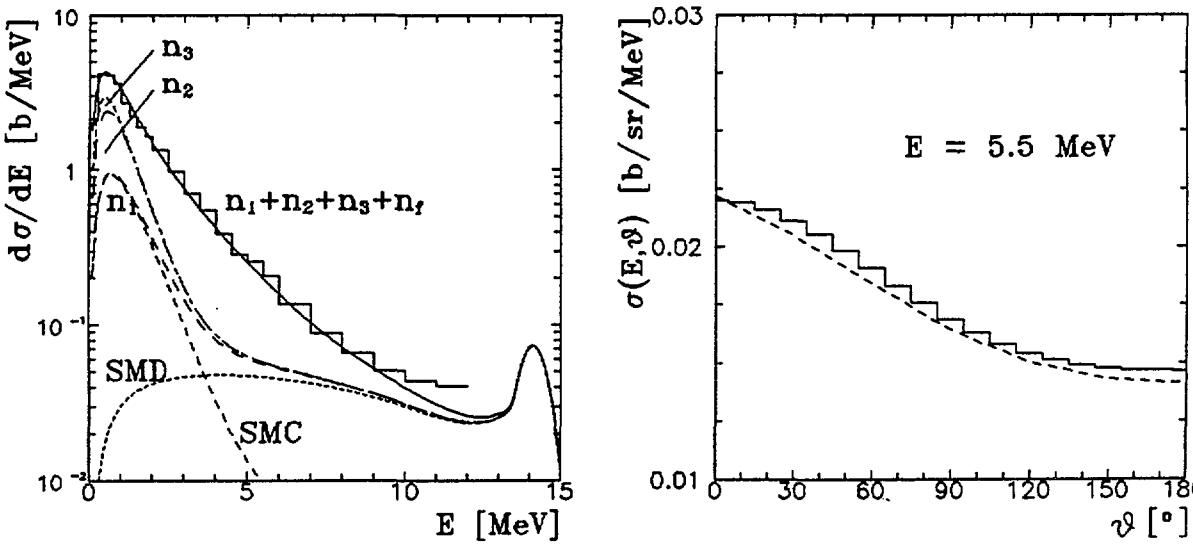


**Fig. 6:** Comparison of the calculated $\sigma$(E) and DDX at E = 5.5 MeV for $E_o$ = 14.1 MeV neutron incidence energy with the evaluated experimental data (histogram).

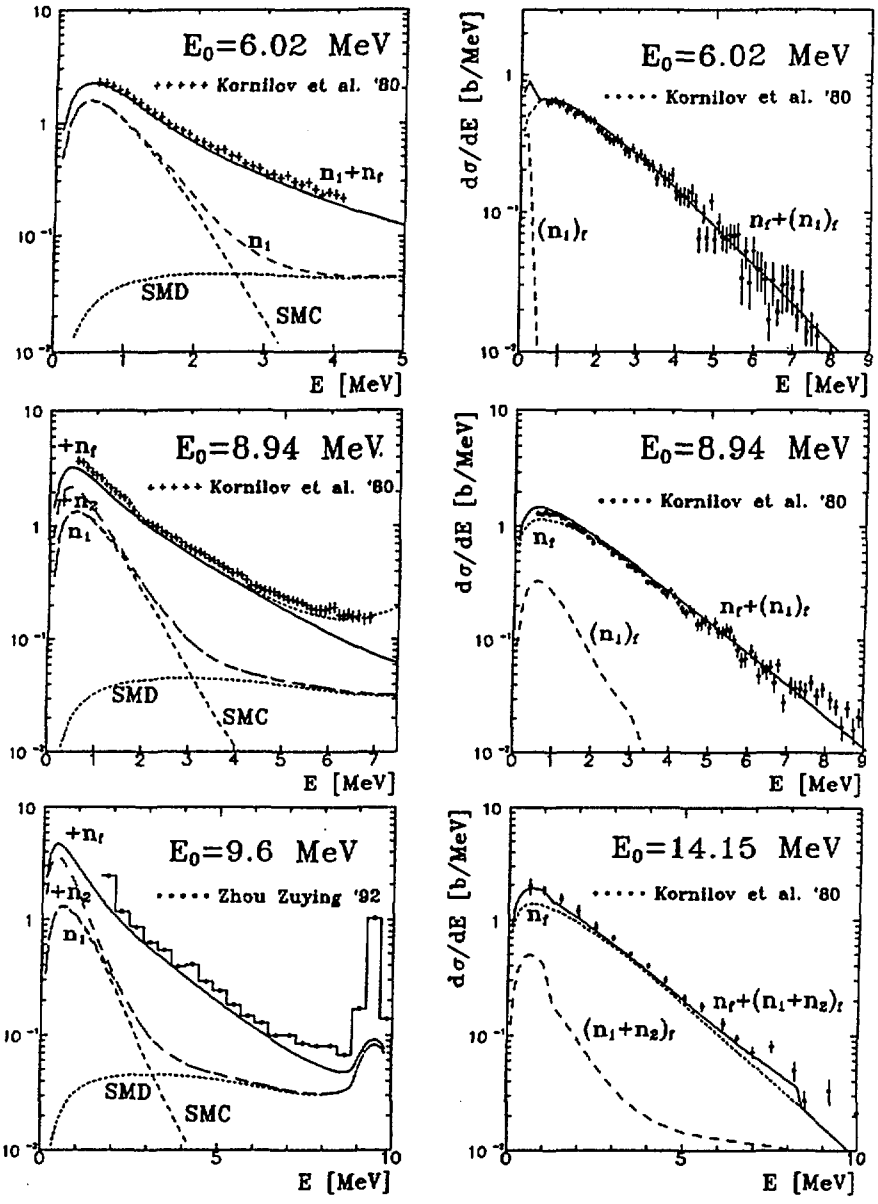


**Fig. 7:** Calculated neutron emission cross sections compared with experimental data. Designation of the components see Fig. 5. Left hand: total emission (exp. data of Ref. [13] (+) and Ref. [14],respectively). Right hand: emission in coincidence with fission (exp. data of Ref. [13])

# 5 Conclusions

Double-differential neutron emission cross sections for $^{238}$U were measured at 14.1 MeV neutron incidence energy. Together with other available data sets the evaluated neutron emission cross sections at $E_o$ = 14.1 MeV were derived. This evaluated cross sections deviate from the library data in some ranges. The origin of the differences is found in the library data, where pre-equilibrium emission components are not taken into account with the accuracy needed. Reaction models like the SMD/SMC-model describe, even with global parameters, the experimental neutron emission cross sections with sufficient quality and can be used to improve the library data. This conclusion should be valid in principle not only for $^{238}$U investigated in the present paper, but for all medium and heavy mass nuclei (with exception of magic nuclei, where shell corrected parameter have to be used).

## References


[1] Nuclear Data for Fusion Reactor Technology, in Proc. Adv. Group Meeting of the IAEA, Gaussig 1986, IAEA-TECDOC-487, IAEA, Vienna, 1988

[2] H. Al Obiesi et al., INDC(GDR)-058/L, IAEA, Vienna, 1990

[3] J.L. Kammerdiener, Thesis, UCRL-51232, Livermore, 1972

[4] J. Voignier et al., CEA-3503 (1968) and EXFOR 21094.004 (1980)

[5] S. Guanren, in Proc. Adv. Group Meeting on Nuclear Theory for Application, Bejing, 1987

[6] D. J. Degtjarev et al., Jadernaja Fizika **34**(1981)299

[7] A. Pavlik and H. Vonach, Physics Data **13 – 4** (1988)

[8] S. Tagesen et al., Physics Data **13 – 1** (1979)

[9] T. Elfruth and T. Hehl, Programme EVALUATE - An Evaluation Programme for DDX, TU Dresden, 1990, unpublished

[10] H. Kalka, INDC(GDR)-059/L, IAEA, Vienna, 1990

[11] T. Hehl, Thesis, TU Dresden, 1990

[12] H. Al Obiesi et al., in Proc. Int. Conf. on Nuclear Data for Science and Technology, 13 - 17 May 1991, Juelich, in press

[13] V. Kornilov et al., in Proc. Conf. on Neutron Physics, 1980, Kiev, Vol. 3, p. 104, Moskva, 1980

[14] Zhou Zuying, private communication, 1992

# Evaluation of the Double-Differential Cross Sections for JENDL Fusion File

Satoshi Chiba, Baosheng Yu* and Tokio Fukahori

Japan Atomic Energy Research Institute
Tokai-mura, Naka-gun, Ibaraki-ken 319-11, Japan

* China Institute of Atomic Energy
Beijing, People's Republic of China

**Abstract**

In order to improve accuracy of the neutron DDX (double differential cross section) data stored in JENDL-3, preparation of JENDL Fusion File is in progress as a part of post JENDL-3 special purpose file activities. The main effort is placed to adopt the energy-angle correlation of neutrons seen in observed data into the evaluated data library. JENDL Fusion File is also intended to contain the DDX of secondary charged particles, which is required in material damage study as basic data for primary knock-on atom spectra (PKAS) and kinetic energy release in materials (KERMA) calculations. The DDXs are calculated by known systematics, and expressed by a compact form in ENDF-6 format. The multistep statistical model was used to calculate various quantities required in the evaluation.

## 1. Introduction

The DDX data are important as a basic information which determines main characteristics of neutron fields in fission and fusion reactor technologies. The neutrons produced from fission or fusion reaction lose their energy by interacting with surrounding nuclei, causing damage by recoil of structural materials, nuclear transmutation, radio-activities, gamma-heating, multiplication, tritium production, etc. All of these processes occur in different rate with respect to energy of the neutrons. On the other hand, the DDX contains information on the dynamics of n + target system, which is also quite interesting in understanding the nucleon many body system. Therefore, detailed knowledge on DDX is significantly required from both the application and basic sciences.

In JENDL-3[1], the DDXs are not given explicitly, so they must be constructed as a product of cross section, angular distribution and energy distribution given independently in MF=3, 4 and 5, respectively. This representation, however, cannot reproduce the energy-angle correlation which is clearly observed in the energy region where the preequilibrium process is dominant[2], and was claimed to be inadequate from both the differential and integral benchmarking[3]. Furthermore, it was also pointed out that the DDXs of secondary charged particles, which are not contained in JENDL-3, are also strongly desirable and therefore be evaluated, because these data are essential in material damage studies as basic data in calculating PKA spectra and KERMA[4]. Then, it was decided by JENDL compilation group

to prepare a special purpose file, JENDL Fusion File, to improve accuracy of the DDX of secondary neutrons as well as that of charged particles to remove these drawbacks of JENDL-3. From discussions with data users, it was decided to include the following elements and their isotopes in JENDL Fusion File: Li, Be, B, C, O, Al, Si, Ca, Ti, Cr, Mn, Fe, Co, Ni, Cu, Ge, As, Zr, Nb, Mo, Sn, Sb, W, Pb and Bi. The project of evaluating JENDL Fusion File was initiated in late 1990. It is intended to be finished by April 1993.

In this paper, basic strategies and requirements for JENDL Fusion File is explained, and general outline of the evaluation method for medium heavy nuclei (heavier than Al) will be given. Evaluation for lighter nuclei will be done completely differently, but it is not decided yet. Some of the results of the evaluation are also presented.

## 2. Basic Strategies and Requirements

After the evaluation of JENDL-3 was completed in 1989, a lot of integral benchmark tests have been carried out for thermal reactors, fast reactors, fusion reactors and shielding problems[3-5]. It was found that JENDL-3 generally gives good C/E results in many cases, establishing the fact that the data given in JENDL-3 is fairly well balanced as a set of nuclear constants. For example, the volume dependency of sodium void coefficient, which was found in JENDL-2, was almost completely removed in JENDL-3. Similar good results were also found in fusion benchmarking. Therefore, it was strongly required to keep the quantities given in JENDL-3 unchanged as much as possible. This requirement put strong constraint in determining the method of evaluating JENDL Fusion File.

In the present work, the double-differential cross sections of about 100 nuclei have to be evaluated by a few evaluators in a few years. Therefore, the evaluation method must be fairly simple and quick. However, it must be reasonably accurate and flexible so as to reflect upon the characteristics of the nuclei participating in the multistep reactions. Particuarly, the discrete level structures and level density parameters must be treated accurately.

The energy-angle correlation appearing in the observed DDX can be theoretically dealt with by several quantum mechanical models (e.g., Refs. 6, 7, 8) or by semi-classical models (e.g., Refs. 9, 10). These theories, however, usually do not meet the requirements explained above, because of the need of a lot of input data, long computation time, inability to predict the whole aspect of the double-differential spectra or to treat the details of level structures. Because of these reasons, it must be concluded at present that these theoretical methods are unfortunately impractical in nuclear data evaluation where a huge amount of computation is needed mostly in trial-and-error base to provide the data for many nuclei (about 100 in this work) in the energy region from $10^{-5}$ eV to 20 MeV. On the other hand, several systematics are available to calculate DDX rather quickly, and it is known that some of these can give quite good agreement with the experimental DDX at 14 MeV[11]. Therefore, we decided to use the systematics in the present evaluation. As described in Ref. 11, the systematics derived by Kumabe et al.[12] was mainly used for the neutron DDX, while that of Kalbach[13] was adopted for the secondary charged particles.

The energy differential cross section (EDX) and fraction of the multistep direct reaction in the EDX have to be known in applying these kinds of systematics. The latter quantity is abbreviated as $f_{MSD}$ in this paper. The distinction between the "multistep direct (MSD)" and "multistep compound (MSC)" reactions are first proposed by Feshbach, Kerman and Koonin[6]. However, it was pointed out by Kalbach and Mann[14], and later by Kumabe et al.[12], that this division between MSD and MSC gives almost equivalent result to that between "preequilibrium + direct reaction" and "equilibrium reaction" as long as the DDX is concerned. Because of this, the MSD cross section was replaced in this work by preequilibrium + direct and MSC by Hauser-Feshbach cross sections, calculated with SINCROS-II code system[15]. This replacement might slightly overestimate MSD because preequilibrium includes a small contribution from the MSC process. However, it is somewhat canceled because the preequilibrium effect is considered only in the first stage of the multistep reaction.

As shown in the upper part of Fig. 1, the SINCROS-II code system consists of three main programs, EGNASH2, DWUCKY and CASTHY2Y. Many evaluations for JENDL-3 were carried out by using these programs, therefore the present evaluation will be a natural extension of JENDL-3. Another merit of using this code systems is an ability to control sophisticated aspects of the multistep statistical model calculation with a simple input by 1) building in such model parameters as optical model potential (OMP) and level density parameters (LDP) as defaults, 2) storing the discrete level structures retrieved from Evaluated Nuclear Data Structure File (ENSDF)[16] and atomic masses in databases, 3) interconnecting the databases and outputs from various programs, and 4) preparing a rich set of processing programs to convert the outputs to the ENDF format.

## 3. General Outline of the Evaluation Method

A schematic diagram of the method of evaluation and compilation of JENDL Fusion File is shown in Fig. 1. The SINCROS-II code system was used to calculate the partial reaction cross sections, particle spectra (EDXs) and the fraction of the multistep direct reactions ($f_{MSD}$). The modified Walter-Guss OMP was used for neutron, Perey and Walter-Guss combined OMP for proton as described in Ref. 15. For other particles, default OMPs were used. The level density parameters were mostly taken from the table of Gilbert-and Cameron[17]. However, LDP had to be adjusted in some cases. The F2 parameter needed in EGNASH2 , which is the Kalbach's constant divided by 100, was adjusted to reproduce the observed EDX at 14 and 18 MeV, if the experimental data are available. The parameter adjustment is designated in the middle left part of Fig. 1, as a loop consists of SINCROS-II, output file 15 from EGNASH-II, KMDDX[18] and SPLINT89[19]. The $f_{MSD}$ depends on incident neutron energy, outgoing particle energy, and outgoing particle species, but was assumed to be independent of reaction channels in the present evaluation.

After fixing the model parameters, and accepting this assumption, the DDXs were calculated and saved in the ENDF-6 format by F15TOB program, using the EDXs of

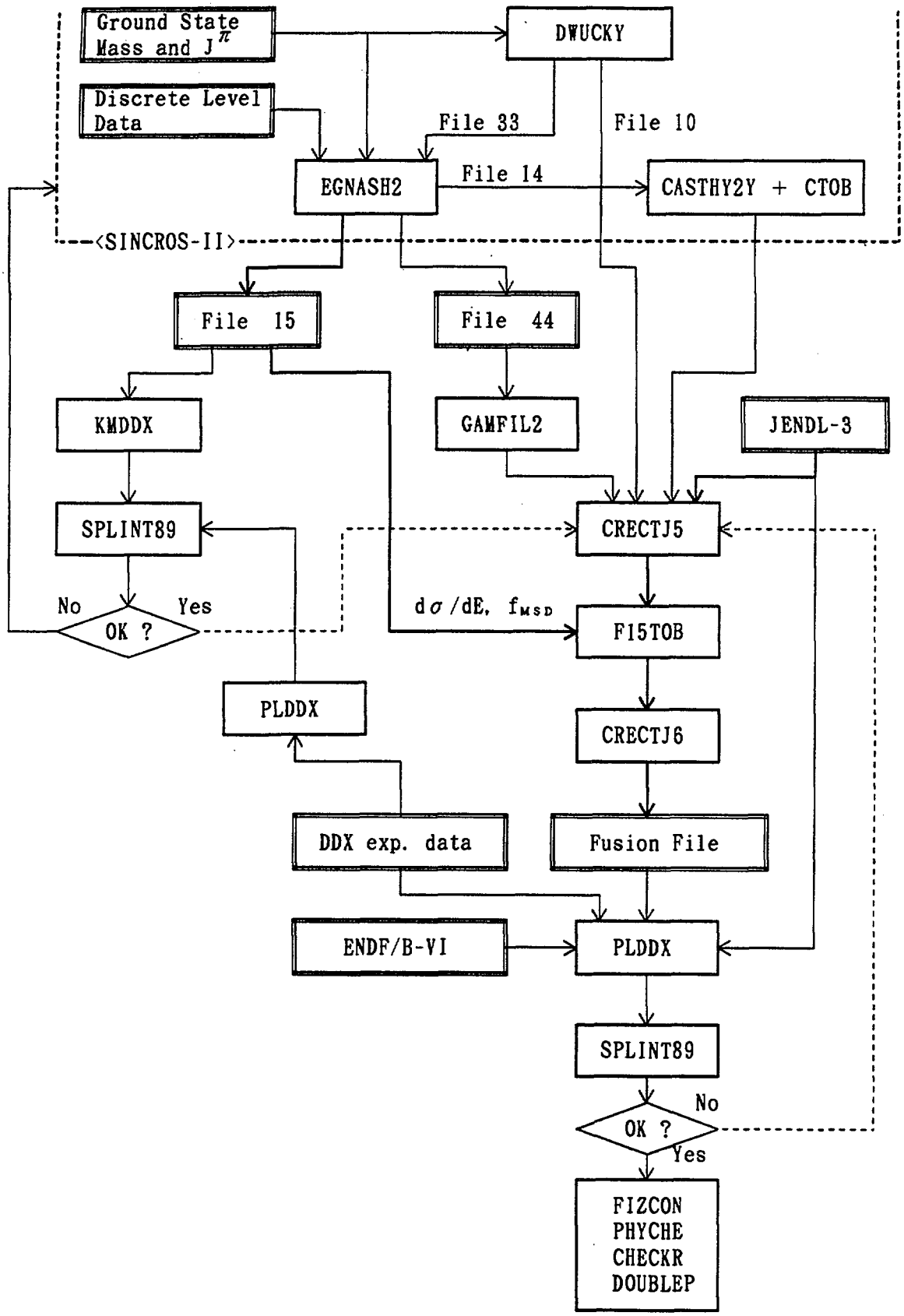


Fig. 1 Schematic flow of evaluation and compilation of JENDL Fusion File

continuum neutrons taken from JENDL-3 and $f_{MSD}$ calculated by EGNASH2. The results were then compared with the experimental data through PLDDX[20] and SPLINT89. If the results are in good agreement with the experimental data, the evaluation process finishes. Otherwise, it is repeated by changing a part of the JENDL-3 data by the results calculated by EGNASH2, CASTHY2Y or DWUCKY through CRECTJ5[21] program. This process is repeated until an acceptable agreement is reached. Then, format and physical consistency of the result are checked by programs provided from BNL/NNDC[22].

As described earlier, the Kumabe's systematics was used in calculating neutron DDX because this systematics can reproduce the observed data in the angular range from 30 to 150 deg. well[11]. However, we found that this systematics sometimes overestimates the cross section in the very forward angles (less than 30 deg.). Therefore, a new formula was sought, by changing the $A_L$ parameter to $A_L = 0.0561 + 0.0377 \cdot L(L+1)$, instead of Eq. (5a) of Ref. 12. The new formula gives slightly smaller cross section in the forward and bigger values at backward angles. This made agreement with the experimental data sometimes better. On the contrary, cross sections calculated by Kumabe's and this formulas are almost indistinguishable in the angular region between 40 and 150 deg. The new formula was used case-by-case.

## 4. Results and Discussion

The results of the present evaluation of DDX are compared with the data measured at Osaka and Tohoku Universities, as well as those reproduced from JENDL-3 and ENDF/B-VI in Figs. 2, 3 and 4 for Al, Fe and Zr, respectively. Generally, DDXs reproduced from JENDL-3 are lower than the observed data at forward angles, and higher at backward angles. This is due to the fact that the energy-angle correlation is not taken into account properly in JENDL-3, and thus too less angular dependence is given. On the contrary, the data calculated from ENDF/B-VI overestimates at forward angles as seen in Fig. 3 on DDX of Fe. This is because the systematics of Kalbach-Mann was adopted in ENDF/B-VI. In our examination[11], it was found that this systematics gives too steep angular dependence for the (n,n') data in the 14 MeV region.

The presently evaluated data can reproduce the general trend of angular dependence of continuum secondary neutron spectra. However, it is slightly smaller than the experimental data at backward angles. A reason of this might be the fact that the preequilibrium + direct reactions were used instead of the MSD process in applying the systematics of Kumabe. This approach is known to overestimate slightly the MSD cross section and therefore the forward peaking is too much emphasized. However, it was shown by Watanabe[23] that even if the MSD cross section calculated by, e.g., EXIFON program[24] is used, the difference from the present approach is very slight, and is found only at the very forward (less than 30 deg.) and backward (greater than 150 deg.) angles. The underestimation at the backward angles seems to show a limitation of using the systematics in calculation of DDX. Nonetheless, the presently evaluated results are in good accord with the measured cross sections on the whole,

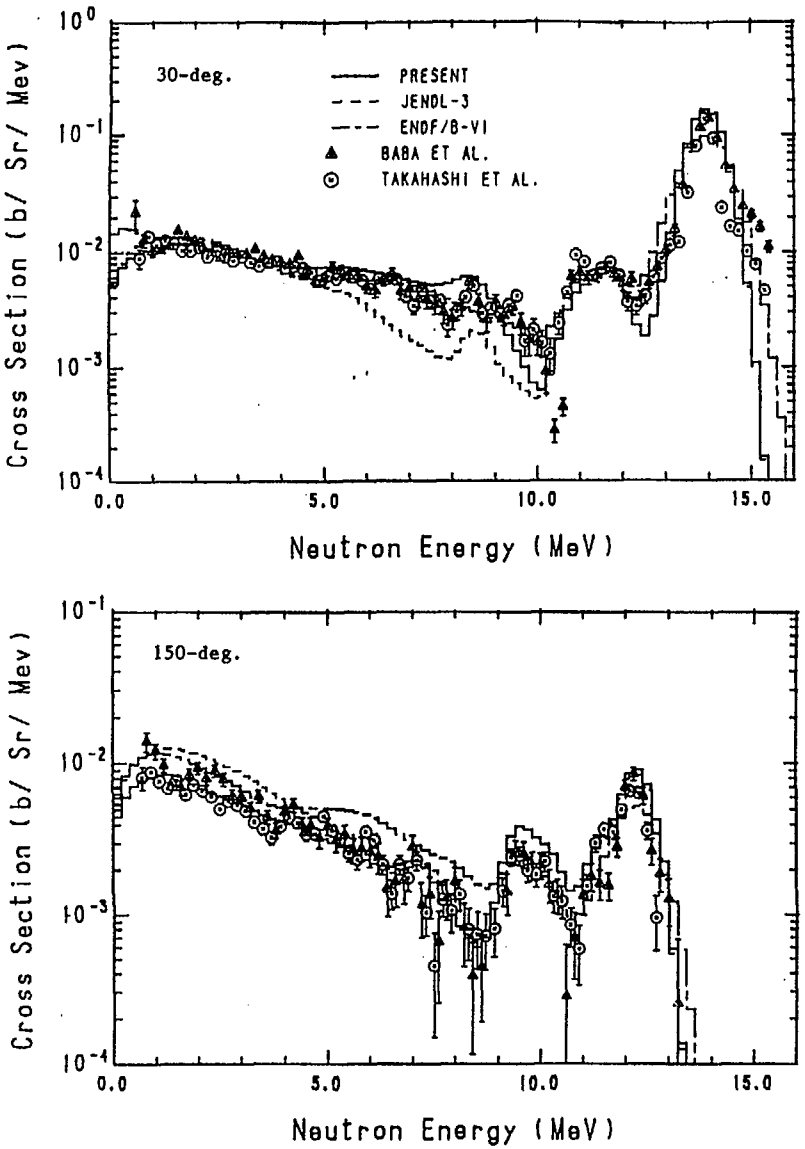


Fig. 2 DDX of $^{27}$Al at 14.1 MeV, 30 and 150 deg.

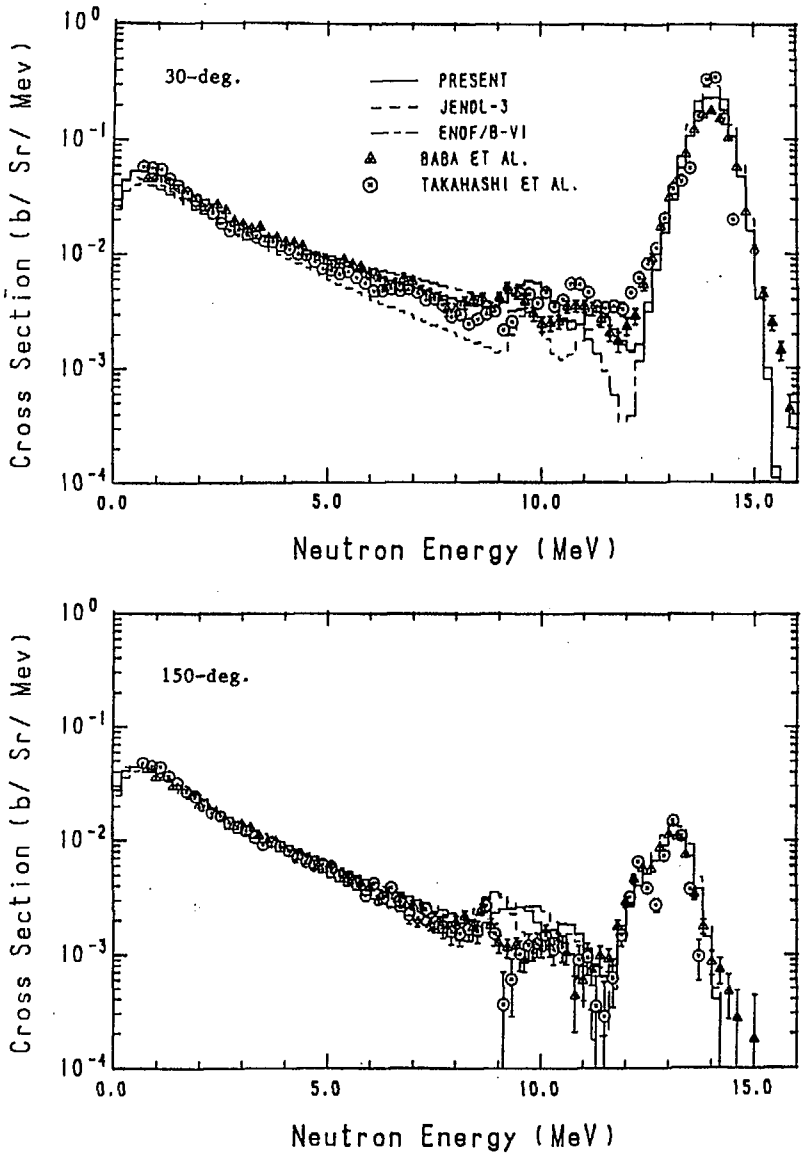


Fig. 3 DDX of Fe at 14.1 MeV, 30 and 150 deg.

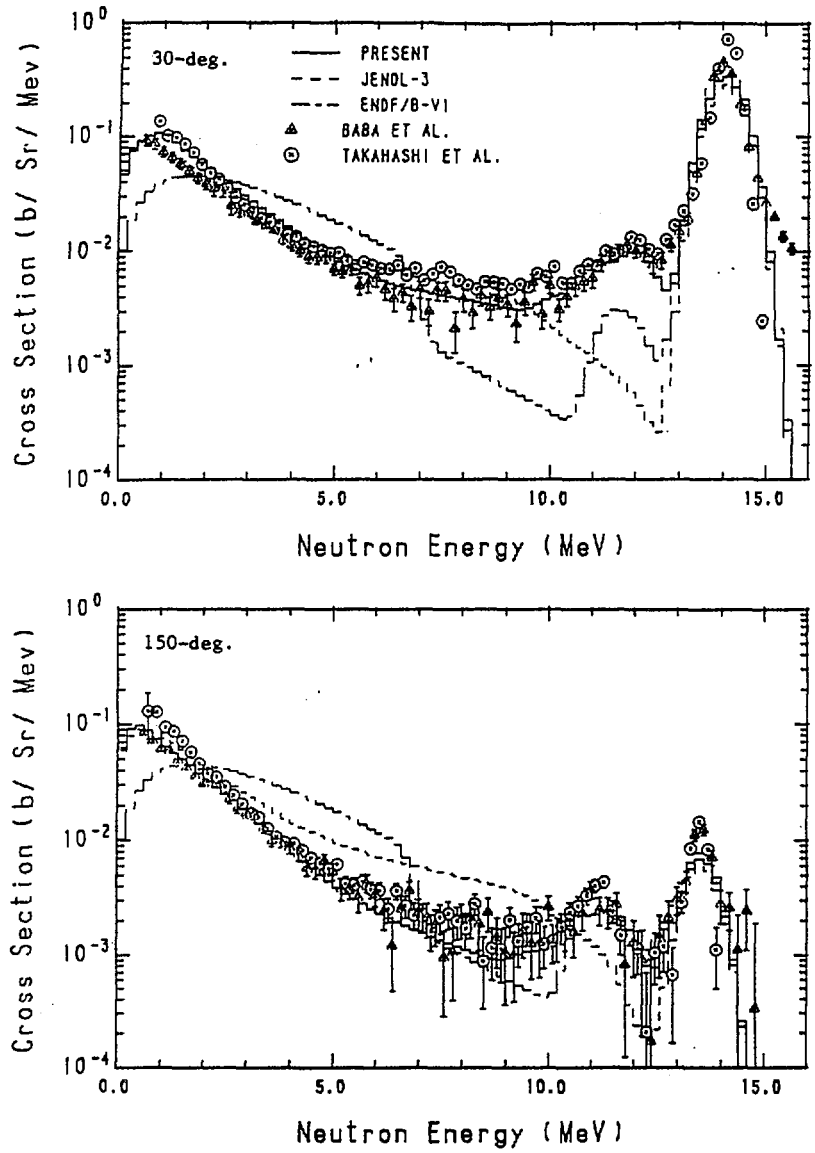


Fig. 4 DDX of Zr at 14.1 MeV, 30 and 150 deg.

and the overall accuracy was estimated to be 5 to 10% for Fe where the two experimental data sets agree quite well, while in other nuclei the accuracy was estimated to be in the range from 10 to 20%.

## 5. Concluding Summary

The double differential cross sections are being evaluated for JENDL Fusion File using systematics supplemented by multistep statistical model calculations. The main effort is placed to take account of the energy-angle correlation in the secondary neutron and charged particle spectra. The results are compiled in the ENDF-6 format.


## Acknowledgements

The authors would like to thank Dr. N. Yamamuro of Data Engineering Corp. for his help in using SINCROS-II code system.

## References


1) K. Shibata, T. Nakagawa, T. Asami, T. Fukahori, T. Narita, S. Chiba, M. Mizumoto, A. Hasegawa, Y. Kikuchi, Y. Nakajima and S. Igarasi : "Japanese Evaluated Nuclear Data Library, Version-3, -JENDL-3 -", JAERI 1319 (1990).
2) e.g., P.E. Hodgeson : "NUCLEAR REACTIONS", Proceedings of a workshop on Applied Nuclear Theory and Nuclear Model Calculations for Nuclear Technology Applications, Trieste, Italy, 15 Feb. - 10 Mar., 1988, edited by M.K. Mehta and J.J. Schmidt, World Scientific.
3) Y. Nakajima and M. Maekawa (Ed.) : Proceedings of the Specialist's Meeting on Nuclear Data for Fusion Reactors, JAERI-M 91-062 (1991).
4) M. Kawai, T. Fukahori and S. Chiba : "STATUS OF JENDL KERMA/PKA FILE", JAERI-M 92-027, p.28 (1992).
5) M. Baba and T. Nakagawa (Ed.) : Proceedings of the 1991 Symposium on Nuclear Data, JAERI-M 92-027 (1992).
6) H. Feshbach, A. Kerman and S. Koonin : Annals of Phys. 125, 429 (1980).
7) T. Tamura, T. Udagawa and H. Lenske : Phys. Rev. C26, 379 (1982).
8) Y.L. Luo and M. Kawai : Phys. Lett. B235, 211 (1990).
9) M. Blann and H.K. Vonach : Phys. Rev. C28, 1475 (1983).
10) J. Zhang : "A Semi-Classical Theory of Multi-Step Nuclear Reaction Processes", presented at Beijing International Symposium on Fast Neutron Physics, Sep. 9 - 13, 1991, Beijing (1991).
11) B. Yu, S. Chiba and T. Fukahori : accepted for publication in Journal of Nuclear Science and Technology.
12) I. Kumabe, Y. Watanabe, Y. Nohtomi and M. Hamada : Nucl. Sci. Eng. 104, 280 (1990).
13) C. Kalbach : Phys. Rev. C37, 2350 (1988).
14) C. Kalbach and F.M. Mann : Phys. Rev. C23, 112 (1981).
15) N. Yamamuro : "A NUCLEAR CROSS SECTION CALCULATION SYSTEM WITH SIMPLIFIED INPUT-FORMAT, VERSION-II (SINCROS-II)", JAERI-M 90-006 (1990).
16) "Evaluated Nuclear Structure Data File", maintained by BNL/NNDC.
17) A. Gilbert and A.G.W. Cameron : Canad. Jour. Phys. 43, 1446 (1965).
18) B. Yu and S. Chiba : "KMDDX", unpublished.
19) T. Nakagawa : "SPINPUT", JAERI-M 9499 (in Japanese) (1981); T. Narita, T. Nakagawa, Y. Kanemori and H. Yamakoshi : "SPLINT, A Computer Code for Superimposed Plotting of the Experimental and the Evaluated Data", JAERI-M 5769 (1974).
20) B. Yu and S. Chiba : "PLDDX", unpublished.
21) T. Nakagawa : "CRECTJ5", to be published.
22) C.L. Dunford : "Release of ENDF Utility Codes, Version 6.6", unpublished memorandum, BNL/NNDC, June 13, 1990.
23) Y. Watanabe : "Statistical Multistep Processes in Nuclear Reactions", JAERI-M 92-027, p. 70 (1992).
24) H. Kalka : "Code EXIFON Version 2" (1991); H. Kalka, M. Torjman and D. Seeliger : Phys. Rev. C40, 1619 (1989).

# Double-differential Neutron Emission Cross Sections for 14, 18 and 2 to 6 MeV Incident Neutrons

M.Baba, S.Matsuyama, T.Ito, H.Wakabayashi,
T.Ohkubo, H.Feijing*) and N. Hirakawa

Department of Nuclear Engineering, Tohoku University
Aramaki, Aoba, Aoba-ku Sendai 980, Japan

Abstract:

Double-differential neutron emission cross sections have been measured for Fe, Mo, Nb, Ta, Bi and U at 14.1 MeV, and for Nb, Bi and U at 18 MeV using Tohoku University Dynamitron TOF spectrometer. For U, data were obtained also at 1.2 to 6 MeV incident energies.

Angle-integrated neutron emission spectra and angular distributions of secondary neutrons were also derived.

The experimental results are compared with other experiments and evaluations. The neutron emission spectra and angular distributions were analyzed, respectively, using a statistical multi-step reaction code EXIFON and systematics by Kalbach-Mann and by Kalbach.

## 1. Introduction

Energy-angular doubly-differential neutron emission cross sections (DDXs) are of prime importance for the design of fusion, fission reactors and accelerator based neutron sources to describe anisotropic transport of fast neutrons. They are indispensable also for assessment of radiation effects caused by knock-on atoms produced by fast neutrons. In addition, experimental DDX data are very useful for validation of models and parameters in theoretical calculations employed in nuclear data evaluation since they provide information on cross sections and emission spectra for neutron emitting reactions.

Systematic experiments on DDXs have been carried out at Tohoku University using Dynamitron Time-of-Flight facility at the incident energies 14 MeV, 18 MeV and MeV region from 1.2 to 7 MeV for light and medium nuclides /1-7/. In these measurements, a care was taken both in experiments and data

---

*) Institute of Heavy Ion Physics, Peking University, PRC

correction to obtain DDX over almost entire range of secondary neutrons with good energy resolution to clarify competition between various reaction processes. From the DDX data, angular distributions of secondary neutrons, angle-integrated emission spectra and various partial cross sections have been deduced. These data will be useful to study the incident energy dependence of DDXs since experimental DDX data for incident neutron energy other than 14 MeV are very scanty.

Recently, we have extended the measurements to medium and heavy nuclides up to Th and U with improving the experimental and data reduction method /7/.

This paper presents the results on Fe, Nb, Mo, Ta, Bi and U. The experimental data are compared with other experiments and evaluated data. The angle-integrated neutron emission spectrum, i.e. energy differential cross section (EDX), and angular distribution of secondary neutrons have been analyzed using a multi-step reaction code EXIFON /8/ and systematics by Kalbach & Mann /9/ and by Kalbach /10/, respectively to study systematic behavior of DDXs.

## 2 Experimental Method

The experimental method has been described previously /2,4,7/.

Figure 1 illustrates the schematic view of experimental setup for DDX measurements. The neutron detector is heavily shielded by a shield-collimator made of paraffin, water and lead to apply fast neutrons up to 20 MeV. It has long beam channel about 2.5 m for tight collimation of neutron detector. This shield is rotatable around the pivot and has adjustable collimator opening. The flight path length is variable between 3.7 and 6.5 m. A pre-shield with double-conical collimator, 60-cm long water tank, was used for measurements using flight path longer than 5 m. A shadow bar for direct neutron shielding is made of copper and iron, 60-cm long.

The absolute value of the cross section was determined relative to n-p scattering cross section by measuring scattered neutron yields from a small polyethylene sample.

### 2.1 Neutron Production and Sample Arrangement

Source neutrons for the experiment were produced by pulsed deuteron or proton beam provided by a 4.5MV Dynamitron accelerator /11/. The Dynamitron delivers pulsed proton and deuteron beam with 1.5- to 2-ns durations in FWHM and about a few mA at peak height using a terminal pulser. The repetition rate is variable from 2 MHz to 7.8kHz in binary step.

In recent experiments, a post-acceleration beam chopper /12,13/ has been employed to improve the energy resolution by eliminating the tail components in accelerated pulsed beam. The post-chopper improved markedly the energy resolution and data quality in high energy region /12,13/.

Primary neutrons were obtained by the T(d,n), D(d,n) and T(p,n) reactions, respectively for 14 and 18 MeV, $4 < En < 7$ MeV and for $En < 2.5$ MeV. The tritium target was tritium-loaded titanium (Ti-T), 1.5-cm diam, with thickness appropriate for each neutron energy. The deuterium target is a gas cell made of Cu tube and Pt beam stop, 1-cm diam by 3-cm long; a Haver foil of 2.2 micro-m thick was used as window of the gas cell.

The target chamber was made as low-mass as practicable and cooled by air blowing to reduce the scattering and attenuation of primary neutrons. In the case of Ti-T target, it is mounted in a thin wall dual-tube chamber, 1.5 cm diam by 6 cm long, to eliminate a flange from the vicinity of the target.

In the 14.1 MeV measurements, the scattering samples were placed at 97.5-deg or 90-deg with respect to the incident beam to obtain primary neutrons with low energy spread. In these angles, the effect of source neutron polarization is negligibly small /14,15/.

In the 97.5-deg arrangement, the scattering samples were placed vertically and the detector was rotated around the samples to change scattering angle /5-7/. When the samples were placed at 90-deg, the detector was fixed at 90-deg and the scattering angle was varied by rotating the samples around target keeping their axes in horizontal plane /2,4/.

For the incident neutrons of 18 MeV and MeV region, the scattering samples were placed at 0-deg emission angle vertically and the detector was rotated around the sample to vary the scattering angle.

In Fig.2, examples of source neutron energy spectrum are shown for 14.1 and 18.0 MeV. For 14 MeV, contaminant neutrons due to target scattering are very few except for parasitic d-D neutrons owing to the low mass structure of the target. For 18 MeV, however, parasitic neutrons due to d-D, d-C and d-O become apparent because of higher deuteron energy. Therefore, experimental data should be corrected appropriately for backgrounds caused by these contaminant neutrons (cf.Sect.4).

## 2.2 Neutron Detector and Electronics

The schematic diagram of electronics system is shown in Fig.3.

Secondary neutrons were detected by a NE213 scintillator, 12.5 cm diam by 5.08 cm thick coupled to Phillips XP2041 photomultiplier tube or 14-cm diam by 10 cm thick coupled to Hamamatsu R1250 tube. The anode signal was fed

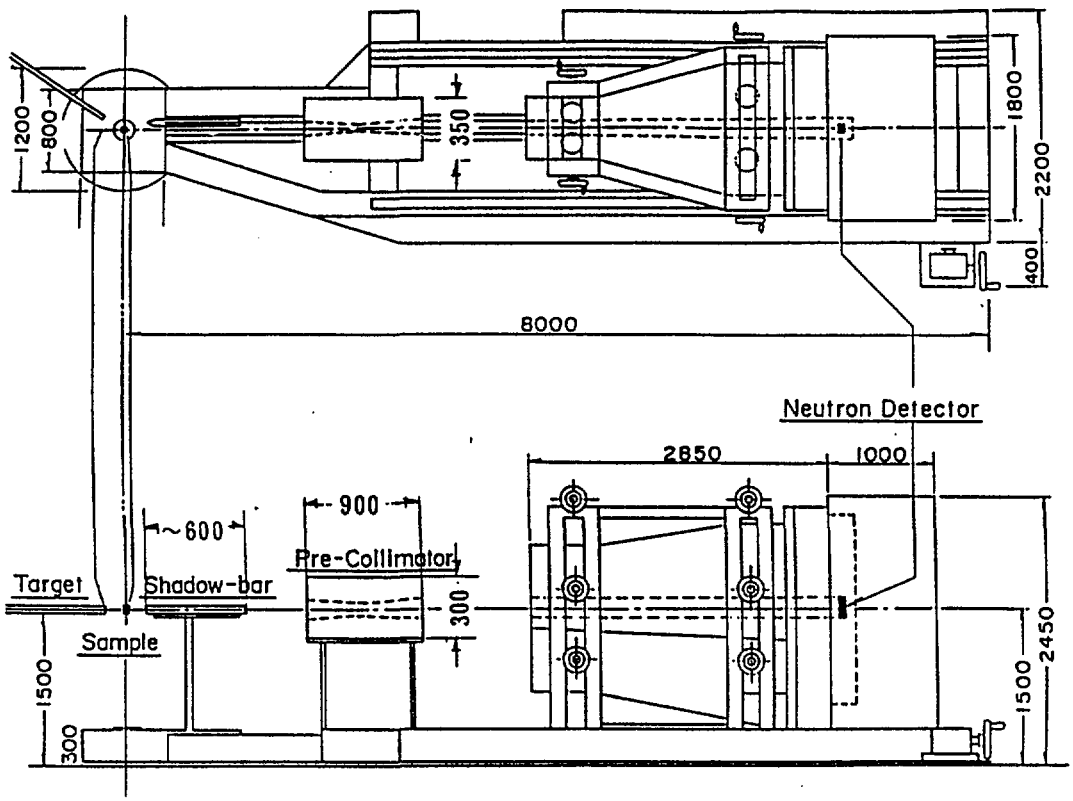


Fig.1: Experimental setup for the present experiment.

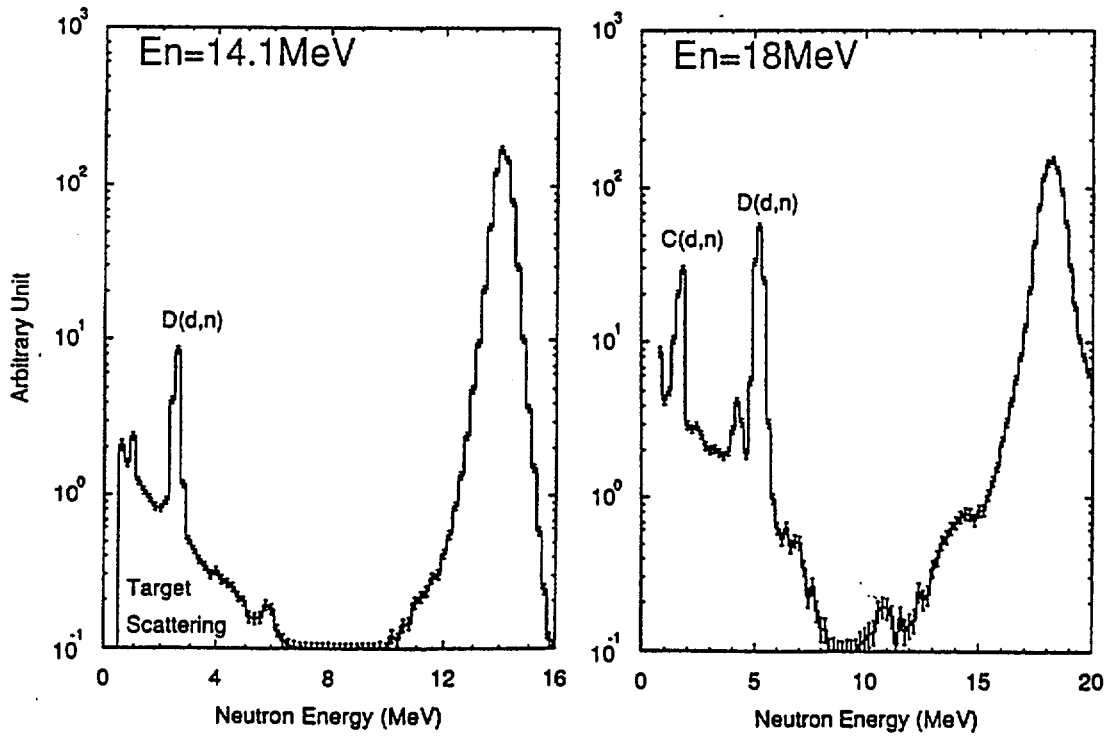


Fig.2: Energy spectra of source neutrons for 14.1 MeV and 18 MeV incident energies.

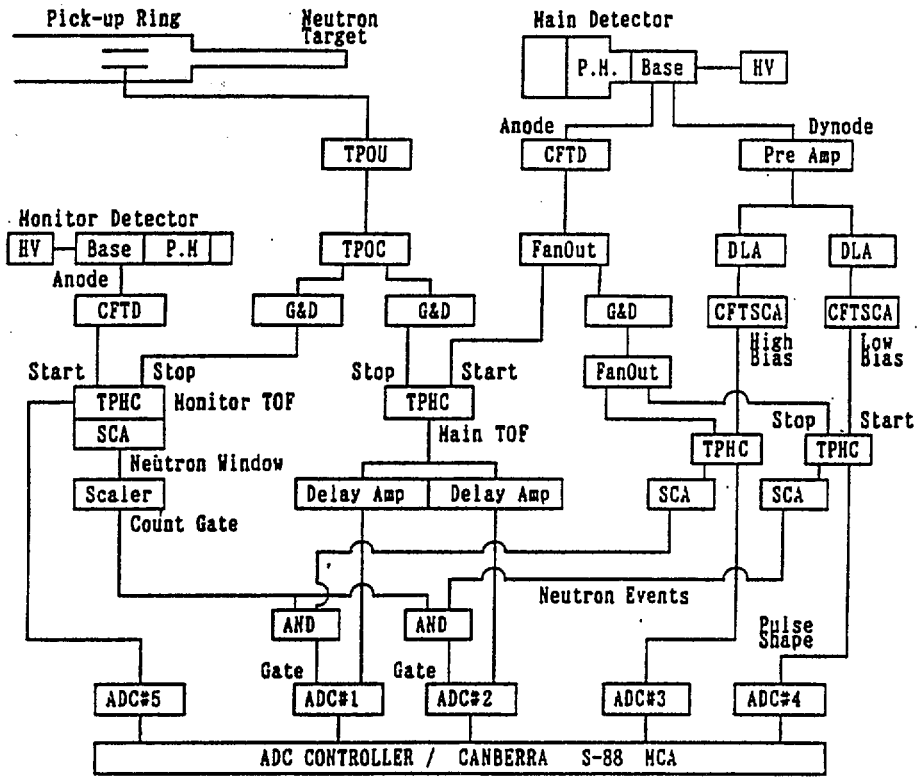


P.M= Photomultiplier, TPOC= Time pick-off unit, TPOC= Time pick-off control, CFTD= Constant-fraction discriminator, G&D= Gate and delay generator, TPHC= Time-to-pulse height convertor, DLA= Delay line amplifier, SCA= Single-channel analyzer, CFTSCA= Constant-fraction timing single-channel analyzer, ADC= Analogue-to-digital convertor, MCA= Multi-channel pulse-height analyzer

Fig.3: Electronics block diagram for the present experiment.

into a constant-fraction timing discriminator (CFTD) and used for TOF measurement. For each photomultiplier, a voltage divider with modified field gradients /16,17/ was employed to get low-walk timing signal over wide range of neutron energy.

For gamma-ray rejection, two-bias pulse shape discriminators (PSD) were employed. The bias level of high-bias system was set at 2-3 MeV proton to get a smooth efficiency curve by ejecting events due to neutron-carbon interaction; this was used for energy range higher than 5-6 MeV. The low-bias system covers lower energy range with bias level of 0.3-0.8 MeV /2,7/.

The energy dependence of the detector efficiency was determined by combining experiments and Monte-Carlo calculation. For neutron energy range higher than 5 MeV, the calculated values by the code O5S /18/ were adopted since they agreed with the experimental values by the n-p scattering method. The efficiency curve for lower energy region was determined experimentally by measuring the TOF spectrum of spontaneous fission neutrons from Cf-252. From the dispersion among repeated measurements, the uncertainty in relative efficiency was estimated to be about 4 %.

A smaller NE213 scintillator, 5.08-cm diam by 5.08-cm thick, was employed as a monitor detector to measure the intensity and spectrum of source neutrons by the TOF method. The monitor count was used for normalization between sample-in and sample-out measurements. It was also housed in a large shield of paraffin or water and surrounded by lead plates. Usually, PSD was not employed since sufficient gamma-ray rejection was possible by TOF. In the measurements for U, it was shadowed from the samples to reject gamma-rays from the samples.

In the data acquisition, a set of five data, i.e. TOF and pulse-shape spectra for the high- and low-bias system of the main detector and the TOF spectrum for monitor detector, was stored in the Canberra S-88 pulse height analyzer.

## 2.3 Scattering Samples

The scattering samples were metallic right cylinders, 3-cm diam by 5-cm long except for U which was 2-cm diam by 5-cm long. A Polyethylene sample, 1.5-cm diam by 5-cm long or 1-cm diam by 4-cm long, was employed to determine the absolute cross section and detector efficiency through the n-p scattering yields. A carbon sample with the same dimension was used to measure backgrounds due to carbon in the polyethylene sample.

These sample sizes were chosen as a compromise between the signal to background ratio and the magnitude of multiple-scattering estimated by an analytic formula /19/.

The samples were placed about 12- or 15-cm from the target and suspended with a thin string by a remotely-controlled sample changer.

## 2.4 Experimental Procedure

The measurements were carried out at the flight path of around 6-m at 14.1 MeV and around 4-m at other incident energies.

The spectrum of source neutrons was measured firstly to determine the energy and its spread of primary neutrons, and the spectrum and intensity of contaminant neutrons (cf.Fig.2). The latter data were used for backgrounds correction.

Then sample-in and sample-out measurements were done at 7-10 laboratory angles. In the measurements using gas target, "gas-out measurements" were also made. The polyethylene and carbon samples were measured at a few forward angles between 25- and 45-deg.

The overall timing resolution of TOF system was around 1.8-2.5 ns.

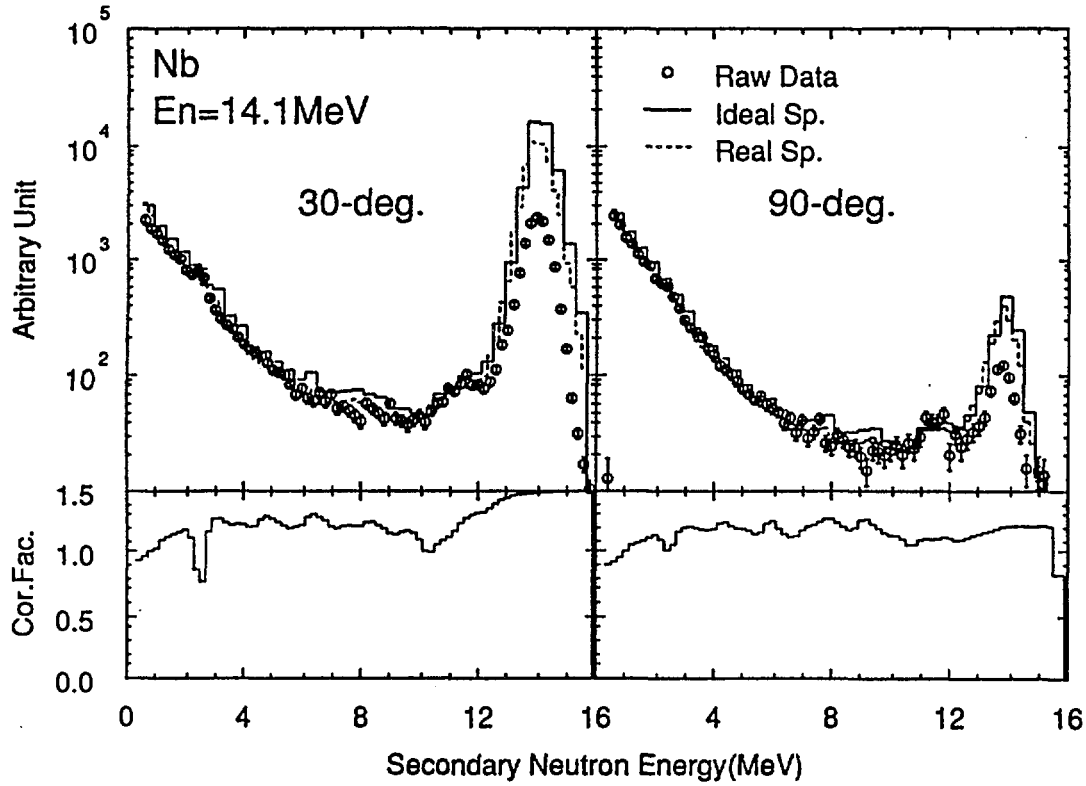


Fig.4: Results of simulation and correction factor for sample-size correction.

## 3 Data Reduction and Correction

### 3.1 Cross Section Derivation

For deduction of DDXs, experimental data were corrected for the effects of 1) sample-out backgrounds, 2) detector efficiency, 3) finite sample-size and 4) sample-dependent backgrounds produced by contaminant components in the source neutrons.

The experimental TOF data were firstly corrected for the sample-out backgrounds and relative detector efficiency, and transformed into energy spectra with 0.2 MeV bin. In the measurements using a gas target, gas-out backgrounds were also subtracted. The correction for sample-activity was also made for U.

The correction factors for finite sample-size effect and sample-dependent backgrounds were obtained using Monte Carlo calculations. The sample-size effect for polyethylene sample was estimated using the analytic formula based on the disk approximation /19/ because only the peak yields for n-p scattering are of concern.

### 3.2 Correction for Sample-size effect and Sample-dependent Backgrounds

To correct the DDX data for finite-sample size effect, it is necessary to trace the energy and angle of multiply-scattered neutrons as well as once-

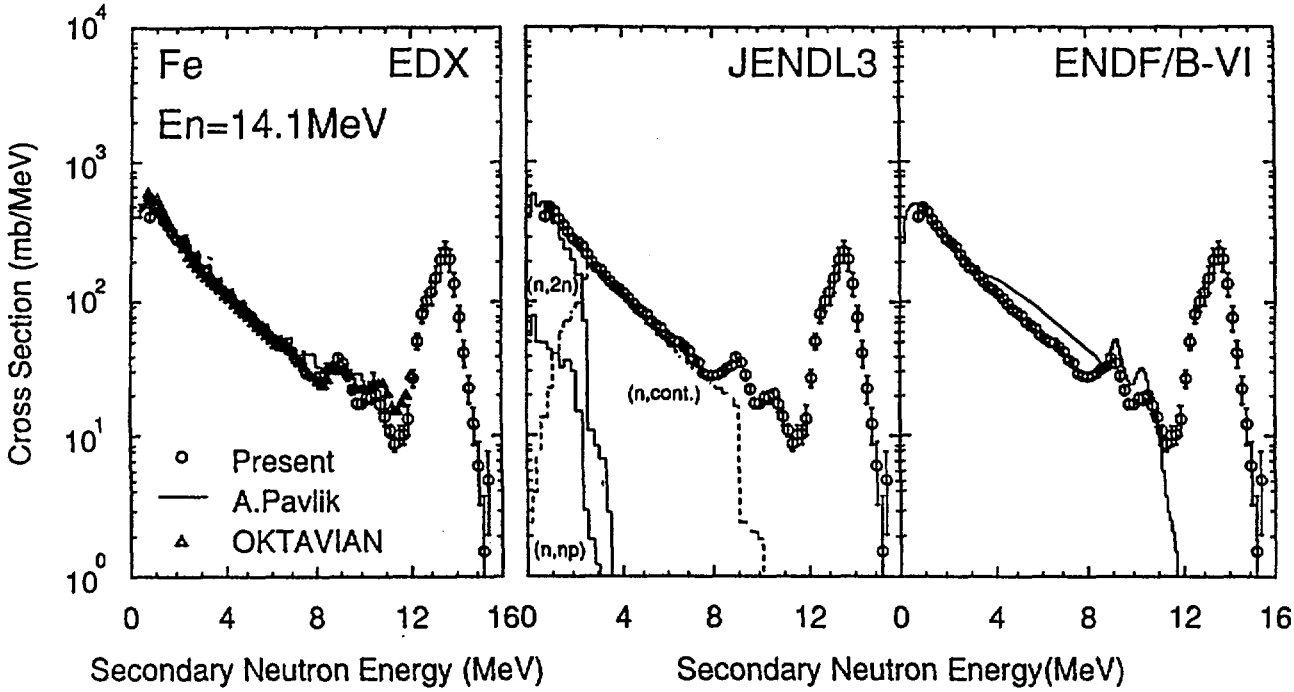


Fig.5: Angle-integrated neutron emission spectrum of Fe at 14.1 MeV.

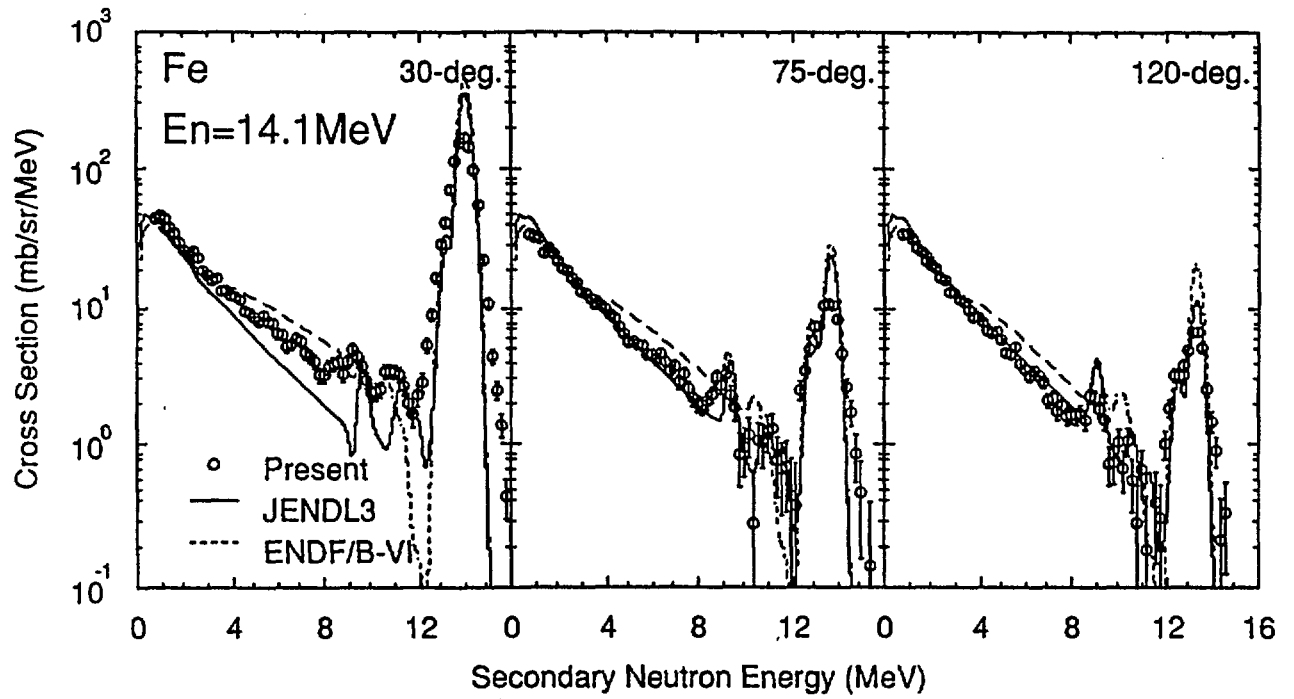


Fig.6: Double-differential neutron emission cross sections of Fe at 14.1 MeV.

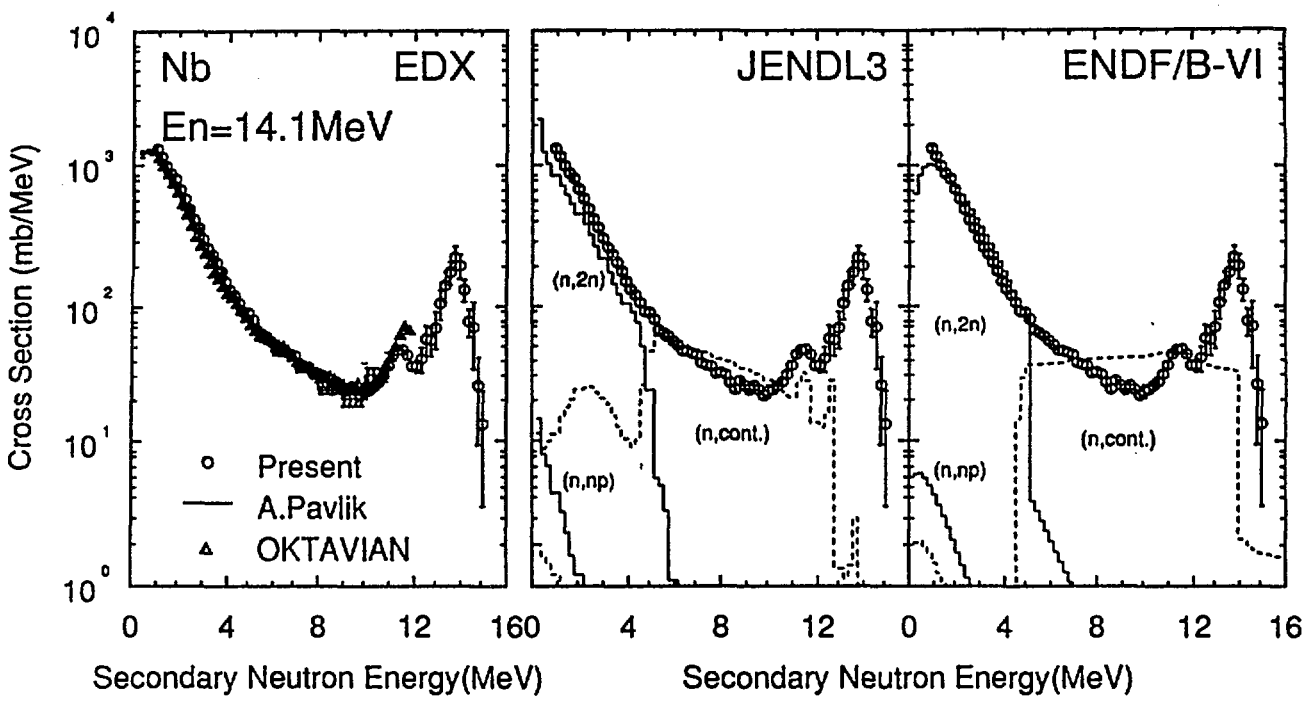


Fig.7: Angle-integrated neutron emission spectrum of Nb at 14.1 MeV.

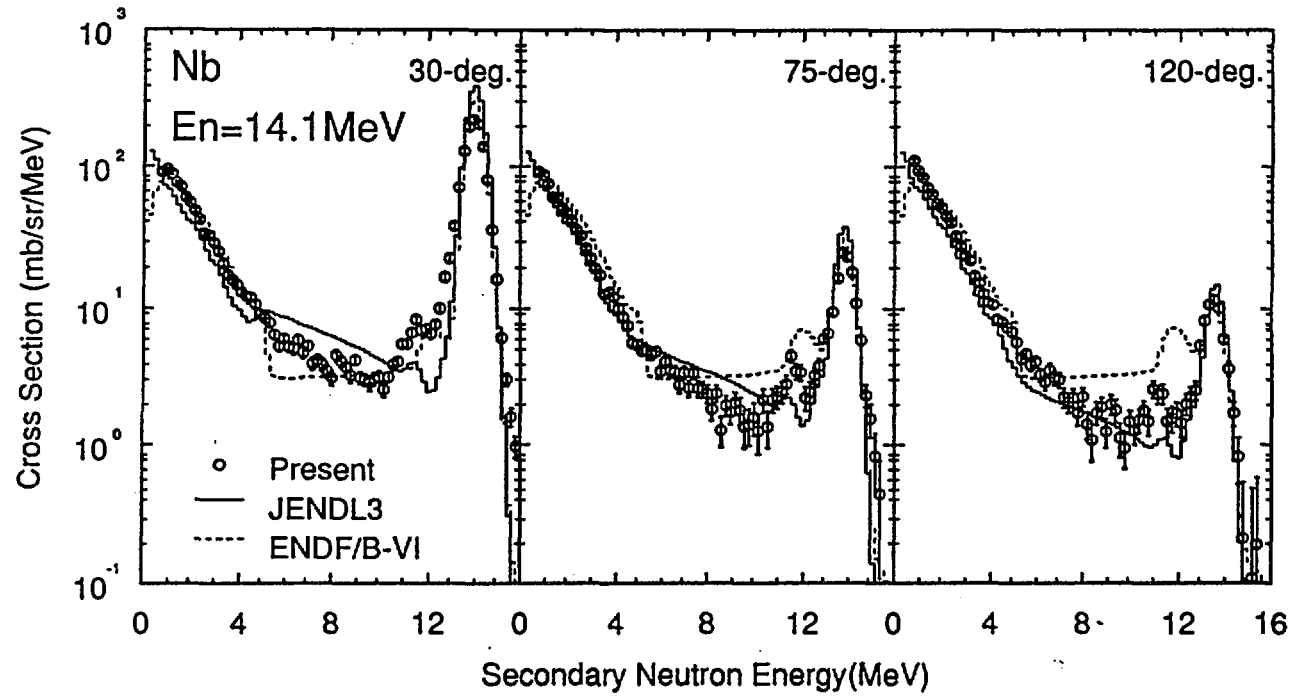


Fig.8: Double-differential neutron emission cross sections of Nb at 14.1 MeV.

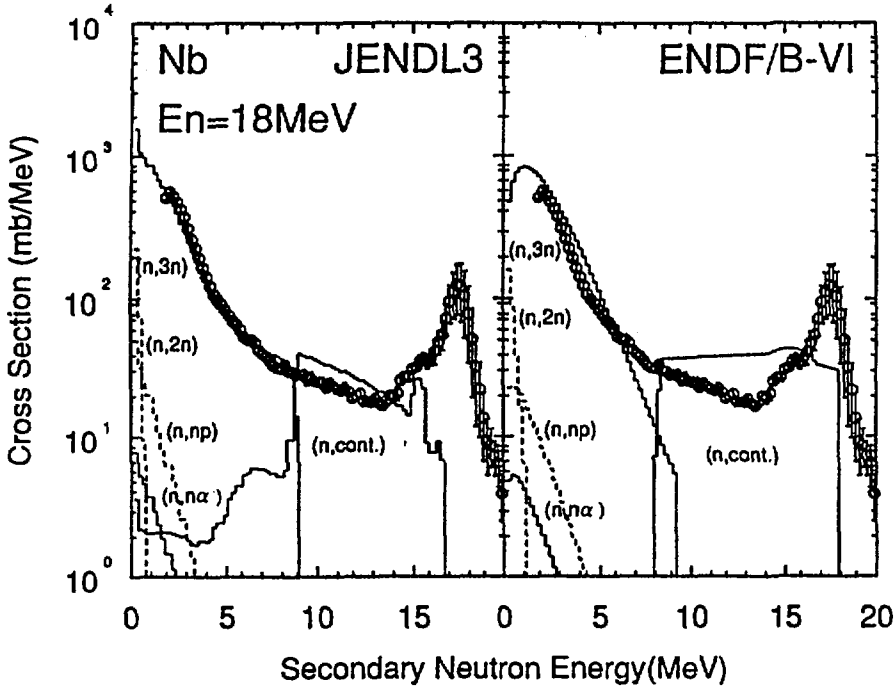


Fig.9: Angle-integrated neutron emission spectrum of Nb at 18.0 MeV.

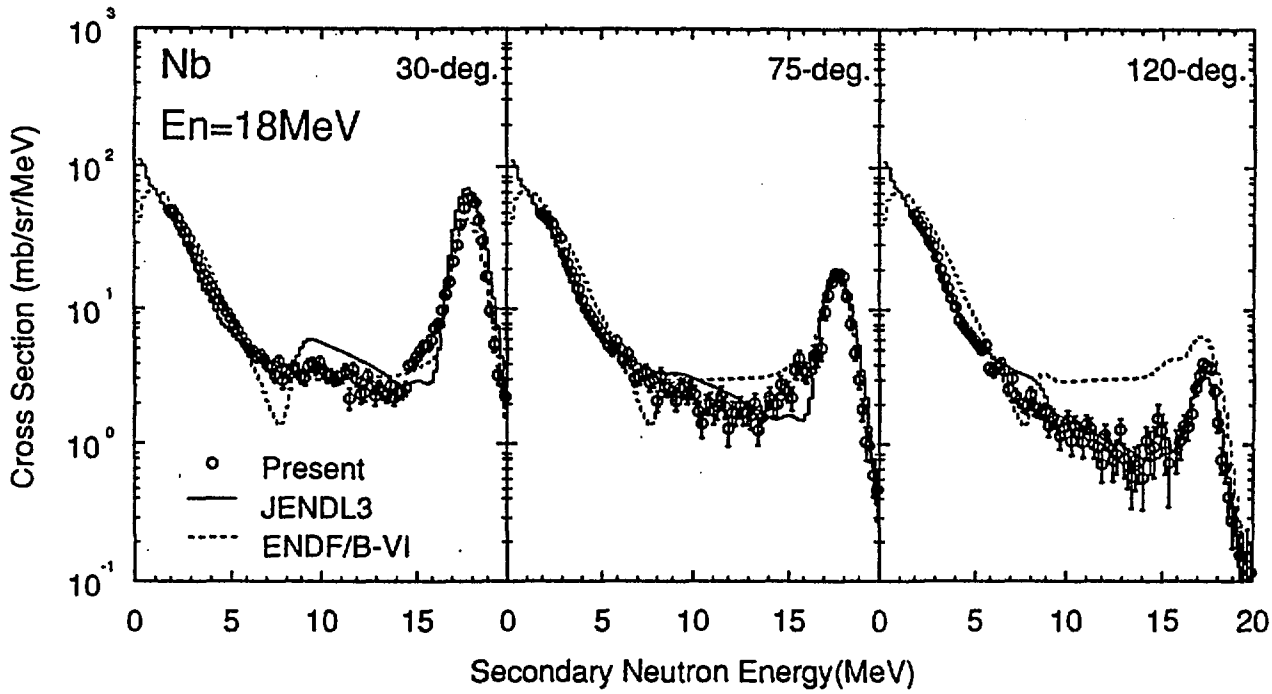


Fig.10: Double-differential neutron emission cross sections of Nb at 18.0 MeV.

scattered neutrons considering finite-geometry between the neutron source and sample, and energy-angle correlation in neutron scattering. This is also the case for sample-dependent backgrounds.

Then, a Monte Carlo code was applied for data correction against finite-sample-size effect and sample-dependent backgrounds /2,4,7/.

This program simulates neutron scattering/reaction process within the sample taking accounts of the a) data for the source reaction and neutron interaction with sample nuclides, b) physical dimensions of target, sample and detector, and c) energy-angle correlation in the scattering/reaction. In the program, neutrons experience forced collision up to five-times with decreasing weight corresponding to the non-escape probability from the sample.

Finally, the program provides three kinds of tabulated data for neutron energy or TOF spectrum to be observed by each detector placed at $\Theta$; 1) $I(E, \Theta, E')$, 2) $N_i(E, \Theta, E')$ (i=1-5) and 3) $R(E, \Theta, E')$. The I-spectrum corresponds to the spectrum observed in an ideal situation without flux attenuation and multiple-scattering. $N_i$-spectrum is that for i-th collision, and the R-spectrum is the sum of $N_i$ over i and corresponds to that in real situation. The correction factor for sample-size effect is obtained by the ratio of I-spectrum to R-spectrum.

The simulation was made using the evaluated nuclear data, JENDL or ENDF/B. In many cases, however, the evaluated data proved not adequate for the simulation since the simulated R-spectrum was largely different from the measured ones. In these cases, the correction factors obtained by the simulation are no more reliable since the fraction of multiply-scattered events are not realistic. As shown in Sect.4, such differences were mainly attributed to inadequate DDX of continuum neutrons in the evaluations. Then, we reconstructed the DDX data by modeling the uncorrected experimental data and applying the systematics as described in Sect.4. In Fig.3, illustrated are the simulation results for I-spectrum (Ideal) and R-spectrum (Real) and corresponding correction factors for Nb.

Final correction factor for both sample-size effect and contaminant neutrons are obtained by

$$Ax(E, \Theta, E') = \frac{I(E, \Theta, E')}{R(E, \Theta, E') + \sum f_i R_i(E_i, \Theta, E')}$$

where, $f_i$ is the fraction of contaminant component i. The spectrum and intensity of parasitic neutrons and target-scattered neutrons were determined, respectively, by the measurement of source neutrons and a Monte-Carlo calculation using the code MCNP. The influence of parasitic neutrons was most seri-

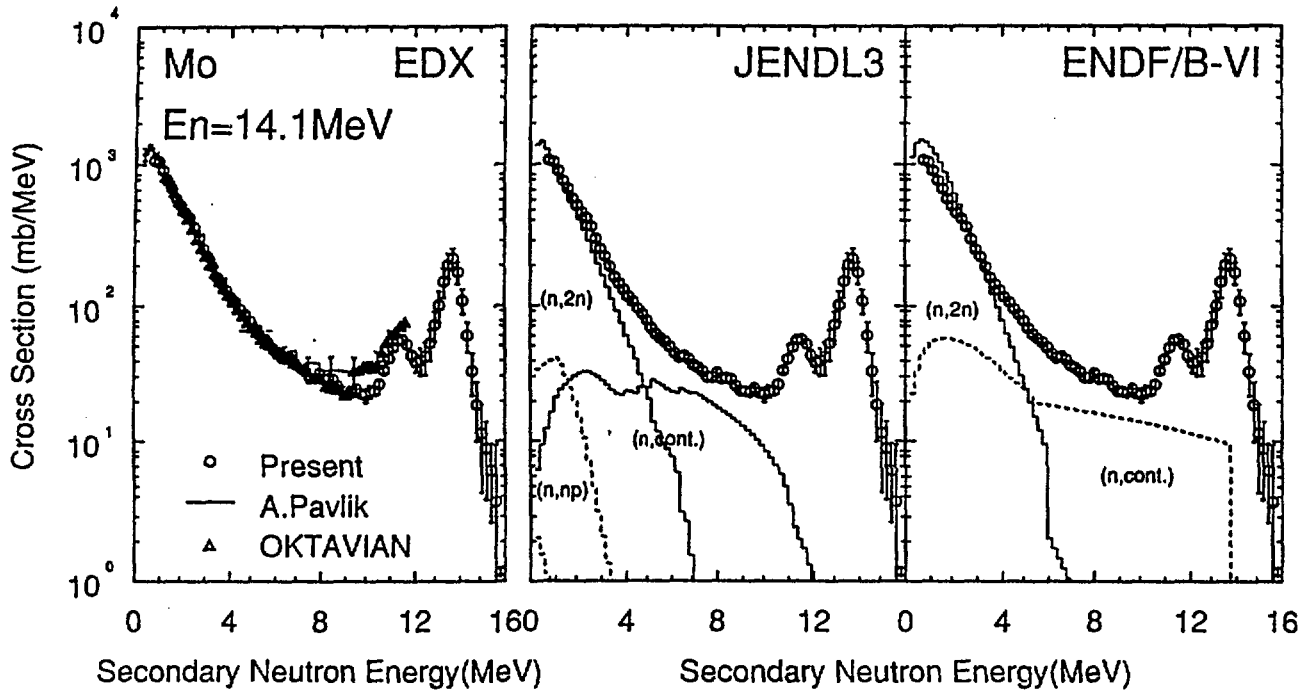


Fig.11: Angle-integrated neutron emission spectrum of Mo at 14.1 MeV.

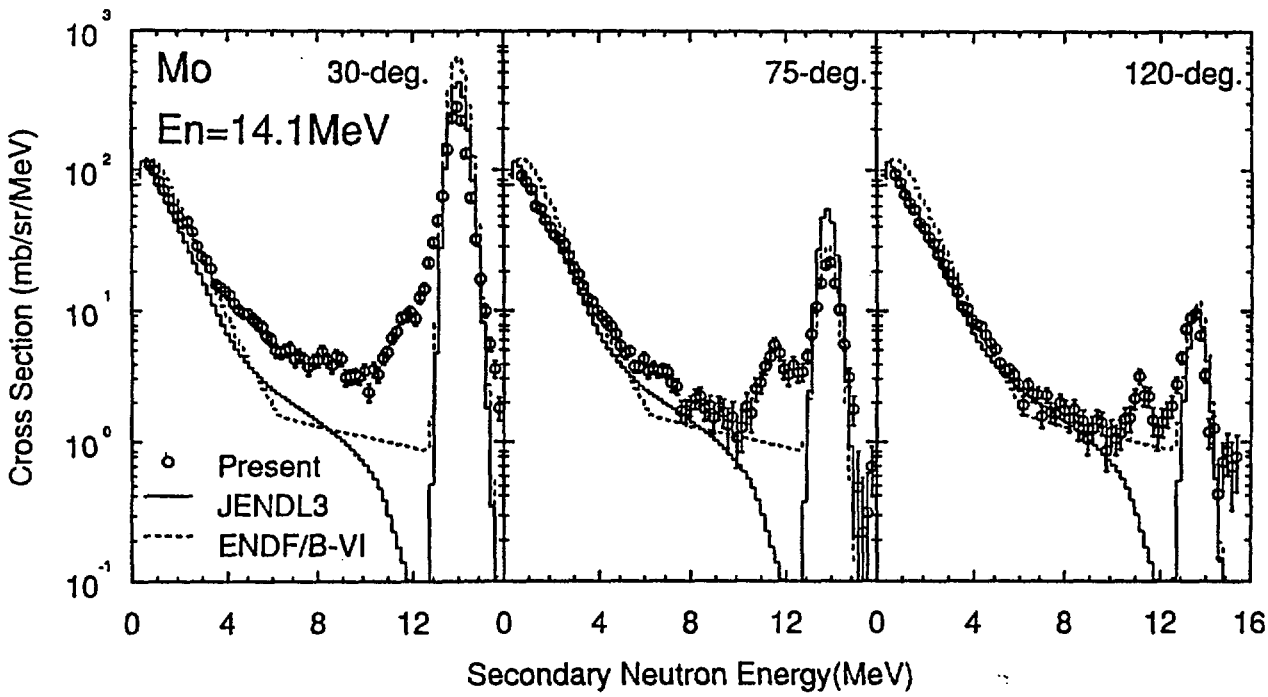


Fig.12: Double-differential neutron emission cross sections of Mo at 14.1 MeV.

ous in the case of 18 MeV measurements because of low intensity of primary neutrons compared with parasitic neutrons due to the d-D, d-C and d-O reactions.

The magnitude of the correction was generally in the range of 0.8 to 1.6 of which 1.1 to 1.4 for flux attenuation and 0.7 to 1.2 for multiple-scattering.

The uncertainty of the correction factor was mainly due to data employed in the simulation than to statistics in the simulation calculation. Then, as the uncertainty of the correction factor, we assigned 10 % of the correction in place of statistical error among a set of "batch" calculation usually defined as the error in the Monte Carlo calculation.

The angular distribution of elastic-scattering was further corrected for the angular resolution using the Kinney's analytic technique /19/.

The error of experimental data was estimated by quadratic sum of each error source, 1)counting statistics, 2) detector efficiency (4%), 3) absolute normalization (5%), and 4) data correction for finite sample-size and sample-dependent backgrounds (10% of correction).

## 4 Results and Discussion

In this section, the present results are presented in comparison with other experiments, evaluated data and with model calculations for emission spectrum and angular distributions.

### 4.1 Data Comparison

In Figs.5-18, illustrated are the angle-integrated spectra (EDXs) and DDXs for Fe, Nb, Mo, Ta and Bi together with those by other experiments and evaluations. EDXs are compared with the data at OKTAVIAN by Takahashi et al. /20,21/ and the evaluations by Pavlik & Vonach /22/, and corresponding values derived from JENDL-3 and ENDF/B-VI. The results at 18 MeV are also presented for Nb and Bi in comparison with the evaluated data; no experimental data are available for direct comparison with them. Figure 19 shows the DDX results for U at 14.1 MeV, 6 MeV and 2 MeV incident energies; the DDX at 14.1 MeV are compared with those by Shen et al. /23/.

(1) For all nuclides, the present EDX results at 14.1 MeV are in good agreement both in shape and magnitude with the data by Takahashi et al. and the evaluations by Pavlik & Vonach mainly based on experimental data, except for slight deviation from Pavlik & Vonach for Mo and from Takahashi et al. for Ta in the energy region above around 7 MeV where the effect of experimental energy resolution is significant. For EDX, the deviation among the data compared here will be within a few tens %. Besides, the present DDX data for U also agree very well with those by Shen et al. at both emission angles.

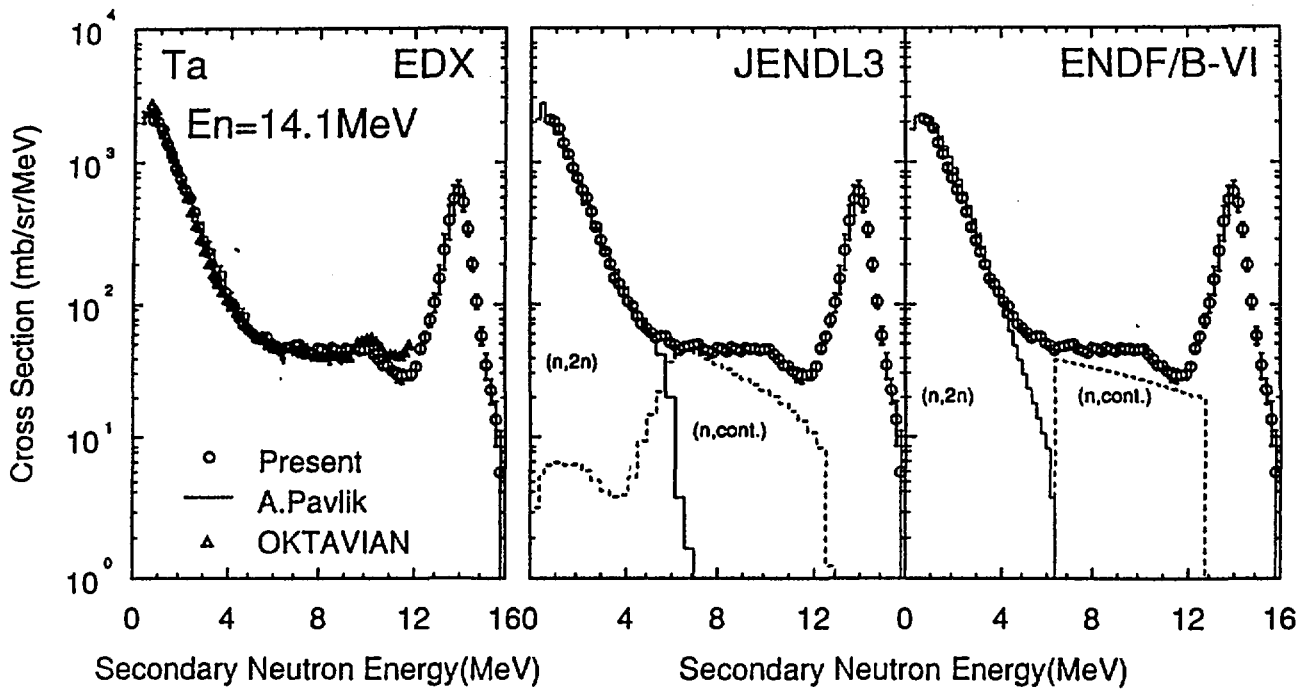


Fig.13: Angle-integrated neutron emission spectrum of Ta at 14.1 MeV.

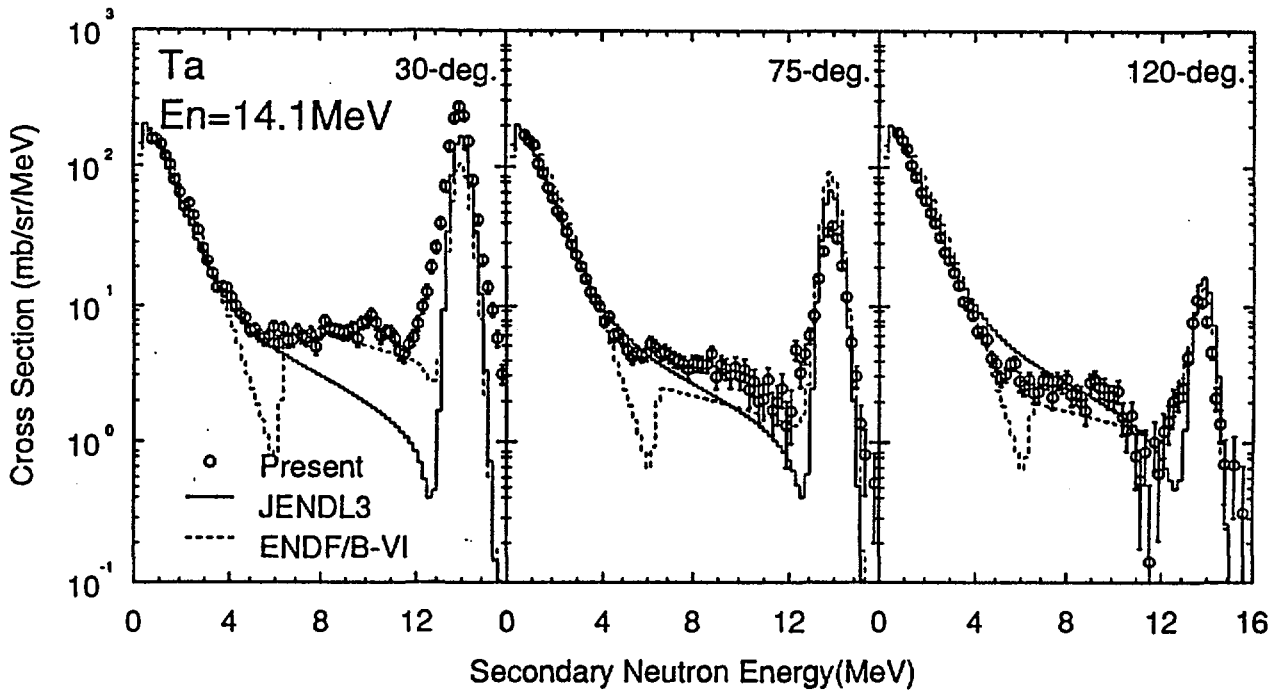


Fig.14: Double-differential neutron emission cross sections of Ta at 14.1 MeV.

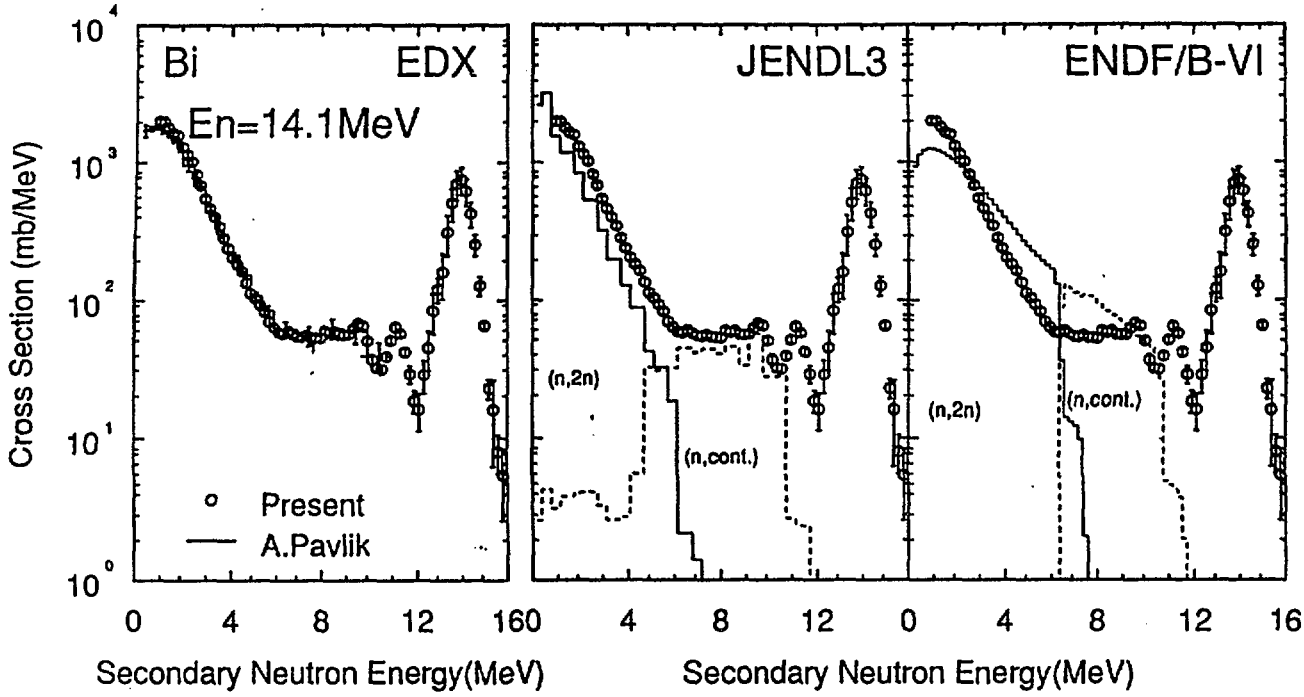


Fig.15: Angle-integrated neutron emission spectrum of Bi at 14.1 MeV.

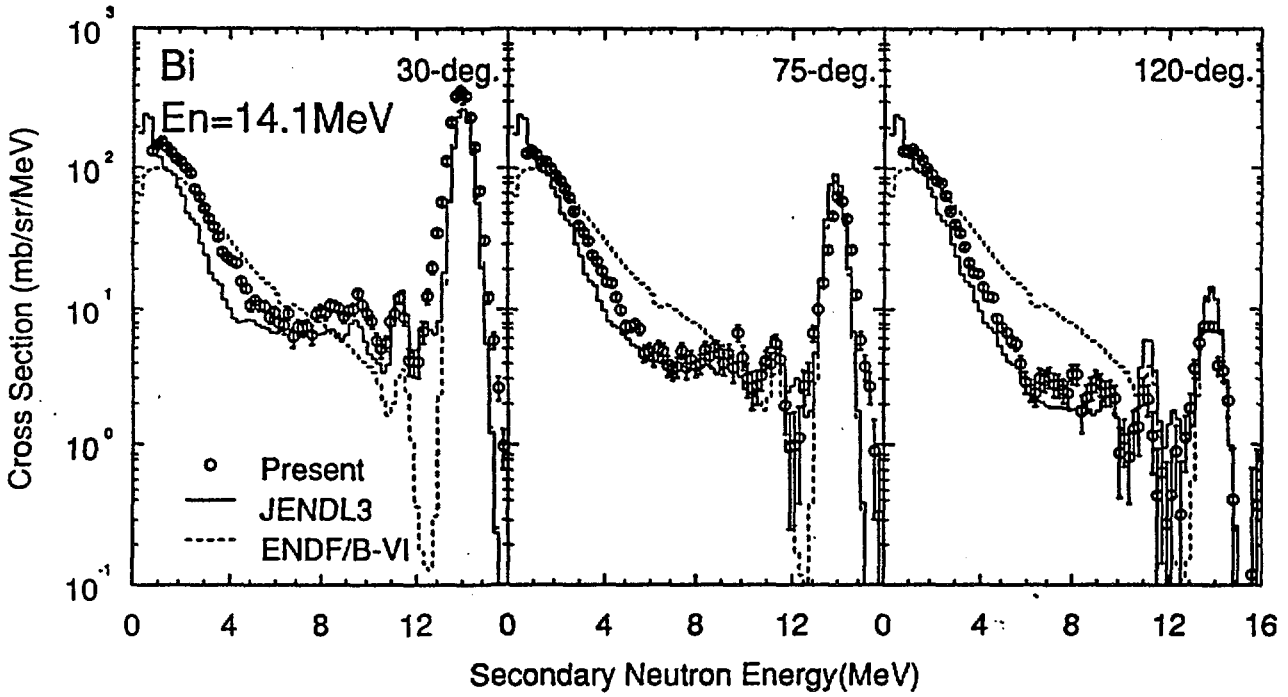


Fig.16: Double-differential neutron emission cross sections of Bi at 14.1 MeV.

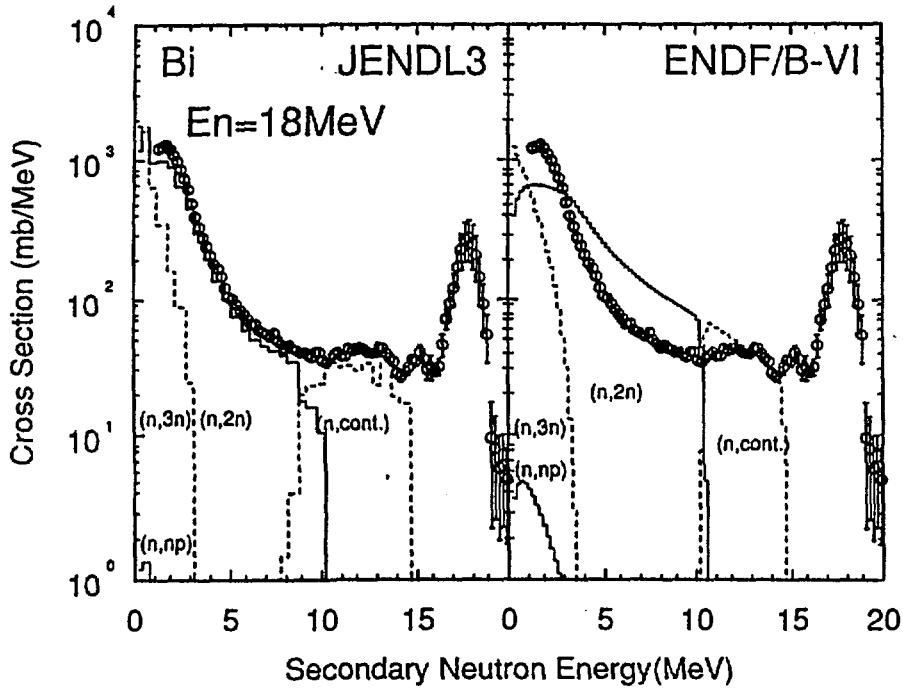


Fig.17: Angle-integrated neutron emission spectrum of Bi at 18.0 MeV.

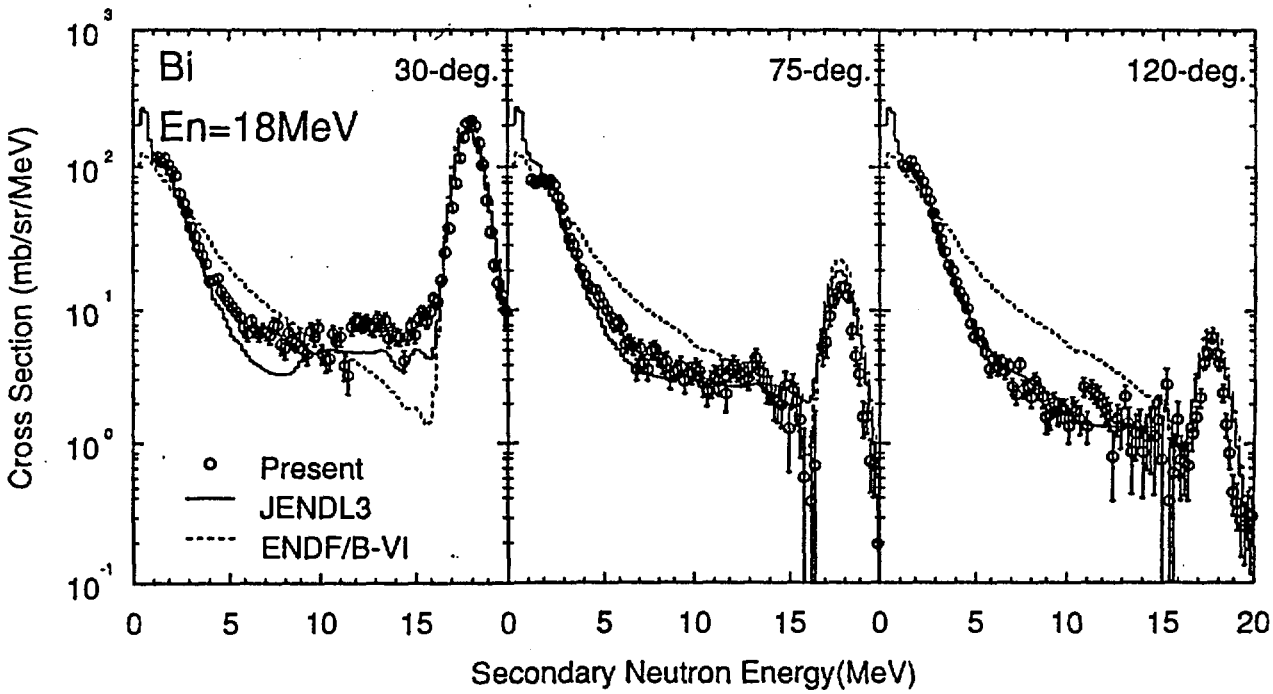


Fig.18: Double-differential neutron emission cross sections of Bi at 18.0 MeV.

(2) On the other hand, marked disagreement exists between the present data and JENDL-3, ENDF/B-VI both in EDXs and DDXs, especially for Mo at 14.1 MeV and for data at 18 MeV. Between the evaluations, the JENDL-3 data show much better agreement than ENDF/B-VI. The discrepancies in EDX will be attributed to the inadequacy of the evaluated data in the cross section and emission spectrum for each reaction process. In addition, evaluated data show discontinuity in the neutron spectrum because of mismatch in the spectrum between low energy part and continuum inelastic-scattering region. Furthermore, structures due to collective excitation are observed apparantly in the experimental data but they are not reproduced at all by the evaluated data.

In the DDXs, discrepancies observed in the EDXs are further enhanced especially in the backward angles since the evaluations do not provide angle-dependence of emission spectra except for Nb and Bi in JENDL-3; they were evaluated using systematics by Kalbach & Mann and reproduce fairy well the angle dependence of emission spectra. Therefore, for proper description of DDX, taking accounts of angle-dependence is indispensable.

(3) It should be noted that the present DDXs for U at 6 and 2 MeV show marked disagreement with the evaluated values even at MeV incident energies. These discrepancies are mainly due to the differences in spectrum shapes than in angular dependence. In these cases, fission neutrons have large contribution to emission spectrum in addition to inelastic-scattering /7/. As noted in Ref.7, these discrepancies are attributed primarily to the differences in cross section and emission spectrum of inelastic-scattering than in fission spectrum. Thus, DDX data are useful also for assessment of inelastic-scattering cross sections of nuclides having complicated level structures.

## 4.2 Analyses of Emission Spectra and Angular Distributions

(1) The present results of EDXs are compared with the calculation by the code EXIFON /8/ based on the statistical multi-step reaction model. This code takes accounts of the direct excitation of vibrational levels and single-particle levels as well as the statistical multi-step direct (SMD) and statistical multi-step compound (SMC) processes.

Figures 20-22 illustrate the results of calculation together with the experimental data. These calculations were done using model parameters built in the code as default values without any adjustment. The calculations reproduce the experiments excellently both in shape and magnitude even in the energy region of collective excitation except for the underestimation of the Bi data at 14.1 MeV. It is very impressive that the EXIFON code reproduces the experiments over wide range of target-mass and secondary neutron energy

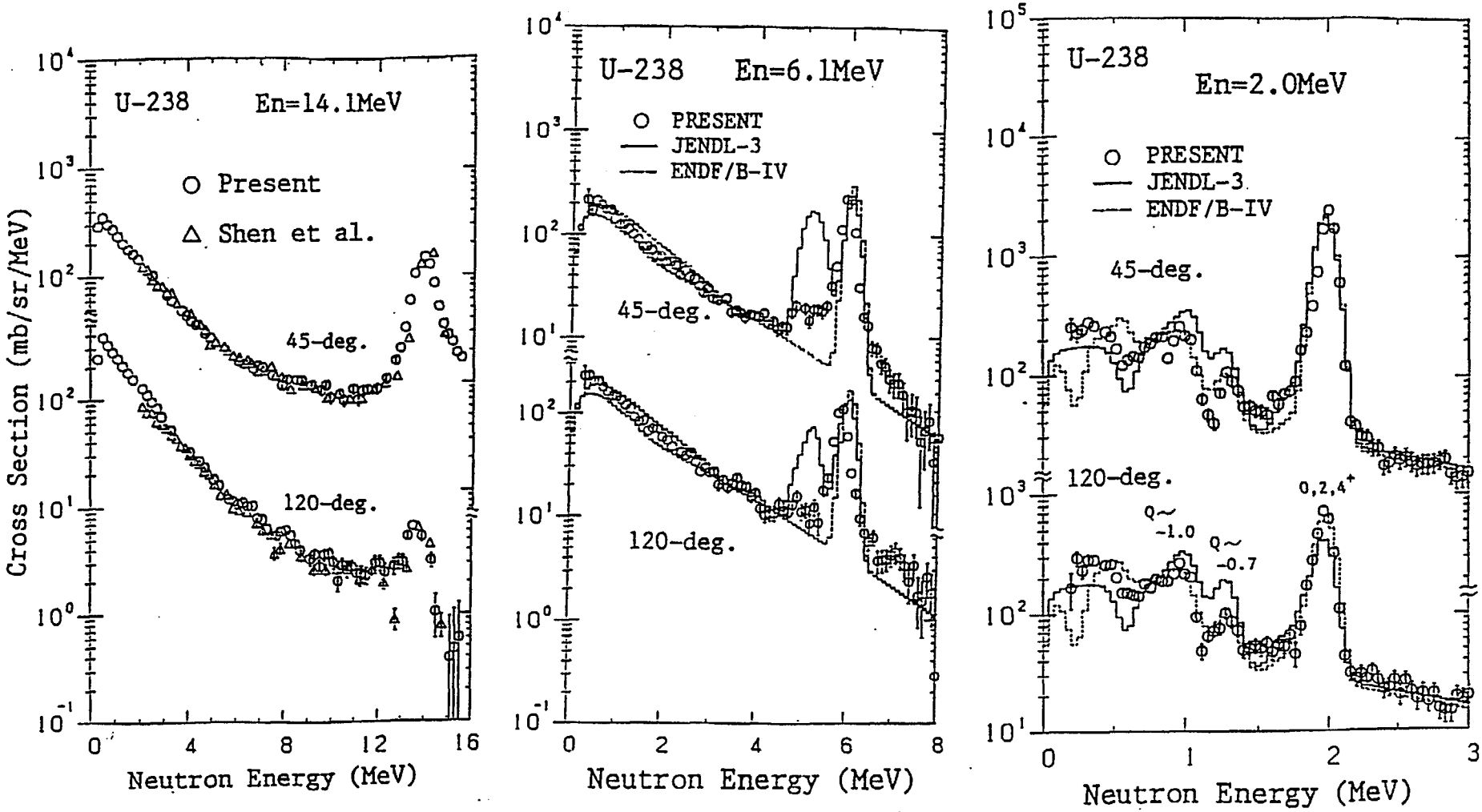


Fig.19: Double-differential neutron emission cross sections of U at 14.1 MeV (left), 6 MeV (middle) and 2 MeV (right).

with a single set of model parameters. These results of calculation indicate the importance of direct inelastic-scattering leading to low-lying levels for description of high energy parts of emission spectra.

(2) Then, the experimental data for angular distribution are compared with those derived from the systematics by Kalbach & Mann /9/ and that by Kalbach /10/ to see the applicability of them as the practical tool for prediction of angular distributions. These systematics represents the angular distributions by superposition of the forward-peaked distribution for SMD process and the isotropic or 90-deg symmetric distribution for SMC.

In the present calculation, the fractions of SMD and SMC were derived from the above mentioned EXIFON calculation. In our previous calculation, we employed a semiclassical modeling for SMD and SMC /6,7/; in these calculations, we assumed that the emission spectra from the SMD and SMC processes are, respectively, equivalent with those by exciton and evaporation model, and determined relative strength so as to reproduce the experimental EDX. Figure 23 illustrates an example of the comparison between the calculations using EXIFON and the previous method. The "SMD" spectrum by the exciton model extends to lower energy region than in the EXIFON calculation since in this model the neutrons emitted from the exciton states of large exciton number are also regarded as the SMD process. This difference will affect the results of angular distributions using the systematics.

The results of the present calculation for angular distribution are shown in Figs.24-25 for typical outgoing neutron energy together with the experimental data. The angular distribution becomes forward-peaking with outgoing energy because of increase of the SMD fraction. Generally, the present data are reproduced fairly well by both systematics in nearly same quality despite the fact that both systematics were derived mainly from the data at much higher incident energies /9,10/.

It is noted that the present calculation using EXIFON reproduces the experiments markedly better than previous one using semiclassical model. In previous analyses, both systematics in particular Kalbach & Mann's one tended to overemphasize the forward rise as a results of over weighting the SMD as mentioned above, and agreement between the calculation and experiment became worse with decreasing target mass.

Then, to quantify the degree of anisotropy, we derived and compared the 1-st order reduced Legendre coefficient b1 = $a_1/a_0$ for experimental data and the calculation using Kalbach & Mann systematics, where $a_0$, $a_1$ are the Legendre coefficients for each angular distribution. Figure 26 presents the results of b1 for typical outgoing energies as a function of target mass

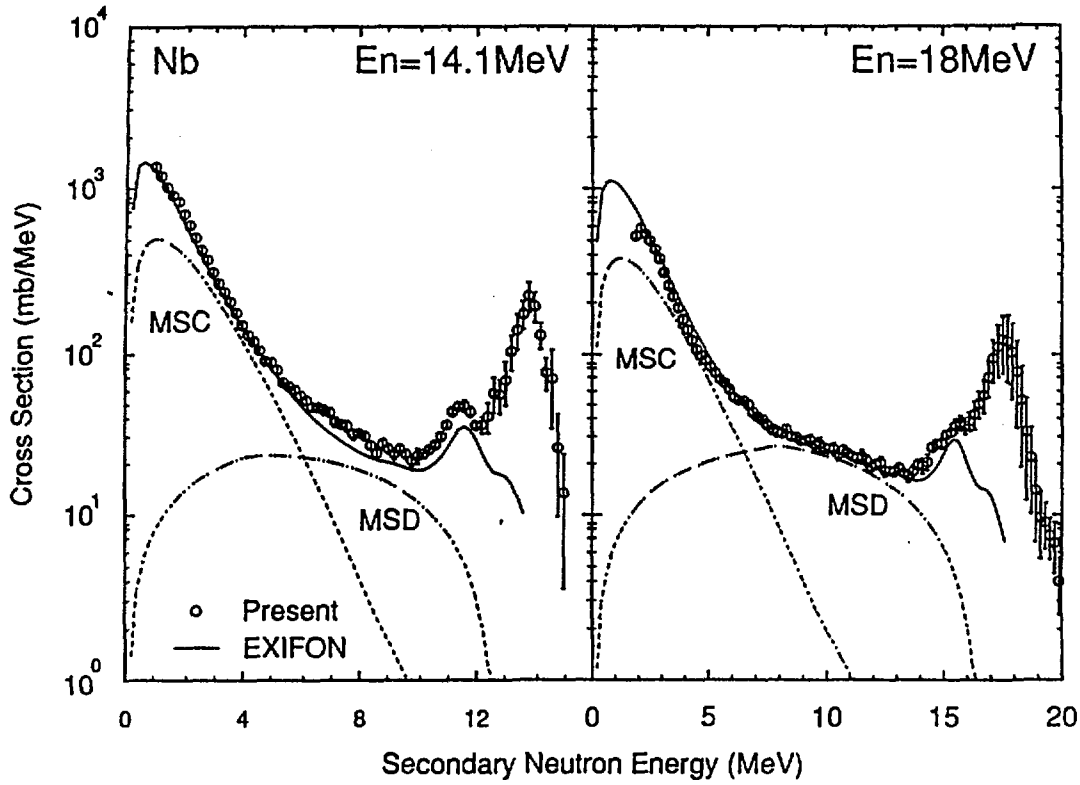


Fig.20: Comparison of angle-integrated neutron emission spectrum of Nb at 14.1 and 18.0 MeV, between the present experiment and EXIFON calculation.

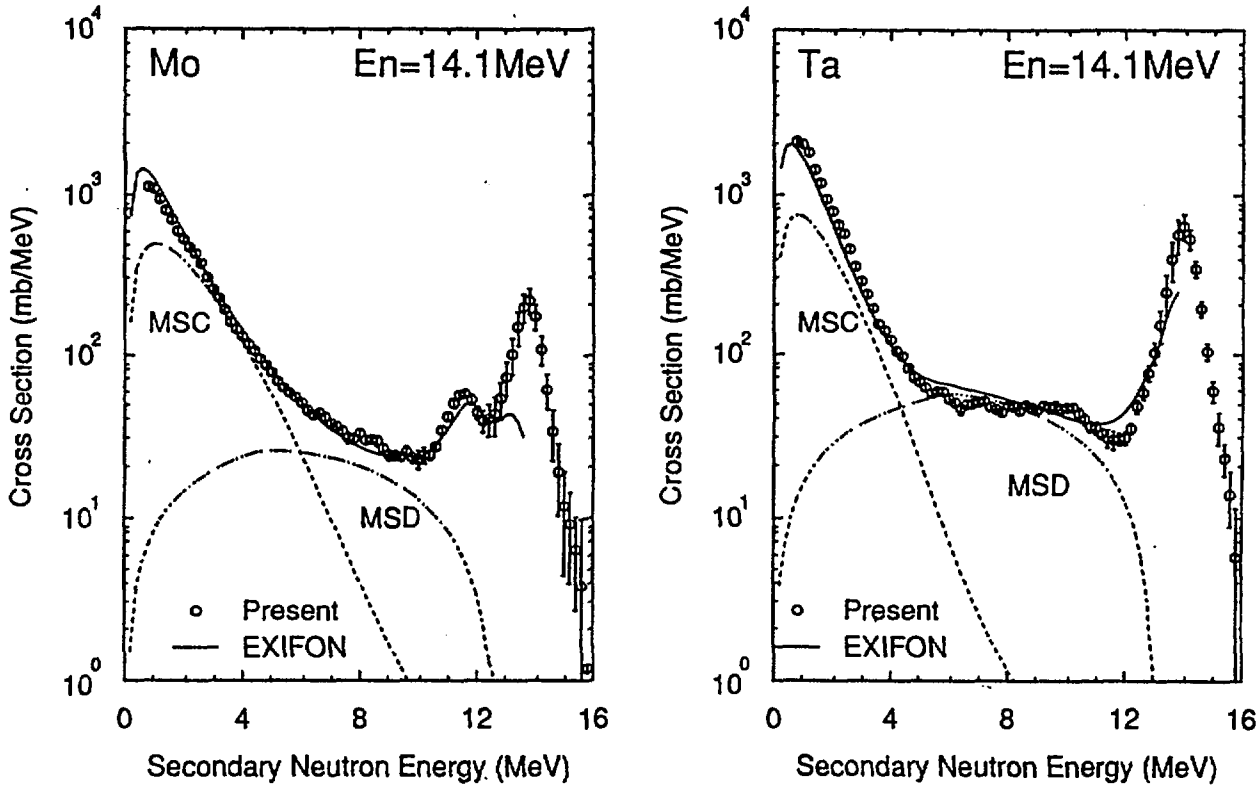


Fig.21: Comparison of angle-integrated neutron emission spectrum of Mo and Ta at 14.1 MeV, between the present experiment and EXIFON calculation.

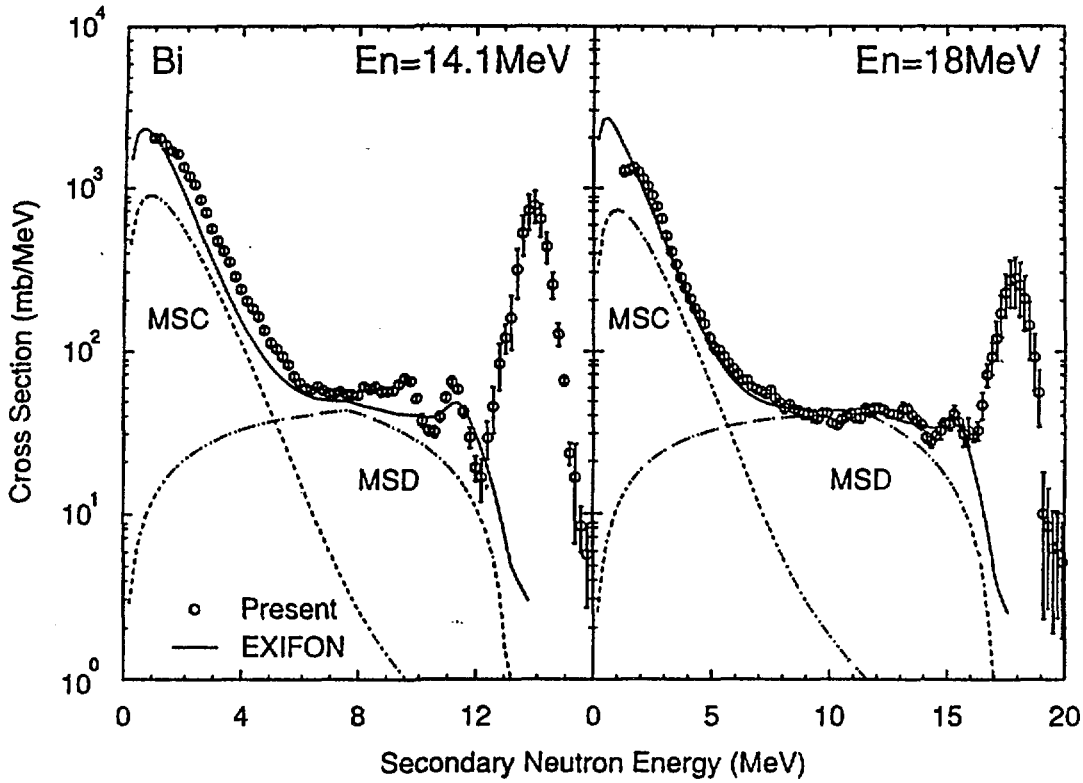


Fig.22: Comparison of angle-integrated neutron emission spectrum of Nb at 14.1 and 18.0 MeV, between the present experiment and EXIFON calculation.

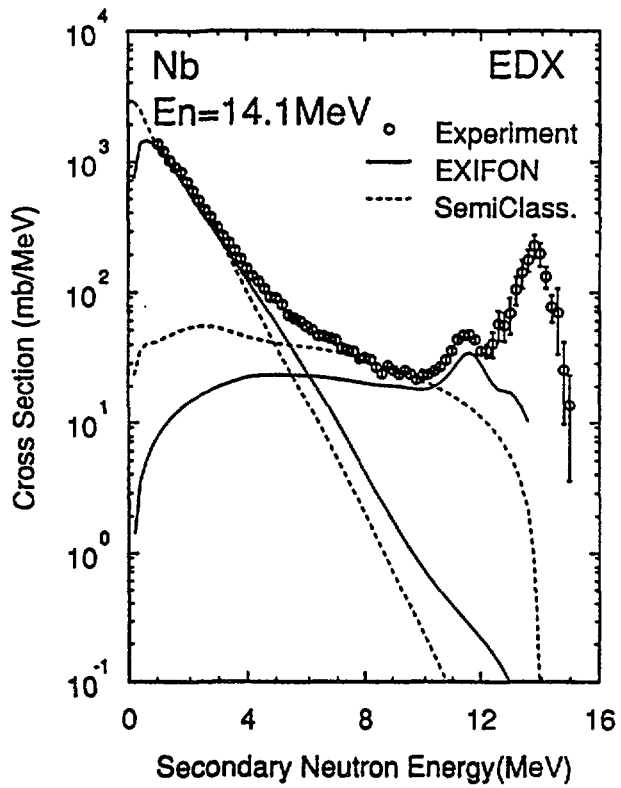


Fig.23: Comparison of angle-integrated neutron emission spectrum of Nb at 14.1 MeV, between the calculations using EXIFON and semi-classical model.

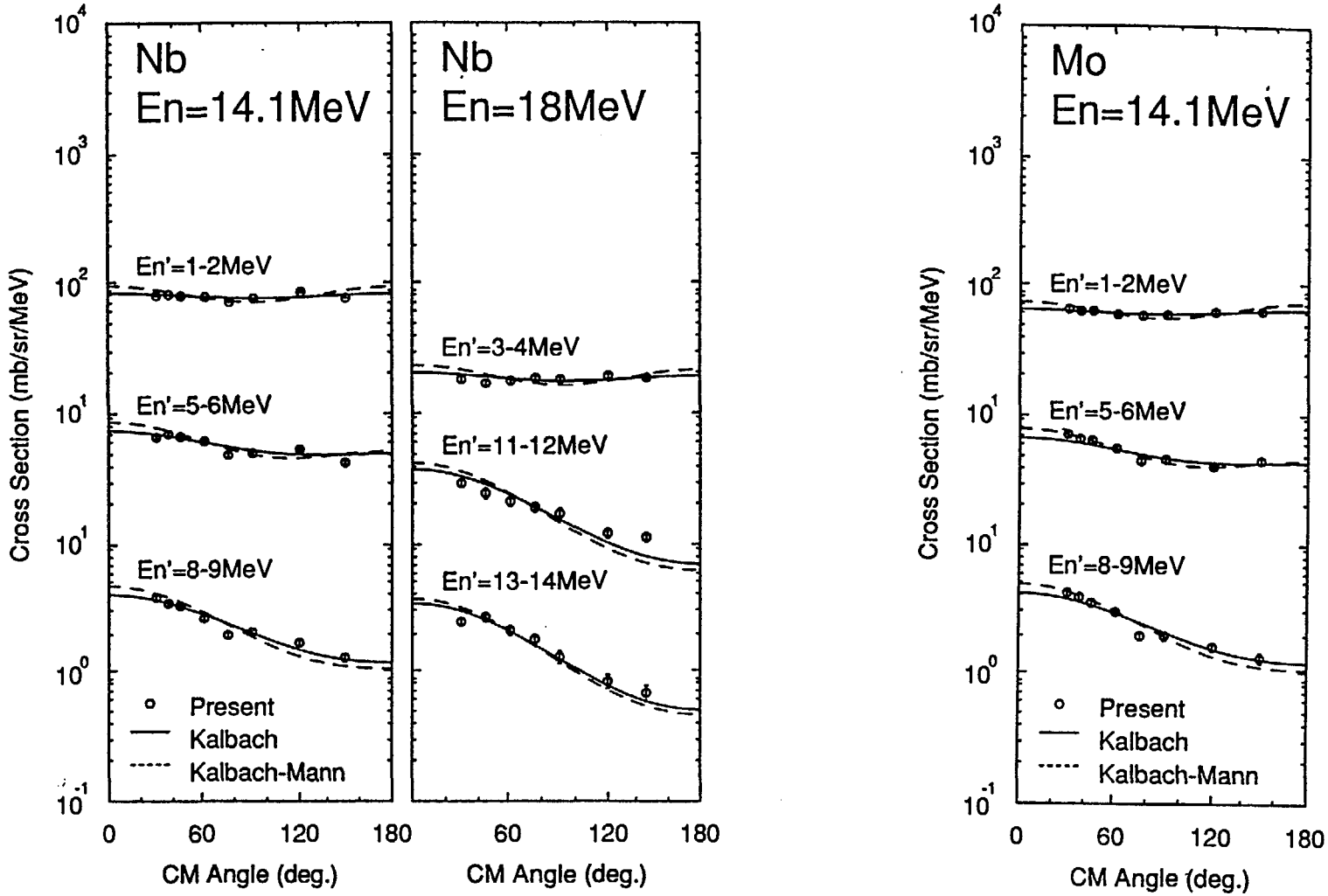


Fig.24: Comparison of angular distributions of secondary neutrons of Nb (left) and of Mo (right) between the present experiment and the systematics by Kalbach-Mann and by Kalbach.

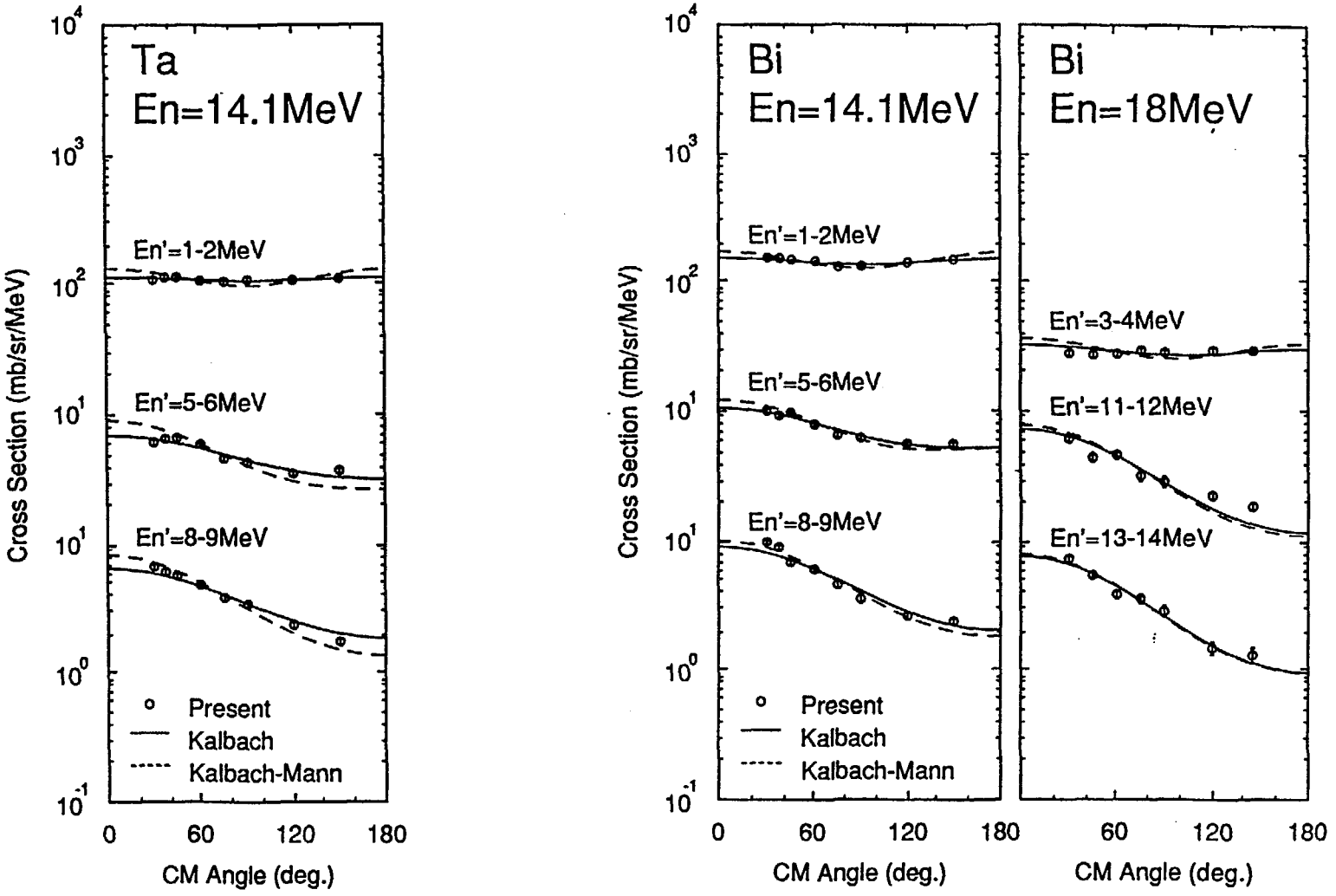


Fig.25: Comparison of angular distributions of secondary neutrons of Ta (left) and of Bi (right) between the present experiment and the systematics by Kalbach-Mann and by Kalbach.

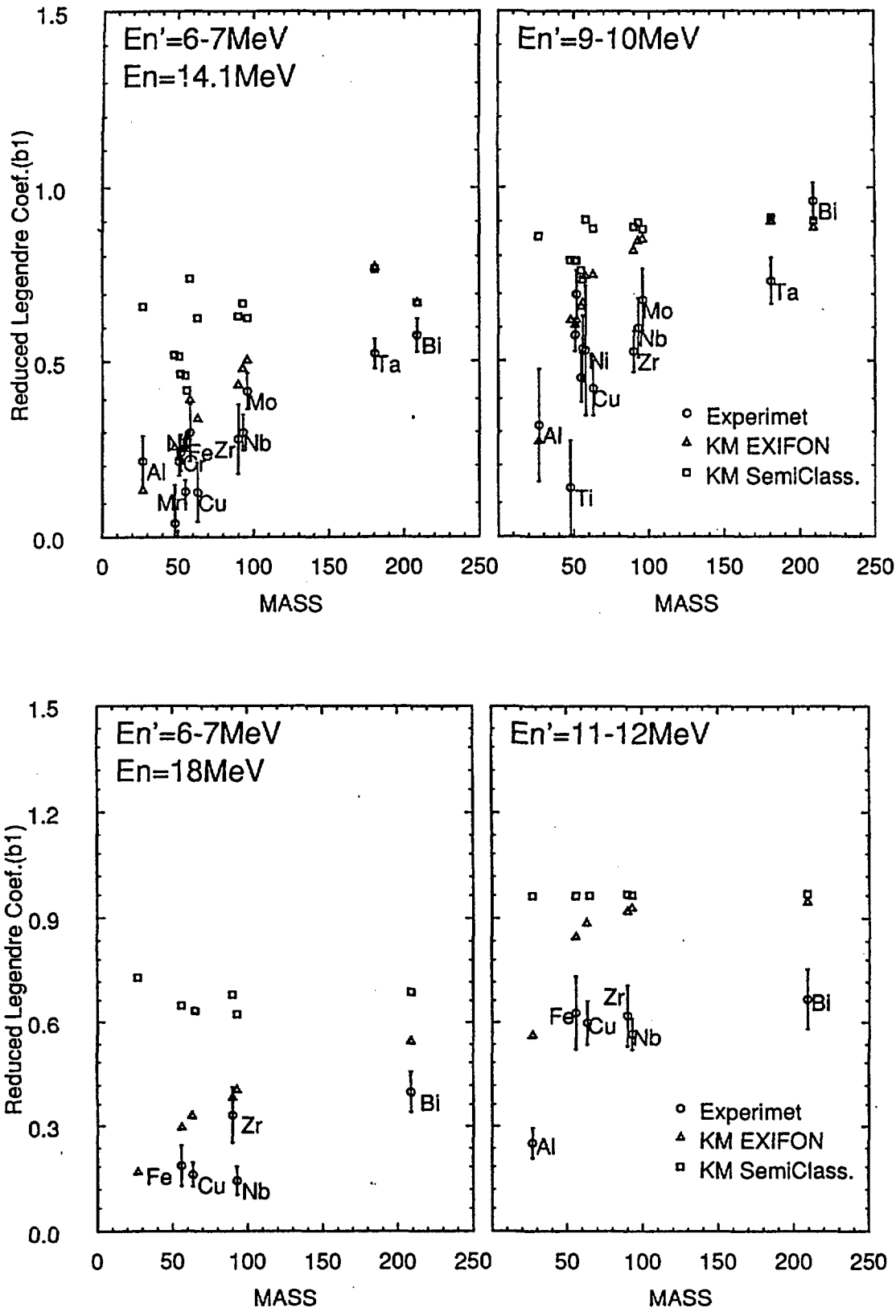


Fig.26: Reduced Legendre coefficients for secondary neutrons as a function of target mass; the experimental results are compared with calculations using Kalbach-Mann systematics with SMD/SMC partition by EXIFON and semi-classical model.

number including the data for lighter mass which were measured previously /6/; the results by semiclassical model are shown as well as those by EXIFON.

The experimental bl tends to decrease with mass number and this trend is traced better by the calculation based on the SMD/SMC partition with EXIFON than that by semiclassical treatment. This is in agreement with the observation reported by Watanabe et al. /24/. Nevertheless the $b_1$ by experiments still show differences from the systematics and it should be traced more for better understanding.

## 5 Summary

Double differential neutron emission cross sections for Fe, Nb, Mo, Ta, Bi and U measured at Tohoku University are presented in comparison with other experiments, evaluated data and model calculations. .

From the data comparison, it is confirmed that experimental data for angle-integrated emission spectrum show fair agreement each other. However, the evaluated data, JENDL-3 and ENDF/B-VI, show marked disagreement with these experimental data in spectrum shapes. In addition, the anisotropic angular distribution of high energy neutrons observed in the experiments are not reproduced by the evaluated data because of lacks in angular information except for Nb and Bi in JENDL-3.

The experimental emission spectra were reproduced very well by the calculations using the EXIFON code based on the quantum mechanical modeling. The angular distributions of continuum neutrons were reproduced by the systematics of Kalbach & Mann and of Kalbach; better agreement was obtained by using SMD/SMC partition with EXIFON than with exciton/evaporation treatment. For better reproduction of angular distribution, further studies will be required.

## Acknowledgement

The authors would like to thank Dr.H.Kalka of T.U Dresden and Dr.Y.Watanabe of Kyushu University for providing them with the EXIFON code. They are indebted to T.Iwasaki, M.Fujisawa, and R.Sakamoto for their helps in experiments. This work was partly supported by Japan Atomic Energy Research Institute.

References:


1 M.Baba et al.: Proc.Conf. Neutron Physics and Nuclear Data (Harwell 1978) p.198

2 S.Chiba et al.: J.Nucl.Sci.Technol., 22(10) 1(1985)

3 M.Baba et al.: Radiation Effects 92-96 223(1986)

4 M.Baba: JAERI-M 86-029 (JAERI 1986) p.119

5 M.Baba et al.: Proc.Conf. Nuclear Data for Science and Technology (Mito 1988) p.209

6 M.Baba et al.: ibid., p.291

7 M.Baba et al.: J.Nucl.Sci.Technol., 27(7) 601(1990)

8 H.Kalka: Z.Phys., A341 298(1992) and private communication

9 C.Kalbach and F.M.Mann, Phys. Rev., C23(1) 112 (1981)

10 C.Kalbach: ibid., C23(1) 124(1981)

11 M.Baba: JAERI-M 86-080 (JAERI 1986) p.270

12 M.Baba et al.: JAERI-M 90-025 (JAERI 1990) p.383

13 S.Matsuyama et al.: Proc.Conf. Nuclear Data for Sci. Technol. (Julich 1991) to be published

14 P.J.Pasma: Nucl.Phys., 6 141(1958)

15 J.R.Smith and S.T.Thoronton: ibid., A187 433(1972)

16 G.Randers-Pehrson et al.: Nucl.Instr.Methods 215 433(1983)

16 S.Iwasaki: NETU-41 (Dep. Nucl. Eng., Tohoku University, 1983) p.5

17 M.Baba et al.: NETU-47 (Dep. Nucl. Eng., Tohoku University, 1986) p.110

18 R.E.Textor & V.V.Verbinski; ORNL-4160 (ORNL 1965)

19 W.E.Kinney: Nucl.Instr.Methods 83 15(1970)

20 A.Takahashi et al.: J.Nucl.Sci.Technol., 25(3) 215(1988)

21 A.Takahashi et al..: OKTAVIAN Report A87-01 (1987)

22 A.Pavlik and H.Vonach: Physics Data No.13-4, ISSN 0344-8401 (Fachinformationszentrum Karsruhe 1988)

23 G.Shen et al..: Proc.Conf. Nuclear Data for Science and Technology (Mito 1988) p.201

24 Y.Watanabe et al.: Proc. 1991 Nuclear Data Symposium, to be published from JAERI

# DOUBLE DIFFERENTIAL NEUTRON EMISSION CROSS SECTIONS OF Fe INDUCED BY 14.1 MeV NEUTRONS

T. VILAITHONG, D. BOONYAWAN, S. KONKLONG, W. PAIRSUWAN AND S.SINGKARAT

**Fast Neutron Research Facility, Department of Physics, Faculty of Science, Chiang Mai University, Chiang Mai 50002, THAILAND**

We measured the energy spectra and yields of neutrons above 2 MeV emitted from collisions of 14.1 MeV neutrons with an iron target. The measurements were made using the pulsed neutron time-of-flight technique with a 10 m long flight path. The data were obtained at 13 angles between 30 to 150 degrees and the angle-integrated spectrum was determined. The results are compared with the most recent measurements and with the calculated spectra based on the JENDL-3 and ENDF/B-VI data.

## 1. Introduction

Iron has been one of the few elements proposed as a candidate for fusion reactor structural materials, and accurate measurement of its double differential neutron emission spectra have been requested [1]. Several measurements of its double differential cross sections (DDX) at 14 MeV were made in the sixties and seventies. Most of these measurements were carried out at a few emission angles only. For those intensive measurements where angular distributions were taken over many angles [2-3], the measured spectra do not agree over the entire energy region.

In the eighties, attempts were made to remeasure the DDX with better energy resolution [4-6] in order to obtain better data in the high energy region where pre-equilibrium and direct neutron spectra overlap. Takahashi et al. [4] used an 8.3 m long TOF facility at Osaka University to measure neutron emission spectra. They observed three states (0.85, 3.23, and 4.40 MeV) strongly excited at 14.1 MeV. At Tohoku University, Baba et al. [5] carried out similar measurement at 14.1 MeV using the Dynamitron Time-of-Flight neutron spectrometer with a flight path of 6 m. They also observed three states excited at about the same energy as seen by Takahashi et al. Lychageen et al. [6] measured the DDX spectra from iron with time resolution of about 0.45 ns/m and a path length of 7.1 m. They observed strongly excited states $2^+$ and $3^-$ with energies of 0.85 and 4.51 MeV. The TOF spectrometers employed by Baba et al. and Lychageen et al. are approximately equivalent in energy resolution. The 3.23 MeV state was not clearly observed in the latter experiment. Mellema et al. [7] observed scattered neutrons in a seven-fold array of liquid scintillator detectors at a flight path of 13 m. They measured eleven inelastic levels for $^{56}$Fe at 11 MeV incident neutron but observed only two states (0.85, 4.51 MeV) strongly excited at 26 MeV. Based on data of Mellema et al. at 11 MeV, the $2^+$ (4.40 MeV) and $3^-$ (4.51 MeV) were both excited, with the probability of exciting the $3^-$ state three times stronger. The 3.23 MeV state observed by Takahashi et al. [4] should be the unresolved $4^+$ (3.12 MeV) and $2^+$ (3.37 MeV) states. Both of these states have equal probability of being excited.

The result of spectral comparison indicates that in the continuum region where compound and pre-compound reaction dominate, the three measurements are in reasonable agreement. Difference could be observed in the direct reactions region where collective excitations of low-lying states could take place. This difference becomes obvious when one compares the experimental data with ENDF/B-IV and JENDL-3T data [4]. The measurements reported here provide an important independent determination of these spectra.

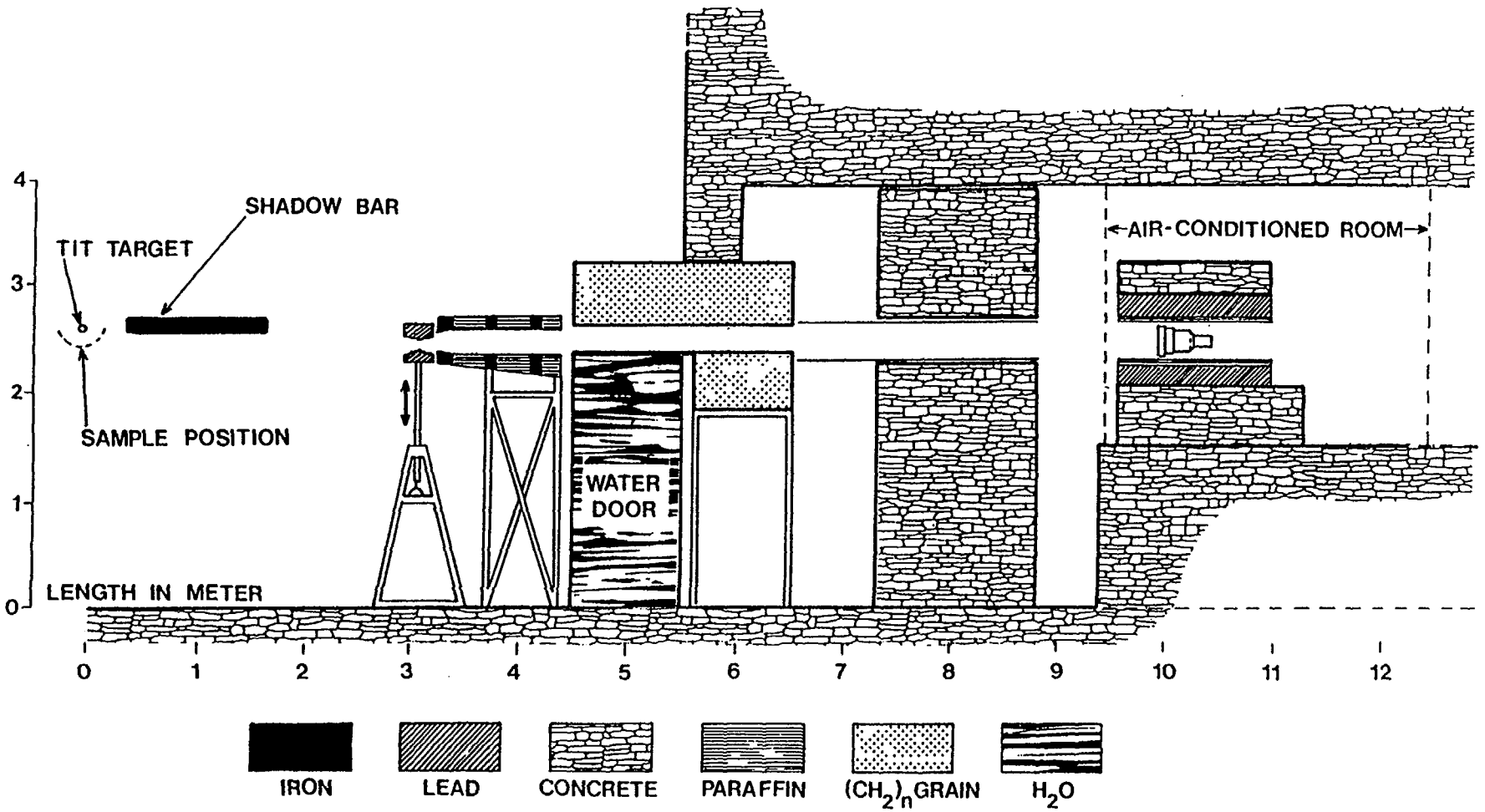


Fig. 1 Experimental arrangement for DDX measurement.

## 2. Experimental Method

The production of ns pulsed neutron beam has been described in an earlier publication [8]. Briefly, neutrons are produced from the high stability Cockcroft-Walton type accelerator by the $T(d,n)^4He$ reaction. The 140 keV deuteron beam is analyzed by an analyzing magnet. The beam is chopped by a double-plate deflecting system and then bunched to pulse with widths of 1.5 to 2.0 ns at the neutron production target by a double-gap klystron buncher. Beam sizes both in horizontal and vertical axes are monitored by means of cross-wire beam profile monitors. For the present work, an average beam current of about 15 $\mu$A was attained, with a neutron pulse width of about 1.8 ns at 1 Mhz repetition rate.

A schematic diagram of the present system is shown in Fig.1. A cylindrical sample of natural iron ($^{54}Fe$ = 5.9%, $^{56}Fe$ = 91.72%, $^{57}Fe$ = 2.1%, $^{58}Fe$ = 0.28%), 3 cm in diameter and 7 cm long, was positioned at 90° relative to the incident deuteron beam with its axis along the axis of the beam line. The sample was set on top of a thin aluminum pipe about 17 cm from the neutron production target. Holes were drilled in the pipe so as to leave the pipe with little material as possible. In order to reduce material around the scattering sample, the tritium target was housed in a 1.5 mm thick and 30 cm long stainless steel tubing. The target was cooled by forced air. The beam line is about 2.5 m above floor level. At this position and with this dimension of the sample, Monte Carlo calculation [9] indicates that the incident neutron energy is about 14.06 $\pm$ 0.09 MeV. A sample rotation technique provides the capability of measuring scattered neutrons over an angular range of 20 to 160 degrees.

Neutrons were detected in BC-501A liquid scintillator detector of diameter 25.0 cm and thickness 10.0 cm. The main detector was coupled to a RCA 8854 photomultiplier tube (PMT) via a partially coated taper light pipe [10]. The photomultiplier base was a modified version of the one suggested by Randers-Pehrson et al. [11]. The neutron detector was located at an extended flight path of 10 m inside a well-shielded underground tunnel. The collimating column has polyethylene lining. We estimated the effect of in-scattered neutron by Monte Carlo calculation to be less than 1 percent for the present collimating system. Also, a pre-collimator made of lead with adjustable height limits the main detector to view only small space of solid angle where the sample is placed. The neutron detector was housed in a temperature controlled room to minimize photomultiplier tube gain drift.

The flux-monitor detectors are three 5 cm diameter by 5 cm thick NE-102A and NE-213 scintillators. The detectors are positioned above the reaction plane and view the neutron production target directly at 90° on the opposite side of the main neutron detector. The discriminating threshold of each detector was set at about 8 MeV proton energy during the experiment. The ratio of count rates registered between each pair of detectors were recorded after each run and compared against one another throughout the entire measurement. In this way we are confident that our flux monitoring system is accurate to better than 1 percent.

The timing detector is a 2.54 cm diameter by 2.54 cm thick NE - 102A scintillator. It is located about 3 m from the tritium target. This detector is used to monitor the timing width of the pulsing system. The width of the timing pulse was adjusted to be between 1.6-2.0 ns during the entire measurement. This is the condition at which the pulsing system is most stable.

The block diagram of the measuring system is shown in Fig.2. A pulse-shape discrimination system (PSD) based on a zero-cross over method was incorporated into the main electronics system to reduce the gamma-ray background. The neutron pulse height information (PHA) is acquired directly from a dynode of the PMT base for a proper threshold selection for off-line analysis. The neutron flight time (TOF) is determined by utilizing a fast beam pick-off

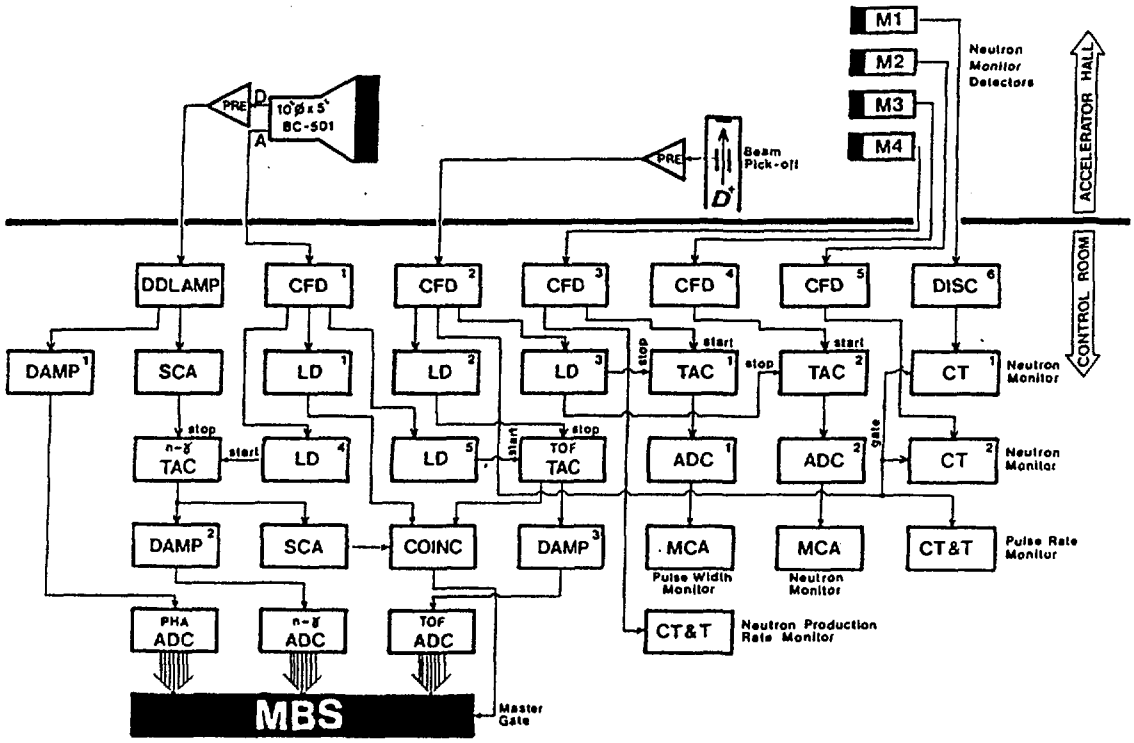


Fig.2(a) Block diagram of the electronic system.

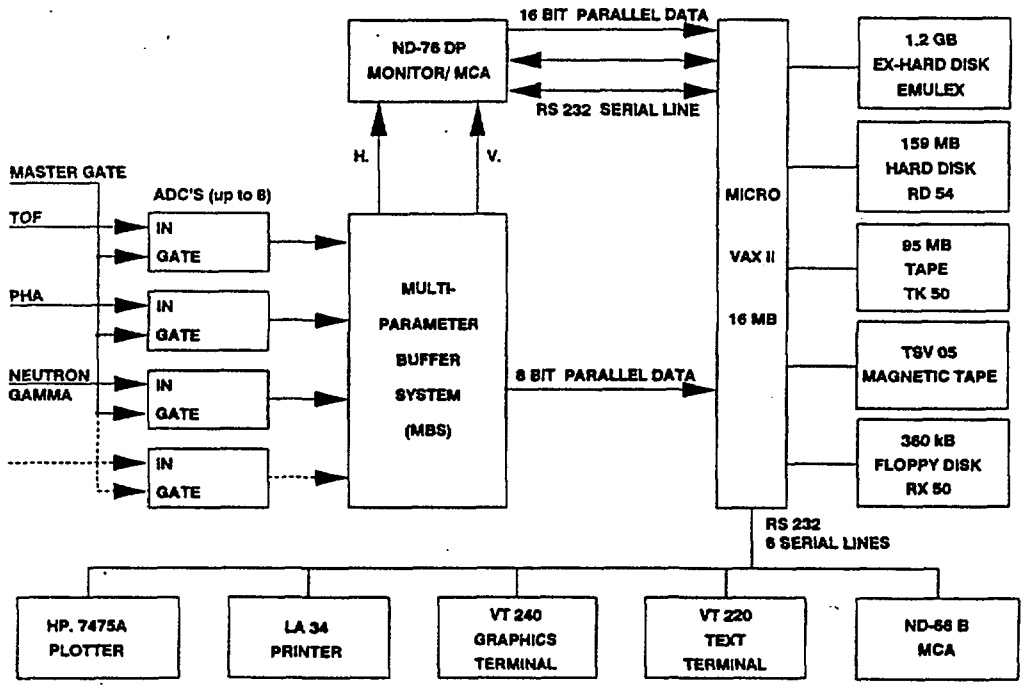


Fig.2(b) Multiparameter data acquisition and analysis system.

signal of a 1 Mhz rate with 2-3 ns rise time as a time reference signal. The TOF, PHA and PSD signals are synchronized and a coincidence signal is produced to trigger a master gate input of the multi-parameter buffer system (MBS) unit to record the three parameters corresponding to each neutron event. The data-acquisition system is controlled by a 16 MB MicroVAX II computer through the MBS unit. Each reaction event detected by the main detector is recorded sequentially in list mode on disk. Our off-line analysis software allows dynamic selections for each correlated parameter in contrast to a conventional hardware-resolution routine.

The pulse height from the main counter was calibrated in about 6 hours intervals before and after each scattering angle with $^{137}Cs$ and $^{22}Na$ radioactive gamma sources. The pulse-height threshold was set at about 1 MeV proton energy. At this bias setting, the overall timing resolution observed from the width of the prompt $\gamma$- ray peak in the TOF spectrum is 2.3 ns (FWHM). The source neutron spectrum measured with the main detector displays resolutions at 14 MeV of about 3.5 ns (FWHM) and 7.9 ns (FWTM) which are equivalent to 513 kev and 1141 kev, respectively.

## 3. Time-of-Flight Measurements.

The measurements were performed at angles from about 30° to 150° in 10° increment. For each set, a "sample-in" spectrum was taken followed by a "sample-out" spectrum. The sample-out background run was used for measurements at angles $\theta$ and (180-$\theta$). Since at these two scattering angles the conditions at the pre-collimator and the shadow bar are similar. Each run took about 2-3 hours. Therefore the main detector was calibrated every six hours before and after each set of measurement. The stability of the electronics was better than 1 percent. It should be noted that all the electronics modules used for the production of ns pulses and radiation measurement are housed in a temperature and humidity controlled area.

A polyethylene sample of same dimension as that of the iron sample was used as standard. Scattered neutrons were recorded at 25° relative to the incident neutron. These polyethylene spectra were recorded at regular intervals. The use of standard sample having the same dimension as the iron sample is a compromise between good counting statistics and multiple and attenuation corrections. Also, the flux monitors were checked regularly. Our experience with three counter monitoring system indicates that there were few occasions where one of the detectors gave inconsistent reading while the other two were functioning properly.

The source neutron spectrum at 90° shown in Fig.3 was measured by a NE-102A scintillator of 5 cm diameter and 5 cm thickness using similar electronic system as in Fig.2. According to Takahashi et al. [12], the low energy part in the energy region of less than about 10 MeV is attributed to the inelastic scattering of 14 MeV neutrons with the structure of the target assembly. They also did an experiment to verify that the scattered-in neutrons from the collimator assembly has no significant contribution to this effect. This fact seems to support the result of our Monte Carlo calculation. Since our source neutron spectrum was taken with a small detector we do not expect multiple scattering of 14 MeV incident neutrons in the detector to be appreciable. The spectral shape in the region between 10-15 MeV can be considered as a representation of the source spectrum for our experiment. This spectrum between 2 and 15 MeV was used in the multiple scattering correction process to account also for the effect of neutrons scattering from target assembly.

A typical TOF spectrum of natural iron at 40° is shown in Fig.4. Also shown in this figure is the sample-out spectrum. The n - $\gamma$ pulse shape discriminating was set to admit some gamma radiations. This prompt gamma ray peak is used as reference for conversion TOF to energy spectrum. Three states at 0.81, 3.25, 4.51 MeV are clearly observed. The background spectrum is clean and shows no structure in the region of interest. The only noticeable region in the background spectrum is around channel 710-730 which is probably the contribution coming from the elastic scattering of neutrons from air surrounding the sample.

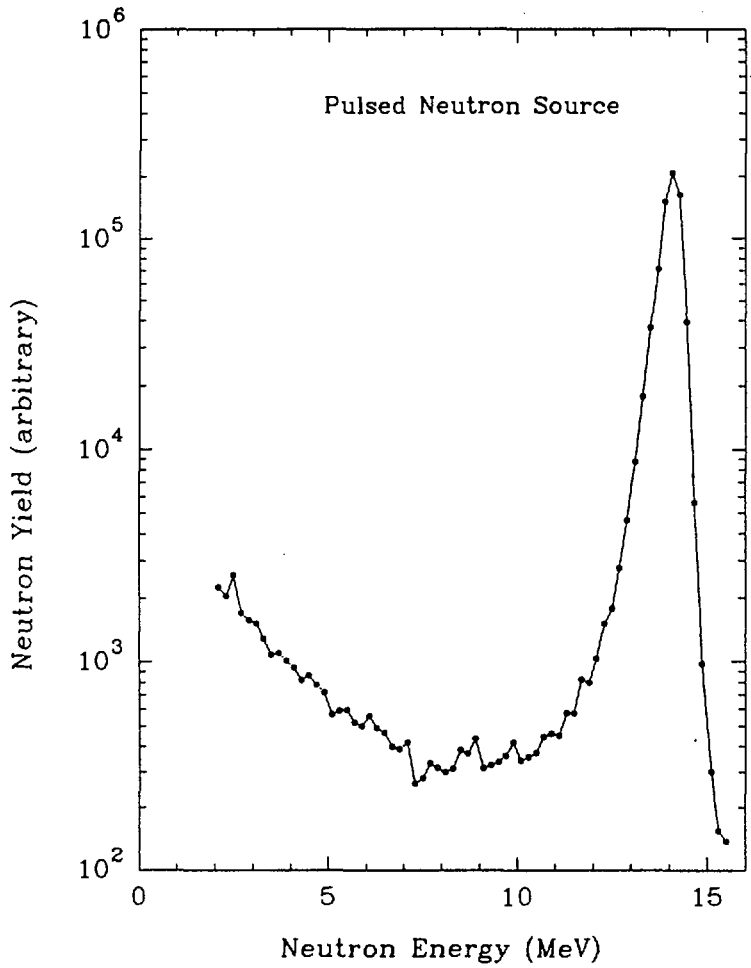


Fig. 3 Measured source neutron spectrum at 90°.

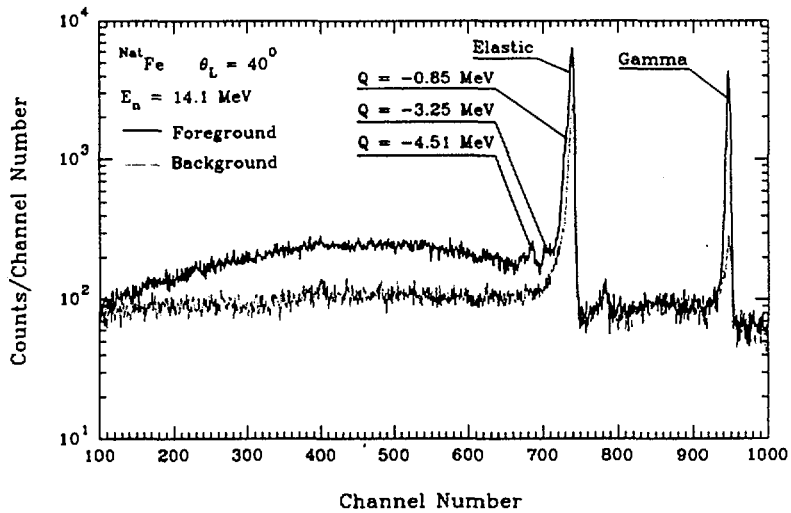


Fig. 4 Typical time-of-flight spectrum of Fe at 40°.

## 4. Data Reduction

The DDX in units of barns per steradian per MeV for each energy internal $E$ of the spectrum is given by the expression:

$$\frac{d^2\sigma(E_o,\theta,E)}{d\Omega\, dE} = \frac{Y(\theta,E)}{Y_H(\varphi)} \frac{M_H N_H}{M_{Fe} N_{Fe}} \frac{\varepsilon_H(E_\varphi)}{\varepsilon(E)} \frac{A(E_o,\theta,E)}{A_H(E_o,\varphi)} \frac{d\sigma(E_o,\varphi)}{d\Omega} \frac{1}{\Delta E} \qquad (1)$$

where

$\frac{d^2\sigma(E_o,\theta,E)}{d\Omega\, dE}$ : Double-differential cross section of neutrons incident energy $E_o$ through angle $\theta$ with secondary neutron energy $E$.

$Y(\theta,E)$ : Neutron yield for iron sample in the energy bin $\Delta E$ around $E$ at angle $\theta$.

$Y_H(\varphi)$ : Neutron yield for polyethylene sample in the measured elastic peak at scattering angle $\varphi=25°$ in the laboratory system.

$M_H$, $M_{Fe}$ : Monitor counts for polyethylene and iron sample, respectively.

$N_H$, $N_{Fe}$ : Number of hydrogen nuclei in polyethylene and iron nuclei in iron samples, respectively.

$\varepsilon_H(E_\varphi)$, $\varepsilon(E)$ : Detecting efficiency of neutron with mean kinetic energy $E_\varphi$ and $E$, respectively.

$A(E_o,\theta,E)$, $A_H(E_o,\varphi)$ : Attenuation and multiple scattering correction factors for iron and polyethylene samples, respectively.

$\frac{d\sigma(E_o,\varphi)}{d\Omega}$ : Differential elastic scattering of hydrogen at an angle $\varphi = 25°$ for incident neutron energy $E_o$.

$\Delta E$ : Width of the energy interval.

The width of the energy interval was taken to be 200 keV which is about a half of the energy resolution of the system at 14 MeV. The differential elastic cross section of hydrogen at 25° for 14.1 MeV neutron taken from the ENDF/B-VI cross section library [13] is 191.4 mb/sr.

The relative neutron detecting efficiency $\varepsilon_H(E_\varphi)/\varepsilon(E)$ was calculated with the Monte Carlo computer program of Cecil et al. [14]. The light output function for the BC-501A scintillator was a semi-empirical fit to twenty experimental light response data set of NE-213 scintillator [15]. These efficiency calculations were compared with the measured values obtained by TOF technique using a Cf-252 fission neutron source [16]. The agreement is better than 3 percent prior to normalization. Therefore, an uncertainty in the Monte Carlo calculation of the relative efficiencies is estimated to be better than 3 percent for a well-known threshold. An uncertainty in the pulse height threshold due to gain shift of the electronic system during each angular distribution measurements was found to be negligible.

The neutron spectrum was determined from the measured TOF spectra in two separate energy regions. The low-energy portion from 1 to 6 MeV were analyzed at a hardware

threshold of 1 MeV proton. Data above 6 MeV were analyzed at a pulse-height threshold of 3 MeV proton to improve energy resolution. The two spectra joined smoothly in the overlap region. The $\gamma$ - rejection was observed for each of the TOF regions because the $\gamma$ - rejection technique was pulse-height dependent. Because of the its big volume, neutron and gamma events in the pulse shape spectrum were not completely separated and some neutrons were lost. This loss was never greater than 1 percent therefore no correction was made.

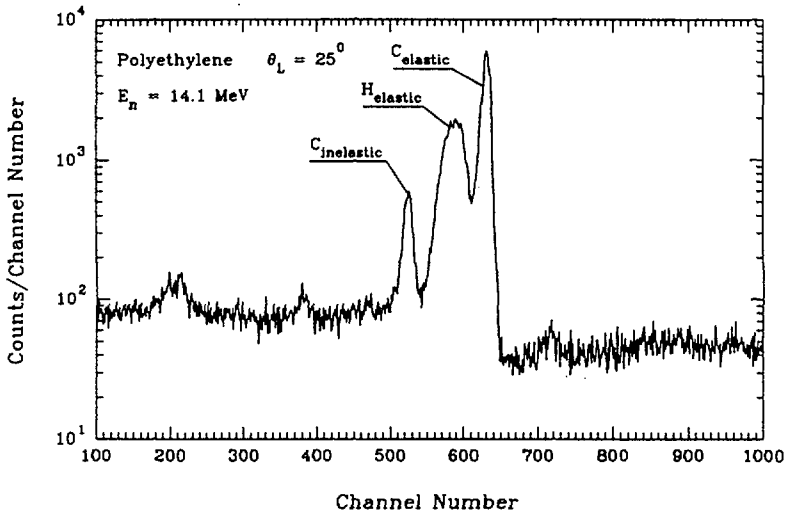


Fig. 5 Time-of-flight spectrum of polyethylene at 25°.

Several corrections were made to the number of detected neutrons. A correction was made to the number of neutrons incident on the iron sample at each scattering angle relative to the polyethylene sample. The hydrogen scattering sample was at 21.9 cm from the neutron production target while separation distance of the iron sample at each scattering distance of the iron sample at each scattering angle varied from 17.25 cm at 90° to 17.63 cm at 30° . Correction for the neutron interactions in the aluminum casing of the main detector was estimated to be less than 1 percent. Correction due to air scattering in flight was estimated to be less than 1.4 percent. Correction for neutron interaction in aluminum casing was not made and an uncertainty of 1 percent is assigned to account for both effects.

Multiple scattering corrections have been carried out with the MUSCC3 computer code [17] which is based on the multi-point collision probability method. This code also treats the correction for the continuous low energy part of the incident neutron spectrum. In this correction 64 angle points and 135 energy groups of DDX-type data processed from JENDL-3 cross sections [18] were used. Multiple scattering correction were made for both the polyethylene and iron samples. The magnitude of the correction factor for polyethylene is 1.18. These corrections are accurate to within about 10 percent for the polyethylene and iron samples. The accuracy of this correction is based on the knowledge of the evaluated cross sections. An accuracy of 20 percent is assigned to the overall correction factor, $A(E_0,\Theta,E)/A_H(E_0,\varphi)$, of these multiple scattering effect. Examples of the magnitude of this relative correction factor is shown in Fig.6 for spectra taken at 60°, 90° and 150°. In the lower energy region below about 4 MeV, the correction is relatively small because more neutrons are emitted in this region. The attenuation and multiple scattering effects almost cancel each other.

The overall systematic error for the value of the DDX is estimated to be $\pm$ 7.3 to $\pm$ 13.7 percent. This number was obtained from the following estimated uncertainties summed as squared values: (1) $\pm$ 3 percent for the neutron detection efficiency ; (2) $\pm$ 2 percent for the

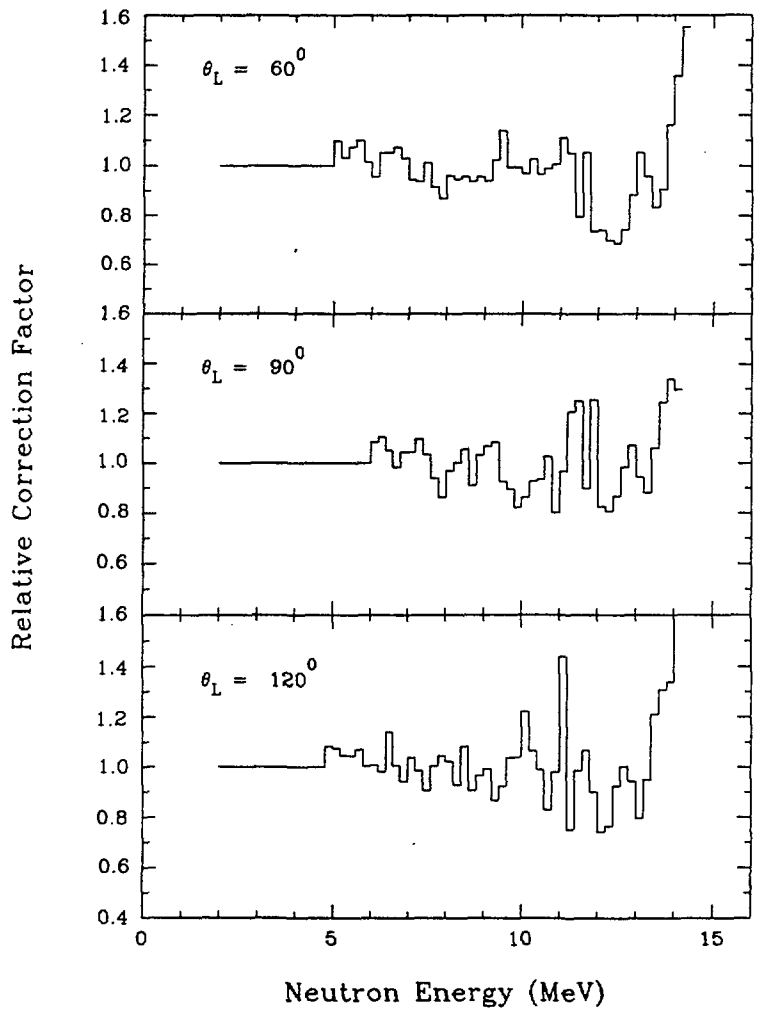


Fig. 6 Correction factor due to multiple scattering and attenuation effects at 60°, 90°, and 120°.

variation of the incident neutron yield; (3) ± 1 percent for the H cross section ; (4) ± 1 percent for the monitor; (5) ± 2 percent for estimating hydrogen scattering yield; (6)± 6 to ± 13 percent for the multiple scattering correction of polyethylene and iron samples; (7) ± 1 percent for air and aluminum interaction effect.

Angle-integrated neutron spectrum in the laboratory system (LAB) was obtained by directly integrating DDX data in the LAB system. An angular distribution for each energy interval was fitted with Legendre polynomial and $P_0$ term is obtained as an integrated value. For angle-integrated neutron emission spectrum in the center-of-mass system (CM), we followed procedure described by Takahashi et al [19]. In this process, DDX data was converted from the LAB system to the CM system, by supposing the kinematics of inelastic scattering to by valid for pseudo-excitation levels which were defined by discretizing the secondary energy region of 2.0-15 MeV with 0.2 MeV interval, according to the following equation.

$$E_{n,CMS} = \frac{E_o}{(1+\frac{1}{A})^2} - \frac{Q_i}{(1+\frac{1}{A})} \qquad (2)$$

where $E_{n,CMS}$ is the outgoing neutron in the CM system, $E_0$ is the incident neutron energy (14.1 MeV), $Q_i$ is the discretized excitation energy, and $A$ is the mass number of the target nucleus. As before the angular distribution for each energy bin in the CM system was fitted by Legendre polynomials. The CM neutron spectrum is used for comparison with the calculated data.

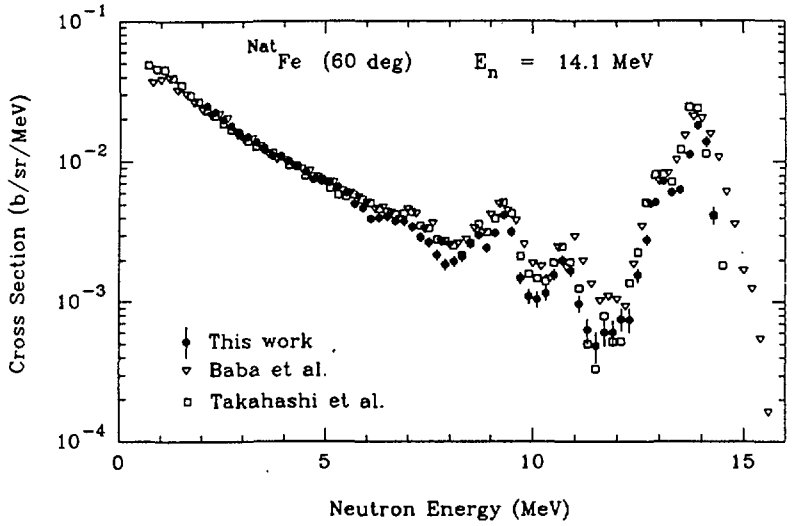


Fig. 7(a) Double differential cross section of Fe at 60°.

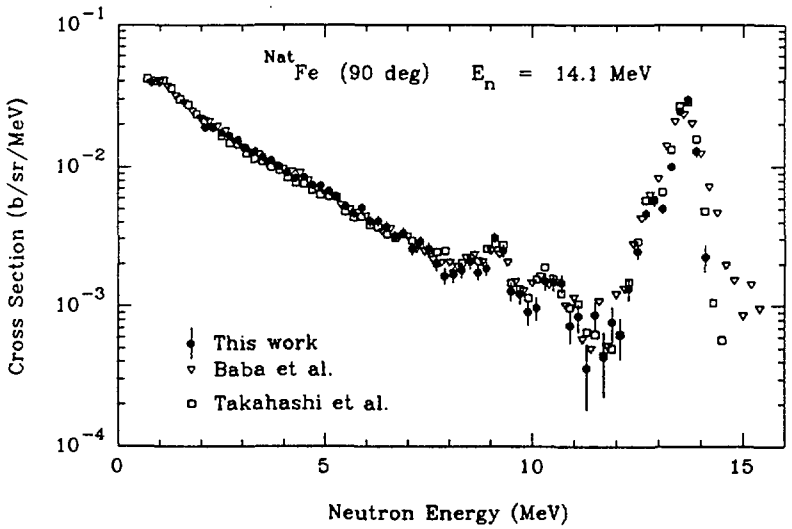


Fig. 7(b) Double differential cross section of Fe at 90°.

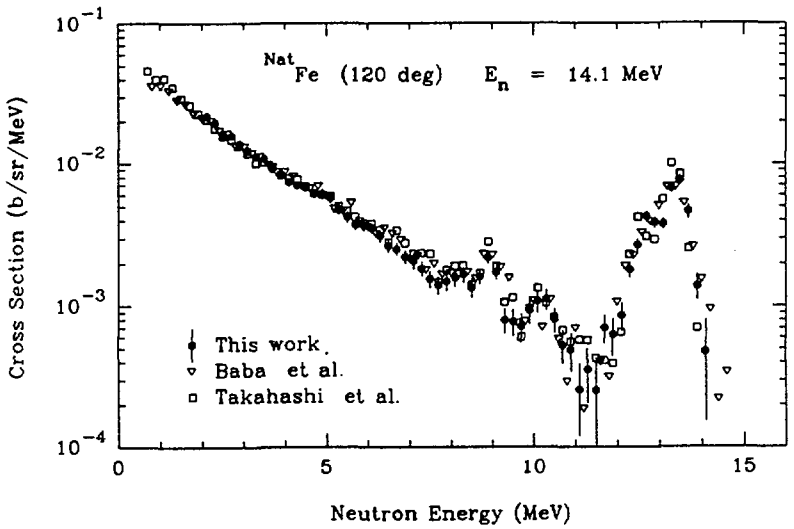


Fig. 7(c) Double differential cross section of Fe at 120°.

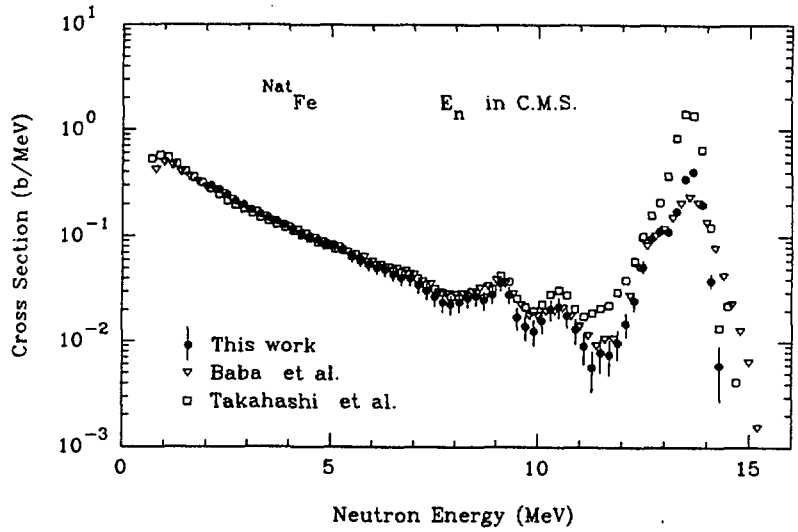


Fig. 8 Angle-integrated spectra of Fe in CM system.

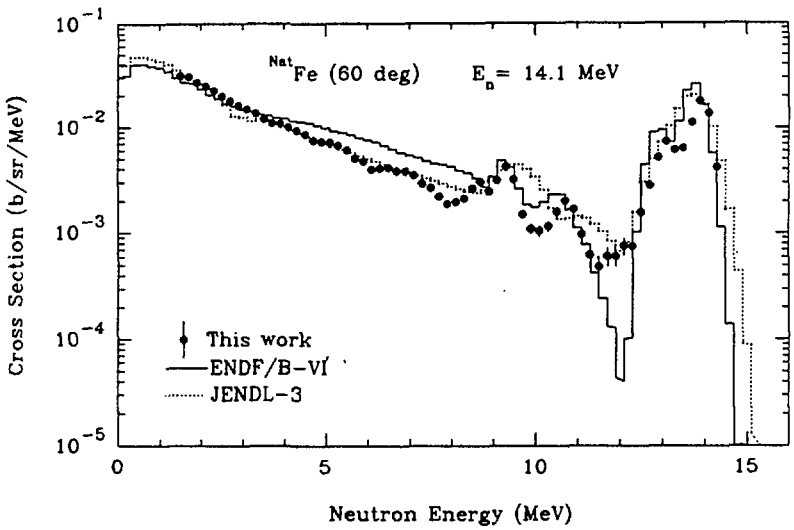


Fig. 9(a) Comparison of DDX of Fe with the calculated spectra at 60°.

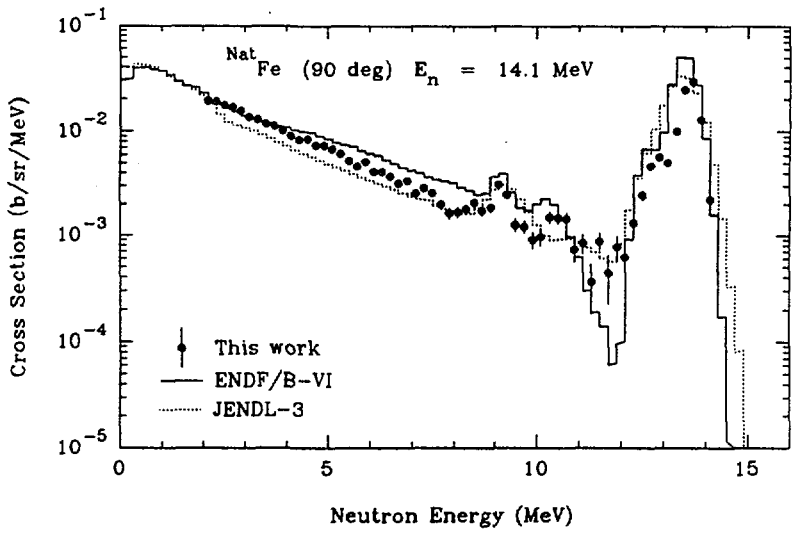


Fig. 9(b) Comparison of DDX of Fe with the calculated spectra at 90°

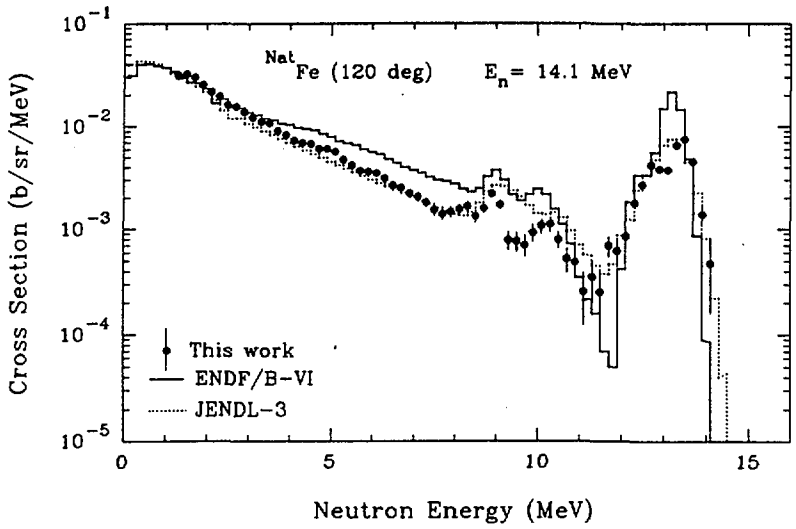


Fig. 9(c) Comparison of DDX of Fe with the calculated spectra at 120°.

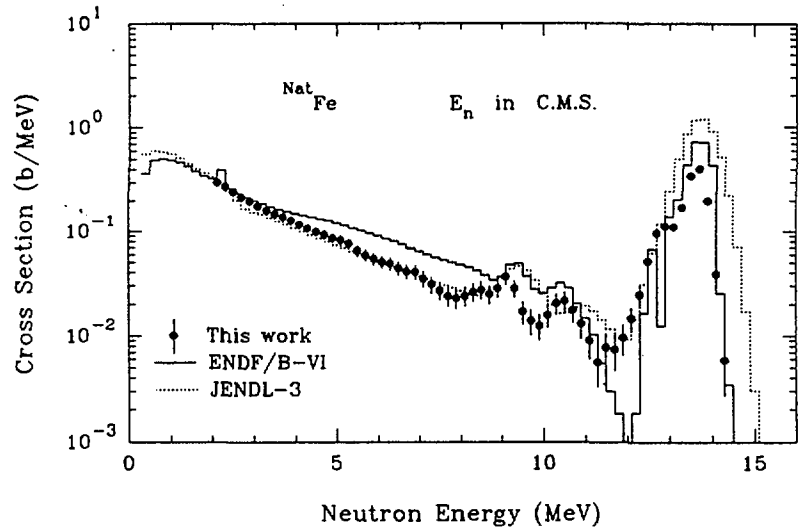


Fig. 10 Comparison of angle-integrated spectra in CM system with calculated spectra.

## 5. Results and Discussions

The DDX obtained from our measurements for iron are tabulated in Table I. In this table we list the statistical uncertainties as well as the estimated experimental uncertainties. The experimental uncertainties were obtained by combining the squared values of the statistical and systematic uncertainties. In Fig.7, we compare our measurements at 60° , 90° , and 120° with those of Takahashi et al. [4] and Baba et al [5]. The angle integrated spectra are compared in Fig.8. The three different sets of measurements agree with one another to within the limit of experimental uncertainty. The discrepancies in the high energy region for the DDX data are due to the systematics and to the difference in energy resolution of the TOF spectrometers.

Baba et al.[5] measured the TOF spectrum with 6 meter flight path whereas Takahashi et al. [4] used a 8.3 meter flight path in their measurements. Our measurements were made with slightly better energy resolution than those of Takahashi et al. However, the three different sets of measurements indicated strong excitation in the regions around 0.85, 3.2 and 4.4 MeV as shown in the angle integrated spectra in Fig.8. The discrepancies in the high energy region

above 10 MeV as shown in the comparison of angle-integrated spectra in Fig.8 are probably due to the systematic in the Legendre fitting process.

In Fig.9 we compare our DDX results with the calculated spectra based on JENDL-3 [20] and ENDF/B-VI data [21]. At forward(60°) and backward (120°) angles, the JENDL-3 library data agree reasonably well with our measurements in the region below about 7 MeV. The ENDF/B-VI overestimates the neutron yield by about 20 percents. In the higher energy region many level can be collectively excited. The calculated spectra, having been smeared out with appropriate energy resolution, do give reasonable representation of experimental data. We present an angle-integrated spectra for comparison in Fig.10. In the region below 7 MeV, the JENDL-3 data reproduces the experimental data very well whereas in the high energy regions the ENDF/B-VI data are in better agreement with our measurements. Both of the two calculations describe the peak at 3.2 MeV excitation fairly well. Based on data of Mellama et al. [7] this state probably results from the collective excitation of the $4^+$ (3.12 MeV) and $2^+$ (3.37) MeV states.

## 6. Conclusion

We measured the double differential neutron emission cross sections from iron at 14.1 MeV from 30° to 150° at 10° interval. We calculated the angle-integrated spectra in the laboratory and the center-of-mass systems. The measured spectra display peaks at 0.85, 3.2 and 4.5 MeV excitation energies. The measurements reported here are in good agreement with the most recent measurements of Takahashi et al. [4] and Baba et al. [5]. The remaining discrepancies are attributed to the energy resolutions and the systematics.

We compare our measurements with calculated spectra based on JENDL-3 and ENDF/B-VI data and found agreement over limited spectral regions. The JENDL-3 data are in better agreement with our data in the region below about 7 MeV. The ENDF/B-VI data give a better representation of the direct spectrum above 7 MeV.

## Acknowledgement.

We are grateful to Professor A. Takahashi and Dr. M. Maekawa for many technical advises and helpful discussions. We thank Dr. S. Chiba and Dr. M. Baba for sending us their DDX and EDX data for comparison. We are indebted to D. Suwannakachorn, G.G. Hoyes, S. Daengtip, R. Charoennugul, S. Wanchai for their helps in the experiments. This work was supported in part by the Institute for Science and Technology Research and Development (Chiang Mai University), the International Program in Physical Science (Uppsala University), and the International Atomic Energy Agency, Vienna, under Contract No. 4885.

## References

[1] E.T. Cheng, Proc. IAEA Advisory Group Meeting on Nuclear Data for Fusion Reactor Technology, Dresden, December (1986).

[2] J.L. Kammerdiener, Lawrence Livermore Laboratory Report No. UCRL-51232 (1972).

[3] D. Hermsdorf, A. Meister, S. Sassonoff, D. Seeliger, K. Siedel, and F. Shaheen, Zentral Institut für Kernforschung, Rossendorf bei Dresden, Report ZFK-277 (1974).

[4] A. Takahashi, Y. Sasaki, and H. Sugimoto, Proc. Conf. Nuclear Data for Science and Technology, Mito, 1988, pp 205-208.

[5] M. Baba, M. Ishikava, N. Yabuta, T. Kikuchi, H. Wakabayashi, and N. Hirakawa, Proc. Conf. Nuclear Data for Science and Technology, Mito, 1988, pp 291-294, and M. Baba private communication (1992).

[6] A.A. Lychageen, V.P. Lunev, B.V. Zhuravlev, O.A. Salnikov, and N.N. Titarenko, Proc. Conf. Nuclear Data for Science and Technology, Mito, 1988, pp 307-309.

[7] S. Mellema, R.W. Finlay, and F.S. Dietrich, Phys. Rev. C 33 (1986) 481.

[8] T. Vilaithong, S. Singkarat, W. Pairsuwan, J.F.Kral, D.Boonyawan, D. Suwannakachorn, S. Konklong, P. Kanjanarat and G.G. Hoyes, Proc. Conf. Nuclear Data for Science and Technology, Jülich (1991).

[9] A. Pavlik and G. Winkler, INDC (AUS) - 011/LI, July (1986), and A. Pavlik, private communication(1992).

[10] H. Schölermann and H.Klein, Nucl. and Meth. 169 (1980) 25.

[11] G. Randers-Pehrson, R.M. Finlay, and D.E. Carter, Nucl. Instr. and Meth, 215 (1983) 433.

[12] A. Takahashi, E. Ichimura, Y. Sasaki, and H. Sugimoto, J. Nucl. Sci. Technol. 25 (1988) 215.

[13] P.F. Rose and C.L. Dunford, ed., "ENDF-102 Data Formats and Procedures for the Evaluated Nuclear Data File ENDF-6," BNL-NCS-44945, July (1990).

[14] R. Cecil, B.D. Anderson, and R. Madey, Nucl. Instr. and Meth. 161 (1979) 439.

[15] T. Vilaithong, S. Na Chiang Mai, N. Chirapatpimol, S. Wiboolsake, V. Teeyasoontranon, and S. Singkarat, Proc. 2nd Int. Symp. on Radiation Physics, Penang, May (1989).

[16] W. Pairsuwan, S. Singkarat, S. Intarasiri, and T. Vilaithong, Proc. Conf. Nuclear Science and Technology, Bangkok, 19-22 April (1988).

[17] E. Ichimura and A. Takahashi, OKTAVIAN Report, A-87-02, Osaka University (1987).

[18] K. Shibata T. Nakagawa, T. Asami, T. Fukahori, T. Narita, S. Chiba, M. Mizumoto, A. Hasegawa, Y. Kikuchi, Y. Nakajima, and S. Igarasi, "JENDL-3 General Purpose File," JAERI 1319 (1990).

[19] A. Takahashi, Y.Sasaki, H. Sugimoto, JAERI-M-88-065, 1988, pp 279-318.

[20] S. Chiba, private communication (1992).

[21] M. Baba, private communication (1992).

Table I : DDX data of natural Fe with En = 14.1 MeV at 30 degrees in LAB system.

| En-min (MeV) | En-max (MeV) | DDX (b/sr/MeV) | Statistical error (b/sr/MeV) | Experimental error (b/sr/MeV) |
|---|---|---|---|---|
| 2.0 | 2.2 | .2629E-01 | .5436E-03 | .1604E-02 |
| 2.2 | 2.4 | .2529E-01 | .5145E-03 | .1540E-02 |
| 2.4 | 2.6 | .2606E-01 | .5065E-03 | .1579E-02 |
| 2.6 | 2.8 | .2255E-01 | .4495E-03 | .1370E-02 |
| 2.8 | 3.0 | .1828E-01 | .3931E-03 | .1121E-02 |
| 3.0 | 3.2 | .1704E-01 | .3707E-03 | .1046E-02 |
| 3.2 | 3.4 | .1596E-01 | .3524E-03 | .9817E-03 |
| 3.4 | 3.6 | .1435E-01 | .3334E-03 | .8889E-03 |
| 3.6 | 3.8 | .1362E-01 | .3264E-03 | .8470E-03 |
| 3.8 | 4.0 | .1354E-01 | .3374E-03 | .8473E-03 |
| 4.0 | 4.2 | .1410E-01 | .3564E-03 | .8843E-03 |
| 4.2 | 4.4 | .1262E-01 | .3429E-03 | .8017E-03 |
| 4.4 | 4.6 | .1174E-01 | .3273E-03 | .7493E-03 |
| 4.6 | 4.8 | .1118E-01 | .3190E-03 | .7168E-03 |
| 4.8 | 5.0 | .1030E-01 | .3054E-03 | .6652E-03 |
| 5.0 | 5.2 | .9091E-02 | .2907E-03 | .5973E-03 |
| 5.2 | 5.4 | .8118E-02 | .2720E-03 | .5396E-03 |
| 5.4 | 5.6 | .7735E-02 | .2683E-03 | .5187E-03 |
| 5.6 | 5.8 | .7017E-02 | .2545E-03 | .4764E-03 |
| 5.8 | 6.0 | .5696E-02 | .2287E-03 | .3990E-03 |
| 6.0 | 6.2 | .5979E-02 | .2451E-03 | .4834E-03 |
| 6.2 | 6.4 | .5089E-02 | .2326E-03 | .3945E-03 |
| 6.4 | 6.6 | .5352E-02 | .2278E-03 | .4235E-03 |
| 6.6 | 6.8 | .4667E-02 | .2139E-03 | .3568E-03 |
| 6.8 | 7.0 | .4353E-02 | .2214E-03 | .3407E-03 |
| 7.0 | 7.2 | .4205E-02 | .2174E-03 | .3476E-03 |
| 7.2 | 7.4 | .3783E-02 | .1959E-03 | .3070E-03 |
| 7.4 | 7.6 | .3148E-02 | .1710E-03 | .2588E-03 |
| 7.6 | 7.8 | .2727E-02 | .1595E-03 | .2403E-03 |
| 7.8 | 8.0 | .2155E-02 | .1449E-03 | .1929E-03 |
| 8.0 | 8.2 | .2255E-02 | .1413E-03 | .1928E-03 |
| 8.2 | 8.4 | .2388E-02 | .1483E-03 | .2073E-03 |
| 8.4 | 8.6 | .2725E-02 | .1591E-03 | .2371E-03 |
| 8.6 | 8.8 | .3065E-02 | .1685E-03 | .2472E-03 |
| 8.8 | 9.0 | .3169E-02 | .1677E-03 | .2706E-03 |
| 9.0 | 9.2 | .2212E-02 | .1404E-03 | .1899E-03 |
| 9.2 | 9.4 | .2563E-02 | .1386E-03 | .2110E-03 |
| 9.4 | 9.6 | .3084E-02 | .1463E-03 | .2349E-03 |
| 9.6 | 9.8 | .3761E-02 | .2103E-03 | .3291E-03 |
| 9.8 | 10.0 | .3356E-02 | .2598E-03 | .3252E-03 |
| 10.0 | 10.2 | .3029E-02 | .2407E-03 | .2946E-03 |
| 10.2 | 10.4 | .3006E-02 | .2389E-03 | .2923E-03 |
| 10.4 | 10.6 | .3224E-02 | .2501E-03 | .3042E-03 |
| 10.6 | 10.8 | .3753E-02 | .2681E-03 | .3243E-03 |
| 10.8 | 11.0 | .4601E-02 | .2793E-03 | .3785E-03 |
| 11.0 | 11.2 | .3895E-02 | .2774E-03 | .3474E-03 |
| 11.2 | 11.4 | .2989E-02 | .2697E-03 | .3075E-03 |
| 11.4 | 11.6 | .2805E-02 | .2710E-03 | .3084E-03 |
| 11.6 | 11.8 | .2184E-02 | .2738E-03 | .2978E-03 |
| 11.8 | 12.0 | .2100E-02 | .2831E-03 | .3117E-03 |
| 12.0 | 12.2 | .2632E-02 | .2877E-03 | .3258E-03 |
| 12.2 | 12.4 | .3401E-02 | .2984E-03 | .3639E-03 |
| 12.4 | 12.6 | .5308E-02 | .3323E-03 | .4673E-03 |
| 12.6 | 12.8 | .8632E-02 | .3785E-03 | .6201E-03 |
| 12.8 | 13.0 | .1747E-01 | .4692E-03 | .9915E-03 |
| 13.0 | 13.2 | .3181E-01 | .5850E-03 | .1680E-02 |
| 13.2 | 13.4 | .4773E-01 | .7118E-03 | .2600E-02 |
| 13.4 | 13.6 | .6804E-01 | .8583E-03 | .3548E-02 |
| 13.6 | 13.8 | .1341E+00 | .1279E-02 | .6851E-02 |
| 13.8 | 14.0 | .3149E+00 | .1929E-02 | .1887E-01 |
| 14.0 | 14.2 | .4691E+00 | .2250E-02 | .3624E-01 |
| 14.2 | 14.4 | .2824E+00 | .1726E-02 | .2511E-01 |
| 14.4 | 14.6 | .6627E-01 | .8964E-03 | .6195E-02 |
| 14.6 | 14.8 | .1211E-01 | .3817E-03 | .1144E-02 |
| 14.8 | 15.0 | .4003E-02 | .2050E-03 | .3959E-03 |

Table I : DDX data of natural Fe with En = 14.1 MeV
at 40 degrees in LAB system.

| En-min (MeV) | En-max (MeV) | DDX (b/sr/MeV) | Statistical error (b/sr/MeV) | Experimental error (b/sr/MeV) |
|---|---|---|---|---|
| 2.0 | 2.2 | .2762E-01 | .4339E-03 | .1644E-02 |
| 2.2 | 2.4 | .2485E-01 | .4112E-03 | .1485E-02 |
| 2.4 | 2.6 | .2252E-01 | .3987E-03 | .1353E-02 |
| 2.6 | 2.8 | .1960E-01 | .3476E-03 | .1177E-02 |
| 2.8 | 3.0 | .1667E-01 | .3119E-03 | .1007E-02 |
| 3.0 | 3.2 | .1537E-01 | .2968E-03 | .9306E-03 |
| 3.2 | 3.4 | .1354E-01 | .2848E-03 | .8279E-03 |
| 3.4 | 3.6 | .1266E-01 | .2706E-03 | .7755E-03 |
| 3.6 | 3.8 | .1141E-01 | .2618E-03 | .7055E-03 |
| 3.8 | 4.0 | .1183E-01 | .2690E-03 | .7305E-03 |
| 4.0 | 4.2 | .1106E-01 | .2735E-03 | .6912E-03 |
| 4.2 | 4.4 | .1055E-01 | .2630E-03 | .6600E-03 |
| 4.4 | 4.6 | .9377E-02 | .2450E-03 | .5914E-03 |
| 4.6 | 4.8 | .8541E-02 | .2403E-03 | .5460E-03 |
| 4.8 | 5.0 | .7947E-02 | .2371E-03 | .5141E-03 |
| 5.0 | 5.2 | .7630E-02 | .2915E-03 | .5440E-03 |
| 5.2 | 5.4 | .7179E-02 | .2665E-03 | .5231E-03 |
| 5.4 | 5.6 | .6606E-02 | .2550E-03 | .4663E-03 |
| 5.6 | 5.8 | .5286E-02 | .2349E-03 | .3850E-03 |
| 5.8 | 6.0 | .4800E-02 | .2146E-03 | .3469E-03 |
| 6.0 | 6.2 | .4714E-02 | .2152E-03 | .3410E-03 |
| 6.2 | 6.4 | .4391E-02 | .2097E-03 | .3189E-03 |
| 6.4 | 6.6 | .3950E-02 | .2060E-03 | .2898E-03 |
| 6.6 | 6.8 | .4015E-02 | .2041E-03 | .3090E-03 |
| 6.8 | 7.0 | .3928E-02 | .2131E-03 | .3073E-03 |
| 7.0 | 7.2 | .3803E-02 | .2016E-03 | .2980E-03 |
| 7.2 | 7.4 | .3484E-02 | .1873E-03 | .2810E-03 |
| 7.4 | 7.6 | .2675E-02 | .1626E-03 | .2235E-03 |
| 7.6 | 7.8 | .1938E-02 | .1540E-03 | .1806E-03 |
| 7.8 | 8.0 | .1940E-02 | .1511E-03 | .1793E-03 |
| 8.0 | 8.2 | .2098E-02 | .1542E-03 | .1966E-03 |
| 8.2 | 8.4 | .2117E-02 | .1580E-03 | .1970E-03 |
| 8.4 | 8.6 | .2610E-02 | .1633E-03 | .2113E-03 |
| 8.6 | 8.8 | .3217E-02 | .1804E-03 | .2658E-03 |
| 8.8 | 9.0 | .2965E-02 | .1731E-03 | .2551E-03 |
| 9.0 | 9.2 | .2072E-02 | .1546E-03 | .1851E-03 |
| 9.2 | 9.4 | .3369E-02 | .1702E-03 | .2513E-03 |
| 9.4 | 9.6 | .3247E-02 | .1659E-03 | .2608E-03 |
| 9.6 | 9.8 | .2139E-02 | .1665E-03 | .2031E-03 |
| 9.8 | 10.0 | .2112E-02 | .1820E-03 | .2155E-03 |
| 10.0 | 10.2 | .1586E-02 | .1742E-03 | .1909E-03 |
| 10.2 | 10.4 | .1966E-02 | .1715E-03 | .1982E-03 |
| 10.4 | 10.6 | .2375E-02 | .1855E-03 | .2235E-03 |
| 10.6 | 10.8 | .2692E-02 | .1954E-03 | .2421E-03 |
| 10.8 | 11.0 | .2704E-02 | .1962E-03 | .2455E-03 |
| 11.0 | 11.2 | .2025E-02 | .1886E-03 | .2206E-03 |
| 11.2 | 11.4 | .1227E-02 | .1822E-03 | .1919E-03 |
| 11.4 | 11.6 | .1065E-02 | .1874E-03 | .1954E-03 |
| 11.6 | 11.8 | .8988E-03 | .1899E-03 | .1962E-03 |
| 11.8 | 12.0 | .9910E-03 | .1881E-03 | .1999E-03 |
| 12.0 | 12.2 | .7484E-03 | .2023E-03 | .2102E-03 |
| 12.2 | 12.4 | .1700E-02 | .2296E-03 | .2512E-03 |
| 12.4 | 12.6 | .2819E-02 | .2633E-03 | .3157E-03 |
| 12.6 | 12.8 | .5054E-02 | .3302E-03 | .4622E-03 |
| 12.8 | 13.0 | .1119E-01 | .4059E-03 | .7296E-03 |
| 13.0 | 13.2 | .2009E-01 | .4998E-03 | .1200E-02 |
| 13.2 | 13.4 | .1860E-01 | .5075E-03 | .1107E-02 |
| 13.4 | 13.6 | .1983E-01 | .5567E-03 | .1207E-02 |
| 13.6 | 13.8 | .3788E-01 | .7103E-03 | .2051E-02 |
| 13.8 | 14.0 | .7451E-01 | .9467E-03 | .4935E-02 |
| 14.0 | 14.2 | .7961E-01 | .1124E-02 | .7104E-02 |
| 14.2 | 14.4 | .2851E-01 | .8582E-03 | .2977E-02 |
| 14.4 | 14.6 | .4802E-02 | .3810E-03 | .6240E-03 |
| 14.6 | 14.8 | .3954E-03 | .1612E-03 | .1647E-03 |
| 14.8 | 15.0 | .2811E-03 | .8417E-04 | .8743E-04 |

Table I : DDX data of natural Fe with En = 14.1 MeV at 50 degrees in LAB system.

| En-min (MeV) | En-max (MeV) | DDX (b/sr/MeV) | Statistical error (b/sr/MeV) | Experimental error (b/sr/MeV) |
|---|---|---|---|---|
| 2.0 | 2.2 | .2672E-01 | .4582E-03 | .1600E-02 |
| 2.2 | 2.4 | .2404E-01 | .4281E-03 | .1445E-02 |
| 2.4 | 2.6 | .2079E-01 | .4216E-03 | .1266E-02 |
| 2.6 | 2.8 | .1925E-01 | .3744E-03 | .1167E-02 |
| 2.8 | 3.0 | .1603E-01 | .3397E-03 | .9809E-03 |
| 3.0 | 3.2 | .1538E-01 | .3263E-03 | .9410E-03 |
| 3.2 | 3.4 | .1339E-01 | .3078E-03 | .8278E-03 |
| 3.4 | 3.6 | .1236E-01 | .2980E-03 | .7697E-03 |
| 3.6 | 3.8 | .1202E-01 | .2939E-03 | .7501E-03 |
| 3.8 | 4.0 | .1107E-01 | .2921E-03 | .6991E-03 |
| 4.0 | 4.2 | .1000E-01 | .2890E-03 | .6429E-03 |
| 4.2 | 4.4 | .9940E-02 | .2760E-03 | .6338E-03 |
| 4.4 | 4.6 | .8399E-02 | .2593E-03 | .5474E-03 |
| 4.6 | 4.8 | .8241E-02 | .2587E-03 | .5391E-03 |
| 4.8 | 5.0 | .7281E-02 | .2526E-03 | .4883E-03 |
| 5.0 | 5.2 | .7040E-02 | .3023E-03 | .5223E-03 |
| 5.2 | 5.4 | .6708E-02 | .2844E-03 | .5066E-03 |
| 5.4 | 5.6 | .5962E-02 | .2791E-03 | .4370E-03 |
| 5.6 | 5.8 | .4716E-02 | .2608E-03 | .3752E-03 |
| 5.8 | 6.0 | .4649E-02 | .2439E-03 | .3632E-03 |
| 6.0 | 6.2 | .3924E-02 | .2291E-03 | .3131E-03 |
| 6.2 | 6.4 | .4004E-02 | .2258E-03 | .3112E-03 |
| 6.4 | 6.6 | .4133E-02 | .2282E-03 | .3364E-03 |
| 6.6 | 6.8 | .3773E-02 | .2267E-03 | .3174E-03 |
| 6.8 | 7.0 | .3566E-02 | .2295E-03 | .3038E-03 |
| 7.0 | 7.2 | .3890E-02 | .2282E-03 | .3126E-03 |
| 7.2 | 7.4 | .2864E-02 | .2131E-03 | .2623E-03 |
| 7.4 | 7.6 | .2883E-02 | .2038E-03 | .2616E-03 |
| 7.6 | 7.8 | .2082E-02 | .1896E-03 | .2181E-03 |
| 7.8 | 8.0 | .2076E-02 | .1971E-03 | .2258E-03 |
| 8.0 | 8.2 | .1776E-02 | .1945E-03 | .2146E-03 |
| 8.2 | 8.4 | .2445E-02 | .1961E-03 | .2371E-03 |
| 8.4 | 8.6 | .2623E-02 | .2004E-03 | .2416E-03 |
| 8.6 | 8.8 | .3605E-02 | .2064E-03 | .3034E-03 |
| 8.8 | 9.0 | .2650E-02 | .1884E-03 | .2385E-03 |
| 9.0 | 9.2 | .3110E-02 | .1982E-03 | .2576E-03 |
| 9.2 | 9.4 | .4465E-02 | .2165E-03 | .3328E-03 |
| 9.4 | 9.6 | .3685E-02 | .1880E-03 | .2993E-03 |
| 9.6 | 9.8 | .1926E-02 | .1674E-03 | .2032E-03 |
| 9.8 | 10.0 | .1578E-02 | .1733E-03 | .1895E-03 |
| 10.0 | 10.2 | .1405E-02 | .1631E-03 | .1785E-03 |
| 10.2 | 10.4 | .1113E-02 | .1667E-03 | .1757E-03 |
| 10.4 | 10.6 | .1866E-02 | .1843E-03 | .2095E-03 |
| 10.6 | 10.8 | .2656E-02 | .2112E-03 | .2660E-03 |
| 10.8 | 11.0 | .1927E-02 | .1940E-03 | .2218E-03 |
| 11.0 | 11.2 | .1343E-02 | .1786E-03 | .1918E-03 |
| 11.2 | 11.4 | .9891E-03 | .1976E-03 | .2038E-03 |
| 11.4 | 11.6 | .5690E-03 | .1829E-03 | .1859E-03 |
| 11.6 | 11.8 | .2198E-03 | .1898E-03 | .1908E-03 |
| 11.8 | 12.0 | .7100E-03 | .2129E-03 | .2169E-03 |
| 12.0 | 12.2 | .9426E-03 | .2234E-03 | .2310E-03 |
| 12.2 | 12.4 | .1406E-02 | .2291E-03 | .2415E-03 |
| 12.4 | 12.6 | .2218E-02 | .2499E-03 | .2796E-03 |
| 12.6 | 12.8 | .4371E-02 | .2853E-03 | .3782E-03 |
| 12.8 | 13.0 | .9332E-02 | .3507E-03 | .5718E-03 |
| 13.0 | 13.2 | .1358E-01 | .4102E-03 | .8819E-03 |
| 13.2 | 13.4 | .1250E-01 | .4498E-03 | .7668E-03 |
| 13.4 | 13.6 | .1540E-01 | .5576E-03 | .1022E-02 |
| 13.6 | 13.8 | .3155E-01 | .7884E-03 | .1747E-02 |
| 13.8 | 14.0 | .5468E-01 | .1029E-02 | .4159E-02 |
| 14.0 | 14.2 | .4257E-01 | .1047E-02 | .4641E-02 |
| 14.2 | 14.4 | .6592E-02 | .9027E-03 | .4583E-02 |

Table I : DDX data of natural Fe with En = 14.1 MeV at 60 degrees in LAB system.

| En-min (MeV) | En-max (MeV) | DDX (b/sr/MeV) | Statistical error (b/sr/MeV) | Experimental error (b/sr/MeV) |
|---|---|---|---|---|
| 2.0 | 2.2 | .2487E-01 | .3393E-03 | .1467E-02 |
| 2.2 | 2.4 | .2242E-01 | .3208E-03 | .1326E-02 |
| 2.4 | 2.6 | .1982E-01 | .3157E-03 | .1181E-02 |
| 2.6 | 2.8 | .1798E-01 | .2853E-03 | .1071E-02 |
| 2.8 | 3.0 | .1615E-01 | .2662E-03 | .9643E-03 |
| 3.0 | 3.2 | .1503E-01 | .2562E-03 | .9000E-03 |
| 3.2 | 3.4 | .1371E-01 | .2411E-03 | .8229E-03 |
| 3.4 | 3.6 | .1212E-01 | .2316E-03 | .7331E-03 |
| 3.6 | 3.8 | .1104E-01 | .2271E-03 | .6733E-03 |
| 3.8 | 4.0 | .1103E-01 | .2223E-03 | .6708E-03 |
| 4.0 | 4.2 | .1018E-01 | .2194E-03 | .6242E-03 |
| 4.2 | 4.4 | .9384E-02 | .2095E-03 | .5780E-03 |
| 4.4 | 4.6 | .8546E-02 | .1982E-03 | .5291E-03 |
| 4.6 | 4.8 | .7526E-02 | .1939E-03 | .4735E-03 |
| 4.8 | 5.0 | .7291E-02 | .1920E-03 | .4605E-03 |
| 5.0 | 5.2 | .7189E-02 | .2316E-03 | .5228E-03 |
| 5.2 | 5.4 | .6669E-02 | .2202E-03 | .4562E-03 |
| 5.4 | 5.6 | .6082E-02 | .2098E-03 | .4379E-03 |
| 5.6 | 5.8 | .5071E-02 | .1932E-03 | .3838E-03 |
| 5.8 | 6.0 | .4743E-02 | .1842E-03 | .3338E-03 |
| 6.0 | 6.2 | .3976E-02 | .1765E-03 | .2792E-03 |
| 6.2 | 6.4 | .4044E-02 | .1760E-03 | .3044E-03 |
| 6.4 | 6.6 | .4139E-02 | .1734E-03 | .3080E-03 |
| 6.6 | 6.8 | .3847E-02 | .1714E-03 | .2971E-03 |
| 6.8 | 7.0 | .3825E-02 | .1752E-03 | .2878E-03 |
| 7.0 | 7.2 | .3484E-02 | .1724E-03 | .2541E-03 |
| 7.2 | 7.4 | .2935E-02 | .1567E-03 | .2210E-03 |
| 7.4 | 7.6 | .2690E-02 | .1535E-03 | .2196E-03 |
| 7.6 | 7.8 | .2205E-02 | .1477E-03 | .1867E-03 |
| 7.8 | 8.0 | .1862E-02 | .1405E-03 | .1677E-03 |
| 8.0 | 8.2 | .1960E-02 | .1358E-03 | .1729E-03 |
| 8.2 | 8.4 | .2126E-02 | .1410E-03 | .1814E-03 |
| 8.4 | 8.6 | .2630E-02 | .1537E-03 | .2098E-03 |
| 8.6 | 8.8 | .3040E-02 | .1545E-03 | .2235E-03 |
| 8.8 | 9.0 | .2454E-02 | .1421E-03 | .1950E-03 |
| 9.0 | 9.2 | .3126E-02 | .1502E-03 | .2241E-03 |
| 9.2 | 9.4 | .4214E-02 | .1635E-03 | .2979E-03 |
| 9.4 | 9.6 | .3195E-02 | .1467E-03 | .2645E-03 |
| 9.6 | 9.8 | .1489E-02 | .1306E-03 | .1557E-03 |
| 9.8 | 10.0 | .1098E-02 | .1197E-03 | .1350E-03 |
| 10.0 | 10.2 | .1042E-02 | .1248E-03 | .1374E-03 |
| 10.2 | 10.4 | .1153E-02 | .1239E-03 | .1416E-03 |
| 10.4 | 10.6 | .1578E-02 | .1248E-03 | .1520E-03 |
| 10.6 | 10.8 | .1999E-02 | .1314E-03 | .1735E-03 |
| 10.8 | 11.0 | .1685E-02 | .1300E-03 | .1625E-03 |
| 11.0 | 11.2 | .9717E-03 | .1157E-03 | .1324E-03 |
| 11.2 | 11.4 | .6282E-03 | .1198E-03 | .1258E-03 |
| 11.4 | 11.6 | .4850E-03 | .1154E-03 | .1180E-03 |
| 11.6 | 11.8 | .6070E-03 | .1174E-03 | .1232E-03 |
| 11.8 | 12.0 | .6076E-03 | .1199E-03 | .1244E-03 |
| 12.0 | 12.2 | .7537E-03 | .1329E-03 | .1390E-03 |
| 12.2 | 12.4 | .7486E-03 | .1441E-03 | .1503E-03 |
| 12.4 | 12.6 | .1560E-02 | .1677E-03 | .1906E-03 |
| 12.6 | 12.8 | .2789E-02 | .1793E-03 | .2345E-03 |
| 12.8 | 13.0 | .5195E-02 | .2166E-03 | .3378E-03 |
| 13.0 | 13.2 | .7319E-02 | .2471E-03 | .5135E-03 |
| 13.2 | 13.4 | .6093E-02 | .2644E-03 | .4245E-03 |
| 13.4 | 13.6 | .6334E-02 | .3025E-03 | .4329E-03 |
| 13.6 | 13.8 | .1120E-01 | .3460E-03 | .6696E-03 |
| 13.8 | 14.0 | .1794E-01 | .4016E-03 | .1334E-02 |
| 14.0 | 14.2 | .1375E-01 | .4145E-03 | .1306E-02 |
| 14.2 | 14.4 | .4193E-02 | .4061E-03 | .6164E-03 |

Table I : DDX data of natural Fe with En = 14.1 MeV at 70 degrees in LAB system.

| En-min (MeV) | En-max (MeV) | DDX (b/sr/MeV) | Statistical error (b/sr/MeV) | Experimental error (b/sr/MeV) |
|---|---|---|---|---|
| 2.0 | 2.2 | .2438E-01 | .4171E-03 | .1460E-02 |
| 2.2 | 2.4 | .2225E-01 | .3906E-03 | .1336E-02 |
| 2.4 | 2.6 | .2010E-01 | .3872E-03 | .1217E-02 |
| 2.6 | 2.8 | .1783E-01 | .3413E-03 | .1079E-02 |
| 2.8 | 3.0 | .1575E-01 | .3203E-03 | .9592E-03 |
| 3.0 | 3.2 | .1489E-01 | .3070E-03 | .9083E-03 |
| 3.2 | 3.4 | .1339E-01 | .2960E-03 | .8236E-03 |
| 3.4 | 3.6 | .1232E-01 | .2834E-03 | .7618E-03 |
| 3.6 | 3.8 | .1131E-01 | .2732E-03 | .7044E-03 |
| 3.8 | 4.0 | .1080E-01 | .2684E-03 | .6755E-03 |
| 4.0 | 4.2 | .9724E-02 | .2637E-03 | .6173E-03 |
| 4.2 | 4.4 | .8855E-02 | .2506E-03 | .5667E-03 |
| 4.4 | 4.6 | .7755E-02 | .2386E-03 | .5050E-03 |
| 4.6 | 4.8 | .7533E-02 | .2387E-03 | .4939E-03 |
| 4.8 | 5.0 | .6996E-02 | .2339E-03 | .4647E-03 |
| 5.0 | 5.2 | .6493E-02 | .2804E-03 | .4670E-03 |
| 5.2 | 5.4 | .6535E-02 | .2661E-03 | .4880E-03 |
| 5.4 | 5.6 | .5471E-02 | .2538E-03 | .4316E-03 |
| 5.6 | 5.8 | .5165E-02 | .2421E-03 | .3860E-03 |
| 5.8 | 6.0 | .4623E-02 | .2284E-03 | .3579E-03 |
| 6.0 | 6.2 | .3942E-02 | .2132E-03 | .3015E-03 |
| 6.2 | 6.4 | .3955E-02 | .2129E-03 | .3049E-03 |
| 6.4 | 6.6 | .3809E-02 | .2013E-03 | .2925E-03 |
| 6.6 | 6.8 | .3489E-02 | .2093E-03 | .2992E-03 |
| 6.8 | 7.0 | .3551E-02 | .2054E-03 | .2884E-03 |
| 7.0 | 7.2 | .3467E-02 | .2028E-03 | .2976E-03 |
| 7.2 | 7.4 | .2782E-02 | .1887E-03 | .2501E-03 |
| 7.4 | 7.6 | .2786E-02 | .1902E-03 | .2478E-03 |
| 7.6 | 7.8 | .1872E-02 | .1781E-03 | .2020E-03 |
| 7.8 | 8.0 | .2044E-02 | .1711E-03 | .2029E-03 |
| 8.0 | 8.2 | .1888E-02 | .1680E-03 | .2060E-03 |
| 8.2 | 8.4 | .2255E-02 | .1741E-03 | .2204E-03 |
| 8.4 | 8.6 | .2781E-02 | .1830E-03 | .2535E-03 |
| 8.6 | 8.8 | .2825E-02 | .1860E-03 | .2438E-03 |
| 8.8 | 9.0 | .2640E-02 | .1773E-03 | .2317E-03 |
| 9.0 | 9.2 | .3128E-02 | .1806E-03 | .2580E-03 |
| 9.2 | 9.4 | .3322E-02 | .1883E-03 | .2680E-03 |
| 9.4 | 9.6 | .2402E-02 | .1707E-03 | .2257E-03 |
| 9.6 | 9.8 | .1109E-02 | .1508E-03 | .1628E-03 |
| 9.8 | 10.0 | .1167E-02 | .1451E-03 | .1588E-03 |
| 10.0 | 10.2 | .9416E-03 | .1455E-03 | .1554E-03 |
| 10.2 | 10.4 | .1359E-02 | .1582E-03 | .1782E-03 |
| 10.4 | 10.6 | .1696E-02 | .1574E-03 | .1881E-03 |
| 10.6 | 10.8 | .1633E-02 | .1526E-03 | .1797E-03 |
| 10.8 | 11.0 | .1181E-02 | .1410E-03 | .1555E-03 |
| 11.0 | 11.2 | .7448E-03 | .1427E-03 | .1475E-03 |
| 11.2 | 11.4 | .4991E-03 | .1316E-03 | .1365E-03 |
| 11.4 | 11.6 | .2780E-03 | .1397E-03 | .1404E-03 |
| 11.6 | 11.8 | .4451E-03 | .1402E-03 | .1421E-03 |
| 11.8 | 12.0 | .7021E-03 | .1446E-03 | .1486E-03 |
| 12.0 | 12.2 | .7263E-03 | .1614E-03 | .1664E-03 |
| 12.2 | 12.4 | .1057E-02 | .1836E-03 | .1930E-03 |
| 12.4 | 12.6 | .1652E-02 | .1927E-03 | .2138E-03 |
| 12.6 | 12.8 | .3370E-02 | .2199E-03 | .2771E-03 |
| 12.8 | 13.0 | .5758E-02 | .2450E-03 | .3859E-03 |
| 13.0 | 13.2 | .6405E-02 | .2578E-03 | .4675E-03 |
| 13.2 | 13.4 | .4828E-02 | .2700E-03 | .3733E-03 |
| 13.4 | 13.6 | .5603E-02 | .3085E-03 | .4137E-03 |
| 13.6 | 13.8 | .8666E-02 | .3838E-03 | .6276E-03 |
| 13.8 | 14.0 | .1048E-01 | .4316E-03 | .9061E-03 |
| 14.0 | 14.2 | .6131E-02 | .4079E-03 | .6779E-03 |
| 14.2 | 14.4 | .7766E-03 | .3846E-03 | .3874E-03 |

Table I : DDX data of natural Fe with En = 14.1 MeV
at 80 degrees in LAB system.

| En-min (MeV) | En-max (MeV) | DDX (b/sr/MeV) | Statistical error (b/sr/MeV) | Experimental error (b/sr/MeV) |
|---|---|---|---|---|
| 2.0 | 2.2 | .2284E-01 | .5033E-03 | .1404E-02 |
| 2.2 | 2.4 | .2147E-01 | .4821E-03 | .1323E-02 |
| 2.4 | 2.6 | .1921E-01 | .4635E-03 | .1196E-02 |
| 2.6 | 2.8 | .1803E-01 | .4528E-03 | .1130E-02 |
| 2.8 | 3.0 | .1604E-01 | .4151E-03 | .1010E-02 |
| 3.0 | 3.2 | .1575E-01 | .3972E-03 | .9877E-03 |
| 3.2 | 3.4 | .1451E-01 | .3789E-03 | .9149E-03 |
| 3.4 | 3.6 | .1341E-01 | .3681E-03 | .8534E-03 |
| 3.6 | 3.8 | .1209E-01 | .3526E-03 | .7782E-03 |
| 3.8 | 4.0 | .1090E-01 | .3437E-03 | .7136E-03 |
| 4.0 | 4.2 | .1072E-01 | .3350E-03 | .7008E-03 |
| 4.2 | 4.4 | .9256E-02 | .3273E-03 | .6240E-03 |
| 4.4 | 4.6 | .8970E-02 | .3177E-03 | .6050E-03 |
| 4.6 | 4.8 | .8000E-02 | .3128E-03 | .5556E-03 |
| 4.8 | 5.0 | .8363E-02 | .3617E-03 | .6044E-03 |
| 5.0 | 5.2 | .7653E-02 | .3426E-03 | .5934E-03 |
| 5.2 | 5.4 | .7006E-02 | .3267E-03 | .5025E-03 |
| 5.4 | 5.6 | .6494E-02 | .3061E-03 | .4799E-03 |
| 5.6 | 5.8 | .4989E-02 | .2945E-03 | .4032E-03 |
| 5.8 | 6.0 | .5647E-02 | .2777E-03 | .4294E-03 |
| 6.0 | 6.2 | .4964E-02 | .2710E-03 | .4038E-03 |
| 6.2 | 6.4 | .4140E-02 | .2556E-03 | .3336E-03 |
| 6.4 | 6.6 | .3879E-02 | .2528E-03 | .3154E-03 |
| 6.6 | 6.8 | .3169E-02 | .2397E-03 | .2861E-03 |
| 6.8 | 7.0 | .3813E-02 | .2514E-03 | .3199E-03 |
| 7.0 | 7.2 | .3153E-02 | .2366E-03 | .2913E-03 |
| 7.2 | 7.4 | .2995E-02 | .2317E-03 | .2736E-03 |
| 7.4 | 7.6 | .2462E-02 | .2216E-03 | .2548E-03 |
| 7.6 | 7.8 | .2255E-02 | .2157E-03 | .2418E-03 |
| 7.8 | 8.0 | .1986E-02 | .2104E-03 | .2340E-03 |
| 8.0 | 8.2 | .2288E-02 | .2082E-03 | .2358E-03 |
| 8.2 | 8.4 | .1977E-02 | .2068E-03 | .2296E-03 |
| 8.4 | 8.6 | .2589E-02 | .2172E-03 | .2513E-03 |
| 8.6 | 8.8 | .2314E-02 | .2122E-03 | .2434E-03 |
| 8.8 | 9.0 | .2068E-02 | .1999E-03 | .2272E-03 |
| 9.0 | 9.2 | .2864E-02 | .2053E-03 | .2623E-03 |
| 9.2 | 9.4 | .3245E-02 | .2202E-03 | .2851E-03 |
| 9.4 | 9.6 | .1847E-02 | .1988E-03 | .2188E-03 |
| 9.6 | 9.8 | .1483E-02 | .1813E-03 | .1966E-03 |
| 9.8 | 10.0 | .1164E-02 | .1867E-03 | .1981E-03 |
| 10.0 | 10.2 | .7766E-03 | .1815E-03 | .1901E-03 |
| 10.2 | 10.4 | .1291E-02 | .1967E-03 | .2096E-03 |
| 10.4 | 10.6 | .1496E-02 | .1976E-03 | .2145E-03 |
| 10.6 | 10.8 | .1525E-02 | .1974E-03 | .2116E-03 |
| 10.8 | 11.0 | .1235E-02 | .1968E-03 | .2061E-03 |
| 11.0 | 11.2 | .1114E-02 | .1869E-03 | .1962E-03 |
| 11.2 | 11.4 | .6377E-03 | .1859E-03 | .1887E-03 |
| 11.4 | 11.6 | .7104E-03 | .1943E-03 | .1981E-03 |
| 11.6 | 11.8 | .7520E-03 | .2062E-03 | .2096E-03 |
| 11.8 | 12.0 | .7474E-03 | .2147E-03 | .2191E-03 |
| 12.0 | 12.2 | .7924E-03 | .2100E-03 | .2147E-03 |
| 12.2 | 12.4 | .1356E-02 | .2296E-03 | .2401E-03 |
| 12.4 | 12.6 | .2012E-02 | .2437E-03 | .2664E-03 |
| 12.6 | 12.8 | .4898E-02 | .3020E-03 | .3945E-03 |
| 12.8 | 13.0 | .8245E-02 | .3582E-03 | .6419E-03 |
| 13.0 | 13.2 | .7540E-02 | .3478E-03 | .5529E-03 |
| 13.2 | 13.4 | .8579E-02 | .3619E-03 | .5508E-03 |
| 13.4 | 13.6 | .1955E-01 | .4941E-03 | .1175E-02 |
| 13.6 | 13.8 | .3459E-01 | .6679E-03 | .2475E-02 |
| 13.8 | 14.0 | .2901E-01 | .7166E-03 | .2627E-02 |
| 14.0 | 14.2 | .5294E-02 | .6268E-03 | .7397E-03 |

Table I : DDX data of natural Fe with En = 14.1 MeV
at 90 degrees in LAB system.

| En-min (MeV) | En-max (MeV) | DDX (b/sr/MeV) | Statistical error (b/sr/MeV) | Experimental error (b/sr/MeV) |
|---|---|---|---|---|
| 2.0 | 2.2 | .1913E-01 | .4349E-03 | .1181E-02 |
| 2.2 | 2.4 | .1890E-01 | .4238E-03 | .1165E-02 |
| 2.4 | 2.6 | .1759E-01 | .4154E-03 | .1092E-02 |
| 2.6 | 2.8 | .1671E-01 | .4137E-03 | .1045E-02 |
| 2.8 | 3.0 | .1558E-01 | .3753E-03 | .9699E-03 |
| 3.0 | 3.2 | .1364E-01 | .3490E-03 | .8572E-03 |
| 3.2 | 3.4 | .1288E-01 | .3346E-03 | .8113E-03 |
| 3.4 | 3.6 | .1178E-01 | .3265E-03 | .7507E-03 |
| 3.6 | 3.8 | .1118E-01 | .3162E-03 | .7154E-03 |
| 3.8 | 4.0 | .1009E-01 | .3087E-03 | .6562E-03 |
| 4.0 | 4.2 | .9043E-02 | .3009E-03 | .6000E-03 |
| 4.2 | 4.4 | .8303E-02 | .2938E-03 | .5599E-03 |
| 4.4 | 4.6 | .8424E-02 | .2867E-03 | .5622E-03 |
| 4.6 | 4.8 | .7373E-02 | .2816E-03 | .5083E-03 |
| 4.8 | 5.0 | .7320E-02 | .2694E-03 | .4992E-03 |
| 5.0 | 5.2 | .6761E-02 | .2605E-03 | .4674E-03 |
| 5.2 | 5.4 | .6158E-02 | .2567E-03 | .4368E-03 |
| 5.4 | 5.6 | .5247E-02 | .2433E-03 | .3871E-03 |
| 5.6 | 5.8 | .4640E-02 | .2454E-03 | .3622E-03 |
| 5.8 | 6.0 | .5122E-02 | .2391E-03 | .3789E-03 |
| 6.0 | 6.2 | .4102E-02 | .2474E-03 | .3604E-03 |
| 6.2 | 6.4 | .4101E-02 | .2451E-03 | .3645E-03 |
| 6.4 | 6.6 | .3721E-02 | .2385E-03 | .3300E-03 |
| 6.6 | 6.8 | .3173E-02 | .2320E-03 | .2927E-03 |
| 6.8 | 7.0 | .3362E-02 | .2337E-03 | .3105E-03 |
| 7.0 | 7.2 | .2549E-02 | .2214E-03 | .2701E-03 |
| 7.2 | 7.4 | .2881E-02 | .2199E-03 | .2888E-03 |
| 7.4 | 7.6 | .2572E-02 | .2129E-03 | .2629E-03 |
| 7.6 | 7.8 | .1996E-02 | .2003E-03 | .2266E-03 |
| 7.8 | 8.0 | .1632E-02 | .1945E-03 | .2102E-03 |
| 8.0 | 8.2 | .1676E-02 | .1899E-03 | .2113E-03 |
| 8.2 | 8.4 | .1787E-02 | .1954E-03 | .2208E-03 |
| 8.4 | 8.6 | .2076E-02 | .1994E-03 | .2369E-03 |
| 8.6 | 8.8 | .1734E-02 | .1893E-03 | .2092E-03 |
| 8.8 | 9.0 | .1850E-02 | .1828E-03 | .2137E-03 |
| 9.0 | 9.2 | .3088E-02 | .2022E-03 | .2799E-03 |
| 9.2 | 9.4 | .2486E-02 | .1989E-03 | .2547E-03 |
| 9.4 | 9.6 | .1267E-02 | .1778E-03 | .1897E-03 |
| 9.6 | 9.8 | .1210E-02 | .1674E-03 | .1783E-03 |
| 9.8 | 10.0 | .9043E-03 | .1666E-03 | .1725E-03 |
| 10.0 | 10.2 | .9717E-03 | .1746E-03 | .1810E-03 |
| 10.2 | 10.4 | .1495E-02 | .1919E-03 | .2073E-03 |
| 10.4 | 10.6 | .1480E-02 | .1922E-03 | .2076E-03 |
| 10.6 | 10.8 | .1455E-02 | .1909E-03 | .2095E-03 |
| 10.8 | 11.0 | .7289E-03 | .1772E-03 | .1809E-03 |
| 11.0 | 11.2 | .8456E-03 | .1787E-03 | .1846E-03 |
| 11.2 | 11.4 | .3595E-03 | .1763E-03 | .1784E-03 |
| 11.4 | 11.6 | .8715E-03 | .1818E-03 | .1945E-03 |
| 11.6 | 11.8 | .4376E-03 | .2119E-03 | .2131E-03 |
| 11.8 | 12.0 | .7712E-03 | .2053E-03 | .2143E-03 |
| 12.0 | 12.2 | .6190E-03 | .1965E-03 | .1989E-03 |
| 12.2 | 12.4 | .1329E-02 | .2264E-03 | .2360E-03 |
| 12.4 | 12.6 | .2459E-02 | .2636E-03 | .2899E-03 |
| 12.6 | 12.8 | .4667E-02 | .3107E-03 | .4063E-03 |
| 12.8 | 13.0 | .5764E-02 | .3382E-03 | .4962E-03 |
| 13.0 | 13.2 | .5071E-02 | .3375E-03 | .4333E-03 |
| 13.2 | 13.4 | .1001E-01 | .3933E-03 | .6357E-03 |
| 13.4 | 13.6 | .2452E-01 | .5311E-03 | .1615E-02 |
| 13.6 | 13.8 | .2943E-01 | .5746E-03 | .2387E-02 |
| 13.8 | 14.0 | .1281E-01 | .4637E-03 | .1220E-02 |
| 14.0 | 14.2 | .2219E-02 | .4511E-03 | .4879E-03 |

Table I : DDX data of natural Fe with En = 14.1 MeV at 100 degrees in LAB system.

| En-min (MeV) | En-max (MeV) | DDX (b/sr/MeV) | Statistical error (b/sr/MeV) | Experimental error (b/sr/MeV) |
|---|---|---|---|---|
| 2.0 | 2.2 | .2337E-01 | .6149E-03 | .1476E-02 |
| 2.2 | 2.4 | .2005E-01 | .5705E-03 | .1285E-02 |
| 2.4 | 2.6 | .1869E-01 | .5576E-03 | .1209E-02 |
| 2.6 | 2.8 | .1726E-01 | .5112E-03 | .1115E-02 |
| 2.8 | 3.0 | .1499E-01 | .4689E-03 | .9798E-03 |
| 3.0 | 3.2 | .1382E-01 | .4494E-03 | .9115E-03 |
| 3.2 | 3.4 | .1222E-01 | .4333E-03 | .8243E-03 |
| 3.4 | 3.6 | .1133E-01 | .4129E-03 | .7704E-03 |
| 3.6 | 3.8 | .1021E-01 | .4027E-03 | .7110E-03 |
| 3.8 | 4.0 | .9084E-02 | .3923E-03 | .6525E-03 |
| 4.0 | 4.2 | .8946E-02 | .3844E-03 | .6414E-03 |
| 4.2 | 4.4 | .8667E-02 | .3749E-03 | .6229E-03 |
| 4.4 | 4.6 | .7728E-02 | .3538E-03 | .5674E-03 |
| 4.6 | 4.8 | .7181E-02 | .4355E-03 | .6181E-03 |
| 4.8 | 5.0 | .6350E-02 | .3969E-03 | .5515E-03 |
| 5.0 | 5.2 | .6362E-02 | .3933E-03 | .5411E-03 |
| 5.2 | 5.4 | .5497E-02 | .3729E-03 | .4928E-03 |
| 5.4 | 5.6 | .4577E-02 | .3386E-03 | .4115E-03 |
| 5.6 | 5.8 | .4081E-02 | .3223E-03 | .3801E-03 |
| 5.8 | 6.0 | .3668E-02 | .3160E-03 | .3775E-03 |
| 6.0 | 6.2 | .3423E-02 | .3032E-03 | .3632E-03 |
| 6.2 | 6.4 | .3508E-02 | .2901E-03 | .3459E-03 |
| 6.4 | 6.6 | .2915E-02 | .2898E-03 | .3242E-03 |
| 6.6 | 6.8 | .3073E-02 | .2893E-03 | .3302E-03 |
| 6.8 | 7.0 | .3146E-02 | .2889E-03 | .3402E-03 |
| 7.0 | 7.2 | .2574E-02 | .2699E-03 | .3032E-03 |
| 7.2 | 7.4 | .2130E-02 | .2685E-03 | .2941E-03 |
| 7.4 | 7.6 | .1791E-02 | .2583E-03 | .2778E-03 |
| 7.6 | 7.8 | .1744E-02 | .2505E-03 | .2664E-03 |
| 7.8 | 8.0 | .1604E-02 | .2408E-03 | .2534E-03 |
| 8.0 | 8.2 | .1748E-02 | .2463E-03 | .2631E-03 |
| 8.2 | 8.4 | .2032E-02 | .2458E-03 | .2678E-03 |
| 8.4 | 8.6 | .1347E-02 | .2216E-03 | .2310E-03 |
| 8.6 | 8.8 | .1957E-02 | .2313E-03 | .2522E-03 |
| 8.8 | 9.0 | .1652E-02 | .2288E-03 | .2431E-03 |
| 9.0 | 9.2 | .2248E-02 | .2469E-03 | .2780E-03 |
| 9.2 | 9.4 | .1300E-02 | .2209E-03 | .2425E-03 |
| 9.4 | 9.6 | .6759E-03 | .1927E-03 | .1957E-03 |
| 9.6 | 9.8 | .8008E-03 | .1961E-03 | .2013E-03 |
| 9.8 | 10.0 | .9149E-03 | .1992E-03 | .2050E-03 |
| 10.0 | 10.2 | .1208E-02 | .2221E-03 | .2312E-03 |
| 10.2 | 10.4 | .1684E-02 | .2186E-03 | .2344E-03 |
| 10.4 | 10.6 | .1744E-02 | .2318E-03 | .2571E-03 |
| 10.6 | 10.8 | .1209E-02 | .2047E-03 | .2197E-03 |
| 10.8 | 11.0 | .9046E-03 | .1966E-03 | .2139E-03 |
| 11.0 | 11.2 | .1652E-03 | .2156E-03 | .2159E-03 |
| 11.2 | 11.4 | .5238E-03 | .2098E-03 | .2116E-03 |
| 11.4 | 11.6 | .5247E-03 | .2224E-03 | .2239E-03 |
| 11.6 | 11.8 | .6758E-03 | .2524E-03 | .2547E-03 |
| 11.8 | 12.0 | .6038E-03 | .2323E-03 | .2347E-03 |
| 12.0 | 12.2 | .7841E-03 | .2546E-03 | .2599E-03 |
| 12.2 | 12.4 | .1236E-02 | .2988E-03 | .3094E-03 |
| 12.4 | 12.6 | .2805E-02 | .3381E-03 | .3663E-03 |
| 12.6 | 12.8 | .3986E-02 | .3878E-03 | .4401E-03 |
| 12.8 | 13.0 | .4646E-02 | .4065E-03 | .4724E-03 |
| 13.0 | 13.2 | .4692E-02 | .4027E-03 | .4649E-03 |
| 13.2 | 13.4 | .6364E-02 | .4804E-03 | .5819E-03 |
| 13.4 | 13.6 | .1137E-01 | .5690E-03 | .9004E-03 |
| 13.6 | 13.8 | .8486E-02 | .5674E-03 | .9439E-03 |
| 13.8 | 14.0 | .2649E-02 | .4459E-03 | .4799E-03 |
| 14.0 | 14.2 | .7509E-03 | .3823E-03 | .3854E-03 |
| 14.2 | 14.4 | .2136E-02 | .5306E-03 | .5426E-03 |

Table I : DDX data of natural Fe with En = 14.1 MeV at 110 degrees in LAB system.

| En-min (MeV) | En-max (MeV) | DDX (b/sr/MeV) | Statistical error (b/sr/MeV) | Experimental error (b/sr/MeV) |
|---|---|---|---|---|
| 2.0 | 2.2 | .2207E-01 | .4463E-03 | .1343E-02 |
| 2.2 | 2.4 | .2065E-01 | .4212E-03 | .1258E-02 |
| 2.4 | 2.6 | .1784E-01 | .4049E-03 | .1101E-02 |
| 2.6 | 2.8 | .1676E-01 | .3823E-03 | .1035E-02 |
| 2.8 | 3.0 | .1431E-01 | .3447E-03 | .8906E-03 |
| 3.0 | 3.2 | .1331E-01 | .3279E-03 | .8316E-03 |
| 3.2 | 3.4 | .1158E-01 | .3104E-03 | .7337E-03 |
| 3.4 | 3.6 | .1126E-01 | .3013E-03 | .7132E-03 |
| 3.6 | 3.8 | .9723E-02 | .2854E-03 | .6268E-03 |
| 3.8 | 4.0 | .8677E-02 | .2794E-03 | .5711E-03 |
| 4.0 | 4.2 | .8317E-02 | .2768E-03 | .5518E-03 |
| 4.2 | 4.4 | .8080E-02 | .2707E-03 | .5370E-03 |
| 4.4 | 4.6 | .7274E-02 | .2573E-03 | .4904E-03 |
| 4.6 | 4.8 | .6400E-02 | .2518E-03 | .4454E-03 |
| 4.8 | 5.0 | .5769E-02 | .2451E-03 | .4120E-03 |
| 5.0 | 5.2 | .5587E-02 | .2454E-03 | .4038E-03 |
| 5.2 | 5.4 | .5020E-02 | .2685E-03 | .4039E-03 |
| 5.4 | 5.6 | .4329E-02 | .2521E-03 | .3635E-03 |
| 5.6 | 5.8 | .3784E-02 | .2464E-03 | .3299E-03 |
| 5.8 | 6.0 | .4043E-02 | .2347E-03 | .3399E-03 |
| 6.0 | 6.2 | .3600E-02 | .2184E-03 | .3251E-03 |
| 6.2 | 6.4 | .3081E-02 | .2139E-03 | .2718E-03 |
| 6.4 | 6.6 | .2785E-02 | .2069E-03 | .2538E-03 |
| 6.6 | 6.8 | .2691E-02 | .2046E-03 | .2449E-03 |
| 6.8 | 7.0 | .2882E-02 | .2157E-03 | .2855E-03 |
| 7.0 | 7.2 | .2049E-02 | .2029E-03 | .2290E-03 |
| 7.2 | 7.4 | .2004E-02 | .2002E-03 | .2309E-03 |
| 7.4 | 7.6 | .1994E-02 | .1875E-03 | .2174E-03 |
| 7.6 | 7.8 | .1866E-02 | .1807E-03 | .2215E-03 |
| 7.8 | 8.0 | .1709E-02 | .1766E-03 | .2089E-03 |
| 8.0 | 8.2 | .1271E-02 | .1834E-03 | .1934E-03 |
| 8.2 | 8.4 | .1978E-02 | .1909E-03 | .2206E-03 |
| 8.4 | 8.6 | .1612E-02 | .1835E-03 | .2045E-03 |
| 8.6 | 8.8 | .1421E-02 | .1790E-03 | .1926E-03 |
| 8.8 | 9.0 | .2632E-02 | .1820E-03 | .2555E-03 |
| 9.0 | 9.2 | .2059E-02 | .1793E-03 | .2201E-03 |
| 9.2 | 9.4 | .1113E-02 | .1627E-03 | .1742E-03 |
| 9.4 | 9.6 | .7375E-03 | .1566E-03 | .1627E-03 |
| 9.6 | 9.8 | .8643E-03 | .1503E-03 | .1562E-03 |
| 9.8 | 10.0 | .8149E-03 | .1501E-03 | .1558E-03 |
| 10.0 | 10.2 | .9695E-03 | .1517E-03 | .1592E-03 |
| 10.2 | 10.4 | .1472E-02 | .1554E-03 | .1824E-03 |
| 10.4 | 10.6 | .1117E-02 | .1584E-03 | .1733E-03 |
| 10.6 | 10.8 | .4437E-03 | .1419E-03 | .1448E-03 |
| 10.8 | 11.0 | .4855E-03 | .1313E-03 | .1375E-03 |
| 11.0 | 11.2 | .2064E-03 | .1272E-03 | .1280E-03 |
| 11.2 | 11.4 | .4662E-03 | .1317E-03 | .1339E-03 |
| 11.4 | 11.6 | .4053E-03 | .1361E-03 | .1377E-03 |
| 11.6 | 11.8 | .4057E-03 | .1402E-03 | .1418E-03 |
| 11.8 | 12.0 | .4087E-03 | .1567E-03 | .1586E-03 |
| 12.0 | 12.2 | .1056E-02 | .1581E-03 | .1663E-03 |
| 12.2 | 12.4 | .1263E-02 | .1815E-03 | .1946E-03 |
| 12.4 | 12.6 | .2674E-02 | .2082E-03 | .2502E-03 |
| 12.6 | 12.8 | .4039E-02 | .2349E-03 | .3360E-03 |
| 12.8 | 13.0 | .3130E-02 | .2344E-03 | .2973E-03 |
| 13.0 | 13.2 | .3222E-02 | .2342E-03 | .2834E-03 |
| 13.2 | 13.4 | .5266E-02 | .2648E-03 | .3749E-03 |
| 13.4 | 13.6 | .7826E-02 | .2912E-03 | .6266E-03 |
| 13.6 | 13.8 | .5738E-02 | .2670E-03 | .5241E-03 |
| 13.8 | 14.0 | .1418E-02 | .2312E-03 | .2480E-03 |
| 14.0 | 14.2 | .4086E-03 | .2405E-03 | .2415E-03 |

Table I : DDX data of natural Fe with En = 14.1 MeV
at 120 degrees in LAB system.

| En-min (MeV) | En-max (MeV) | DDX (b/sr/MeV) | Statistical error (b/sr/MeV) | Experimental error (b/sr/MeV) |
|---|---|---|---|---|
| 2.0 | 2.2 | .2177E-01 | .4543E-03 | .1330E-02 |
| 2.2 | 2.4 | .1960E-01 | .4126E-03 | .1198E-02 |
| 2.4 | 2.6 | .1626E-01 | .3921E-03 | .1012E-02 |
| 2.6 | 2.8 | .1566E-01 | .3800E-03 | .9759E-03 |
| 2.8 | 3.0 | .1379E-01 | .3419E-03 | .8624E-03 |
| 3.0 | 3.2 | .1229E-01 | .3210E-03 | .7751E-03 |
| 3.2 | 3.4 | .1125E-01 | .3053E-03 | .7145E-03 |
| 3.4 | 3.6 | .1078E-01 | .2980E-03 | .6868E-03 |
| 3.6 | 3.8 | .9174E-02 | .2806E-03 | .5966E-03 |
| 3.8 | 4.0 | .8404E-02 | .2745E-03 | .5550E-03 |
| 4.0 | 4.2 | .7392E-02 | .2721E-03 | .5040E-03 |
| 4.2 | 4.4 | .7037E-02 | .2645E-03 | .4829E-03 |
| 4.4 | 4.6 | .6817E-02 | .2601E-03 | .4698E-03 |
| 4.6 | 4.8 | .6132E-02 | .2533E-03 | .4337E-03 |
| 4.8 | 5.0 | .6108E-02 | .2992E-03 | .4923E-03 |
| 5.0 | 5.2 | .5699E-02 | .2942E-03 | .4660E-03 |
| 5.2 | 5.4 | .4781E-02 | .2717E-03 | .3983E-03 |
| 5.4 | 5.6 | .4244E-02 | .2564E-03 | .3637E-03 |
| 5.6 | 5.8 | .3753E-02 | .2371E-03 | .3348E-03 |
| 5.8 | 6.0 | .3670E-02 | .2369E-03 | .3178E-03 |
| 6.0 | 6.2 | .3540E-02 | .2276E-03 | .3063E-03 |
| 6.2 | 6.4 | .3132E-02 | .2215E-03 | .2825E-03 |
| 6.4 | 6.6 | .2671E-02 | .2100E-03 | .2793E-03 |
| 6.6 | 6.8 | .2534E-02 | .2093E-03 | .2556E-03 |
| 6.8 | 7.0 | .2227E-02 | .1997E-03 | .2326E-03 |
| 7.0 | 7.2 | .2076E-02 | .2023E-03 | .2380E-03 |
| 7.2 | 7.4 | .1839E-02 | .1939E-03 | .2198E-03 |
| 7.4 | 7.6 | .1551E-02 | .1983E-03 | .2136E-03 |
| 7.6 | 7.8 | .1403E-02 | .1822E-03 | .1994E-03 |
| 7.8 | 8.0 | .1479E-02 | .1808E-03 | .2020E-03 |
| 8.0 | 8.2 | .1572E-02 | .1857E-03 | .2076E-03 |
| 8.2 | 8.4 | .1675E-02 | .1929E-03 | .2120E-03 |
| 8.4 | 8.6 | .1344E-02 | .1807E-03 | .2002E-03 |
| 8.6 | 8.8 | .1605E-02 | .1730E-03 | .1915E-03 |
| 8.8 | 9.0 | .2205E-02 | .1818E-03 | .2185E-03 |
| 9.0 | 9.2 | .1723E-02 | .1816E-03 | .2063E-03 |
| 9.2 | 9.4 | .7946E-03 | .1549E-03 | .1597E-03 |
| 9.4 | 9.6 | .7736E-03 | .1602E-03 | .1652E-03 |
| 9.6 | 9.8 | .7103E-03 | .1617E-03 | .1673E-03 |
| 9.8 | 10.0 | .9249E-03 | .1758E-03 | .1844E-03 |
| 10.0 | 10.2 | .1075E-02 | .1695E-03 | .1883E-03 |
| 10.2 | 10.4 | .1116E-02 | .1713E-03 | .1849E-03 |
| 10.4 | 10.6 | .7982E-03 | .1475E-03 | .1543E-03 |
| 10.6 | 10.8 | .5266E-03 | .1382E-03 | .1406E-03 |
| 10.8 | 11.0 | .4880E-03 | .1439E-03 | .1465E-03 |
| 11.0 | 11.2 | .2556E-03 | .1342E-03 | .1366E-03 |
| 11.2 | 11.4 | .3524E-03 | .1463E-03 | .1475E-03 |
| 11.4 | 11.6 | .2529E-03 | .1490E-03 | .1497E-03 |
| 11.6 | 11.8 | .6977E-03 | .1491E-03 | .1554E-03 |
| 11.8 | 12.0 | .6254E-03 | .1816E-03 | .1844E-03 |
| 12.0 | 12.2 | .8554E-03 | .1838E-03 | .1896E-03 |
| 12.2 | 12.4 | .1800E-02 | .1997E-03 | .2212E-03 |
| 12.4 | 12.6 | .2691E-02 | .2244E-03 | .2649E-03 |
| 12.6 | 12.8 | .4232E-02 | .2500E-03 | .3491E-03 |
| 12.8 | 13.0 | .3855E-02 | .2556E-03 | .3282E-03 |
| 13.0 | 13.2 | .3782E-02 | .2629E-03 | .3256E-03 |
| 13.2 | 13.4 | .6644E-02 | .2934E-03 | .4624E-03 |
| 13.4 | 13.6 | .7589E-02 | .3040E-03 | .6479E-03 |
| 13.6 | 13.8 | .4588E-02 | .2732E-03 | .4765E-03 |
| 13.8 | 14.0 | .1381E-02 | .2580E-03 | .2853E-03 |
| 14.0 | 14.2 | .4745E-03 | .3143E-03 | .3216E-03 |

Table I : DDX data of natural Fe with En = 14.1 MeV at 130 degrees in LAB system.

| En-min (MeV) | En-max (MeV) | DDX (b/sr/MeV) | Statistical error (b/sr/MeV) | Experimental error (b/sr/MeV) |
|---|---|---|---|---|
| 2.0 | 2.2 | .2174E-01 | .4393E-03 | .1323E-02 |
| 2.2 | 2.4 | .1998E-01 | .4159E-03 | .1220E-02 |
| 2.4 | 2.6 | .1660E-01 | .3945E-03 | .1031E-02 |
| 2.6 | 2.8 | .1642E-01 | .3932E-03 | .1021E-02 |
| 2.8 | 3.0 | .1427E-01 | .3449E-03 | .8888E-03 |
| 3.0 | 3.2 | .1283E-01 | .3275E-03 | .8059E-03 |
| 3.2 | 3.4 | .1140E-01 | .3104E-03 | .7242E-03 |
| 3.4 | 3.6 | .1106E-01 | .3008E-03 | .7026E-03 |
| 3.6 | 3.8 | .9308E-02 | .2888E-03 | .6073E-03 |
| 3.8 | 4.0 | .8446E-02 | .2795E-03 | .5596E-03 |
| 4.0 | 4.2 | .7553E-02 | .2710E-03 | .5113E-03 |
| 4.2 | 4.4 | .7111E-02 | .2626E-03 | .4854E-03 |
| 4.4 | 4.6 | .6819E-02 | .2553E-03 | .4673E-03 |
| 4.6 | 4.8 | .5971E-02 | .2439E-03 | .4207E-03 |
| 4.8 | 5.0 | .6355E-02 | .3054E-03 | .5219E-03 |
| 5.0 | 5.2 | .5340E-02 | .2889E-03 | .4247E-03 |
| 5.2 | 5.4 | .5039E-02 | .2668E-03 | .4390E-03 |
| 5.4 | 5.6 | .4382E-02 | .2500E-03 | .3773E-03 |
| 5.6 | 5.8 | .4191E-02 | .2505E-03 | .3591E-03 |
| 5.8 | 6.0 | .3814E-02 | .2396E-03 | .3263E-03 |
| 6.0 | 6.2 | .3216E-02 | .2252E-03 | .2836E-03 |
| 6.2 | 6.4 | .3241E-02 | .2193E-03 | .2981E-03 |
| 6.4 | 6.6 | .2928E-02 | .2090E-03 | .2667E-03 |
| 6.6 | 6.8 | .2603E-02 | .2132E-03 | .2576E-03 |
| 6.8 | 7.0 | .2773E-02 | .2078E-03 | .2698E-03 |
| 7.0 | 7.2 | .1957E-02 | .2138E-03 | .2381E-03 |
| 7.2 | 7.4 | .1971E-02 | .2110E-03 | .2357E-03 |
| 7.4 | 7.6 | .1930E-02 | .2083E-03 | .2438E-03 |
| 7.6 | 7.8 | .1352E-02 | .1856E-03 | .2039E-03 |
| 7.8 | 8.0 | .1458E-02 | .1902E-03 | .2122E-03 |
| 8.0 | 8.2 | .1366E-02 | .1895E-03 | .2023E-03 |
| 8.2 | 8.4 | .1227E-02 | .1868E-03 | .2010E-03 |
| 8.4 | 8.6 | .1751E-02 | .1865E-03 | .2186E-03 |
| 8.6 | 8.8 | .1419E-02 | .1852E-03 | .1992E-03 |
| 8.8 | 9.0 | .2633E-02 | .1905E-03 | .2448E-03 |
| 9.0 | 9.2 | .1522E-02 | .1737E-03 | .2007E-03 |
| 9.2 | 9.4 | .8653E-03 | .1656E-03 | .1756E-03 |
| 9.4 | 9.6 | .6389E-03 | .1565E-03 | .1595E-03 |
| 9.6 | 9.8 | .3719E-03 | .1500E-03 | .1517E-03 |
| 9.8 | 10.0 | .8776E-03 | .1511E-03 | .1585E-03 |
| 10.0 | 10.2 | .1003E-02 | .1592E-03 | .1679E-03 |
| 10.2 | 10.4 | .9393E-03 | .1627E-03 | .1721E-03 |
| 10.4 | 10.6 | .6726E-03 | .1639E-03 | .1773E-03 |
| 10.6 | 10.8 | .7572E-03 | .1630E-03 | .1719E-03 |
| 10.8 | 11.0 | .4001E-03 | .1489E-03 | .1503E-03 |
| 11.0 | 11.2 | .2237E-03 | .1560E-03 | .1567E-03 |
| 11.2 | 11.4 | .4660E-03 | .1618E-03 | .1641E-03 |
| 11.4 | 11.6 | .6612E-03 | .1666E-03 | .1701E-03 |
| 11.6 | 11.8 | .4187E-03 | .1788E-03 | .1809E-03 |
| 11.8 | 12.0 | .8190E-03 | .1787E-03 | .1833E-03 |
| 12.0 | 12.2 | .1058E-02 | .2113E-03 | .2186E-03 |
| 12.2 | 12.4 | .1894E-02 | .2378E-03 | .2596E-03 |
| 12.4 | 12.6 | .3435E-02 | .2823E-03 | .3380E-03 |
| 12.6 | 12.8 | .3314E-02 | .2763E-03 | .3391E-03 |
| 12.8 | 13.0 | .2965E-02 | .2588E-03 | .2956E-03 |
| 13.0 | 13.2 | .5048E-02 | .2925E-03 | .3890E-03 |
| 13.2 | 13.4 | .9475E-02 | .3543E-03 | .6950E-03 |
| 13.4 | 13.6 | .8222E-02 | .3511E-03 | .7806E-03 |
| 13.6 | 13.8 | .1982E-02 | .3107E-03 | .3981E-03 |

Table I : DDX data of natural Fe with En = 14.1 MeV at 140 degrees in LAB system.

| En-min (MeV) | En-max (MeV) | DDX (b/sr/MeV) | Statistical error (b/sr/MeV) | Experimental error (b/sr/MeV) |
|---|---|---|---|---|
| 2.0 | 2.2 | .2366E-01 | .4512E-03 | .1431E-02 |
| 2.2 | 2.4 | .2157E-01 | .4289E-03 | .1310E-02 |
| 2.4 | 2.6 | .1798E-01 | .4024E-03 | .1108E-02 |
| 2.6 | 2.8 | .1580E-01 | .3945E-03 | .9889E-03 |
| 2.8 | 3.0 | .1478E-01 | .3539E-03 | .9190E-03 |
| 3.0 | 3.2 | .1374E-01 | .3380E-03 | .8580E-03 |
| 3.2 | 3.4 | .1246E-01 | .3205E-03 | .7836E-03 |
| 3.4 | 3.6 | .1107E-01 | .3044E-03 | .7046E-03 |
| 3.6 | 3.8 | .9667E-02 | .2941E-03 | .6280E-03 |
| 3.8 | 4.0 | .9085E-02 | .2863E-03 | .5949E-03 |
| 4.0 | 4.2 | .8310E-02 | .2758E-03 | .5510E-03 |
| 4.2 | 4.4 | .7396E-02 | .2629E-03 | .4994E-03 |
| 4.4 | 4.6 | .6816E-02 | .2562E-03 | .4677E-03 |
| 4.6 | 4.8 | .6165E-02 | .2497E-03 | .4331E-03 |
| 4.8 | 5.0 | .6167E-02 | .3115E-03 | .4711E-03 |
| 5.0 | 5.2 | .6109E-02 | .2951E-03 | .4860E-03 |
| 5.2 | 5.4 | .5045E-02 | .2746E-03 | .4147E-03 |
| 5.4 | 5.6 | .4607E-02 | .2587E-03 | .3857E-03 |
| 5.6 | 5.8 | .4063E-02 | .2518E-03 | .3516E-03 |
| 5.8 | 6.0 | .3556E-02 | .2373E-03 | .3073E-03 |
| 6.0 | 6.2 | .3969E-02 | .2338E-03 | .3248E-03 |
| 6.2 | 6.4 | .3034E-02 | .2246E-03 | .2752E-03 |
| 6.4 | 6.6 | .2986E-02 | .2176E-03 | .2764E-03 |
| 6.6 | 6.8 | .2843E-02 | .2177E-03 | .2714E-03 |
| 6.8 | 7.0 | .2294E-02 | .2045E-03 | .2400E-03 |
| 7.0 | 7.2 | .2287E-02 | .2093E-03 | .2428E-03 |
| 7.2 | 7.4 | .2178E-02 | .2123E-03 | .2421E-03 |
| 7.4 | 7.6 | .1887E-02 | .1998E-03 | .2247E-03 |
| 7.6 | 7.8 | .1616E-02 | .1892E-03 | .2138E-03 |
| 7.8 | 8.0 | .1393E-02 | .1818E-03 | .2020E-03 |
| 8.0 | 8.2 | .1436E-02 | .1864E-03 | .1995E-03 |
| 8.2 | 8.4 | .1386E-02 | .1893E-03 | .2010E-03 |
| 8.4 | 8.6 | .1549E-02 | .1834E-03 | .1991E-03 |
| 8.6 | 8.8 | .2125E-02 | .1824E-03 | .2221E-03 |
| 8.8 | 9.0 | .2479E-02 | .1952E-03 | .2531E-03 |
| 9.0 | 9.2 | .1128E-02 | .1683E-03 | .1781E-03 |
| 9.2 | 9.4 | .8391E-03 | .1529E-03 | .1591E-03 |
| 9.4 | 9.6 | .4331E-03 | .1554E-03 | .1573E-03 |
| 9.6 | 9.8 | .7292E-03 | .1720E-03 | .1764E-03 |
| 9.8 | 10.0 | .9001E-03 | .1717E-03 | .1778E-03 |
| 10.0 | 10.2 | .1147E-02 | .1774E-03 | .1892E-03 |
| 10.2 | 10.4 | .5174E-03 | .1756E-03 | .1777E-03 |
| 10.4 | 10.6 | .5709E-03 | .1593E-03 | .1625E-03 |
| 10.6 | 10.8 | .6395E-03 | .1592E-03 | .1622E-03 |
| 10.8 | 11.0 | .4473E-03 | .1536E-03 | .1555E-03 |
| 11.0 | 11.2 | .4819E-03 | .1555E-03 | .1573E-03 |
| 11.2 | 11.4 | .8473E-03 | .1598E-03 | .1689E-03 |
| 11.4 | 11.6 | .5923E-03 | .1556E-03 | .1589E-03 |
| 11.6 | 11.8 | .4043E-03 | .1721E-03 | .1736E-03 |
| 11.8 | 12.0 | .8556E-03 | .1952E-03 | .1995E-03 |
| 12.0 | 12.2 | .1445E-02 | .2096E-03 | .2256E-03 |
| 12.2 | 12.4 | .2870E-02 | .2393E-03 | .2779E-03 |
| 12.4 | 12.6 | .4218E-02 | .2719E-03 | .3588E-03 |
| 12.6 | 12.8 | .3430E-02 | .2692E-03 | .3239E-03 |
| 12.8 | 13.0 | .4548E-02 | .3014E-03 | .3822E-03 |
| 13.0 | 13.2 | .7030E-02 | .3468E-03 | .4943E-03 |
| 13.2 | 13.4 | .1065E-01 | .3917E-03 | .8390E-03 |
| 13.4 | 13.6 | .5842E-02 | .3296E-03 | .5935E-03 |
| 13.6 | 13.8 | .1880E-02 | .2790E-03 | .3221E-03 |
| 13.8 | 14.0 | .4179E-03 | .2937E-03 | .2980E-03 |

Table I : DDX data of natural Fe with En = 14.1 MeV at 150 degrees in LAB system.

| En-min (MeV) | En-max (MeV) | DDX (b/sr/MeV) | Statistical error (b/sr/MeV) | Experimental error (b/sr/MeV) |
|---|---|---|---|---|
| 2.0 | 2.2 | .2205E-01 | .4794E-03 | .1353E-02 |
| 2.2 | 2.4 | .2056E-01 | .4539E-03 | .1264E-02 |
| 2.4 | 2.6 | .1720E-01 | .4214E-03 | .1074E-02 |
| 2.6 | 2.8 | .1563E-01 | .4123E-03 | .9872E-03 |
| 2.8 | 3.0 | .1331E-01 | .3707E-03 | .8492E-03 |
| 3.0 | 3.2 | .1306E-01 | .3587E-03 | .8310E-03 |
| 3.2 | 3.4 | .1182E-01 | .3387E-03 | .7581E-03 |
| 3.4 | 3.6 | .1049E-01 | .3257E-03 | .6848E-03 |
| 3.6 | 3.8 | .1001E-01 | .3124E-03 | .6541E-03 |
| 3.8 | 4.0 | .8079E-02 | .3005E-03 | .5526E-03 |
| 4.0 | 4.2 | .7737E-02 | .2968E-03 | .5341E-03 |
| 4.2 | 4.4 | .6836E-02 | .2823E-03 | .4834E-03 |
| 4.4 | 4.6 | .6857E-02 | .2796E-03 | .4828E-03 |
| 4.6 | 4.8 | .6047E-02 | .2720E-03 | .4410E-03 |
| 4.8 | 5.0 | .5844E-02 | .2672E-03 | .4289E-03 |
| 5.0 | 5.2 | .5546E-02 | .2601E-03 | .4111E-03 |
| 5.2 | 5.4 | .4918E-02 | .2944E-03 | .4263E-03 |
| 5.4 | 5.6 | .4693E-02 | .2707E-03 | .4016E-03 |
| 5.6 | 5.8 | .3957E-02 | .2568E-03 | .3494E-03 |
| 5.8 | 6.0 | .3809E-02 | .2523E-03 | .3490E-03 |
| 6.0 | 6.2 | .3422E-02 | .2380E-03 | .3039E-03 |
| 6.2 | 6.4 | .2968E-02 | .2339E-03 | .2910E-03 |
| 6.4 | 6.6 | .2303E-02 | .2210E-03 | .2552E-03 |
| 6.6 | 6.8 | .2449E-02 | .2192E-03 | .2661E-03 |
| 6.8 | 7.0 | .2225E-02 | .2152E-03 | .2485E-03 |
| 7.0 | 7.2 | .2102E-02 | .2148E-03 | .2564E-03 |
| 7.2 | 7.4 | .2096E-02 | .2114E-03 | .2558E-03 |
| 7.4 | 7.6 | .1502E-02 | .2079E-03 | .2251E-03 |
| 7.6 | 7.8 | .1788E-02 | .1984E-03 | .2318E-03 |
| 7.8 | 8.0 | .1602E-02 | .1981E-03 | .2187E-03 |
| 8.0 | 8.2 | .1383E-02 | .2007E-03 | .2215E-03 |
| 8.2 | 8.4 | .1294E-02 | .1986E-03 | .2085E-03 |
| 8.4 | 8.6 | .1710E-02 | .2040E-03 | .2234E-03 |
| 8.6 | 8.8 | .2284E-02 | .1950E-03 | .2414E-03 |
| 8.8 | 9.0 | .1384E-02 | .1861E-03 | .2011E-03 |
| 9.0 | 9.2 | .6671E-03 | .1731E-03 | .1764E-03 |
| 9.2 | 9.4 | .5006E-03 | .1745E-03 | .1768E-03 |
| 9.4 | 9.6 | .9000E-03 | .1821E-03 | .1883E-03 |
| 9.6 | 9.8 | .1110E-02 | .1805E-03 | .1945E-03 |
| 9.8 | 10.0 | .1073E-02 | .1665E-03 | .1779E-03 |
| 10.0 | 10.2 | .8346E-03 | .1784E-03 | .1870E-03 |
| 10.2 | 10.4 | .8962E-03 | .1765E-03 | .1833E-03 |
| 10.4 | 10.6 | .8815E-03 | .1761E-03 | .1825E-03 |
| 10.6 | 10.8 | .9072E-03 | .1759E-03 | .1819E-03 |
| 10.8 | 11.0 | .4354E-03 | .1565E-03 | .1581E-03 |
| 11.0 | 11.2 | .6990E-03 | .1728E-03 | .1777E-03 |
| 11.2 | 11.4 | .5012E-03 | .1800E-03 | .1817E-03 |
| 11.4 | 11.6 | .4686E-03 | .1803E-03 | .1818E-03 |
| 11.6 | 11.8 | .8844E-03 | .1956E-03 | .2015E-03 |
| 11.8 | 12.0 | .1425E-02 | .1990E-03 | .2147E-03 |
| 12.0 | 12.2 | .2695E-02 | .2384E-03 | .2728E-03 |
| 12.2 | 12.4 | .4800E-02 | .2893E-03 | .3968E-03 |
| 12.4 | 12.6 | .5337E-02 | .2932E-03 | .4461E-03 |
| 12.6 | 12.8 | .4288E-02 | .2664E-03 | .3423E-03 |
| 12.8 | 13.0 | .5621E-02 | .2885E-03 | .4051E-03 |
| 13.0 | 13.2 | .1052E-01 | .3483E-03 | .7246E-03 |
| 13.2 | 13.4 | .1151E-01 | .3673E-03 | .1018E-02 |
| 13.4 | 13.6 | .4138E-02 | .3106E-03 | .4824E-03 |
| 13.6 | 13.8 | .1167E-02 | .3025E-03 | .3240E-03 |
| 13.8 | 14.0 | .3013E-03 | .3531E-03 | .3578E-03 |

# DIFFERENTIAL NEUTRON EMISSION CROSS-SECTION FOR BERYLLIUM AND TUNGSTEN AT 14 MeV INCIDENT NEUTRON ENERGY*

S.P.Simakov, B.V.Devkin, M.G.Kobozev, A.A.Lychagin, V.A.Talalaev
Institute of Physics and Power Engineering, Obnisk,
Rusian Federation

C.Sandin
Institute of Nuclear Science and Technology,
Havana, Cuba

ABSTRACT

Neutron emission cross-section have been measured with the time of flight spectrometer based on a pulsed neutron generator KG-0,3 (IPPE). The experimental arrangement, measuring and data reduction procedures are described. The obtained results are compared with known experimental and evaluated data. The numerical experimental data are listed in tables.

*KEYWORDS: double differential cross sections, 14 MeV, fusion reactor materials, time of flight technique*

## 1. INTRODUCTION

The study of the interaction cross-section of fast neutron with beryllium and tungsten nuclei is an actual problem from fundamental and applied point of view. In the MeV incident neutron energy range almost all nonelastic cross-sections for beryllium are determined by the (n,2n) reaction, because of this, the beryllium is supposed to be used as a neutron multiplier material in conceptual design of fusion reactors. Due to the large nonelastic cross section and high melting temperature the tungsten is considered as moderating and shielding material. With this point of view, the differential neutron emission cross-section (DDCS) at 14 MeV neutron incident energy have to be determined with relative high accuracy [1].

From the theoretical point of view the interest is caused by the possible different ways that this reaction can proceed in the case of Be and large contribution of nonstatistical procecces for deformed isotopes of W.

---

*) This work was done under the Research Agreement No 6241/Cf between IAEA and IPPE.

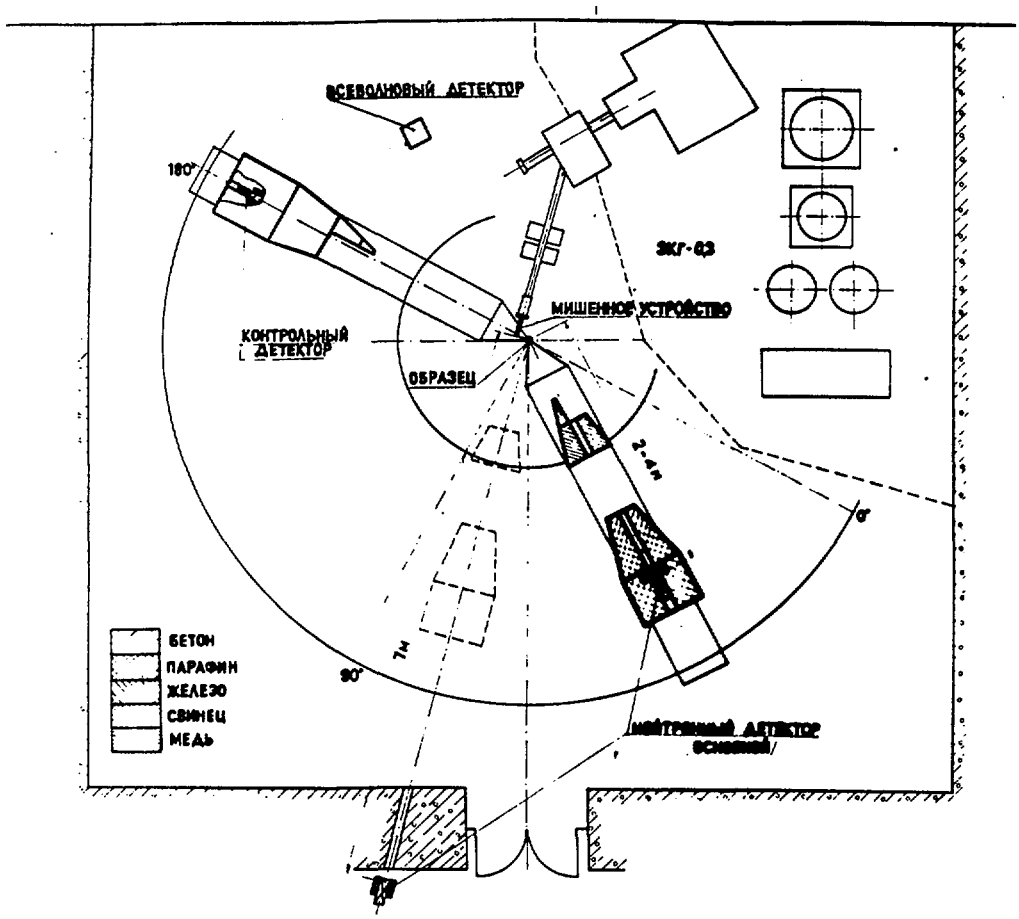


Fig.1. Geometrical arrangement of the time-of-flight spectrometer.

## EXPERIMENT

The geometrical arrangement of fast neutron spectrometer [2] is shown in fig.1. The neutron generator operated in a pulsed mode with the following parameters : energy of accelerated deuterons was 250KeV with pulse duration of 2.5ns and 2.5MHz repetition rate, the mean deuteron current - 1.5μA. The neutron yield of about $10^8$neut./s was produced in a air cooled solid TiT target.

Source neutrons scattered on a beryllium or tungsten sample allocated at 13-27 cm distance from the target. The scattering angle was change by shifting the sample near the target. This resulted in the changing of the incident neutron energy at different angles: 14.8($30^0$), 14.5($60^0$), 14.1($90^0$), 13.7($120^0$), 13.5($150^0$). The samples had a hollow cylinder form with parameters listed in the Tabl.1.

Scattered neutrons were registered by a detector consisted of a NE-218 liquid scintillator of 10 cm in diameter and 5 cm length coupled with a XP-2041 photomultiplier. The detector was housed in a lead block behind the concrete wall. The direct neutron flux

Table 1. The parameters of the samples used in the experiment.

| Element | Diameter, cm outer | Diameter, cm inner | Height cm | Weight g | Number of nucleus |
|---|---|---|---|---|---|
| Beryllium | 4.50 | 3.00 | 5.64 | 91.44 | $6.108*10^{24}$ |
| Tungsten | 4.20 | 2.00 | 5.00 | 561.25 | $1.838*10^{24}$ |

from the target was attenuated by shadow bar of iron, copper and massive paraffin shield.

With the flight path of 709 cm and 3ns overall time resolution the spectrometer energy resolution was 0.6 and 0.01 MeV at 14 and 1 MeV, correspodingly.

The generator pulse mode was controlled by a time-of-flight detector ( TOF Monitor ) consisted of fast plastic scintillator СПС-15Б of Ø2x2 cm and ФЭУ-87 photomultiplier. The time resolution of this detector measured by $\gamma$-$\gamma$ coincidence technique was 0.4 ns at 0.5 MeV $\gamma$-energy threshold. The TOF Monitor measured the TOF spectrum of source neutrons simultaneously with main detector. For monitoring the neutron yield from the target and normalization of different runs a Long Counter was used.

The detector signals fed into electronic CAMAC modules connected on line with SM-1420 Computer. The anode signals from main and monitor detectors were used for constant fraction timing (start) as well as for neutron-gamma pulse shape discrimination. The signal of pick-up electrode located before the target gave the stop pulses. The channel width of time-to-digit converter was measured dividing by factor 2 the stop rate. In that case two peaks, separated well known period, were accumulated in TOF spectrum. The channel width deduced in this method was equal 0.948 ns. The duration of each acquisition run was determined by presetting the total counts of Long Counter blocked for dead time of spectrometer.

The neutron detector efficiency was experimentally determined by two methods. In the first one, a specially designed $^{252}Cf$ ionization chamber ($1.3x10^5$ fission rate ) replaced the sample. Spectrum of prompt neutrons was measured by TOF method. The detector efficiency was then obtained from comparison of measured spectrum with standard one [3].

In the neutron energy range above 6 - 8 MeV, where the statistical accuracy with $^{252}Cf$ become poor, the efficiency was measured relative to n-p scattering cross-section [4]. In this case we placed a fast scintillate detector with a stilbene crystal

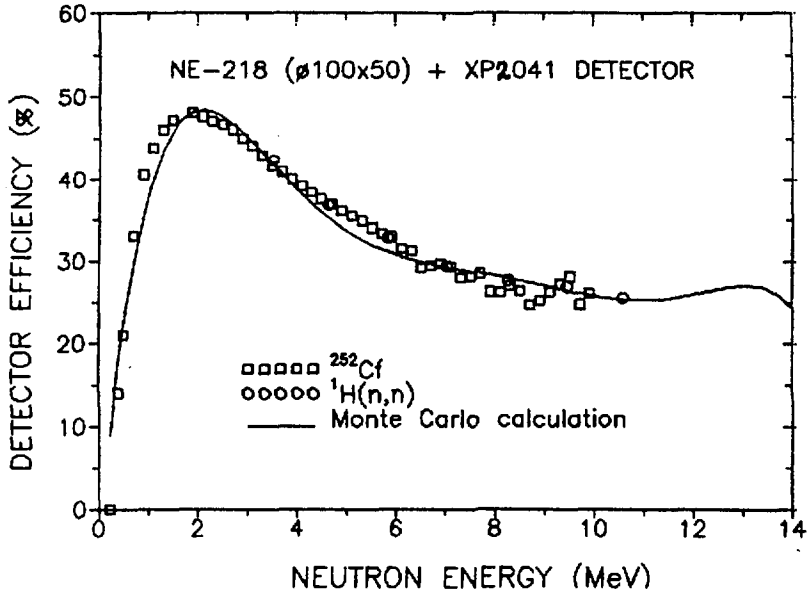


Fig.2. Efficiency of the neutron detector.

(Ø1x4cm), which gave the stop pulses for the time-of-flight separation of hydrogen scattered neutrons.

The neutron detector efficiency versus the energy is shown in fig. 2. The efficiency measured relative to n-p scattering was normalized to californium one in overlapping energy interval. The energy threshold determined by extrapolation of the efficiency curve to zero was about 0.2 MeV. The efficiency was also calculated Monte-Carlo code [5] by Kapote (INST). It is seen in the fig.2 that calculated efficiency agrees with the experimental one rather well.

The stability of the detectors and electronics was checked by long time measurements with radioactive sources. Moreover the main detector efficiency was measured several times during the whole experiment. The mean square deviations of different measurements estimated the unstability as 2 - 3 %.

The acquisition procedure consisted of sequential measurements with the sample in and sample out (several times at every angle).

Conversion from neutron spectra to double differential cross section was accomplished by comparison with the n-p scattering cross section ( as described above ) and by aluminum foil activation method. In the later case, two Al foils (Ø1.9x0.1cm) replaced the sample and were irradiated during the $T_{1/2}$=15h period, the target neutron yield been monitoring by Long Counter. The activity of irradiated foils was then measured by $\beta$-$\gamma$ coincidences spectrometer. This data and the standard Al(n,$\alpha$)

reaction cross section [4] were used for calculation of the incident neutron flux at sample position.

## 3. DATA REDUCTION PROCEDURE

At first, the TOF spectra and corresponding Long Counter counts, accumulated at every angle, were summed. Then the effect spectra were calculated as a difference of spectra obtained with the sample in and out, taking into account the possible different counts of Long Counter. After that the TOF spectra were transformed into energy one $N(E,\theta)$ and double differential cross sections were calculated by expression:

$$\frac{d^2\sigma}{dE\,d\Omega}\left[\frac{B}{MeV\cdot sr}\right]=\frac{N(E,\theta)[1/MeV]}{\varepsilon(E)\cdot\Omega[sr]}\cdot\frac{1}{M}\cdot\frac{1}{F[1/cm^2]}\cdot\frac{1}{cor(E,\theta)} \qquad (1)$$

where $\varepsilon(E)$ – is the absolute neutron detector efficiency,

$\Omega$ – is the solid angle subtended by the detector,

$M$ – is the total number of sample nuclei,

$cor(E,\theta)$ – is the correction for attenuation of in- and out-coming neutron fluxes and multiple scattering in the sample,

$F$ – is the integral neutron flux, the sample was irradiated during the experiment.

It is obvious that there is a direct correspondence between F and Long Counter counts LC :

$$F\ [1/cm^2] = k\ [1/cm^2]\cdot LC \qquad (2)$$

where k – is unknown factor, that should be determined to make absolute normalization of measured spectra. It was mentioned above that it was performed experimentally by two methods.

In the case of Al-foils activation method, the corresponding values $F_{Al}$ and $LC_{Al}$ were measured directly, hence the factor k can be determined from :

$$k=\frac{F_{Al}}{LC_{Al}} \qquad (3)$$

From the expressions (1)–(3) we can find that

$$\frac{d^2\sigma}{dEd\Omega}=\frac{N(E,\theta)}{\varepsilon(E)\cdot\Omega}\cdot\frac{1}{M}\cdot\frac{LC_{Al}}{LC}\cdot\frac{1}{cor(E,\theta)} \qquad (4)$$

In the second case the neutron flux or factor k were deduced from n–p scattering :

$$F_H = k \cdot LC_H = \frac{N_H}{\frac{\sigma_H}{\pi} \cdot \cos(\theta) \cdot \varepsilon(E_H) \cdot \Omega \cdot M_H \cdot cor_H(\theta)} \qquad (5)$$

where $\sigma_H$ – cross-section of n-p scattering [4],

$M_H$ – number of hydrogen nuclei in stilbene crystal,

$N_H$ – area under the n-p scattering peak in TOF spectra,

$cor_H(\theta)$ – correction for neutron flux attenuation and recoil proton leakage in stilbene crystal,

$E_H = E_0 \cos^2(\theta)$ – energy of neutrons scattered by protons at the angle $\theta_H$

From (1), (2) and (5) in the case of the n-p scattering normalization method we finally receive:

$$\frac{d^2\sigma}{dE\, d\Omega} = \frac{\sigma_H}{\pi} \cdot \cos(\theta_H) \cdot \frac{N(E,\theta)}{N_H} \cdot \frac{\varepsilon(E_H)}{\varepsilon(E)} \cdot \frac{LC_H}{LC} \cdot \frac{M_H}{M} \cdot \frac{cor_H(\theta_H)}{cor(E,\theta)} \qquad (6)$$

In the present experiment the absolute scaling procedure was carried out by both methods, resulting to the normalization uncertainty of 3 %.

The elastically scattered neutrons were subtracted from total neutron emission spectrum in the following way. During the experiment the spectrum of neutrons scattered by $^{208}Pb$ sample was measured. Due to high excitation of the first level (2.7MeV) the elastically and inelastically scattered neutron groups are separated. The $^{208}Pb$ elastic peak was then fitted to the upper part of elastic peak in the time of flight spectrum of neutrons scattered by W.

In the case of light nucleus $^{9}Be$ the situation is more complicated: elastically scattered neutrons decrease its energy strongly that results in the broadening of the elastic peak. This effect is illustrated in fig.3, for the case of $90^{o}$. The solid line curve is calculated spectrum of neutrons elastically scattered by the beryllium sample. The calculations were done by Monte-Carlo method using SSE code. The multiple elastic collisions, kinematic effects were taking into account to calculate the time of flight spectrum in the detector, i.e. the real experimental conditions were simulated. The time of flight spectrum was then transformed to the energy one and folded with the time resolution function of the spectrometer. Finally, the spectrum obtained was fitted to the upper part of elastic peak in the Be neutron emission spectrum. The dashed curves in the fig.3 are the contributions of single and multiple elastic collisions. It is seen that single elastic

Table 2. DDCS and absolute errors [mb/MeV/sr] in lab. system for Be.
The values in the brackets indicates the incident energies.

| E, MeV | $30^0$ (14.78) | $60^0$ (14.49) | $90^0$ (14.10) | $120^0$ (13.72) | $150^0$ (13.45) |
|---|---|---|---|---|---|
| .8 | 33.10±22.96 | 24.29±2.64 | 15.37±1.61 | 16.06±1.12 | 19.90±5.50 |
| 1.0 | 27.05± 8.33 | 17.15±1.52 | 13.70±1.10 | 15.19±1.17 | 11.74± .83 |
| 1.2 | 21.41± 2.46 | 17.24±1.38 | 12.93± .99 | 13.21±1.01 | 11.93±1.13 |
| 1.4 | 19.57± 3.06 | 14.48±1.16 | 11.37± .86 | 11.03± .77 | 10.24± .73 |
| 1.6 | 16.58± 1.70 | 13.99±1.08 | 10.66± .80 | 9.43± .67 | 8.01±1.19 |
| 1.8 | 12.76± 1.44 | 12.22± .96 | 9.47± .71 | 7.72± .59 | 6.63± .63 |
| 2.0 | 15.27± 1.50 | 10.61± .84 | 8.05± .61 | 6.41± .57 | 6.15± .47 |
| 2.2 | 12.27± 1.30 | 9.65± .77 | 6.47± .50 | 5.27± .37 | 5.60± .63 |
| 2.4 | 14.80± 1.42 | 9.36± .75 | 5.80± .46 | 4.77± .34 | 5.82± .59 |
| 2.6 | 17.33± 1.56 | 8.44± .70 | 5.11± .42 | 4.24± .30 | 4.92± .43 |
| 2.8 | 13.98± 1.39 | 7.12± .61 | 4.33± .37 | 3.93± .38 | 3.98± .30 |
| 3.0 | 10.78± 1.20 | 5.95± .55 | 4.00± .35 | 3.60± .26 | 3.88± .27 |
| 3.2 | 8.59± 1.05 | 5.70± .52 | 3.41± .31 | 3.58± .25 | 3.80± .30 |
| 3.4 | 9.05± 1.04 | 4.82± .45 | 3.03± .28 | 3.33± .25 | 3.90± .35 |
| 3.6 | 7.29± 1.01 | 4.66± .45 | 2.88± .27 | 3.32± .31 | 3.71± .48 |
| 3.8 | 6.71± .93 | 4.54± .44 | 2.89± .28 | 3.49± .25 | 3.63± .35 |
| 4.0 | 5.64± .88 | 4.25± .44 | 3.08± .28 | 3.97± .28 | 3.38± .25 |
| 4.2 | 6.42± .95 | 4.43± .43 | 3.22± .30 | 4.05± .42 | 3.35± .24 |
| 4.4 | 5.23± 1.01 | 3.66± .43 | 3.32± .30 | 3.95± .34 | 3.30± .29 |
| 4.6 | 6.51± .90 | 3.48± .38 | 3.60± .32 | 3.40± .32 | 2.70± .52 |
| 4.8 | 5.52± .91 | 3.62± .40 | 3.87± .32 | 3.06± .28 | 2.74± .32 |
| 5.0 | 4.90± .99 | 3.65± .39 | 4.11± .37 | 2.49± .23 | 2.31± .18 |
| 5.2 | 4.01± .81 | 3.55± .41 | 4.30± .36 | 2.14± .20 | 1.80± .16 |
| 5.4 | 4.24± .90 | 4.04± .43 | 4.40± .38 | 1.94± .16 | 1.37± .11 |
| 5.6 | 4.64± .85 | 3.94± .42 | 4.20± .36 | 1.87± .16 | 1.10± .09 |
| 5.8 | 3.68± .99 | 3.99± .42 | 3.74± .32 | 1.72± .14 | .96± .22 |
| 6.0 | 4.47± .82 | 4.63± .44 | 3.24± .29 | 1.62± .21 | 1.01± .07 |
| 6.2 | 5.76± .95 | 5.38± .52 | 2.73± .29 | 1.44± .20 | 1.54± .11 |
| 6.4 | 5.80± .81 | 5.70± .49 | 2.31± .23 | 1.47± .15 | 2.17± .36 |
| 6.6 | 4.15± .84 | 5.89± .53 | 2.05± .23 | 1.45± .11 | 3.11± .36 |
| 6.8 | 4.57± .84 | 6.12± .54 | 1.94± .23 | 1.66± .12 | 5.39±1.21 |
| 7.0 | 5.59± 1.13 | 5.46± .49 | 1.94± .22 | 2.03± .19 | 5.06± .65 |
| 7.2 | 5.52± .86 | 4.80± .54 | 1.50± .26 | 3.27± .43 | 2.29± .40 |
| 7.4 | 6.92± .90 | 4.25± .43 | 1.47± .20 | 4.84± .44 | |
| 7.6 | 7.15± 1.18 | 4.00± .49 | 1.51± .20 | 5.99± .56 | |
| 7.8 | 6.59± .92 | 3.89± .40 | 1.38± .25 | 5.98± .44 | |
| 8.0 | 5.27± 1.07 | 2.63± .44 | 1.65± .24 | 5.12± .65 | |
| 8.2 | 5.51± 1.01 | 2.81± .39 | 1.82± .20 | 2.78± .53 | |
| 8.4 | 5.97± .99 | 2.77± .31 | 2.47± .27 | 1.32± .26 | |
| 8.6 | 5.33± .93 | 2.52± .35 | 4.02± .37 | .73± .21 | |
| 8.8 | 5.11± .89 | 2.50± .35 | 5.60± .46 | | |
| 9.0 | 4.17± .85 | 2.25± .33 | 5.73± .47 | | |
| 9.2 | 3.80± .80 | 2.11± .33 | 6.05± .49 | | |
| 9.4 | 3.63± .77 | 2.20± .33 | 6.20± .50 | | |
| 9.6 | 3.49± .74 | 2.35± .33 | 4.75± .40 | | |
| 9.8 | 3.26± .72 | 2.93± .35 | 2.73± .26 | | |
| 10.0 | 3.29± .70 | 4.41± .43 | 1.25± .29 | | |
| 10.2 | 2.61± .68 | 7.10± .59 | .46± .35 | | |
| 10.4 | 2.91± .67 | 9.09± .73 | | | |
| 10.6 | 2.97± .66 | 10.56± .83 | | | |
| 10.8 | 3.10± .66 | 10.41± .81 | | | |
| 11.0 | 3.56± .69 | 8.75± .71 | | | |
| 11.2 | 5.42± .75 | 5.78± .50 | | | |
| 11.4 | 6.92± .83 | 2.90± .31 | | | |
| 11.6 | 11.77± 1.12 | 1.51± .25 | | | |
| 11.8 | 15.23± 1.33 | 1.01± .29 | | | |
| 12.0 | 15.93± 1.38 | .89± .41 | | | |
| 12.2 | 11.78± 1.10 | .76± .58 | | | |
| 12.4 | 7.57± .86 | .87± .35 | | | |
| 12.6 | 4.49± .66 | .42± .41 | | | |
| 12.8 | 3.71± .61 | | | | |

Table 3. The same as in table 2, but for W.

| E, MEV | 30° (14.78) | 60° (14.49) | 90° (14.10) | 120° (13.72) | 150° (13.45) |
|---|---|---|---|---|---|
| .6 | 260.8±18.9 | 187.6±13.5 | 225.3±17.0 | 226.9±16.1 | 185.9±13.3 |
| .8 | 247.1±17.4 | 187.5±13.2 | 210.5±15.0 | 202.4±14.2 | 168.6±11.9 |
| 1.0 | 220.2±16.2 | 175.5±13.9 | 187.4±13.1 | 171.1±12.0 | 146.6±10.7 |
| 1.2 | 192.2±14.1 | 156.5±11.2 | 164.9±11.5 | 145.4±10.4 | 136.8±11.2 |
| 1.4 | 161.4±11.3 | 132.5± 9.4 | 139.3± 9.7 | 121.7± 8.5 | 119.0± 8.6 |
| 1.6 | 133.5± 9.5 | 110.8± 7.9 | 113.5± 8.4 | 99.3± 7.0 | 95.7± 7.1 |
| 1.8 | 111.4± 8.4 | 90.2± 6.3 | 90.9± 6.3 | 80.0± 5.7 | 78.9± 5.6 |
| 2.0 | 91.8± 6.9 | 72.6± 5.5 | 73.7± 5.3 | 63.7± 4.4 | 64.8± 4.6 |
| 2.2 | 75.7± 5.9 | 57.9± 4.1 | 58.2± 4.0 | 49.7± 3.5 | 51.2± 3.6 |
| 2.4 | 64.5± 5.5 | 47.1± 3.3 | 47.0± 3.7 | 39.3± 3.1 | 37.8± 2.6 |
| 2.6 | 59.6± 4.2 | 39.8± 3.3 | 38.0± 2.6 | 31.5± 2.2 | 31.4± 3.7 |
| 2.8 | 52.9± 5.7 | 33.3± 2.4 | 31.6± 2.2 | 25.8± 1.8 | 24.9± 3.8 |
| 3.0 | 40.9± 3.8 | 27.7± 2.0 | 24.5± 1.8 | 20.6± 1.5 | 20.9± 2.7 |
| 3.2 | 31.0± 3.0 | 21.9± 1.8 | 19.8± 2.2 | 16.4± 1.1 | 15.9± 1.2 |
| 3.4 | 25.9± 2.0 | 17.3± 1.2 | 15.6± 1.2 | 13.0± .9 | 16.4± 2.6 |
| 3.6 | 22.2± 1.5 | 15.4± 1.1 | 13.9± 1.0 | 10.7± .9 | 19.5± 2.3 |
| 3.8 | 16.1± 1.3 | 14.3± 1.0 | 11.4± .8 | 9.1± .7 | 13.9± 1.1 |
| 4.0 | 16.7± 3.3 | 12.7± 1.1 | 9.9± .9 | 7.8± .6 | 7.9± .5 |
| 4.2 | 15.8± 4.4 | 11.0± 1.1 | 8.2± .7 | 6.0± .5 | 10.0± .7 |
| 4.4 | 17.3± 2.6 | 9.9± .7 | 7.3± .6 | 4.7± .3 | 12.0± 1.0 |
| 4.6 | 15.1± 3.1 | 9.8± .8 | 6.4± .4 | 4.3± .3 | 8.9± 1.2 |
| 4.8 | 11.8± .9 | 9.4± .6 | 6.4± .4 | 4.3± .3 | 5.7± .9 |
| 5.0 | 10.3± 1.4 | 8.5± .6 | 6.1± .7 | 3.9± .5 | 5.0± .7 |
| 5.2 | 9.6± 1.0 | 6.9± .7 | 5.9± .7 | 3.8± .6 | 3.9± .2 |
| 5.4 | 9.4± 1.2 | 6.0± 1.0 | 5.2± .5 | 3.2± .5 | 4.1± .3 |
| 5.6 | 7.6± .9 | 4.7± .5 | 5.1± .3 | 3.6± .4 | 4.1± .3 |
| 5.8 | 7.1± .8 | 4.6± .3 | 4.5± .3 | 3.3± .6 | 3.9± .3 |
| 6.0 | 8.8± .8 | 5.1± .7 | 4.4± .4 | 3.5± .6 | 3.2± .2 |
| 6.2 | 10.7± 1.9 | 5.1± 1.0 | 4.2± .5 | 3.1± .7 | 2.1± .4 |
| 6.4 | 10.2± .7 | 4.8± .4 | 3.7± .2 | 4.1± .6 | .9± .2 |
| 6.6 | 8.4± .7 | 4.0± .3 | 3.1± .2 | 4.3± .8 | 1.5± .1 |
| 6.8 | 7.7± .6 | 3.4± .3 | 2.7± .2 | 3.8± .3 | 2.3± .2 |
| 7.0 | 6.8± 1.5 | 3.6± .6 | 2.7± .2 | 3.4± .2 | 1.1± .1 |
| 7.2 | 6.9± 1.4 | 4.0± .3 | 2.6± .3 | 2.9± .5 | .2± .2 |
| 7.4 | 5.6± 1.0 | 4.6± .8 | 2.5± .2 | 2.6± .5 | 4.3± .3 |
| 7.6 | 7.0± .8 | 4.4± .6 | 2.5± .1 | 2.1± .2 | 3.3± .2 |
| 7.8 | 7.4± 1.5 | 3.7± .4 | 2.5± .3 | 2.0± .2 | 2.4± .2 |
| 8.0 | 7.8± 1.2 | 4.3± .4 | 3.2± .4 | 1.8± .2 | 2.8± .4 |
| 8.2 | 6.9± 1.5 | 4.3± .5 | 3.5± .6 | 1.4± .2 | 3.9± .4 |
| 8.4 | 7.8± 1.1 | 4.1± .3 | 3.5± .2 | 1.4± .2 | 1.7± .1 |
| 8.6 | 7.8± .8 | 3.5± .2 | 3.3± .2 | 1.2± .2 | 1.5± .1 |
| 8.8 | 7.5± 1.2 | 3.0± .2 | 2.9± .4 | 1.7± .2 | 1.4± .1 |
| 9.0 | 6.2± 1.1 | 3.3± .4 | 2.8± .4 | 1.9± .4 | 2.0± .2 |
| 9.2 | 5.6± .6 | 3.6± .5 | 2.2± .4 | 2.0± .2 | 1.9± .1 |
| 9.4 | 7.5± .6 | 3.6± .2 | 2.6± .3 | 1.7± .3 | 2.6± .2 |
| 9.6 | 8.9± .9 | 3.4± .2 | 2.5± .5 | 1.8± .3 | 3.4± .2 |
| 9.8 | 10.3± 1.1 | 3.4± .2 | 2.5± .3 | 1.7± .3 | 3.0± .4 |
| 10.0 | 10.7± 1.3 | 3.1± .5 | 2.3± .1 | 1.8± .1 | 2.6± .5 |
| 10.2 | 10.4± .7 | 2.9± .5 | 2.4± .2 | 1.9± .1 | 1.7± .1 |
| 10.4 | 9.2± .7 | 2.6± .2 | 2.2± .1 | 2.1± .1 | .8± .1 |
| 10.6 | 10.3± 1.4 | 3.5± .2 | 1.6± .1 | 2.2± .2 | .01± .01 |
| 10.8 | 10.9± 2.5 | 3.8± .3 | 1.3± .2 | 2.2± .2 | .02± .02 |
| 11.0 | 10.5± 1.2 | 3.8± .3 | 1.2± .1 | 1.9± .3 | .7± .7 |
| 11.2 | 8.5± .6 | 3.3± .3 | 1.9± .2 | 1.5± .1 | 1.6± .9 |
| 11.4 | 8.2± .6 | 3.2± .3 | 2.6± .2 | 1.2± .1 | 1.1± .2 |
| 11.6 | 8.4± .7 | 3.3± .2 | 3.1± .3 | 1.2± .1 | .05± .01 |
| 11.8 | 9.1± .7 | 3.7± .3 | 3.0± .2 | 1.7± .2 | .04± .12 |
| 12.0 | 9.4± .7 | 3.5± .4 | 2.7± .2 | 2.2± .4 | |
| 12.2 | 8.2± .8 | 3.1± .4 | 2.8± .2 | 1.9± .2 | |
| 12.4 | 7.4± 1.1 | 2.8± .8 | 2.7± .4 | 1.5± .3 | |
| 12.6 | 7.0± 2.0 | 3.2± .8 | 2.7± .4 | 1.0± .6 | |
| 12.8 | 6.2± 1.9 | 3.3± .8 | 2.6± .8 | | |

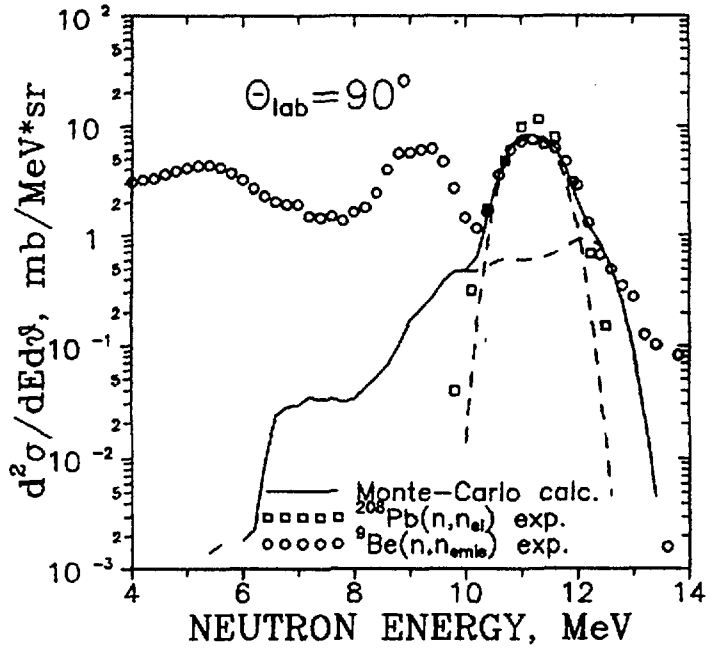


Fig.3. Elastic peak separation procedure for $^{9}Be$ at $90^{\circ}$.

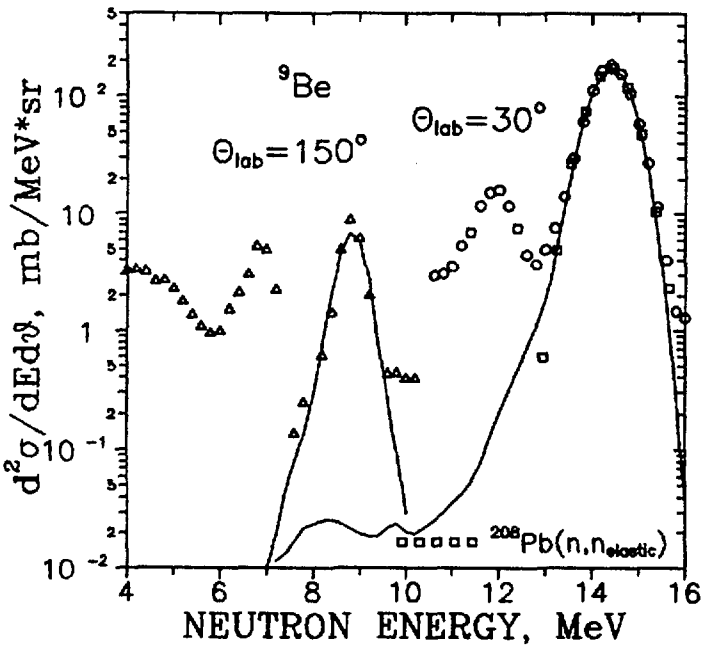


Fig.4. Elastic peak separation procedure for $^{9}Be$ at $30^{\circ}$and $150^{\circ}$.

scattered neutrons peak have the shape close to $^{208}Pb(n,n_{elastic})$ peak, but multiple elastic scattering contribution changes this shape noticeably. In the fig.4 the elastic peak separation procedure is shown for the $30^{\circ}$ and $150^{\circ}$ scattering angles.

The same SSE code was used to calculate the neutron multiple scattering and flux attenuation corrections. It can be defined as the ratio of differential cross-section disturbed by the sample

Table 4. Angle-integrated neutron emission cross-sections and abs. errors [mb/MeV] for Be and W in center of mass system.

| E, MeV | Beryllium σ(E) | Beryllium Δσ(E) | Tungsten σ(E) | Tungsten Δσ(E) | E, MeV | Beryllium σ(E) | Beryllium Δσ(E) | Tungsten σ(E) | Tungsten Δσ(E) |
|---|---|---|---|---|---|---|---|---|---|
| .8 | 114. | ± 68. | .255E+04 | ±.18E+03 | 6.6 | 38.2 | ± 3.3 | .476E+02 | ±.48E+01 |
| 1.0 | 110. | ± 88. | .227E+04 | ±.16E+03 | 6.8 | 34.5 | ± 3.0 | .458E+02 | ±.48E+01 |
| 1.2 | 161. | ± 12. | .198E+04 | ±.14E+03 | 7.0 | 30.1 | ± 2.6 | .457E+02 | ±.40E+01 |
| 1.4 | 215. | ± 35. | .168E+04 | ±.12E+03 | 7.2 | 28.2 | ± 2.5 | .488E+02 | ±.44E+01 |
| 1.6 | 193. | ± 24. | .139E+04 | ±.98E+02 | 7.4 | 25.2 | ± 2.4 | .453E+02 | ±.45E+01 |
| 1.8 | 161. | ± 13. | .113E+04 | ±.79E+02 | 7.6 | 23.8 | ± 2.2 | .419E+02 | ±.41E+01 |
| 2.0 | 135. | ± 9.7 | .912E+03 | ±.64E+02 | 7.8 | 22.6 | ± 2.1 | .461E+02 | ±.47E+01 |
| 2.2 | 120. | ± 8.8 | .735E+03 | ±.52E+02 | 8.0 | 21.6 | ± 2.1 | .496E+02 | ±.42E+01 |
| 2.4 | 102. | ± 7.4 | .603E+03 | ±.43E+02 | 8.2 | 23.9 | ± 2.2 | .475E+02 | ±.42E+01 |
| 2.6 | 88.3 | ± 6.8 | .494E+03 | ±.36E+02 | 8.4 | 27.9 | ± 2.4 | .431E+02 | ±.38E+01 |
| 2.8 | 75.6 | ± 6.1 | .403E+03 | ±.29E+02 | 8.6 | 38.4 | ± 3.3 | .410E+02 | ±.34E+01 |
| 3.0 | 66.9 | ± 5.1 | .318E+03 | ±.24E+02 | 8.8 | 58.2 | ± 4.5 | .412E+02 | ±.36E+01 |
| 3.2 | 63.8 | ± 4.8 | .259E+03 | ±.20E+02 | 9.0 | 79.6 | ± 6.1 | .420E+02 | ±.36E+01 |
| 3.4 | 57.8 | ± 4.4 | .209E+03 | ±.15E+02 | 9.2 | 96.3 | ± 7.3 | .435E+02 | ±.37E+01 |
| 3.6 | 52.9 | ± 4.3 | .182E+03 | ±.14E+02 | 9.4 | 99.5 | ± 7.4 | .462E+02 | ±.40E+01 |
| 3.8 | 49.8 | ± 4.0 | .169E+03 | ±.14E+02 | 9.6 | 81.4 | ± 6.4 | .458E+02 | ±.38E+01 |
| 4.0 | 48.7 | ± 3.8 | .148E+03 | ±.13E+02 | 9.8 | 51.1 | ± 4.2 | .428E+02 | ±.36E+01 |
| 4.2 | 46.1 | ± 3.6 | .125E+03 | ±.10E+02 | 10.0 | 27.0 | ± 2.5 | .446E+02 | ±.39E+01 |
| 4.4 | 46.8 | ± 3.6 | .110E+03 | ±.86E+01 | 10.2 | 15.3 | ± 2.5 | .485E+02 | ±.56E+01 |
| 4.6 | 49.8 | ± 3.9 | .102E+03 | ±.74E+01 | 10.4 | 9.22 | ± 5.0 | .477E+02 | ±.39E+01 |
| 4.8 | 49.4 | ± 3.8 | .952E+02 | ±.71E+01 | 10.6 | 1.84 | ± 3.3 | .420E+02 | ±.32E+01 |
| 5.0 | 52.0 | ± 4.0 | .834E+02 | ±.69E+01 | 10.8 | | | .387E+02 | ±.29E+01 |
| 5.2 | 56.6 | ± 4.5 | .726E+02 | ±.66E+01 | 11.0 | | | .370E+02 | ±.29E+01 |
| 5.4 | 58.6 | ± 4.5 | .634E+02 | ±.53E+01 | 11.2 | | | .390E+02 | ±.29E+01 |
| 5.6 | 60.1 | ± 4.6 | .619E+02 | ±.47E+01 | 11.4 | | | .412E+02 | ±.33E+01 |
| 5.8 | 57.9 | ± 4.4 | .659E+02 | ±.58E+01 | 11.6 | | | .397E+02 | ±.34E+01 |
| 6.0 | 51.5 | ± 4.0 | .647E+02 | ±.55E+01 | 11.8 | | | .379E+02 | ±.43E+01 |
| 6.2 | 46.2 | ± 3.8 | .603E+02 | ±.48E+01 | 12.0 | | | .350E+02 | ±.50E+01 |
| 6.4 | 42.1 | ± 3.6 | .526E+02 | ±.43E+01 | 12.2 | | | .360E+02 | ±.49E+01 |

Table 5. Legendre coefficients and absolute errors in c.m. systems.

| $E_i - E_{i+1}$ MeV | Beryllium $a_0$ [mb/sr] | Beryllium $b_1$ | Beryllium $b_2$ | Tungsten $a_0$ [mb/sr] | Tungsten $b_1$ | Tungsten $b_2$ |
|---|---|---|---|---|---|---|
| 1 - 2 | | | | 1542±55 | .04±.05 | .03±.08 |
| 2 - 3 | 97.5±1.0 | -.48±.02 | .33±.02 | 566±25 | .05±.07 | .14±.10 |
| 3 - 4 | 56.5±1.3 | -.30±.05 | .46±.06 | 208± 7 | .07±.06 | .24±.09 |
| 4 - 5 | 48.5±0.4 | -.10±.01 | .24±.02 | 109±10 | .33±.17 | .54±.23 |
| 5 - 6 | 57.1±1.3 | .18±.04 | .12±.05 | 67± 5 | .37±.15 | .31±.19 |
| 6 - 7 | 40.3±1.7 | .36±.08 | .43±.10 | 49± 5 | .49±.20 | .21±.23 |
| 7 - 8 | 25.1±1.0 | .38±.08 | .26±.09 | 44± 5 | .62±.24 | .34±.26 |
| 8 - 9 | 39.3±2.5 | .20±.12 | -.04±.15 | 41± 5 | .65±.24 | .63±.33 |
| 9 - 10 | 76.2±2.8 | .62±.07 | .20±.09 | 39± 7 | .84±.37 | .57±.42 |

finite effects and the true one, the later corresponding to the infinite small sample :

$$cor(E,\theta) = \frac{\sigma(raw)}{\sigma(true)} \qquad (7)$$

This function was calculated using the evaluated and/or experimental neutron data [6].

The statistical uncertainty of the measured spectra varies from 2 to 25%, the overall error in the determination of neutron detector efficiency was 4-6%, systematic uncertainty of absolute normalization was 3%, calculation of mulltiple scattering correction in the sampe - 3%. These factors contributed to the total uncertainty in the double differential cross section of 6-25%.

## 4. EXPERIMENTAL RESULTS AND DISCUSSION.

Double differential cross sections in laboratory system are listed in the tables 2(Be) and 3(W). The angle-integrated cross-sections in center of mass system for both nuclei in the table 4. The absolute errors listed in these tables are full uncertainties of experimental data.

In the table 5 the reduced Legendre coefficients for a $P_2$ fit to the experimental data in the center of mass system are given:

$$\int_{E_i}^{E_{i+1}} \frac{d^2\sigma}{dE\, d\Omega} dE = a_0 [1 + b_1 P_1(\cos\theta) + b_2 P_2(\cos\theta)], \qquad (8)$$

where neutron energy bins $E_{i+1} - E_i$ = 1MeV. The errors of $a_0$, $b_1$ and $b_2$ were calculated taking into account the statistical errors and normalization uncertainty of the spectra at different angles.

Beryllium. We compared our measurements with M.Baba e.a.[7] and A.Takahashi e. a. [8] data in fig 5 a)-e). It is seen that agreement with A.Takahashi e.a. experiment is much better then with the one of M.Baba e.a. In the experiment of H.Hogue e.a. [9] the cross-section of inelastic neutron scattering to the 2.43MeV level was measured at 14.94MeV incident energy. The angular distributions of these neutrons compared to our results are shown in fig.6 in the center of mass system.

In the same figures the evaluated data from ENDF/B6 file is shown. It is obvious that evaluation underestimates the low energy part of the double differential cross-section at backward angles.

In the fig.7 the angle-integrated cross section is shown. The arrows indicate the level scheme of the $^9$Be nucleus. It's interesting to notice that only definite states are populated through the inelastic scattering. In this figure experimental results of two our experiments are shown: the data of present one (flight path 7.1m) and of the previous experiment that have been performed at 3.1m flight path. It is seen that increasing of the

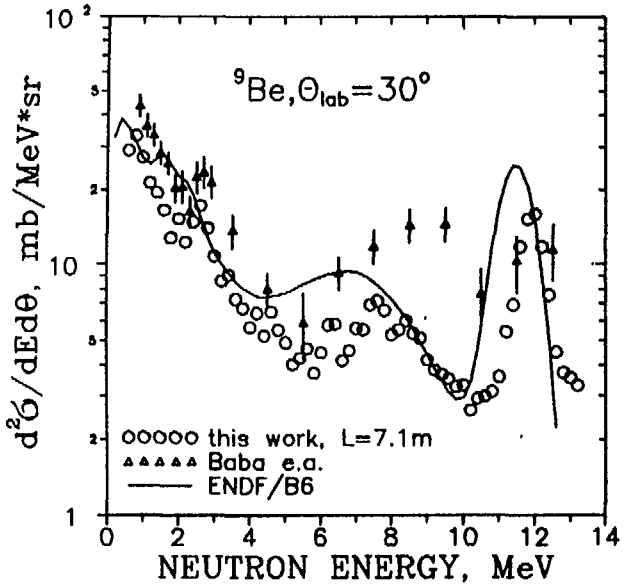


Fig.5a. Cross-section for Be at 30°.

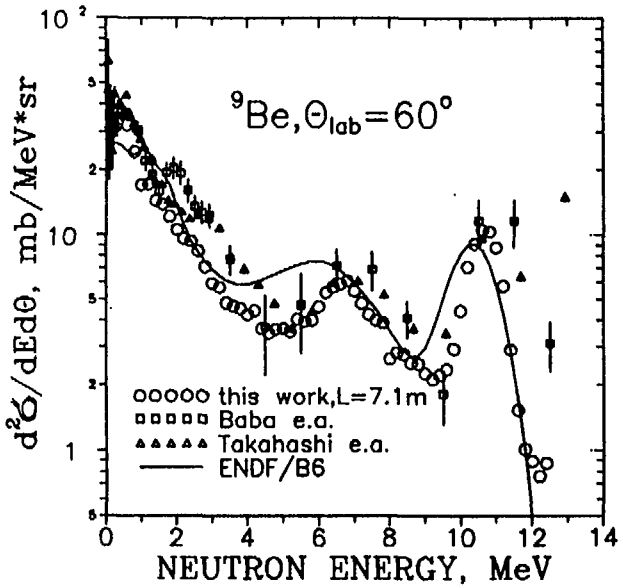


Fig.5b. Cross-section for Be at 60°.

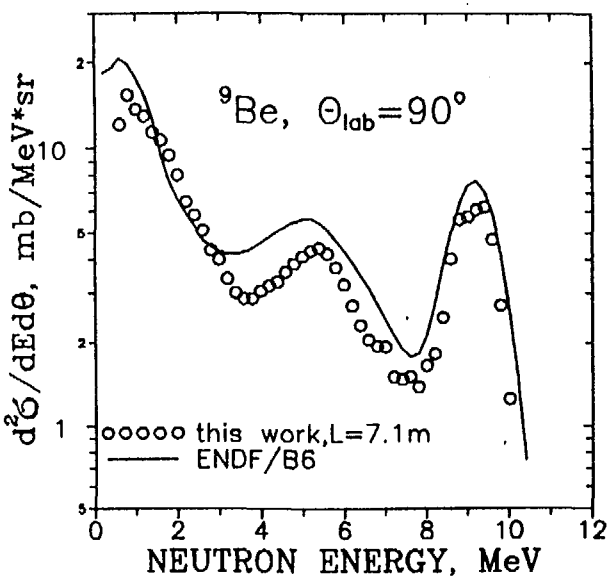


Fig.5c. Cross-section for Be at 90°.

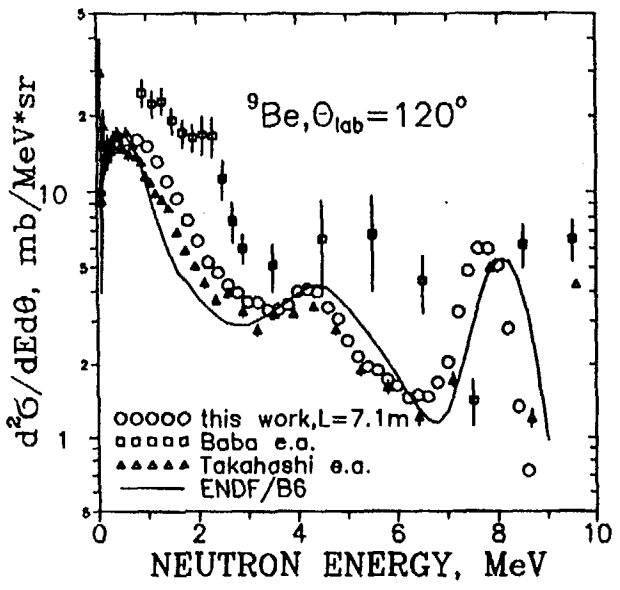


Fig.5d. Cross-section for Be at 120°.

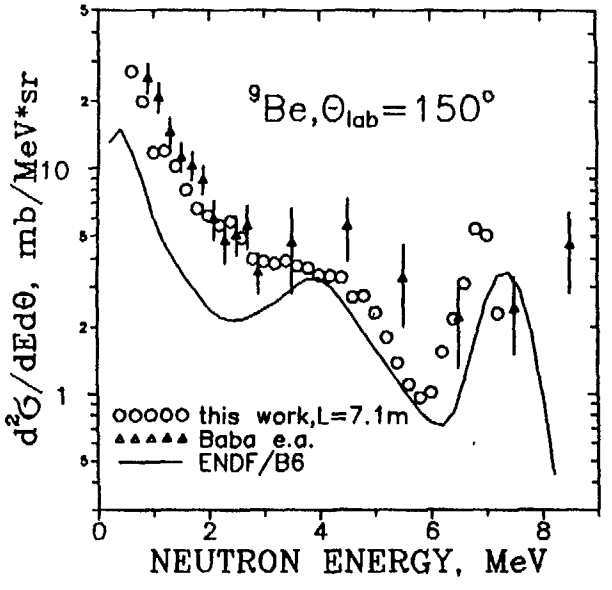


Fig.5e. Cross-section for Be at 150°.

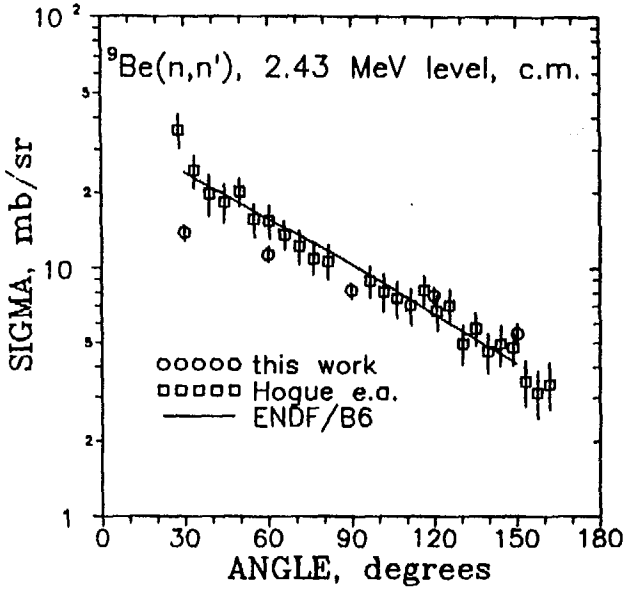


Fig.6. Cross-section of $^9Be(n,n')^9Be^*(2.43MeV)$.

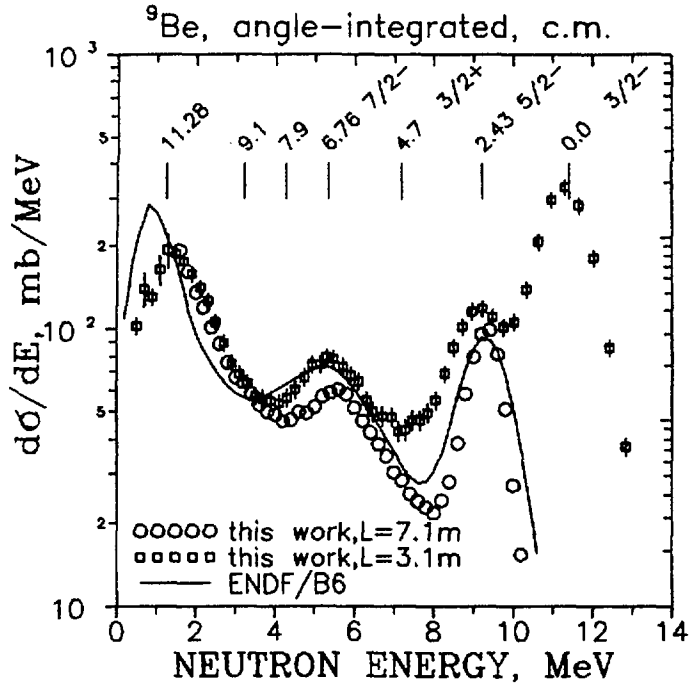


Fig.7. Angle-integrated neutron emission cross-section. The arrows indicate the level scheme for $^{9}$Be residual nucleus.

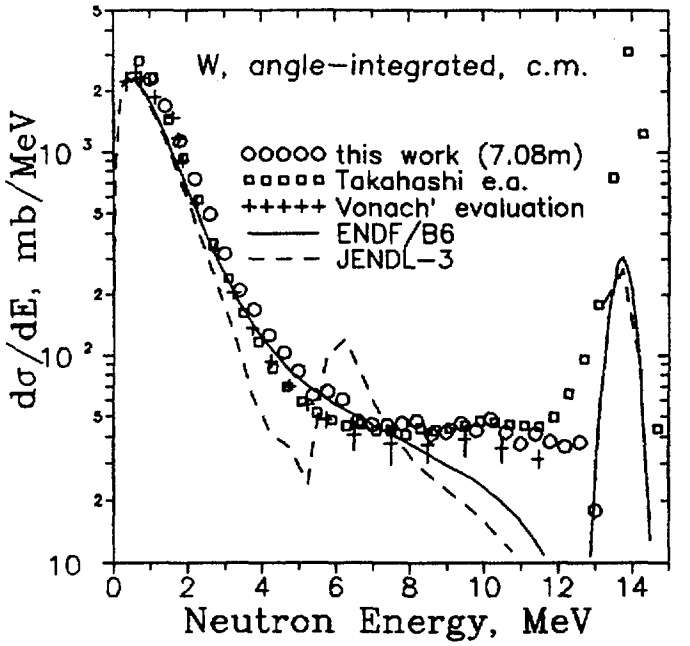


Fig.8. Angle-integrated neutron emission cross-section for W.

flight path increase the energy resolution of the spectrometer. This results in to the better separation of the neutron groups, corresponding the excitation of $^{9}$Be levels.

Tungsten. In fig.8 our experimental results are compared with A.Takahashi e.a. experimental [10] and A.Pavlik and H.Vonach compilation [11] data. The agreement is rather good.

The experimental data are compared with ENDF/B6 and JENDL-3 evaluated data as well. It is seen that both files underestimate the emission spectra in 8-13 MeV energy interval. The peak near 14MeV corresponds the inelastic scattering with excitation of low lying discrete levels (folded with the energy resolution of the spectrometer). It seems that such evaluation contradicts the energy behavior of high energy part of the spectrum. Besides in the JENDL-3 the conjunction of spectra of neutrons from (n,2n) and (n,n') reactions is not correct. All these files do not take into account the angular anisotropy of the inelastically scattered neutrons, that is rather strong for the high energy part of the spectrum.

REFERENCES.


1. World Request List for Nuclear Data. INDC(SEC)-88/URSF, IAEA, Vienna, 1988
2. В.Б.Ануфриенко и др. Вопросы атомной науки и техники. Сер.Ядерные константы. 1989,вып.5(9), с.34
3. W.Mannhart. Report IAEA-TECDOC-410, Vienna,1987 ,p.158
4. Data Standards for Nuclear Measurements. Report IAEA-TECDOC-227,IAEA, Vienna, 1989
5. R.A.Cecil,B.D.Anderson,R.Madey.Nucl.Instr. and Methods,1979,v.161,p.439
6. Neutron Cross Section. Academic Press, INC, New York,1988,v.2
7. M.Baba,T.Sakase e.a.Repot NETU-27,Tohoku University,1979
8. A.Takahashi,J.Yamamoto e.a. Oktavian Report A-87-01,Osaka,1987
9. H.H.Hoque,P.L.Von Behren e.a. Nucl.Sci.Eng.,1978,v.68,p.38
10. A.Takahashi,Y.Sasaki e.a. Report JAERI-M 89-214,Tokio,1989
11. A.Pavlik and H.Vonach. Physics Data, Karslruhe,1988

# NEUTRON INELASTIC SCATTERING AT 5 - 8.5 MeV FOR $^{59}Co$, $^{89}Y$, $^{93}Nb$, Mo, $^{113}In$, $^{115}In$, $^{181}Ta$ and $^{209}Bi$.

S.P.Simakov, G.N.Lovchikova, V.P.Lunev,
V.G.Pronyaev, N.N.Titarenko, A.M.Trufanov

Institute of Physics and Power Engineering,
Obninsk, Rusian Federation

ABSTRACT

The brief review of neutron inelastic scattering double differential cross section measurements and its theoretical analyses for a few construction elements is made. The measurements have been performed by time-of- flight technique at tandem accelerator EGP-10M with the gas tritium target as a neutron source. From theoretical analyses of the experimental data the levels density parameters set and the contribution of the compound and direct reaction mechanisms were deduced. The numerical experimental data and parameters of analyses are listed in tables.

## 1. INTRODUCTION

For incident neutron energies up to binding energy of neutrons in nucleus (6-8 MeV), the dominant reaction channels is (n,n') process. From the analyses of energy and/or angular distributions of secondary neutrons from this reaction the information about reaction mechanism and excited states structure can be deduced. On other hand the Double Differential cross Sections (DDCS) are needed for applied purposes with relatively high accuracy of 10-20% [1].

The main goal of present work is to collect in one report the main experimental and theoretical analyses results, that was published early in a few journals [2], that sometimes not easy to

## 2. Experiment

The measurements have been performed at time-of-flight fast neutron spectrometer [3] of IPPE. The experimental set up is shown in fig.1.

The monoenergetic neutrons were produced by gas tritium target bombarded by pulsed proton beam from tandem accelerator EGP-10M. The target arrangement is shown in fig.2. The gaseous tritium filled up to 2 atm the stainless steel cell (Ø1x4cm), that was separated from vacuum system of accelerator by two $^{58}Ni$ foils (8mg/cm$^2$). The foils were cooled by helium circulated between them.

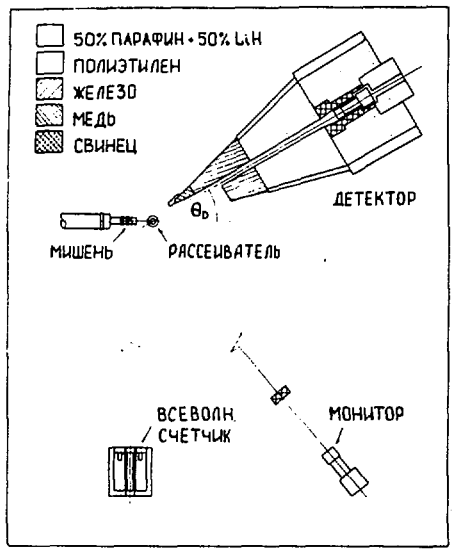


Fig.1. The lay-out of the fast neutron spectrometer

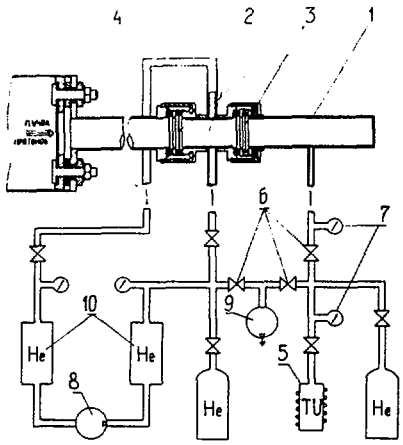


Fig.2. The lay-out of the gas tritium target:
1 - tritium cell,
2 - cooling cell,
3 - $^{58}Ni$ foils,
4 - $^{58}Ni$ sector diaphragm
5 - Uran absorber
6 - valves
7 - pressur indicator
8 - He compressor
9 - vacuum pump
10- He volumes

The parameters of gas target as the neutron source are listed in the table 1 (details see in [4]). It is seen that gas tritium is rather intensive and monoenergetic neutron source suitable for fast neutron spectrometry.

Table 1. Parameters of gas tritium target as a neutron source.

| N | Parameter | Values | | | |
|---|---|---|---|---|---|
| 1 | Neutron energy along the beam axis, MeV | 5 | 6 | 7 | 8 |
| 2 | Neutron yield, $10^8$ n/(s sr μA) | 1.3 | 1 | 0.8 | 0.7 |
| 3 | Proton energy, MeV | 6.5 | 7.4 | 8.4 | 9.3 |
| 4 | Proton angle spread, degrees | 3.5 | 3.0 | 2.7 | 2.4 |
| 5 | Neutron energy resolution, MeV | 0.07 | 0.06 | 0.05 | 0.05 |
| 6 | Non T(p,n) reaction neutron yield, % | 0.03 | 0.08 | 0.30 | 1 |

During the measurements the sample under investigation was installed along the proton beam axis at 15cm distance from the target. The parameters of the samples are listed in the table 2.

Table 2. Parameters of the samples.

| N | Nucleus | Purity, % | Diameter, cm | | Height, cm | Mass, g |
|---|---|---|---|---|---|---|
| | | | outer | inner | | |
| 1 | $^{59}Co$ | 99.8 | 4.00 | 3.01 | 5.14 | 244.4 |
| 2 | $^{89}Y$ | 99.8 | 4.49 | 3.02 | 4.40 | 172.8 |
| 3 | $^{93}Nb$ | 99.8 | 4.50 | 3.00 | 4.52 | 298.3 |
| 4 | Mo | 99.7 | 3.10 | 1.60 | 5.00 | 282.1 |
| 5 | $^{113}In$ | 99.9 | 2.39 | 1.4 | 3.95 | 82.9 |
| 6 | $^{115}In$ | 99.9 | 3.00 | 1.4 | 4.52 | 182.8 |
| 7 | $^{181}Ta$ | 99.5 | 3.40 | 2.40 | 5.00 | 373.2 |
| 8 | $^{209}Bi$ | 99.8 | 4.49 | 3.01 | 5.00 | 429.1 |

The hollow cylinder form and relative thin walls result in the low value of correction (about 15%) for attenuation and multiple scattering in the sample.

The neutrons scattered by the sample were registered by the scintillation detector consisted of the stilbene crystal (Ø6.3x4 cm) and photo multiplier ФЭУ-30. The detector was installed in the massive shield of paraffin and metals that can be rotated around the sample. The spectrometer flight pass was 2m, the overall time resolution - 3.5 ns.

The data processing consists the next procedures:

- summation of the spectra and subtraction of the background (sample out of beam);
- transformation of time-of-flight spectrum to energy one;
- correction for neutron detector efficiency, the latter was measured by the time-of-flight spectrometry of $^{252}Cf$ fission neutrons and polyethylene scattered neutrons;
- elastic peak separation from the total emission spectra. For this purpose the target neutron spectrum (measured by detector at $0^{0}$) was fitted to the upper part of elastic peak;
- correction for flux attenuation and multiple scattering of neutrons in the samples.

The estimated total experimental errors include the next factors: statistical uncertainties (3 - 20%); detector efficiency calibration (4%); absolute normalization of DDCS (3%) and correction for the multiple scattering (3%).

Double differential cross-section can be found in the EXFOR library: EXFOR number 40519 - Mo, In; 40530 - Co; 40603 - Ta, Bi; 40623 - Nb; 40627 - Y. The angle-integrated differential cross-sections in laboratory system are listed in table 3.

Table 3. Angle-integrated neutron inelastic cross-section and absolute errors [mb/MeV] in laboratory system.

| E, MeV | Cobalt-59 | | | | Yttrium-89 | | | |
|---|---|---|---|---|---|---|---|---|
| | 4.99 | 5.97 | 7.00 | 8.09 | 4.86 | 6.08 | 7.02 | 7.94 |
| .6 | 599±10 | 635±63 | 524±52 | 435±44 | 903±57 | 891±53 | 1041±62 | 967±61 |
| .8 | 683±68 | 598±60 | 575±57 | 463±46 | 969±59 | 968±58 | 934±56 | 843±52 |
| 1.0 | 758±76 | 696±70 | 568±57 | 445±44 | 726±44 | 871±52 | 842±51 | 724±44 |
| 1.2 | 600±60 | 614±61 | 580±58 | 420±42 | 729±44 | 727±44 | 736±44 | 625±38 |
| 1.4 | 469±47 | 511±51 | 530±53 | 389±39 | 552±34 | 595±36 | 649±39 | 563±35 |
| 1.6 | 520±52 | 429±43 | 469±47 | 373±37 | 662±40 | 409±25 | 566±34 | 505±31 |
| 1.8 | 480±48 | 402±40 | 386±39 | 338±34 | 541±33 | 378±23 | 513±31 | 438±27 |
| 2.0 | 332±33 | 404±40 | 378±38 | 324±32 | 325±20 | 314±19 | 423±25 | 374±23 |
| 2.2 | 271±27 | 327±33 | 358±36 | 305±31 | 317±20 | 304±18 | 371±22 | 317±20 |
| 2.4 | 251±25 | 279±28 | 287±29 | 276±28 | 201±13 | 270±16 | 315±19 | 283±18 |
| 2.6 | 276±28 | 281±28 | 244±24 | 230±23 | 166±11 | 210±13 | 237±14 | 264±17 |
| 2.8 | 195±20 | 242±24 | 236±24 | 194±19 | 176±12 | 243±15 | 201±12 | 223±15 |
| 3.0 | 136±14 | 172±17 | 225±23 | 194±19 | 359±22 | 198±12 | 171±10 | 190±13 |
| 3.2 | 203±20 | 141±14 | 179±18 | 176±18 | 293±18 | 160±10 | 155± 9 | 166±12 |
| 3.4 | 263±26 | 140±14 | 159±16 | 149±15 | 128± 9 | 140± 8 | 127± 8 | 140±10 |
| 3.6 | 232±23 | 135±14 | 150±15 | 133±13 | 94± 8 | 103± 6 | 112± 7 | 116±10 |
| 3.8 | 132±13 | 108±11 | 126±13 | 128±13 | 144±11 | 75± 4 | 121± 7 | 93± 8 |
| 4.0 | 53± 5 | 98±10 | 93± 9 | 123±12 | 103± 9 | 89± 5 | 127± 8 | 84± 8 |
| 4.2 | 45± 5 | 129±13 | 80± 8 | 103±10 | | 113± 7 | 110± 7 | 73± 7 |
| 4.4 | | 161±16 | 74± 7 | 88± 9 | | 103± 6 | 96± 6 | 66± 6 |
| 4.6 | | 148±15 | 75± 8 | 81± 8 | | 87± 5 | 78± 5 | 55± 6 |
| 4.8 | | 98±10 | 66± 7 | 73± 7 | | 95± 6 | 65± 4 | 66± 6 |
| 5.0 | | | 72± 7 | 58± 6 | | 115± 7 | 65± 4 | 70± 6 |
| 5.2 | | | 94± 9 | 53± 5 | | 100± 6 | 74± 4 | 67± 6 |
| 5.4 | | | 107±11 | 51± 5 | | 66± 4 | 78± 5 | 63± 6 |
| 5.6 | | | 102±10 | 51± 5 | | | 75± 4 | 58± 6 |
| 5.8 | | | 70± 7 | 55± 6 | | | 76± 5 | 48± 5 |
| 6.0 | | | 31± 3 | 66± 7 | | | 71± 4 | 51± 5 |
| 6.2 | | | | 87± 9 | | | 56± 3 | 55± 5 |
| 6.4 | | | | 102±10 | | | 18± 1 | 56± 5 |
| 6.6 | | | | 108±11 | | | | 58± 6 |
| 6.8 | | | | 102±10 | | | | 72± 6 |
| 7.0 | | | | 95± 9 | | | | 76± 7 |

Table 3. (continued).

| E, MeV | Niobium-93 | | | | Molibdenum | | | |
|---|---|---|---|---|---|---|---|---|
| | 5.23 | 6.22 | 7.23 | 8.01 | 4.91 | 5.98 | 6.98 | 8.01 |
| .6 | 1239±76 | 1082±66 | 1009±64 | 876±54 | 1309±79 | 1187±72 | 1220±75 | 1048±64 |
| .8 | 1127±68 | 1019±62 | 897±54 | 816±49 | 1153±70 | 1061±64 | 1034±62 | 890±54 |
| 1.0 | 984±59 | 920±56 | 796±48 | 689±42 | 940±57 | 932±56 | 909±55 | 744±45 |
| 1.2 | 837±51 | 835±50 | 742±45 | 623±38 | 751±45 | 828±50 | 799±48 | 654±40 |
| 1.4 | 712±43 | 684±41 | 696±42 | 567±34 | 632±38 | 701±42 | 685±41 | 583±35 |
| 1.6 | 584±35 | 591±36 | 570±35 | 509±31 | 517±31 | 591±36 | 573±35 | 505±31 |
| 1.8 | 532±32 | 497±30 | 492±30 | 448±27 | 486±29 | 491±30 | 483±29 | 430±26 |
| 2.0 | 511±31 | 437±27 | 432±26 | 392±24 | 368±22 | 406±25 | 402±24 | 360±22 |
| 2.2 | 417±25 | 386±24 | 359±22 | 344±21 | 304±19 | 330±20 | 354±22 | 310±19 |
| 2.4 | 308±19 | 326±20 | 312±19 | 296±18 | 255±16 | 275±17 | 295±18 | 259±16 |
| 2.6 | 228±14 | 276±17 | 276±17 | 256±16 | 197±12 | 230±14 | 246±15 | 218±14 |
| 2.8 | 217±13 | 246±15 | 234±15 | 219±14 | 150±10 | 212±13 | 205±13 | 189±12 |
| 3.0 | 224±14 | 233±15 | 204±13 | 185±12 | 113± 7 | 177±11 | 168±11 | 160±10 |
| 3.2 | 178±11 | 194±12 | 179±12 | 160±10 | 128± 8 | 151± 9 | 140± 9 | 140± 9 |
| 3.4 | 144±10 | 147±10 | 153±10 | 129± 9 | 108± 7 | 141± 9 | 121± 8 | 119± 8 |
| 3.6 | 135± 9 | 126± 9 | 133± 9 | 113± 7 | 83± 6 | 124± 8 | 112± 7 | 100± 7 |
| 3.8 | 146±10 | 131± 9 | 125± 9 | 101± 7 | 117± 8 | 103± 7 | 109± 8 | 86± 6 |
| 4.0 | 171±11 | 127± 9 | 119± 8 | 93± 6 | 153±10 | 83± 6 | 95± 7 | 74± 5 |

Table 3. (continued).

| E, MeV | Niobium-93 | | | | Molibdenum | | | |
|---|---|---|---|---|---|---|---|---|
| | 5.23 | 6.22 | 7.23 | 8.01 | 4.91 | 5.98 | 6.98 | 8.01 |
| 4.2 | 186±12 | 110± 7 | 102± 7 | 79± 5 | | 77± 5 | 89± 6 | 61± 5 |
| 4.4 | 152±27 | 102± 7 | 92± 6 | 72± 5 | | 74± 6 | 94± 7 | 56± 4 |
| 4.6 | 82±33 | 104± 7 | 90± 6 | 71± 5 | | 76± 6 | 91± 6 | 57± 4 |
| 4.8 | | 125± 9 | 90± 6 | 67± 5 | | 94± 8 | 83± 6 | 57± 4 |
| 5.0 | | 141±12 | 85± 6 | 67± 5 | | 108±10 | 73± 5 | 65± 5 |
| 5.2 | | | 80± 6 | 65± 5 | | 98±11 | 67± 5 | 64± 5 |
| 5.4 | | | 80± 6 | 64± 4 | | | 68± 5 | 66± 5 |
| 5.6 | | | 75± 7 | 72± 5 | | | 80± 6 | 70± 5 |
| 5.8 | | | 86±11 | 75± 5 | | | 104± 7 | 69± 5 |
| 6.0 | | | 90±19 | 75± 5 | | | 112± 8 | 65± 5 |
| 6.2 | | | 93±23 | 66± 5 | | | 85± 7 | 57± 5 |
| 6.4 | | | 90±30 | 77± 5 | | | | 57± 5 |
| 6.6 | | | | 85± 6 | | | | 65± 5 |
| 6.8 | | | | 92± 6 | | | | 72± 6 |
| 7.0 | | | | 96± 6 | | | | 77± 7 |
| 7.2 | | | | 80± 6 | | | | 63± 6 |

Table 3. (continued).

| E, MeV | Indium-113 | | | | Indium-115 | | | |
|---|---|---|---|---|---|---|---|---|
| | 5.34 | 6.47 | 7.49 | 8.53 | 5.19 | 6.47 | 7.49 | 8.53 |
| .6 | 1639±164 | 1414±141 | 1283±128 | 1120±112 | 1639±164 | 1547±139 | 1197±108 | 1081±97 |
| .8 | 1443±144 | 1242±124 | 1150±115 | 1040±104 | 1664±150 | 1348±121 | 1024± 92 | 982±88 |
| 1.0 | 1230±123 | 1066±107 | 1016±102 | 925± 93 | 1487±134 | 1198±108 | 912± 82 | 873±79 |
| 1.2 | 961± 96 | 921± 92 | 899± 90 | 815± 82 | 1255±113 | 1034± 93 | 818± 74 | 775±70 |
| 1.4 | 762± 76 | 751± 75 | 806± 81 | 708± 71 | 972± 87 | 841± 76 | 710± 64 | 677±61 |
| 1.6 | 590± 59 | 613± 61 | 661± 66 | 607± 61 | 767± 69 | 675± 61 | 607± 55 | 578±52 |
| 1.8 | 464± 46 | 491± 49 | 533± 53 | 496± 50 | 595± 54 | 537± 48 | 483± 43 | 472±42 |
| 2.0 | 362± 36 | 373± 37 | 432± 43 | 423± 42 | 448± 40 | 434± 39 | 404± 36 | 383±34 |
| 2.2 | 265± 27 | 303± 30 | 354± 35 | 344± 34 | 338± 30 | 336± 30 | 333± 30 | 314±28 |
| 2.4 | 192± 19 | 234± 23 | 286± 29 | 296± 30 | 249± 22 | 268± 24 | 256± 23 | 266±24 |
| 2.6 | 156± 16 | 192± 19 | 231± 23 | 233± 23 | 184± 17 | 206± 19 | 204± 18 | 218±20 |
| 2.8 | 156± 16 | 155± 15 | 189± 19 | 189± 19 | 166± 15 | 167± 15 | 175± 16 | 183±17 |
| 3.0 | 139± 14 | 129± 13 | 147± 15 | 152± 15 | 158± 14 | 134± 12 | 144± 13 | 152±14 |
| 3.2 | 105± 11 | 108± 11 | 120± 12 | 139± 14 | 128± 11 | 113± 10 | 118± 11 | 130±12 |
| 3.4 | 80± 8 | 85± 8 | 103± 10 | 122± 12 | 79± 7 | 97± 9 | 95± 9 | 110±10 |
| 3.6 | 91± 9 | 82± 8 | 90± 9 | 108± 11 | 63± 6 | 90± 8 | 88± 8 | 90± 8 |
| 3.8 | 106± 11 | 89± 9 | 77± 8 | 86± 9 | 92± 8 | 102± 9 | 78± 7 | 77± 7 |
| 4.0 | 132± 13 | 90± 9 | 78± 8 | 74± 7 | 137± 12 | 104± 9 | 68± 6 | 65± 6 |
| 4.2 | 111± 11 | 79± 8 | 70± 7 | 68± 7 | 145± 13 | 89± 8 | 63± 6 | 55± 5 |
| 4.4 | 97± 10 | 57± 6 | 63± 6 | 53± 5 | 85± 8 | 67± 6 | 63± 6 | 54± 5 |
| 4.6 | 90± 9 | 58± 6 | 66± 7 | 54± 5 | 56± 5 | 54± 5 | 70± 6 | 45± 4 |
| 4.8 | | 72± 7 | 76± 8 | 45± 4 | 91± 8 | 68± 6 | 81± 7 | 44± 4 |
| 5.0 | | 103± 10 | 89± 9 | 50± 5 | | 101± 9 | 84± 8 | 45± 4 |
| 5.2 | | 97± 10 | 86± 9 | 56± 6 | | 115± 10 | 78± 7 | 50± 4 |
| 5.4 | | 80± 8 | 74± 7 | 54± 5 | | 107 10 | 71± 6 | 46± 4 |
| 5.6 | | 75± 7 | 70± 7 | 51± 5 | | 98 9 | 71± 6 | 54± 5 |
| 5.8 | | 95± 9 | 76± 8 | 65± 7 | | 116 10 | 82± 7 | 62± 6 |
| 6.0 | | | 99± 10 | 84± 8 | | | 109± 10 | 79± 7 |
| 6.2 | | | 108± 11 | 77± 8 | | | 118± 11 | 81± 7 |
| 6.4 | | | 90± 9 | 74± 7 | | | 98± 9 | 66± 6 |
| 6.6 | | | 54± 5 | 83± 8 | | | 85± 8 | 67± 6 |
| 6.8 | | | | 79± 8 | | | | 79± 7 |
| 7.0 | | | | 89± 9 | | | | 90± 8 |
| 7.2 | | | | 104± 10 | | | | 101± 9 |
| 7.4 | | | | 115± 12 | | | | 110±10 |
| 7.6 | | | | 120± 12 | | | | 110±10 |

Table 3. (continued).

| E, MeV | Tantalum-181 | | | | Bismuth-209 | | | |
|---|---|---|---|---|---|---|---|---|
| | 5.19 | 6.47 | 7.45 | 7.94 | 4.99 | 5.97 | 7.00 | 8.09 |
| .6 | 2059±124 | 1549±94 | 1785±108 | 1519±93 | 1791±109 | 1151±72 | 782±51 | 860±55 |
| .8 | 1875±113 | 1494±90 | 1544± 93 | 1357±82 | 2039±123 | 1267±77 | 893±55 | 853±52 |
| 1.0 | 1570± 95 | 1320±80 | 1364± 82 | 1182±72 | 1806±109 | 1338±81 | 952±58 | 835±51 |
| 1.2 | 1245± 75 | 1134±69 | 1186± 72 | 1009±61 | 1151± 69 | 1179±71 | 1041±63 | 829±50 |
| 1.4 | 971± 59 | 901±55 | 999± 60 | 856±52 | 854± 52 | 975±59 | 970±59 | 780±47 |
| 1.6 | 736± 44 | 699±42 | 814± 49 | 696±42 | 766± 46 | 1188±72 | 991±60 | 728±44 |
| 1.8 | 548± 33 | 550±34 | 640± 39 | 546±34 | 752± 46 | 1157±70 | 920±56 | 641±39 |
| 2.0 | 416± 25 | 418±26 | 513± 31 | 453±28 | 403± 25 | 872±53 | 845±51 | 649±39 |
| 2.2 | 315± 19 | 337±21 | 407± 25 | 360±22 | 678± 41 | 561±34 | 723±44 | 610±37 |
| 2.4 | 237± 15 | 265±17 | 310± 19 | 294±19 | 522± 32 | 392±24 | 624±38 | 527±32 |
| 2.6 | 177± 11 | 206±13 | 251± 16 | 230±15 | 75± 6 | 326±20 | 627±38 | 458±28 |
| 2.8 | 133± 9 | 161±11 | 207± 13 | 192±13 | 28± 4 | 279±17 | 512±31 | 398±25 |
| 3.0 | 106± 7 | 129± 9 | 172± 11 | 159±11 | 41± 4 | 209±14 | 355±22 | 349±22 |
| 3.2 | 82± 6 | 104± 8 | 145± 10 | 138±10 | 100± 7 | 285±18 | 213±14 | 277±17 |
| 3.4 | 70± 5 | 83± 7 | 125± 9 | 113±10 | 104± 8 | 218±14 | 156±11 | 246±16 |
| 3.6 | 76± 6 | 71± 6 | 109± 8 | 101± 8 | 59± 6 | 61± 7 | 144±10 | 252±17 |
| 3.8 | 87± 7 | 65± 5 | 97± 8 | 89± 8 | 112± 9 | 23± 4 | 130±10 | 227±15 |
| 4.0 | 84± 6 | 55± 5 | 86± 7 | 79± 7 | 177± 12 | 26± 5 | 132±10 | 171±12 |
| 4.2 | 74± 6 | 50± 5 | 71± 6 | 71± 7 | 124 10 | 40± 5 | 169±12 | 114± 9 |
| 4.4 | 111± 8 | 44± 5 | 68± 6 | 70± 7 | | 52± 6 | 136±10 | 82± 7 |
| 4.6 | 204± 14 | 48± 5 | 65± 6 | 58± 6 | | 52± 6 | 54± 6 | 76± 6 |
| 4.8 | | 51± 5 | 59± 5 | 53± 6 | | 60± 6 | 17± 5 | 76± 6 |
| 5.0 | | 62± 5 | 61± 5 | 52± 5 | | 48± 6 | 16± 4 | 84± 7 |
| 5.2 | | 66 6 | 60± 5 | 44± 5 | | 98±11 | 23± 5 | 102± 7 |
| 5.4 | | 76 6 | 65± 5 | 43± 5 | | | 29± 5 | 105± 7 |
| 5.6 | | 101 8 | 69± 5 | 45± 5 | | | 28± 5 | 66± 6 |
| 5.8 | | 134 10 | 75± 6 | 53± 5 | | | 25± 5 | 38± 4 |
| 6.0 | | 142 11 | 84± 6 | 52± 5 | | | 24± 6 | 33± 4 |
| 6.2 | | | 95± 7 | 63± 6 | | | | 43± 5 |
| 6.4 | | | 102± 7 | 65± 6 | | | | 48± 5 |
| 6.6 | | | 112 8 | 70± 6 | | | | 50± 5 |
| 6.8 | | | 96 8 | 81± 7 | | | | 59± 6 |
| 7.0 | | | | 89± 7 | | | | 61± 6 |
| 7.2 | | | | 91± 8 | | | | |

## 3. THEORETICAL ANALYSES

In theoretical interpretation of experimental data we try to use the basic approaches without free (where it was possible) parameters. From this point of view the contribution of the compound and direct processes can be estimated without large ambiguities.

The Hauser-Feshbach model [5] have been used to calculate the statistical part of cross section ( code SMT [6]). These calculations need some parameters:

- Spherical optical model potential (SOMP) for estimation of the neutron transmission coefficients. For the better prediction we used the best "individual" but not "global" SOMP known for given nucleus (see references in Table 3).
- Discrete level parameters up to maximum (as possible) excitation energy (Uc). It was taken from Nuclear Data Sheets.

- For energies grater than Uc, the back-shifted Fermi gas model [7] was used to calculate the energy and spin distribution of excited states:

$$\rho(U,I) = \frac{\sqrt{\pi}}{24}\,\frac{\exp[2\sqrt{a(U-\Delta)}]}{a^{1/4}(U-\Delta)^{\sigma}}\,\frac{(2I+1)}{2\sqrt{2\pi}\sigma^{2}}\,\exp\left[-\frac{(I+1/2)^{2}}{2\sigma^{2}}\right]$$

$$\sigma^{2}(U) = 0.00957\,\eta\,\sqrt{\frac{U-\Delta}{a}}\,r_{o}^{2}\,A^{5/3}$$

where there are three free parameters:

$a$ - level density energy dependence parameter

$\Delta$ - back shift

$\eta = F/F_{rigid}$ - the ratio of inertia moment to equivalent rigid body one

Unfortunately, the systematics of Dilg e.a. [7] or Gilbert and Cameron [8] for parameters $a, \Delta$ and $\eta$ did not reproduce well the experimental spectra. That is why we deduced these parameters from the fit of the Hauser-Feshbach model cross-section, calculated with back-shifted level density function, to the low energy part of DDCS, where the contribution of non-statistical processes is negligible. In the fitting procedure three set of experimental data was used to find three unknown parameters: energy dependence of spectra and low discrete level number ( these data influenced mainly on $a$ and $\Delta$), angular distribution of scattered neutrons ($\eta$).

The result values are listed in tab. 4 and fig.3. It is seen that parameters obtained differ from systematic [7,8]. In fig.4 the dependence of relative moment of inertia $\eta$ versus the excitation energy U is shown. The solid curve is fenomenological superfluid model calculations [15]. The arrows and characters p or n indicate the energies of superfluid-Fermi gas transitions $U_{tr}$ in proton or neutron shells. Above $U_{tr}$ the $\eta$ is energy independent ( Fermi gas

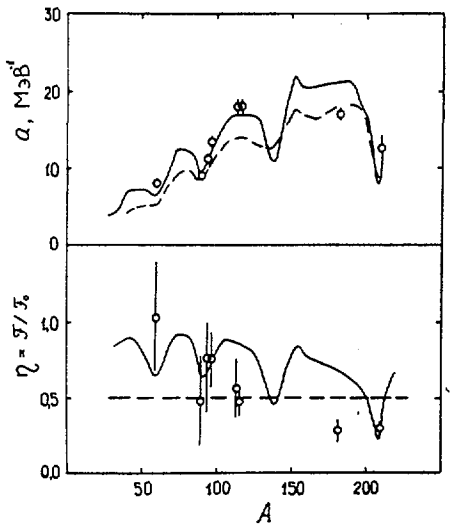


Fig.3. The mass dependence of level density parameters $a$ and relative inertia moment $\eta$. Points - this work, solid curve - systematic of Gilbert and Cameron [8], dashed - Dilg e.a. [7].

Table 4. Parameters for Hauser-Feshbach model

| Nucleus | SOMP | Uc, MeV | $\alpha$, MeV$^{-1}$ | $\Delta$, MeV | $\eta$ |
|---|---|---|---|---|---|
| $^{59}$Co | [9] | 2.8 | 7.9 | 0.6 | 1.02±0.37 |
| $^{89}$Y | [10] | 3.8 | 8.9 | 1.8 | 0.44±0.28 |
| $^{93}$Nb | [10] | 1.7 | 11.2 | -0.2 | 0.51±0.17 |
| Mo | [11] | 1.3 | 13.3 | 0.8 | 0.53±0.12 |
| $^{113}$In | [12] | 1.6 | 17.9 | 0.8 | 0.50±0.17 |
| $^{115}$In | [12] | 1.5 | 18.0 | 0.8 | 0.41±0.09 |
| $^{181}$Ta | [13] | 1.4 | 17.1 | 0.8 | 0.24±0.06 |
| $^{209}$Bi | [14] | 3.3 | 12.7 | 1.6 | 0.29±0.04 |

model prediction). Unfortunately, the experimental uncertainties are too large to conclude whether superfluid or Fermi gas model is more suitable for description of energy dependence of $\eta$.

Strong channel coupling (SCC) method and distorted wave Born approximation (DWBA) we used to calculate the direct reaction cross section. To do these calculations we used the collective vibrational model for the first excited states (phonon with spin $\lambda$) in nucleus. In this approach the form-factor F(r) of inelastic transitions depends on dynamic deformation parameter $\beta_\lambda$ and first derivative from real part of the optical model potential V:

$$F(r) \approx (2\lambda+1) \times \beta_\lambda \times \frac{dV}{dr}$$

For the odd nuclei we used the weak coupling model: it supposed that odd nucleon (hole) does not affect the collective excitation modes of even-even core. The experimental information about parameters U, $\beta$ were taken from analyses of (p,p') reaction cross-sections. For the higher excitation energies the harmonic vibrational model and SCC method were used to evaluate the

Table 5. Comparison of experimental cross-section(mb) with calculated. $\sigma_c$ - compound, $\sigma_{dir}$ - direct scattering, $\sigma_\Sigma = \sigma_c + \sigma_{dir}$.

| Nucl. | E, MeV | experim. $\sigma_{nn'}$ | theory $\sigma_c$ | $\sigma_{dir}$ | $\sigma_\Sigma$ | Nucl. | E, MeV | experim. $\sigma_{nn'}$ | theory $\sigma_c$ | $\sigma_{dir}$ | $\sigma_\Sigma$ |
|---|---|---|---|---|---|---|---|---|---|---|---|
| $^{59}$Co | 4.99 | 1500±100 | 1488 | 64 | 1552 | $^{113}$In | 5.34 | 2420±190 | 2135 | 216 | 2365 |
| | 5.97 | 1530±120 | 1489 | 70 | 1558 | | 6.47 | 2250±180 | 2119 | 226 | 2345 |
| | 7.00 | 1530±120 | 1479 | 75 | 1554 | | 7.49 | 2270±180 | 2088 | 220 | 2308 |
| | 8.09 | 1420±110 | 1459 | 72 | 1531 | | 8.53 | 2250±180 | 2080 | 206 | 2286 |
| $^{89}$Y | 4.86 | 1730±140 | 1884 | 78 | 1962 | $^{115}$In | 5.19 | 2440±200 | 2121 | 228 | 2349 |
| | 6.08 | 1890±150 | 1836 | 87 | 1923 | | 6.47 | 2510±200 | 2103 | 234 | 2337 |
| | 7.02 | 1970±160 | 1843 | 92 | 1935 | | 7.49 | 2090±160 | 2072 | 227 | 2299 |
| | 7.94 | 1870±150 | 1848 | 89 | 1937 | | 8.53 | 2130±170 | 2070 | 211 | 2281 |
| $^{93}$Nb | 5.23 | 2170±170 | 1782 | 269 | 2051 | $^{181}$Ta | 5.19 | 3010±240 | | | |
| | 6.22 | 2130±170 | 1807 | 244 | 2051 | | 6.47 | 2640±210 | | | |
| | 7.23 | 2010±160 | 1830 | 227 | 2057 | | 7.49 | 2890±230 | | | |
| | 8.01 | 1890±130 | 1834 | 218 | 2052 | | 7.94 | 2640±210 | | | |
| Mo | 4.91 | 1940±140 | 1888 | 267 | 2155 | $^{209}$Bi | 4.99 | 3110±250 | 2466 | 112 | 2578 |
| | 5.98 | 2050±140 | 1799 | 254 | 2053 | | 5.97 | 2650±210 | 2502 | 140 | 2642 |
| | 6.98 | 2100±150 | 1777 | 243 | 2020 | | 7.00 | 2510±200 | 2548 | 170 | 2718 |
| | 8.01 | 1950±130 | 1784 | 237 | 2021 | | 8.09 | 2450±200 | 2386 | 163 | 2551 |

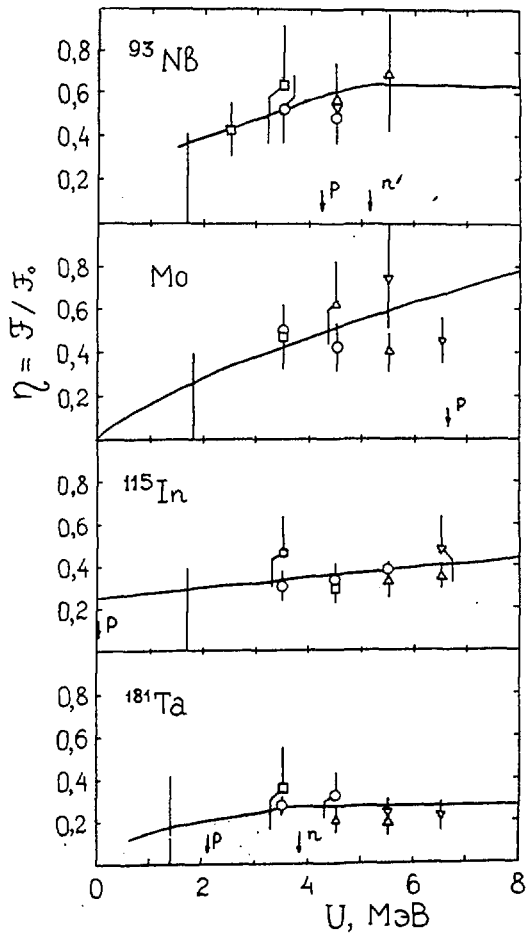


Fig.4. The dependence of $\eta$ versus the excitation energy U. Points - experiment. Solid curve - superfluid model calculation, arrows - $U_{tr}$, vertical line - $U_c$.

contribution of the two phonon states. Of cause, this approach is not valid for deformed nucleus $^{181}$Ta.

The calculated cross-sections are compared with experimental ones in Table 5 and Fig. 5-12. The experimental total (n,n') cross-section was obtained by integrating the double differential cross section and extrapolation under the detector threshold using Hauser-Feshbach model prediction. It is seen in Tabl.5 and Fig.5-11 that models used reproduce the energy and angular distribution of the secondary neutrons as well as the total (n,n') cross-section rather good. Hence we can conclude that compound and direct processes dominates in (n,n') reaction for incident neutron energies and spherical nuclei under interest.

At 8 MeV for Mo and In isotopes the calculation underestimates the experimental DDCS. It is possible that this is caused by models drawbacks and/or absence of information about excited states. The second reason is possible connected with the small contribution of third mechanism, e.g. precompound, doorway etc. Since the it contribution have to increase with increasing of incident neutron energy, it is interesting to analyze the neutron spectra in the more wide energy range.

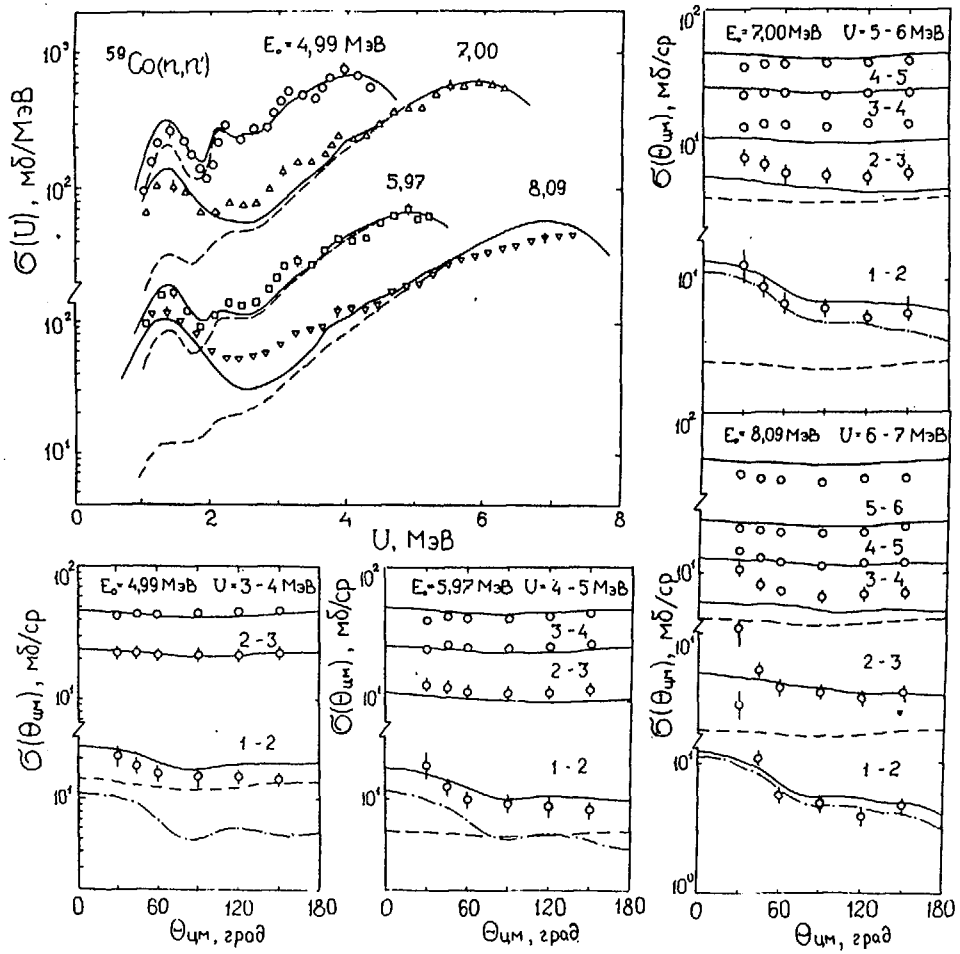


Fig.5. Angle-integrated neutron inelastic scattering for $^{59}Co$ as a function of excitation energy U. Energy integrated DDCS for intervals indicated. Points - experimental data. Dashed curve - compound process, dashed-dotted - direct, solid - its sum.

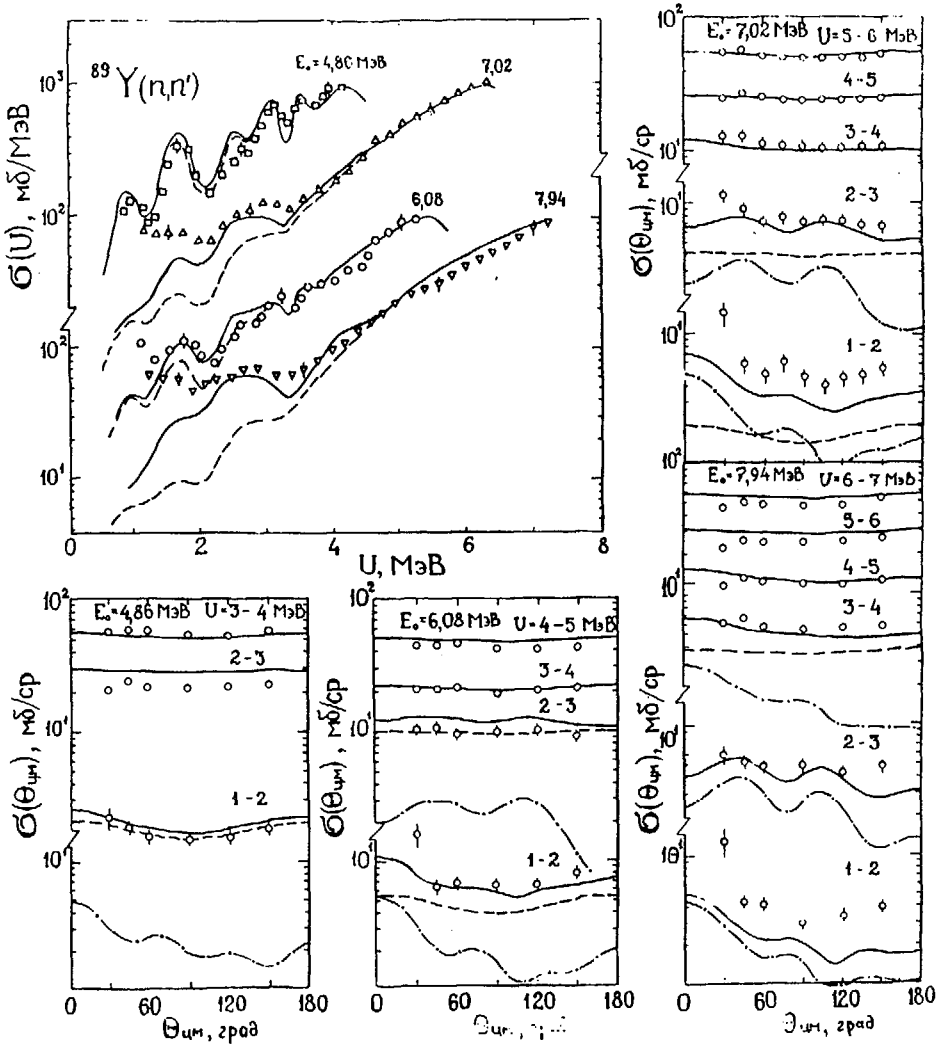


Fig.6. The same as for fig.5, but for $^{89}Y$.

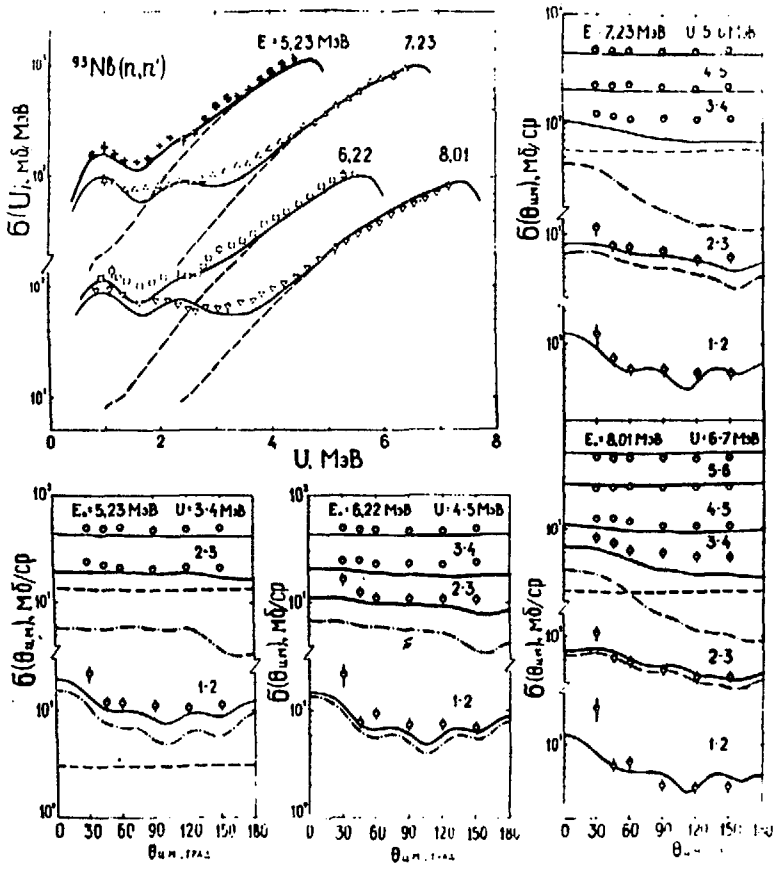


Fig.7. The same as for fig.5, but for $^{93}$Nb.

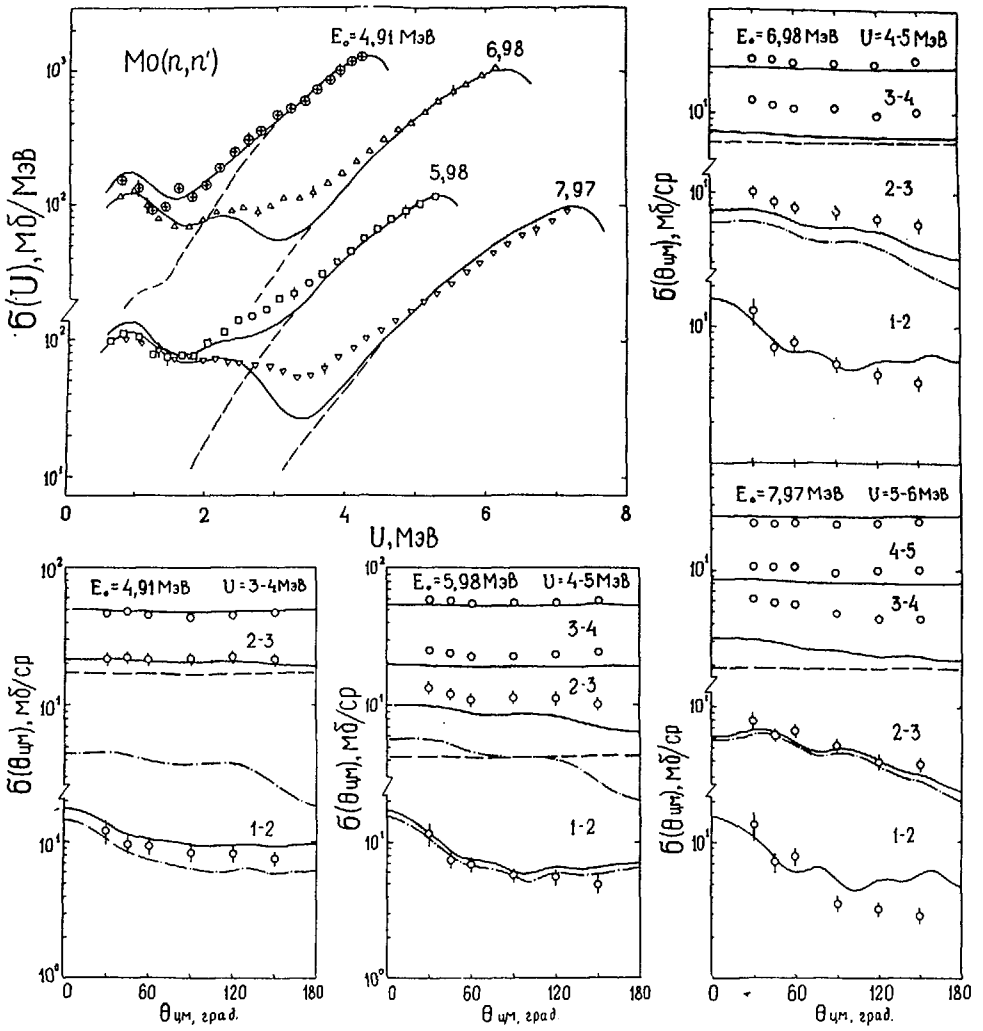


Fig.8. The same as for fig.5, but for Mo.

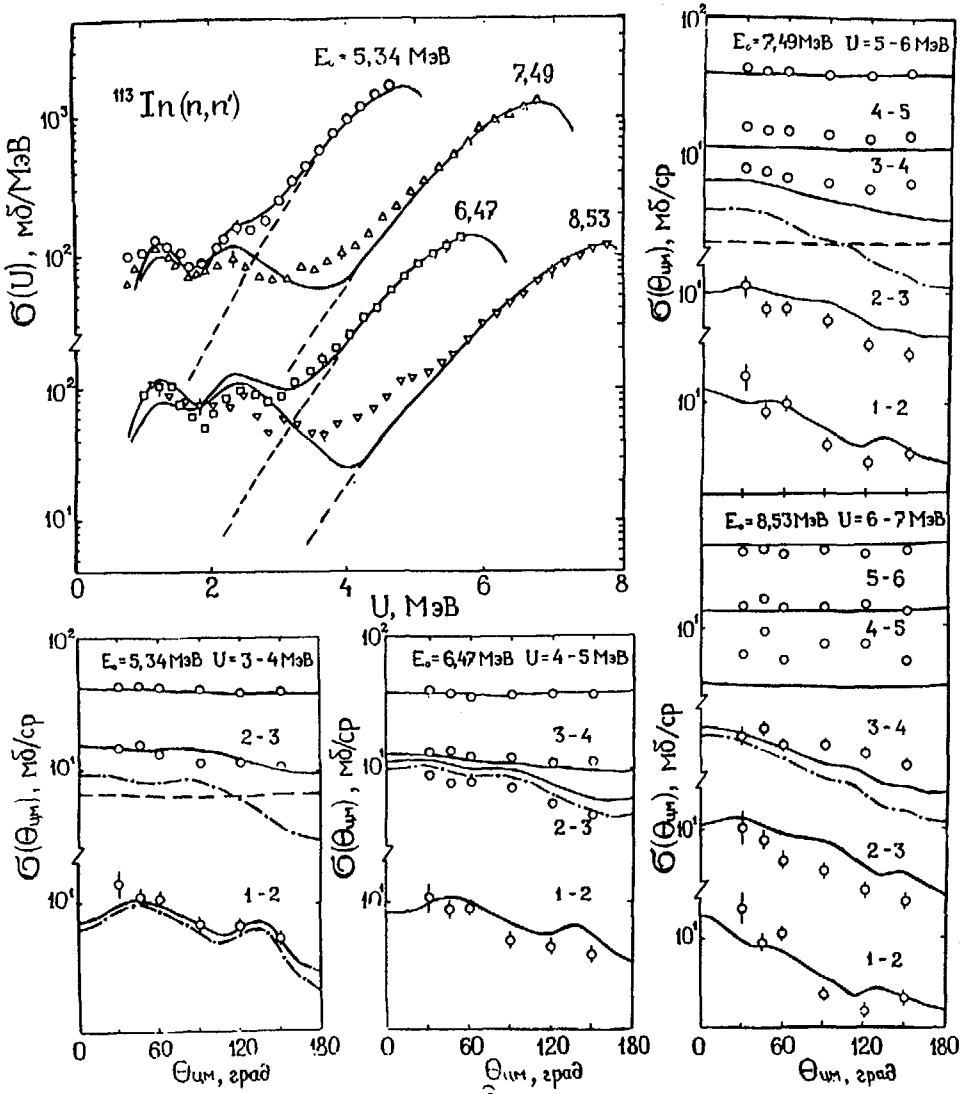


Fig.9. The same as for fig.5, but for $^{113}$In.

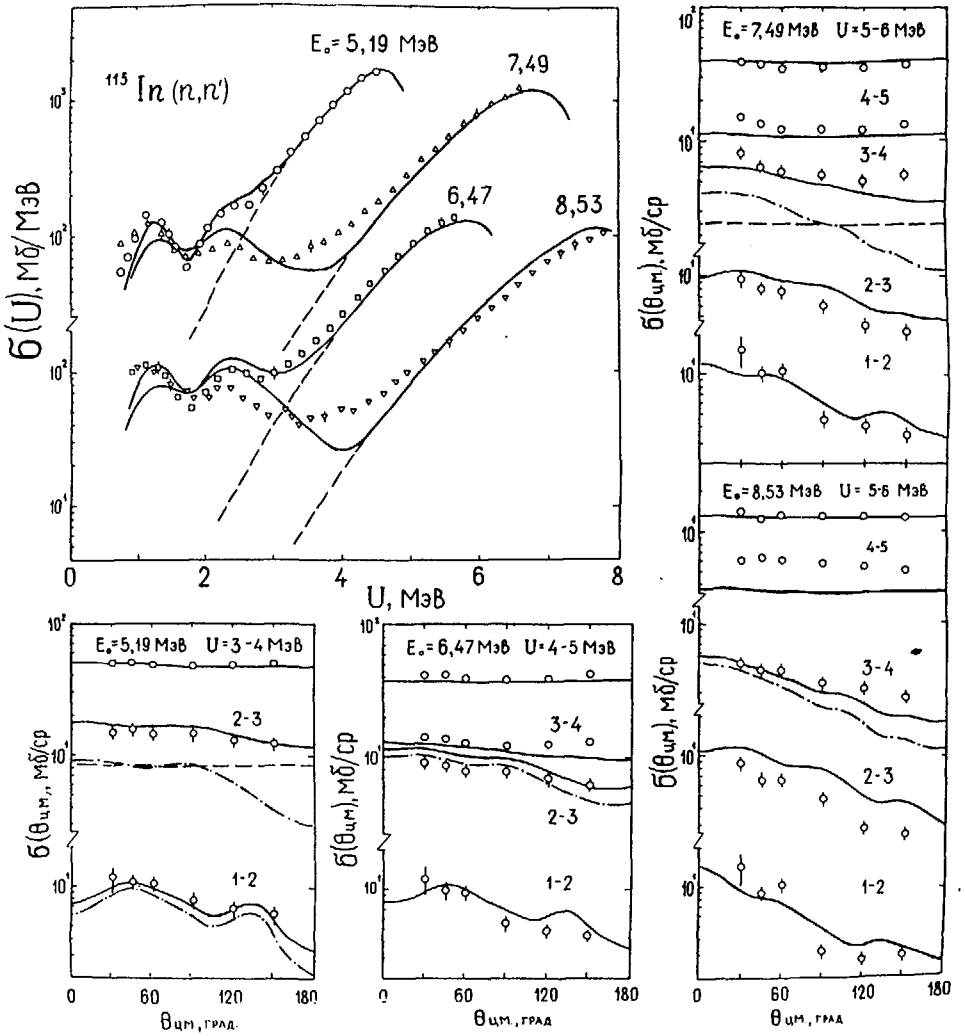


Fig.10. The same as for fig.5, but for $^{115}$In.

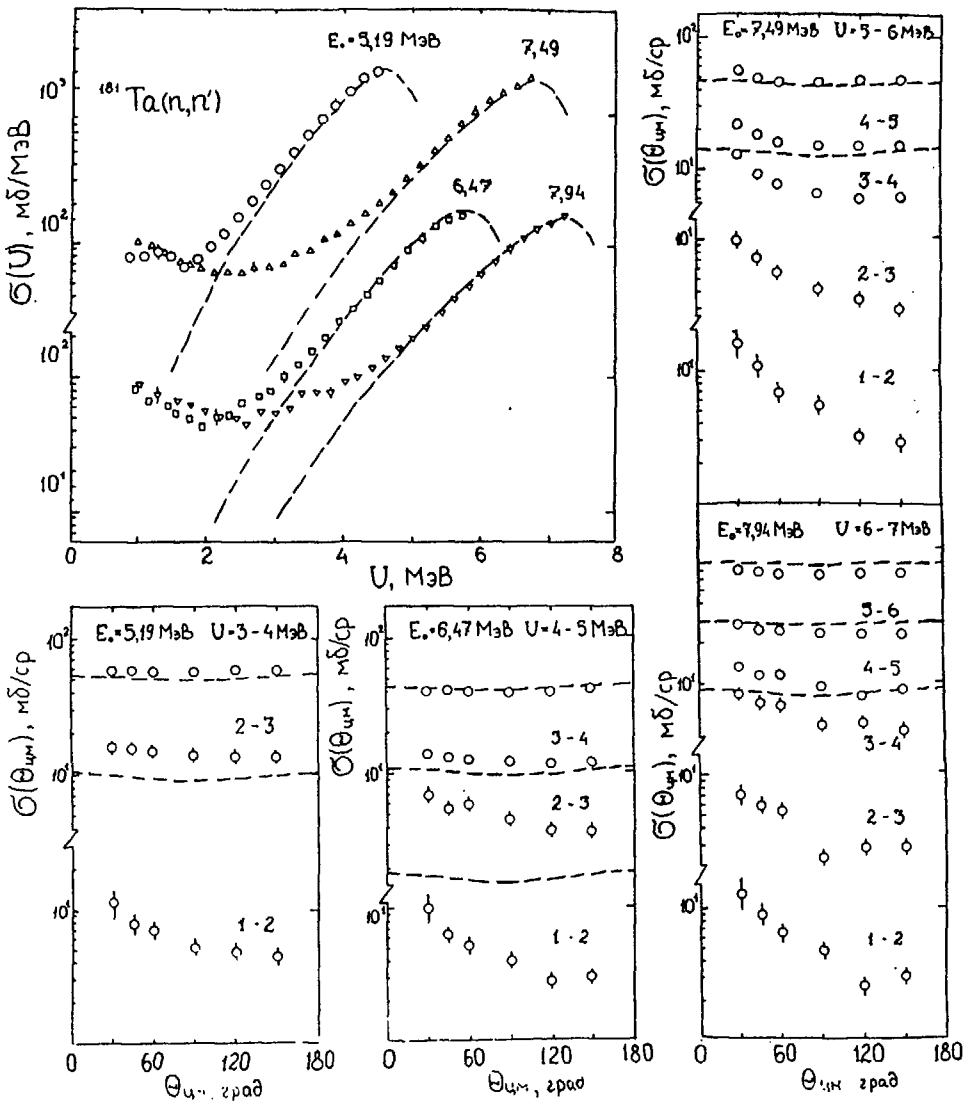


Fig. 11. The same as for fig. 5, but for $^{181}$Ta.

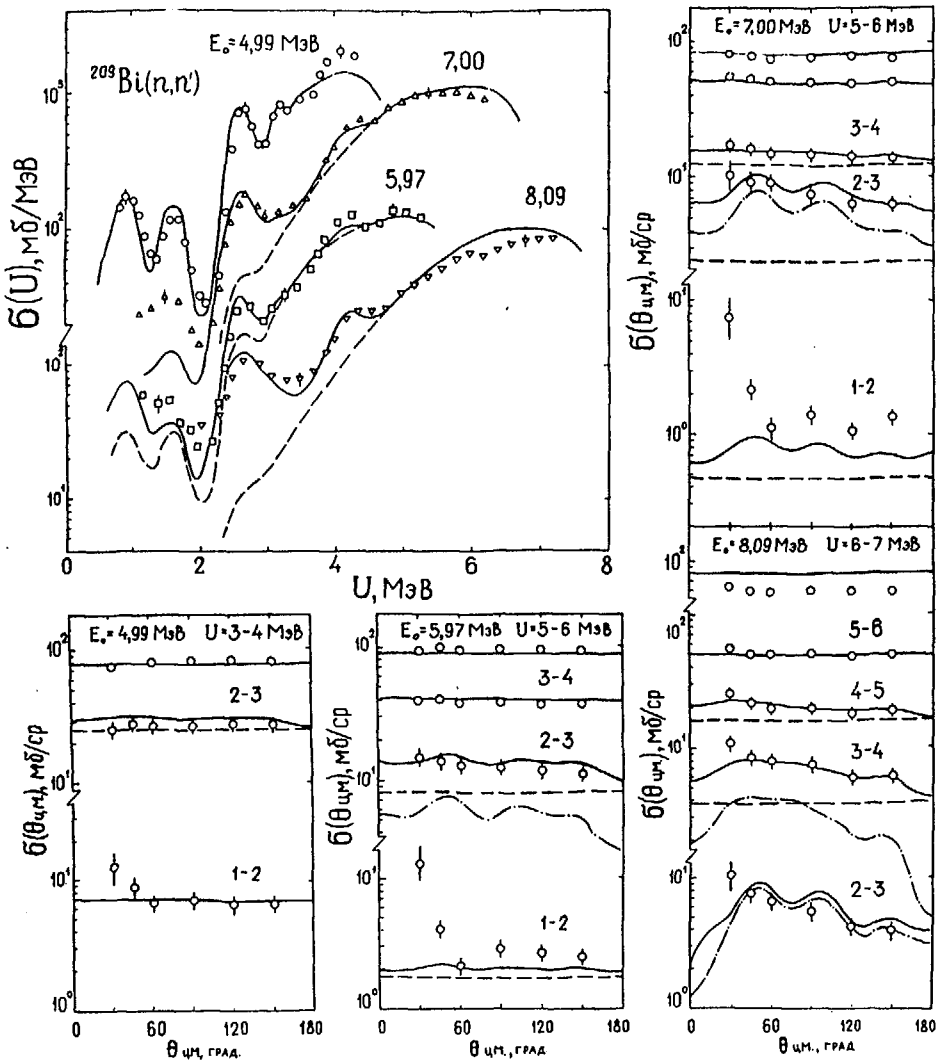


Fig. 12. The same as for fig. 5, but for $^{209}$Bi.

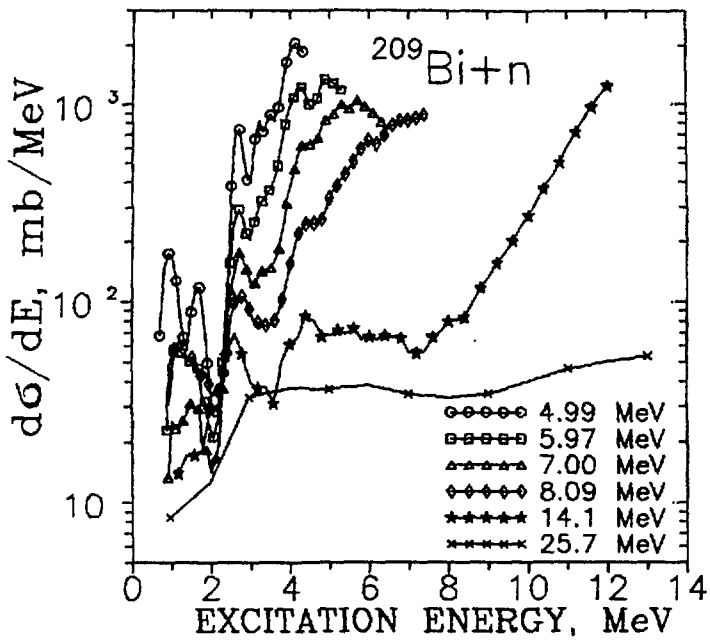


Fig.13. Angle-integrated DDCS versus the excitation energy of residual nucleus $^{209}$Bi. Points - experimental data (references see in the text); curves - eye guided.

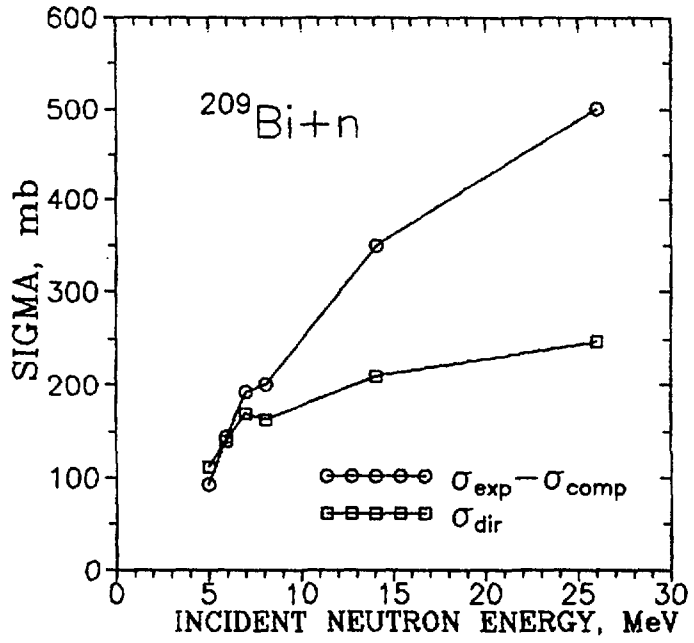


Fig.14. Energy dependence of $\sigma_{noncomp}=\sigma_{exp}-\sigma_{comp}$ and $\sigma_{dir}$ for $^{209}$Bi.

We took $^{209}$Bi for which, besides 5 - 8 MeV data, there are DDCS at 14MeV [16] and 26MeV [17]. In Fig.13 these experimental angle-integrated cross-sections as a function of the residual nucleus excitation energy are shown in the center of mass system. The main tendency with increasing of incident energy is following: shifting of the compound processes to the higher excitation energy

(where the level density is large) and broadening of the non-compound part. In Fig.14 the non-compound part of spectra $\sigma_{noncomp} = (\sigma_{exp} - \sigma_{comp})$ and $\sigma_{dir}$ are shown versus the incident energy. It is seen that the differences between these two values increase. The analyses performed at 26 MeV [18] have shown that it can be eliminated by taking into account the pre-compound decay from closed configuration.

REFERENCES


1. World Request List for Nuclear Data. INDC(SEC)-88/URSF, IAEA, Vienna, 1988
2. С.П.Симаков и др. В сб"Нейтронная физика", Москва, 1984, т.1. с.185 Report ZFK-491, Dresden, 1982, p.206; Ядерная физика, 1983, т.37, с.801; Атомная энергия, 1981, т.51., с.244
3. А.М.Труфанов и др. Приборы и техника эксперимента. 1979, N2, с.50 С.П.Симаков и др. В сб"Нейтронная физика", Москва, 1980, т.1, с.320
4. Н.И.Фетисов и др. Приборы и техника эксперимента. 1980, N4, с.22 G.N.Lovchikova e.a. Report IAEA-TECDOC-410, Vienna 1987, p.296
5. W.Hauser, H.Feshbach. Phys.Rev., 1952, v.87, p.366
6. Н.Н.Титатенко. Препринт ФЭИ-1260, Обнинск, 1982
7. W.Dilg, W.Schantl and H.Vonach. Nucl.Phys., 1983, v.A217, p.269
8. A.Gilbert and A.G.W.Cameron Can.J.Phys., 1965, v.43, p.1446
9. В.М.Бычков и др. В сб"Нейтронная физика", Москва, 1976, т.1, с.160
10. Ch.Lagrange. Ibid, v.3, p.65
11. A.B.Smith, P.Guenther, J.Whalen. Nucl.Phys., 1975, v.A244, p.213
12. J.Rapaport, M.Mirzaa e.a. Nucl.Phys., 1980, v.A341, p.56
13. J.P.Delaroche e.a. Phys.Rev., 1981, v.C23, p.136
14. S.Tanaka. Report JAERI-M5984, 1975, p.212
15. Шубин Ю.Н. и др. Ядерная физика, 1979, т.30, с.1236
16. S.P.Simakov, B.V.Devkin e.a. Report INDC(CCP)-315/L, Vienna, 1990
17. A.Marcinkowski e.a. Nucl.Sci.Eng., 1983, v.83, p.13
18. V.P.Lunev, V.G.Pronyaev, S.P.Simakov. Report FEI-2218, Obninsk, 1991

APPENDIX I

IAEA Research Co-ordination Meeting on
"Measurement and Analysis of 14 MeV Neutron-Induced
Double-Differential Neutron Emission Cross Sections Needed
for Fission and Fusion Reactor Technology"

31 March - 2 April 1992
Fast Neutron Research Facility, Department of Physics,
Faculty of Science, Chiang Mai University
Chiang Mai, Thailand

AGENDA

Tuesday, 31 March

09:00-09:15 1. Opening ceremony by Dean of Faculty of Science

09:15-09:30 Break

09:30-09:45 - Adoption of Agenda

09:15-12.00 2. Progress reports of the CRP participants of experiments

- A. Priller
  "The IRK time-of-flight facility for measurements of double-differential neutron emission cross sections"

- Zhou Zuying
  "Measurements of double-differential neutron emission cross sections for $^{209}Bi(n,n')^{209}Bi$ and $^{238}U(n,n')^{238}U$"

- T. Elfruth
  "Measurement, analysis and evaluation of double differential neutron emission cross sections for $^{238}U$ at 14.1 MeV incident energy

12:00-14:00 Lunch

14:00-15:30 - J. Rahighi

- A. Takahashi
"Double differential neutron emission cross sections at 14 MeV for Li-6, Li-7, Be-9 and other light nuclei"

15:30-15:45 Break

15:45-17:15 - S.P. Simakov
"Measurement of double-differential neutron emission cross section at 14 MeV incident energy for beryllium and tungsten"

"Neutron inelastic scattering at 5-8.5 MeV for Co, V, Mo, Nb, Ni, Ta and Bi"

- T. Vilaithong
"Measurement of double differential neutron emission cross sections for Fe and Ta at 14 MeV"

17:15-18:00 Visit of the Fast Neutron Research Facility of the Chiang Mai University

Wednesday, 1 April

09:00-10:30 - T.Elfruth
"Correction of the influence of finite sample size, target holding and experimental background in time-of-flight DDX-measurements at 14 MeV"

3. Recent Japanese measurements of DDX

- M. Baba
"Double-differential Neutron Emission Cross Sections for 14, 18 MeV and 2-6 MeV Incident Neutrons"

Discussions of technical problems with experiments

10:30-10:45 Break

10:45-12:00 4. Progress reports of the CRP participants of evaluation of DDX

- A. Priller
  "Evaluation of the angle-integrated neutron emission cross sections for Cr, Fe, Ni, Nb, Mo, Ta, W and Bi"

- T. Elfruth
  "Evaluation of double-differential neutron emission cross sections of $^{51}V$ at 14 MeV"

12:00-14:00 Lunch

14:00-14:45 5. Japanese evaluation of DDX

- S. Chiba
  "Evaluation of the double differential cross sections for JENDL fusion file"

14:45-16:30 6. Computer code for nuclear reaction calculation

- T. Elfruth
  "Introduction of the EXIFON program for the DDX calculations"

A demonstration of the computer program

16:30-16:45 Break

16:45-18:00 Discussions of technical problems with evaluations

Thursday, 2 April

| | |
|---|---|
| 09:00-10:30 | 7. Review of the data status and recommendation of the "best" data from this CRP |
| 10:30-10:45 | Break |
| 10:45-12:00 | Discussions of the final reports of the CRP |
| 12:00-14:00 | Lunch |
| 14:00-17:45 | Discussions of conclusions and recommendations |
| 17:45-18:00 | 8. Closing ceremony |

Appendix II

Coordinated Research Programme on "Measurement and Analysis of 14 MeV Neutron-induced Double-differential Neutron Emission Cross Sections needed for Fission and Fusion Reactor Technology"

Third Research Co-ordination Meeting
Chiang Mai, Thailand, 31 March-2 April 1992

## LIST OF PARTICIPANTS

### AUSTRIA

Mr. Alfred Priller
Research Agreement
No. 4880/CF

Institut für Radiumforschung
und Kernphysik
Boltzmanngasse 3
A-1090 Vienna

### CHINA, P.R.

Dr. Zhou Zuying
Research Contract
No. 4881/RB

Institute of Atomic Energy
P.O. Box 275 (3)
Beijing

### GERMANY

Dr. T. Elfruth
Research Agreement
No. 4937/CF

Sektion Physik
Technische Universität
Mommsenstrasse 13
D-O 8027 Dresden

### IRAN

Dr. J. Rahighi
Research Contract
No. 4883/RB

Esfahan Nuclear Technology Centre
Nuclear Engineering Department
P.O. Box 81465/1589
Esfahan

JAPAN

Dr. A. Takahashi
Research Agreement
No. 4884/CF

Dept. of Nuclear Engineering
Faculty of Engineering
Osaka University
2-1 Yamada-Oka, Suita
Osaka 565

Dr. M. Baba (Observer)

Dept. of Nuclear Engineering
Tohoku University
Sendai 980

Dr. S. Chita (Observer)

Nuclear Data Centre
JAERI
Tokai-Mura, Naka-gun
Ibaraki-ken 319

RUSSIAN FEDERATION

Dr. S.P. Simakov

Physical Power Institute (PPI)
Ploshchad Bondarenko
249 020 Obninsk, Kaluga Region

THAILAND

Dr. T. Vilaithong
Research Contract
No. 4885/RB

Fast Neutron Research Facility
Department of Physics
Faculty of Science
Chiang Mai University
Chiang Mai

# SUMMARY ACTIVITY

| Group/ Nuclide | V | | Cr | | Fe | | Nb | | Ta | | U-238 | | Li-6 | | Li-7 | | 9-Be | | Mo | | W | | Bi | | Co | | Ni | |
|---|---|---|---|---|---|---|---|---|---|---|---|---|---|---|---|---|---|---|---|---|---|---|---|---|---|---|---|---|
| | Exp. | Eval. | Exp. | Eval. | Exp. | Eval. | Exp. | Eval. | Exp. | Eval. | Exp. | Eval. | Exp. | Eval. | Exp. | Eval. | Exp. | Eval. | Exp. | Eval. | Exp. | Eval. | Exp. | Eval. | Exp. | Eval. | Exp. | Eval. |
| G. Winkler<br>IRK, Vienna | | | | X | | X | | X | | X | | | | | | | | | | X | | X | | X | | | | X |
| Sa Jan<br>IAE, Beijing | | | | | | | X | | | | @ | | | | | | | | | | | | X<br>@ | | | | | |
| K. Seidel<br>TU Dresden | X | X | | | | | | | | X | | X | X | | | | | | | | X | | | | | | | |
| J. Rahighi<br>ENTC, Esfahan | | | | | (X) | | | | | | | | | | | | | | | | | | | | | | | |
| A. Takahashi<br>OKTAVIAN, Osaka | X | | | X | | X | | X | | X | | | | X | | X | | X | | X | | X | | X | | X | | |
| T. Vilaithong<br>FNRF, Chiang Mai | | | | | | X | | | | | | | | | | | | | | | | | | | | | | |
| S.P. Simakov<br>PPI, Obninsk | | # | | | | | | # | | # | | | | | | | | X<br># | | X | | X<br># | | X<br># | | # | | |

* at 14 MeV
@ at 10 MeV
# at 5-8.5 MeV

(X) The experiment is under progress

Appendix IV

## DATA STATUS

(1) "Satisfactory" Data

| | DDX measured at 14 MeV | | Comment to Data Library | |
|---|---|---|---|---|
| Nuclide | EDX | DDX | ENDF/B-6 DDX | JENDL-3 DDX |
| Li-6 | S | N | F | S |
| Li-7 | S | N | F | S |
| Be-9 | S | N | S | S |
| Fe | S | C | N | N |
| Cu | S | C | N | N |
| Nb | S | C | N | N |
| W | S | N | N | N |
| Ta | S | N | N | N |
| Pb | S | N | N | F |
| U-238 | S | N | N | N |

S = Satisfied

N = Not satisfied ($\theta_L < 30^0$, $E_n$, < 1 MeV, $E_n'$ > 8 MeV)

C = to be checked

F = fairly good

Appendix IV contd.

(2) New Data Required

| Nuclide | Comment |
|---|---|
| F-19 | High resolution, Breeder compound material FLiBe |
| Si | High resolution, collective states |
| (Ti) | to be checked |
| V | High resolution |
| Cr | Cr-52 available, High resolution enriched sample |
| (Mn) | to be checked |
| Co-59 | reference data, odd mass |
| Ni | enriched sample desirable |
| Zr | new data desirable |
| Pb | low $E_n$, |
| Na | (n,2n) cross section, coolant NaK |
| Mg | only one data available at most |
| P-31 | " |
| S | " |
| Cl | " |
| K | ", coolant NaK |
| Ca | ", concrete |

* High energy resolution for high mass target is desirable

* Low $E_n$, for (n,2n) reaction